Ionic coupling to plasma polymer surfaces

Mutton, Simon James

Ionic Coupling to Plasma Polymer Surfaces

Ph.D. Thesis

by

Simon James Hutton

Department of Chemistry

University of Durham

2000

For Mum, Dad and Alex

STATEMENT OF COPYRIGHT

DECLARATION

The work described in this thesis was carried out in the Chemistry Department at the University of Durham between October 1996 and September 1999. It is the original work of the author, except where otherwise acknowledged, and has not been submitted previously for a degree at this or any other University.

Wilhelmy plate measurements were carried out by Dr. Jonathan Crowther (chapter 3).

PUBLICATIONS

Work carried out in this thesis has been published as follows:-

S. J. Hutton, J. M. Crowther and J. P. S. Badyal, *Complexation of Fluorosurfactants to Functionalized Solid Surfaces: Smart Behaviour*, Chemistry of Materials, **12** (2000), p2282.

ACKNOWLEDGEMENTS

I would like to thank all the people who have made this work possible and my time in Durham so memorable.

To my supervisor Prof. Jas Pal Badyal for his help and enthusiasm over the last three years and EPSRC and Ron Thomas of Mupor Ltd. for financial support.

To everybody in Lab. 98 past and present for making the work enjoyable.

To George, Kelvin and Barry in the electrical workshop for never giving up. To the glassblowers Gordon, Ray and Malcolm for numerous repairs and advice. To Jim and Neil in the mechanical workshop for all the help and equipment and Jimmy and Joe in the stores for all the last minute orders.

To the members of 14A for all the laughs and good times.

And finally a special thanks to my parents and Alex for always been there for me.

ABSTRACT

The work in this thesis was aimed at the preparation of low energy surfaces via the surface attachment of fluorinated surfactant molecules. Such surface functionalisation routes are highly dependent on the chemical nature of the substrate surface. For this reason the choice of substrate materials is both all important and extremely limited. To make the process of more general appeal a method for pre-treating the substrate, using cold plasma polymerisation reactions, followed by surfactant coupling to the plasma polymer has been devised. Using this approach, the surfactant coupling process is now dependent on the surface chemistry of deposited plasma polymers and independent of substrate characteristics.

In order to form highly functionalised surfaces, likely to undergo further reactions, the plasma polymerisation of acrylic acid, allyl amine and allyl alcohol was investigated. Highly functionalised acid, amine and alcohol surfaces, as shown by X-ray Photoelectron Spectroscopy (XPS) and Infrared Spectroscopy (IR), were produced by optimisation of pulsed plasma conditions. Measurement of deposition rates during plasma polymerisation reactions indicated that polymerisation can occur during the off-time of the pulsed plasma period, most likely via free radical polymerisation pathways.

Highly functionalised plasma polymer surfaces thus formed were shown to couple to fluorinated surfactant molecules. The mechanism of surfactant attachment has been suggested to be ionic attraction between opposite charges on the surfactant molecule and the plasma polymer in aqueous solution. The surfaces formed give rise to oleophobic/hydrophilic behaviour. This is in marked contrast to the usual liquid repellent attributes of conventional polyelectrolyte-fluorosurfactant complexes formed by solution phase synthesis.

CONTENTS

CHAPTER ONE

AN INTRODUCTION TO NON-EQUILIBRIUM GLOW DISCHARGES, PLASMA POLYMERISATION, SURFACES AND CHARACTERISATION TECHNIQUES

1.1 INTRODUCTION

Plasma processing of materials has grown into a multi-billion pound industry world wide, with applications in fields such as organic chemistry, polymer chemistry, biology, solid-state electronics and metallurgy.[1] The industrial use of plasmas may be divided into three main categories:

- Surface modification; plasmas are widely used to alter the surface properties of solid materials via the action of reactive species and ultraviolet radiation.[2] Classes of surface modification include altering the wettability,[3-5] the molecular weight of a polymer,[6] adhesion behaviour,[7-9] hydrophobicity,[10,11] refractive index,[12,13] and composition.[14]
- Surface etching; plasmas can physically etch surfaces. Two distinct types of etching exist; physical etching where ions from the plasma bombard the surface and chemical etching which involves surface reactions and the loss of low molecular weight stable species from the solid.[15]
- Deposition; new materials can be deposited from plasmas.[16] This application will form the basis of the work presented here and will be discussed in further detail in the rest of this chapter.

1.1.1 DEFINITION OF A PLASMA

The term "plasma" was first used by Langmuir to describe the state of ionised gas found in electrical discharges.[17] A plasma can be viewed as a fourth state of matter which is composed of positively charged ions and electrons. Equal numbers of these species mean that plasmas are approximately neutral. As we shall see this picture is an oversimplification and a plasma may be defined more accurately as a "quasineutral gas of charged and neutral particles which exhibits collective behaviour."[18,19] Although comparatively rare on Earth, most of the matter in the universe may well exist in the plasma state.

1.2 GAS DISCHARGES

1.2.1 GAS DISCHARGES

Lightning and the Aurora Borealis are natural examples of the conduction of electricity through gases. Lightning occurs at atmospheric pressures while the Northern Lights are examples of electric currents passing through gases at very low pressures.[20] It has even been suggested that many alleged UFO sightings may be the result of electrical phenomenon occurring over highly charged regions of the earth's surface owing their existence to geological faults.[21] Electrons in gases are strongly bound to the positive nuclei; when electric field strengths are low, gases are highly insulating. Theoretically high electric field strengths would be required to ionise the atoms or molecules of gases. However, gases usually become conducting at much lower field strengths.[20] To explain this phenomenon it has been suggested that free electrons are always present in gases due to the ionisation of particles by cosmic rays and background radioactive decay. The conduction of electricity in gases is complicated by the presence of positive ions. Ionisation of gas particles to produce free electrons liberates an equal number of positive ions. These ions are also accelerated by the electrical field; but in the opposite direction.

Gas discharges can be divided into self sustaining and non-self sustaining discharges.[20] Self sustaining discharges do not require outside sources of electrons for the discharge to be maintained. Non-self sustaining discharges make use of external methods of producing charged particles to perpetuate the discharge. If this aid is removed the discharge is extinguished. Such discharges can be produced by heating the electrodes or the gas itself to liberate free electrons. The discharges utilised in this thesis are examples of non-self sustaining discharges and this class alone will be considered further.

1.2.2 DISCHARGE AND BREAKDOWN

Consider a gas between two parallel flat metal plates. When the voltage between the plates is small the gas is an insulator and no current flows between the electrodes.[20] If the potential difference between the plates is increased the gas eventually becomes conductive and an electric current flows between the plates. The lowest voltage at which current is observed is known as the "breakdown voltage."[20] At atmospheric pressure a spark of high current, lasting only a fraction of a second, passes between the electrodes. At lower pressures the current between the plates may be very small. The discharge voltage can be followed as a function of current passing through the gas, Figure 1.1.

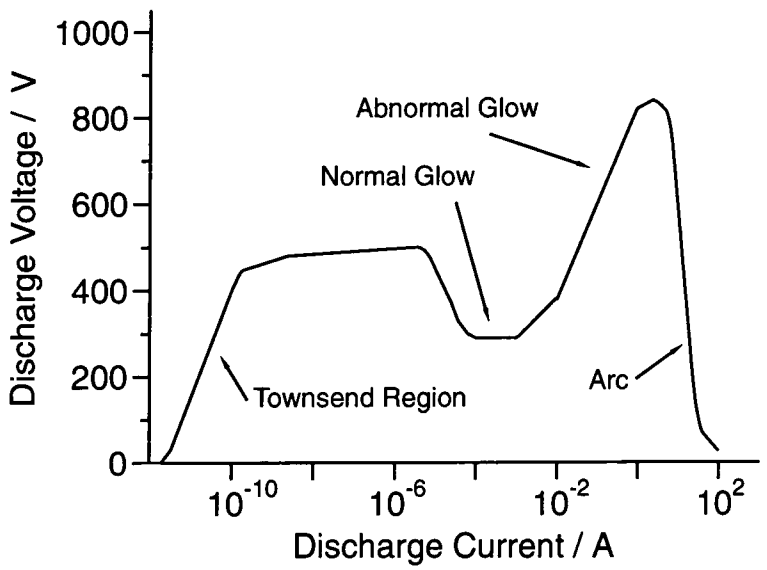

Figure 1.1: Voltage plotted as a function of current for electrical discharges.[20]

At low currents, where the gas has resistance of megaohms, the discharge is known as a Townsend discharge.[20] Breakdown of the gas occurs in this region.

1.2.3 HOW IS THE DISCHARGE MAINTAINED?

The electrical field in Townsend discharges is not strong enough to ionise the gas particles.[20] However, as previously explained (Section 1.2.1), free electrons and ions are always present. These electrons are accelerated by the electric field. If the electrons gain sufficient energy, i.e. the ionisation energy or above, they are capable of ionising gas particles in collisions. These newly formed electrons are also accelerated by the field and may cause further ionisation leading to an avalanche of ionisation processes. However, ionisation of gas particles by free electrons is not very efficient. Collisions of electrons with the massive gas particles are likely to be elastic, with no energy being transferred. Furthermore, inelastic processes include excitation as well as ionisation. It is this excitation of gas particles and the subsequent relaxation pathways which cause the emission of light from gas discharges. In reality the number of electrons produced by the ionisation of gas particles is insufficient to account for the electron currents observed in such discharges. Ions strike the cathode liberating secondary electrons which are accelerated away from the cathode back into the discharge. These extra electrons account for the deficit.

1.2.4 THE GLOW DISCHARGE

When the current observed between the plates reaches the milliamp region the discharged is termed a "Glow discharge," Figure 1.1.[20] The glow discharge is not uniform across the width of the discharge, unlike the Townsend discharge. The discharge consists of 2 main luminous regions and 2 dark spaces.[20] Adjacent to the cathode there is the Crookes dark space followed by the negative glow, the faraday dark space and finally, if the distance between the electrodes is large enough, the positive column. Almost all of the potential difference between the electrodes is concentrated between the cathode and the beginning of the negative glow. The rest of the discharge is relatively field free. Electrons are accelerated across the Crookes dark space by the electric field. These electrons are secondary electrons formed by the mechanism described above. They reach the negative glow with fairly high energies. Collisions in this region cause

ionisation and electronic excitation. This gives rise to the light emitted from the negative glow. The change in potential across the Crookes dark space is given the name the "Cathode Fall."[20] The cathode fall is constant for a range of currents, Figure 1.1. This corresponds to the region where the cathode is only partially covered in glow. Increasing the current extends the glow coverage of the cathode and the current grows in direct proportion to the area of the negative glow. This situation is termed the "Normal Glow."[20] Once the entire surface of the cathode is covered in glow, the cathode fall of potential increases and becomes abnormal. The current density has to increase if the current is to be increased further.[20]

1.3 PLASMA THEORY

1.3.1 PLASMAS

A plasma is a partially ionised gas consisting of equal numbers of positive and negative charge carriers and a different number of neutral particles.[22] The plasmas in question contain a relatively small number of charged particles. Typically the degree of ionisation is approximately 10^{-4}. Under these conditions we assume that the Coulomb interactions between particles sum to zero.

1.3.2 ELECTRON AND ION TEMPERATURES

The mechanisms occurring in plasmas are excitation, relaxation, ionisation and recombination. For a steady state to be reached, i.e. electron and ion densities to be equal, then the rate of ionisation must equal that of recombination.[22] To fulfil this criteria energy must be put into the system. This usually takes the form of an electrical field. As ions have a much larger mass than electrons the action of the field is mainly to give energy to the electrons. The electron energy distribution, for a given mean electron energy (ε), can be predicted by two

models, the Druyvesteyn and the Maxwellian. The former distribution predicts fewer high-energy electrons.[1] Figure 1.2.

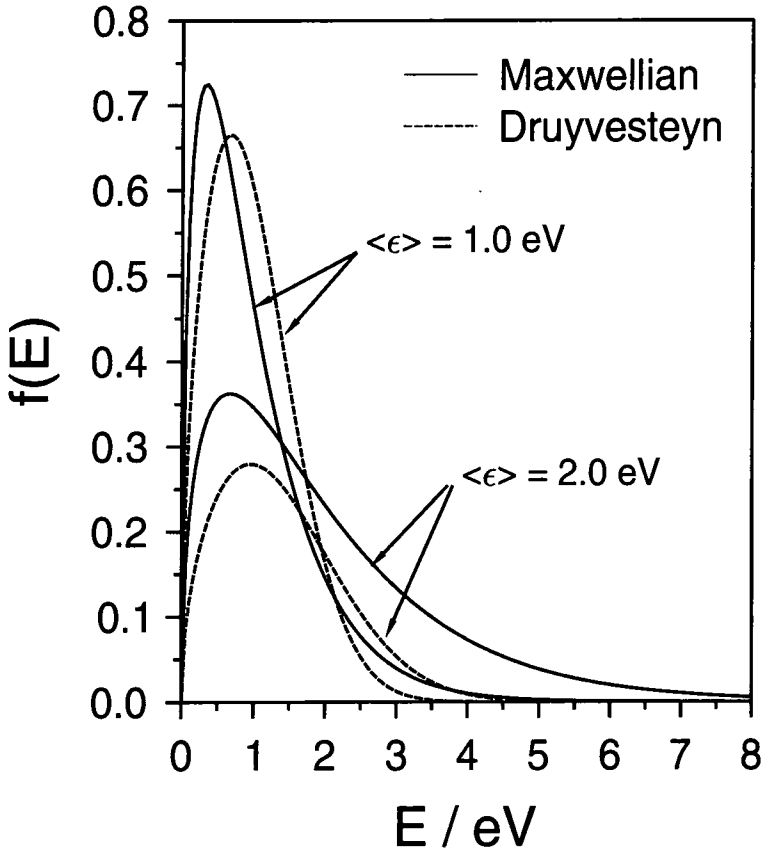

Figure 1.2: Electron energy distribution in a plasma.[1]

Collisions occur at a very high rate in plasmas. Electrons colliding with massive neutrals and ions in the plasma only transfer a small proportion of their energy in such collisions. This is a direct result of the large difference in mass between them. Conversely, ions and neutrals exchange large proportions of their energy on collision with each other and with the container walls. Thus the average kinetic energy of the electrons is high (typically 2 - 8 eV),[22] corresponding to temperatures in the region of 60,00 K (2 eV = 23,200 K). On the other hand the energy of the ions is not much greater than that of the neutral species, i.e. room temperature. This type of plasma is known as a "non-equilibrium plasma."

1.3.3 EQUILIBRIUM AND NON-EQUILIBRIUM PLASMAS

The equilibrium plasma is termed a hot plasma.[16] At temperatures of greater than 10,000 K molecules are ionised and a plasma is formed. In this type of plasma the temperatures of the electrons and other species in the gas are approximately equal. A thermal equilibrium therefore exists between all of the species present. Examples of this type of plasma include stars with temperatures ranging from 5,000 to 70,000 K.[23] Non-equilibrium plasmas, as explained above, occur when the temperature of the electrons greatly exceeds that of other gas species. These are termed "cold plasmas" because the temperature of the species of which the plasmas are formed does not greatly exceed room temperature (except the ionised electrons).[16] Due to the very high temperatures generated equilibrium plasmas are not used for modification or deposition of polymers and will not be considered further.

1.3.4 FLOATING POTENTIAL

The electron and ion density in non-equilibrium plasmas are approximately equal and much smaller than the density of neutral species.[22] The density of ions and electrons is known as the "plasma density."[22] If an electrically isolated substrate is introduced into the plasma it will be bombarded by electrons and ions with

certain charge fluxes (i.e. current densities).[22] The electron flux is given by the following equation,[22] Equation 1.1:

$$j_e = \frac{en_e\overline{c_e}}{4} \qquad \textbf{Eq. 1.1}$$

and the ion flux is,[22] Equation 1.2:

$$j_i = \frac{en_i\overline{c_i}}{4} \qquad \textbf{Eq. 1.2}$$

where j, n and c are the electron (subscript e) or ion (subscript i) flux, number and velocity respectively. As $\overline{c}_e$ is much greater than $\overline{c}_i$, electron fluxes are often three orders of magnitude greater than ion fluxes. Therefore, the substrate is initially bombarded by many more electrons than ions and rapidly acquires a negative charge with respect to the plasma.[1,18] Electrons are repelled from the substrate by the negative charge and ions attracted. A balance is achieved where the electron flux, reduced by repulsion, compensates the ion flux reaching the substrate surface. The potential of the substrate is known as the "floating potential" (V_f, which is the same as the potential of electrically isolated walls of the plasma chamber).[22] This floating potential is measured relative to the "plasma potential" (V_p), which will always be positive.

1.3.5 PLASMA SHEATH

Isolated substrates acquire a positive charge around them as they repel electrons.[22] This is known as a "space charge" and results in the formation of a "sheath" about the substrate.[18,19,22] The electron density in the sheath decreases towards the substrate and a sheath voltage is established. Electron collision with gas species, causing electronic excitation, is responsible for the light emitted by plasmas. As the electron density in plasma sheaths is much lower than that in the bulk plasma this area is less luminescent. The sheath is visible around objects within the plasma as an area of lower luminosity than the glow. Typical

sheath voltages are of the order of +15 V.[22] Only high energy electrons have enough energy to transverse the sheath and arrive at the substrate. The ion flux reaching the substrate is not increased by the magnitude of the floating potential as the flux is limited by arrival of ions at the plasma-sheath interface. However, the kinetic energy of ions at the substrate surface is governed by the sheath voltage. If no collisions occur in the sheath then ions will strike the substrate with a kinetic energy equivalent to the sheath voltage.[22]

1.3.6 DEBYE SHIELDING

Although the net Coulomb interaction between particular charges sums to zero on average; the instantaneous potential at a point due to a disturbance is non-zero and time dependent.[22] If the potential in the plasma is perturbed, the plasma reacts to oppose the change. The "Debye length" (λ_D, typically 100 μm), is a measure of how quickly the perturbation is attenuated in the plasma. The Debye length is defined by the distance required for a perturbation to be reduced to 1/e of its initial value.[22] When considering a particular charge in the plasma we need to take into account the sum of individual interactions with all other charges within a radius of 1 or 2 Debye lengths. Outside this sphere the net interaction is assumed to be zero.[22]

1.4 METHODS OF GENERATING NON-EQUILIBRIUM PLASMAS

1.4.1 DIRECT CURRENT (dc) DISCHARGES

One of the simplest ways to produce an electrical discharge is to pass a dc through a gas situated between two plane electrodes; this is the glow discharge (Section 1.2.4). The actual structure of the gas in the discharge is more complex than previously suggested. A diagrammatic representation of the normal glow discharge, in neon gas at a pressure of 1 torr, reveals the different regions created, Figure 1.3.[20]

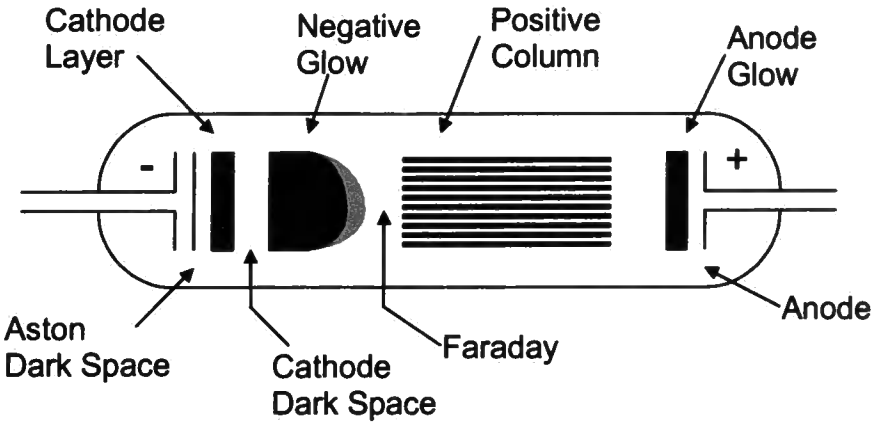

Figure 1.3 dc glow discharge.[20]

The positive column of dc discharge most resembles the idealised plasma (Section 1.2). In this region the discharge is approximately field free. If the electrodes are brought progressively closer together then the length of the positive column is diminished. The Crookes dark space and the negative glow are unaffected. Eventually the positive column and Faraday dark space will be completely consumed and any further inward movement will extinguish the discharge.[20]

1.4.2 CORONA DISCHARGE

To produce discharges at higher gas pressures it is necessary to alter the shape of the electrodes used and a point and plane configuration is often employed,[7,24] Figure 1.4. Using this design discharges can be produced in gases at pressures of up to one atmosphere. Due to the small surface area of the point electrode the electrical current at this position will be very high. The glow of such systems is concentrated at this point and the small volume of active plasma produced limits their use in industry. They do however find an application in such devices as copying machines where they produce charged particles.

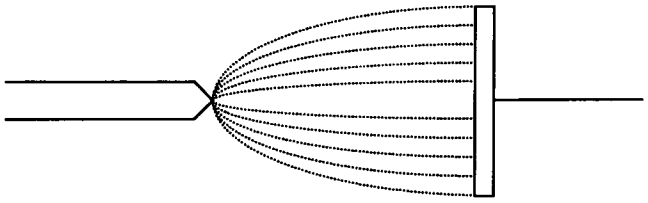

Figure 1.4: Corona Discharge.[24]

1.4.3 SILENT DISCHARGE

The silent discharge is a large volume method with the ability to create industrially useful discharges at atmospheric pressures,[24] Figure 1.5. One electrode in silent discharges is covered in a dielectric material. Micro-discharges take place between the electrodes. The reduced field at the breakdown voltage corresponds to electron energies of 1-10 eV. If high frequency electrical currents are used then high power dissipation can be achieved at low voltages.[24]

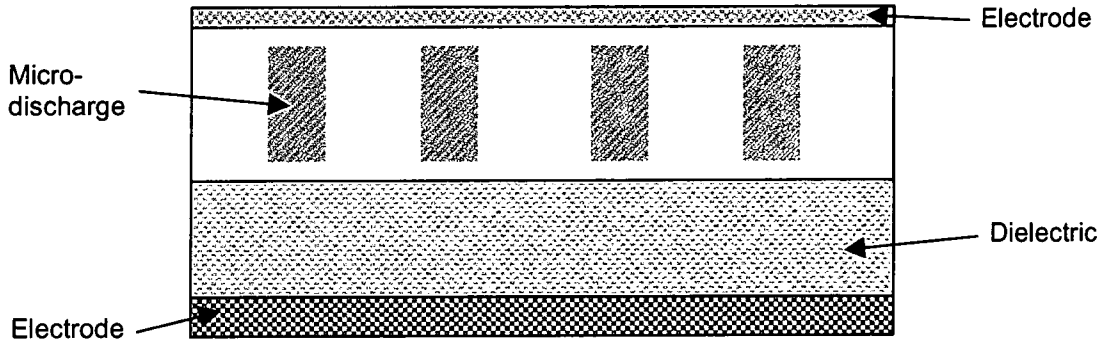

Figure 1.5: The silent discharge.[24]

1.4.4 RADIO FREQUENCY (rf) DISCHARGES

rf discharges are commonly used in polymer processing applications and have several advantages over other types of discharges:[22]

- Direct contact between the electrodes and the plasma is avoided. This overcomes the problem of contamination in plasmas by particles spluttered from the surfaces of electrodes;
- Insulating materials can be studied more easily in these systems than in dc discharges;
- rf discharges are also more efficient than dc systems at producing ionisation and sustaining the discharge;
- The minimum operating pressures are also reduced in rf discharges compared with dc discharges.

Frequencies of alternating current above 1 MHz are used for rf discharges. The frequency most often employed is 13.56 MHz, due to government broadcasting limitations.[20]

1.4.4.1 rf Sheaths

The sheath thickness in rf systems is far less dependent on gas pressure than in the dc case.[22] Little ionisation occurs in the sheath region but it is generally not collision free (depending on gas pressure). The energy distribution of ions which transverse the sheath will be affected by the rf modulation.[16] For example, a 20 eV argon ion has a velocity of 9.8×10^5 cms^{-1}. It would therefore take approximately 1 μs to transverse the 1 cm of the sheath.[22] However, a frequency of 13.56 MHz corresponds to oscillations of 74 ns which means the ion would undergo several oscillations on its journey to the wall. The energy of ions at the substrate surface should be equal to that of the plasma potential, modulated by collisions and the oscillating field. Fast light particles will cross the sheath quickly and be affected by the instantaneous potential. The energy distribution of such particles is narrow, while slow moving, heavier particles see only an average potential. Their energies characteristically show a broad distribution.[22]

1.4.4.2 Matching Networks

A matching network is placed between the rf generator and the discharge. This network increases the power dissipation in the discharge and protects the generator.[22] The matching network is situated close to the discharge to avoid power loss which might occur due to the large reactive currents flowing between the discharge and the matching network.[22] The two methods of matching routinely used are inductive and capacitive coupling, Figure 1.6.

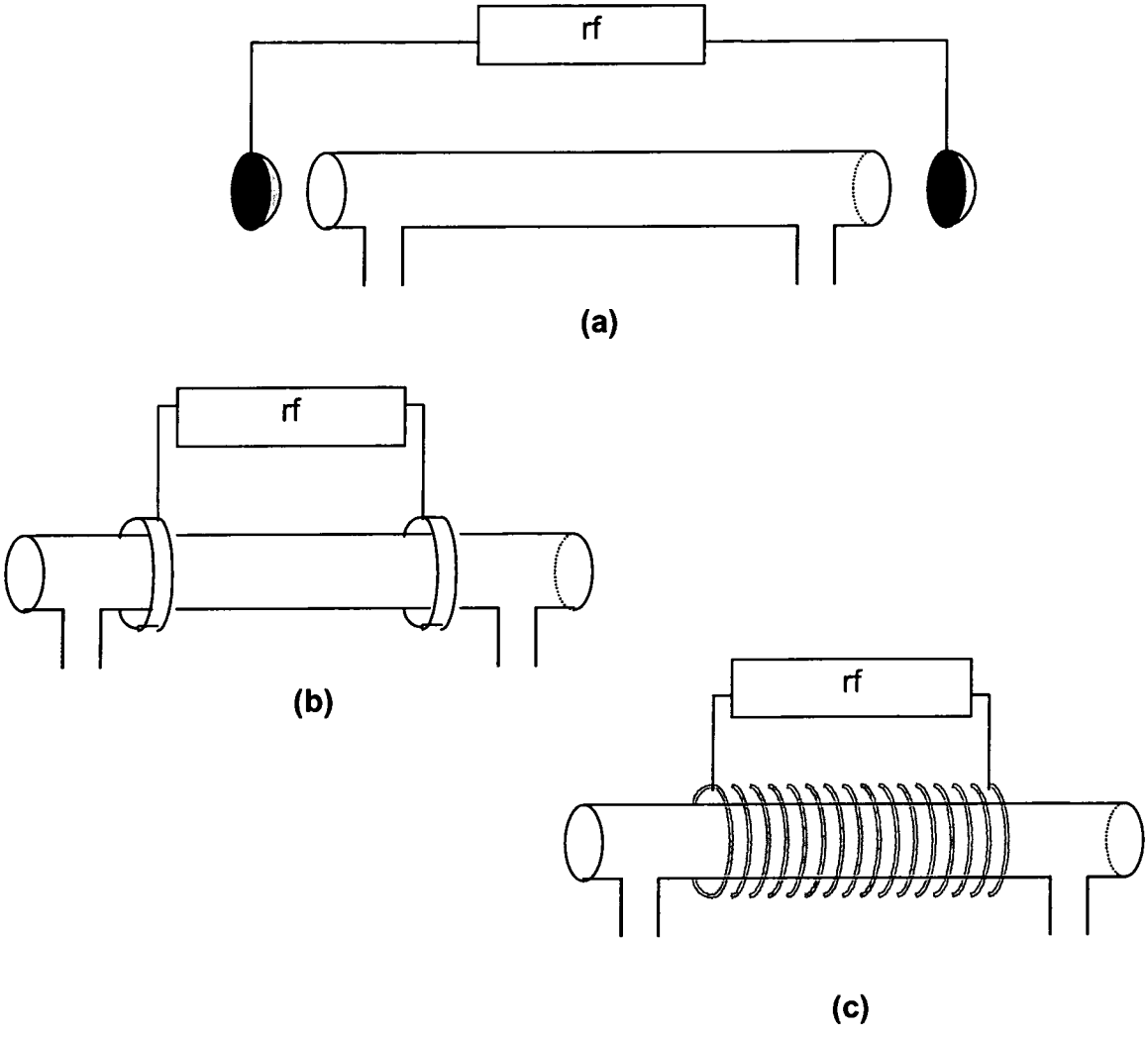

Figure 1.6: Matching in rf discharges: (a) and (b) are capacitively coupled; and (c) is inductively coupled.[1]

1.4.5 MICROWAVE DISCHARGES

Microwave discharges have the advantage that they can be operated in a wide pressure range, from 1 mbar to atmospheric.[22] The frequency of microwave electromagnetic radiation is 0.3 to 10 GHz.[23] As a result the wavelength of the electromagnetic radiation used to maintain the plasma is similar to that of the reactor dimensions and resonance can occur. This makes the discharges efficient but difficult to maintain.[22]

1.5 PLASMA POLYMERISATION

1.5.1 INTRODUCTION

Many organic molecules possess sufficient vapour pressure for the maintenance of an electrical discharge. Under these conditions novel materials may be produced by polymerisation of the organic monomer subject to the discharge.[25] These polymers are typically thin films which bare little resemblance to polymers formed by more conventional routes. This new class of materials are termed "plasma polymers" and are often highly branched, cross-linked, amorphous thin films.[26]

The process of plasma polymerisation is discernible from conventional polymerisation by several important features:[27]

- The polymers formed lack a recognisable repeat unit;
- Polymer properties are highly dependent on the conditions of polymerisation as well as the initial monomer structure;
- Potential monomers do not require a conventional polymerisable functional group such as a double bond.

The chemistry of plasma polymerisation is a nonthermal, nonequilibrium process and the electron temperature in non-equilibrium plasmas is several orders of magnitudes greater than the gas temperature.[27] Chemical reactions can take place at lower temperatures than would be possible under thermal conditions.

An understanding of the mechanism of plasma polymerisation would be useful in the tailoring and optimisation of polymer properties. Before considering likely plasma polymerisation mechanisms a brief review of more conventional polymerisation mechanisms is required.

1.5.2 STEP-GROWTH POLYMERISATION

Step-growth or condensation polymerisation occurs if two difunctional molecules react.[28] The product of such a reaction also possesses two functional groups. It is assumed that the reactivity of these groups is not dependent on the chain length when it is greater than a critical value. A small molecule is eliminated in the polymer forming reaction. This molecule must be removed for efficient polymerisation. For step-growth polymerisation to take place the equilibrium constant for the forward reaction must be large.[16] The formation of the polyamide Nylon from a diacid and a diamine is one example of a polymer formed by a step-growth polymerisation mechanism, Figure 1.7.

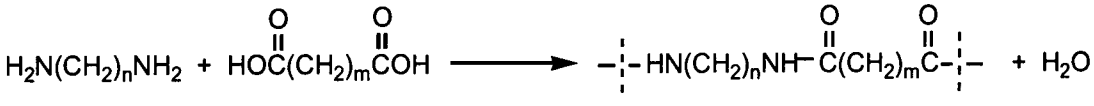

Figure 1.7: Step-Growth Polymerisation.[28]

1.5.3 CHAIN-GROWTH POLYMERISATION

The formation of polymer molecules by chain-growth polymerisation occurs via consecutive reaction of the end of a "living" polymer chain with a monomer molecule. There are three distinct stages in the chain-growth mechanism which can be represented as shown overleaf:[16]

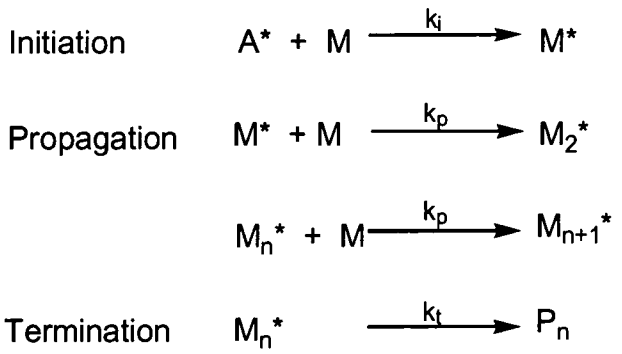

Figure 1.8: Chain-Growth Polymerisation.[16]

The first stage involves the formation of an active site and is termed initiation. The monomer (M) can be activated by collision with an initiator compound (A). The polymer molecule is formed by the rapid reaction of monomer molecules with the active site in the propagation step. The growth process is terminated when the active site is lost by colliding with a second active site. The active site could be cationic, anionic or more commonly a radical. Consideration of the mechanism of free radical polymerisation leads to the following observations:[16]

- The rate of polymerisation is proportional to the square root of the initiator concentration;
- The degree of polymerisation is inversely proportional to the square root of the initiator concentration, i.e. the faster the polymerisation, the shorter the chain length.

1.5.3.1 Thermodynamic Limitation on Chain Propagation

On polymerisation, a large number of randomly oriented, moving monomer molecules become incorporated into a relatively well ordered solid structure. The entropy of the system is significantly decreased. As a result the enthalpy of the polymerisation reaction must be large and negative. Therefore the $-T\Delta S$ term dominates the thermodynamics of the system. Thus there is a ceiling temperature (T_c) to the polymerisation process beyond which polymerisation will not occur.[16]

1.5.4 RADIATION POLYMERISATION

Radiation polymerisation is similar to plasma polymerisation in that initiators are absent in both cases. Monomer molecules are ionised by radiation or high energy electron beams. A cation-radical is formed:[16]

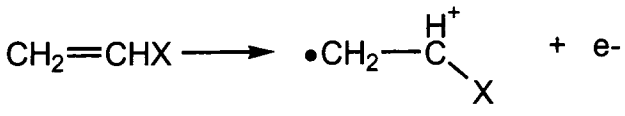

The ejected electron may recombine with the ion or the pair may become separated. If the latter takes place the cation and radical migrate to opposite ends of the molecule. Propagation proceeds independently at both ends of the molecule:[16]

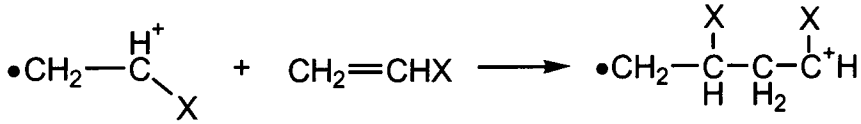

The ejected electron could be captured by a monomer molecule to form an anion-radical pair also capable of initialising propagation reactions.

1.5.5 POLYMERISATION IN A VACUUM

Plasma polymerisation typically takes place at pressures below atmospheric. It is therefore necessary to take the reduced pressure into account when searching for possible plasma polymerisation mechanisms. Two pertinent points concerning polymerisation are highlighted below:[16]

- The number of molecules in a vacuum is considerably less than the number present in the same volume at atmospheric pressure;
- The ceiling temperature to chain-growth polymerisation decreases with decreasing pressure.

The two major classes of polymerisation mechanisms discussed above are therefore ruled out as candidates for plasma polymerisation. The scarce population of monomer molecules would make conventional step-growth polymerisation too slow to account for the rapid polymer formation observed in many plasma systems.[16] In the gas phase the change in entropy on polymerisation is greatly increased. Furthermore, due to the low pressures used in many plasmas, the anticipated ceiling temperature to chain-growth polymerisation is too low to expect appreciable polymer formation by this mechanism.

1.5.6 PLASMA POLYMERISATION

Plasma polymerisation is initiated by the formation of a reactive species by collision, electron impact, or interaction with an energetic photon. Polymer growth occurs by the addition of this reactive species to other species present. Termination may occur by collision of reactive species to form an unreactive polymer chain. This may undergo re-excitation, however, in a process akin to the original initiation. The polymerisation process can occur homogeneously in the gas phase or heterogeneously between gas phase species and activated surfaces. These processes are not mutually exclusive and may occur concurrently in the same system, Figure 1.9.

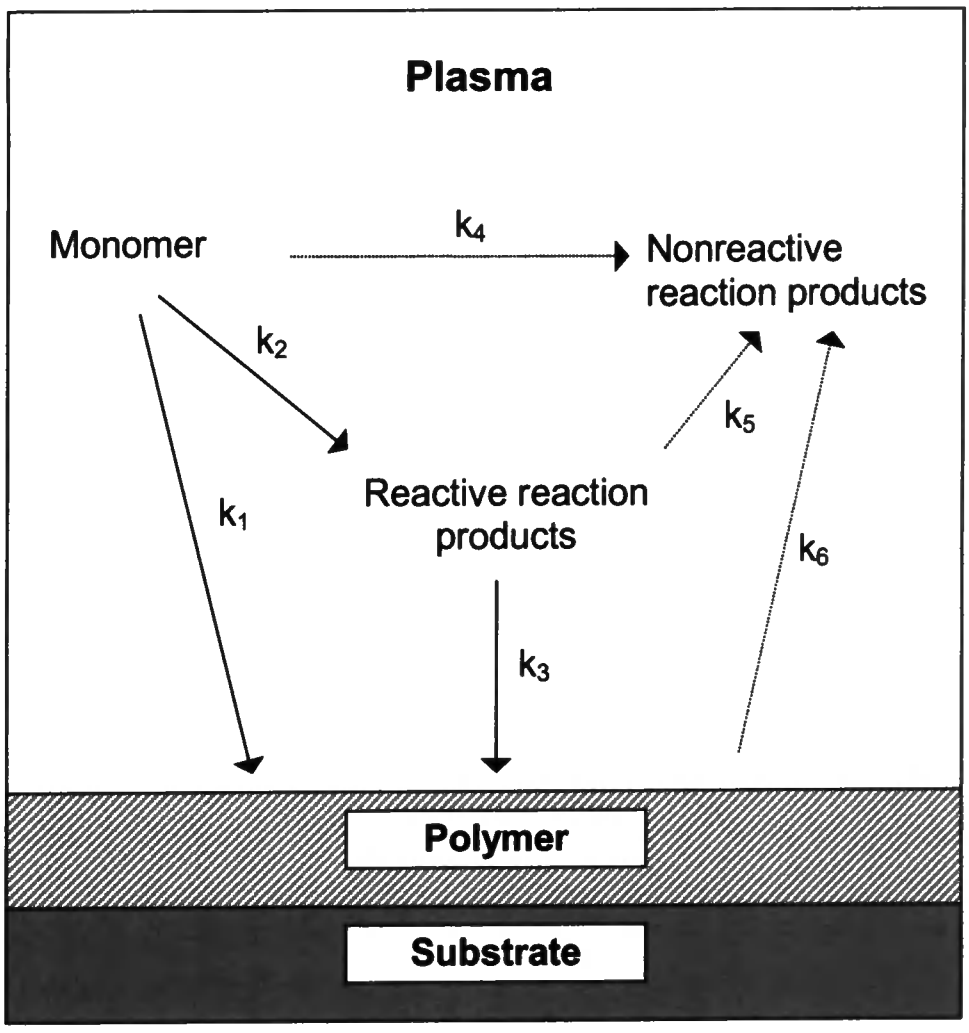

Figure 1.9: Schematic diagram of the various types of reaction involved in plasma polymerisation.[29]

Reaction k_1 where monomer is directly incorporated into the polymer film is called plasma induced polymerisation. Plasma polymerisation is taking place via reactions k_2 and k_3. The nature of the reactive species discussed above can be inferred by consideration of the discharge conditions. Ionisation of molecules by electron collision is essential for maintaining the gas discharge. However, only high energy electrons (>10 eV) have sufficient energy to cause ionisation.[16] The electron energy distribution (Figure 1.2) in a typical plasma ensures that only a small proportion of the electrons in the plasma are energetic enough to cause

ionisation. However, a large proportion of the electrons are capable of breaking the covalent bonds present in many organic molecules, Table 1.1:

H——H	4.5	C——C	3.6	C=C	6.4
H——C	4.3	C——N	3.0	C≡C	8.4
H——O	4.8	C——O	3.6	C=O	7.5
H——Cl	4.5	C——F	2.6	C≡N	9.1
		C——Cl	3.6		

Table 1.1. Average values of bond energies / (eV).[30]

We would therefore expect a far greater number of free radicals than ions present in the plasma. The concentration of free radicals in the plasma is estimated to be approximately five times greater than that of ions.[31] For these reasons it is believed that the most important species in polymer forming plasmas are radicals.[16] However, this assumption has recently been questioned.[32]

1.5.7 MECHANISM OF PLASMA POLYMERISATION

Yasuda has proposed a mechanism based on the rapid step-growth principle,[16] Figure 1.10. There are two main routes of rapid step growth polymerisation. Cycle I represents the repeated reactivation of products from monofunctional activated species. Cycle II involves the reaction of difunctional or multifunctional species.

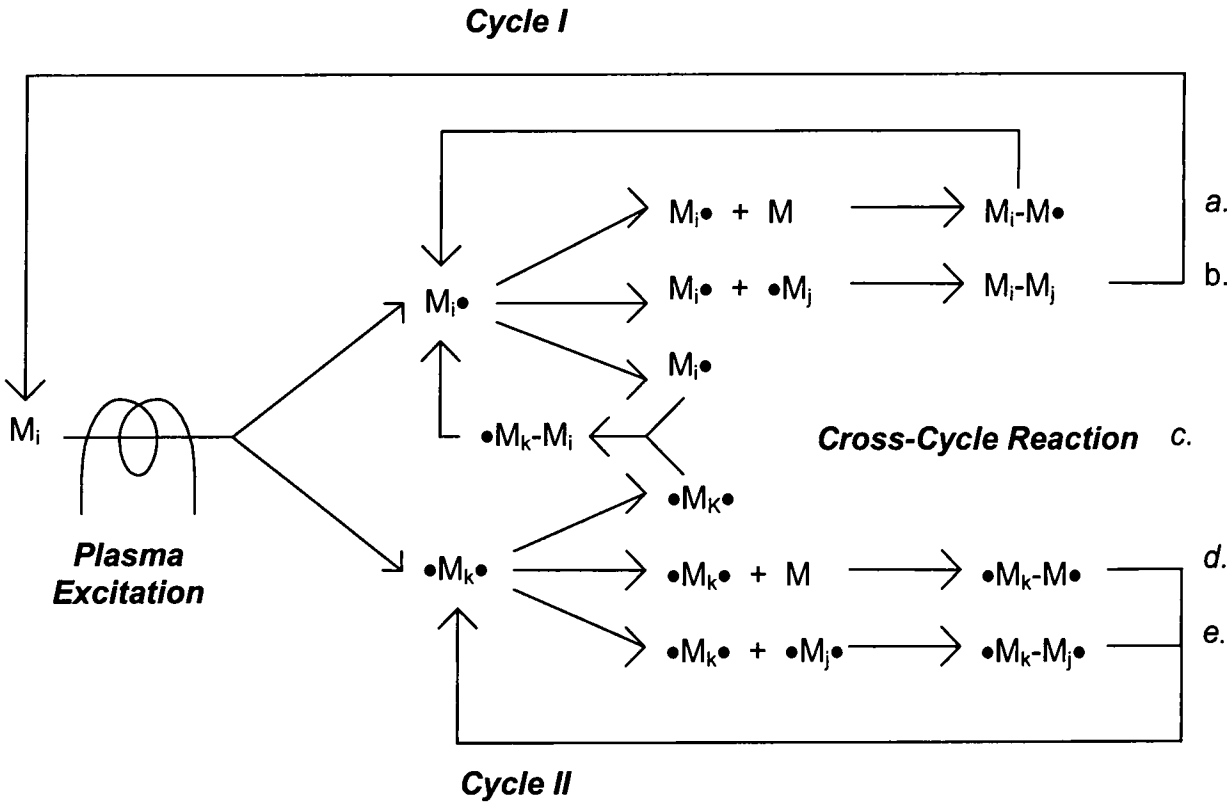

i, j and k represent differences in size between the species.

Figure 1.10: Schematic diagram of the proposed mechanism of plasma polymerisation.[33]

Reactions *a.* and *d.* (Figure 1.10) require the monomer to possess a chemical structure that can add M•. Reaction *b.* is a termination step. Ions may contribute in reactions but reactions between neutral species are more likely.[25]

1.5.8 POLYMERISATION PARAMETERS

The plasma polymerisation technique is very system dependent. Under conditions of constant pressure, the most important parameter affecting the polymer structure is the power (W) to monomer flow-rate (F) ratio, W / F.[34] This parameter is modified by the molecular weight of the monomer (M) to give W / FM.[16,35] The dissociation of monomer molecules into radicals and ions in the

plasma is related to the energy each molecule receives. The chemical structure of the polymer produced is related to this parameter.[27] Different reactors cannot be compared quantitatively as monomer disruption is predominant in the glow discharge volume.[36] This volume is often different even for reactor systems with the same volume.

1.5.9 CONCLUSION

We have seen that one mechanism suggested for plasma polymerisation is rapid step-growth polymerisation. A wide range of species are involved and may consist of cations, anions, or more commonly, radicals. The reactions occurring in the plasma, homogeneously and heterogeneously, are complex and difficult to characterise. It seems unlikely that reaction mechanisms can be confidently described by the analysis of the polymers formed alone.

1.6 PULSED PLASMAS

The properties of plasma polymers are very dependent on the plasma system's parameters. The plasma is often a harsh environment and a large proportion of functional groups are rapidly lost from monomers and leave the plasma as stable molecules such as H_2O or CO_2. Incorporation of desirable functional groups into the plasma polymer is therefore often difficult. Over the last few years a new technique for plasma processing has been developed to tackle these difficulties in which the plasma is pulsed. In most examples of such work an rf plasma is utilised. Typically, the rf power supply is pulsed on and off by an external pulse generator. A quantity known as the duty cycle describes the pulse cycle used,[37] Equation 1.3:

$$\text{Duty Cycle} = \left| \frac{t_{on}}{t_{on} + t_{off}} \right| \qquad \textbf{Eq. 1.3}$$

where t_{on} is the plasma on-time, t_{off} is the plasma the off-time and P_p is the peak rf power supplied to the plasma by the rf generator. A schematic of a typical pulsing experiment is presented below, Figure 1.11:

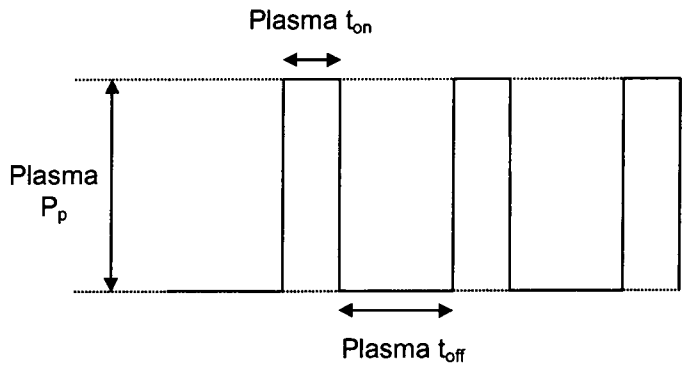

Figure 1.11: Schematic representation of the pulse modulation of plasma discharges.

During pulsed plasma experiments the average power supplied to the plasma can be calculated,[37] Equation 1.4:

$$\langle P \rangle = P_p \times \left| \frac{t_{on}}{t_{on} + t_{off}} \right| \qquad \textbf{Eq. 1.4}$$

where $\langle P \rangle$ is the average power. Examples of structural retention during electrically pulsed plasma include deposition from silicon containing monomers,[38-40] halocarbons,[38,39,41-44] tin containing precursors,[45] alcohols[46] and other reactive molecules.[39,47] Increased structural retention is not only achieved due to low average discharge powers but conventional type polymerisation reactions may occur in the off-time.[38,41,43]

1.7 SURFACES, INTERFACES, CONTACT ANGLES AND SURFACTANT ADSORPTION

1.7.1 INTRODUCTION

An interface is a region of finite thickness where one bulk phase changes to another.[48] If one of the phases is a gas or a vacuum the interface is known as a surface. The atoms and molecules at surfaces or interfaces have chemical and physical properties which differ from those of the bulk material.[49-51] The differences arise from the fact that molecules situated close to the surface are subject to different intermolecular forces than those experienced in the bulk of the material. This results in the total energy of a system being different when a surface exists.[49] This excess energy is often called surface tension or surface energy.[52] The chemical nature of surfaces has a direct influence upon their interaction with other molecules during surface wetting and adsorption. The attractive energy between surfaces and other molecules may be broken down into separate contributions from different types of intermolecular forces such as dispersion, induction and dipole-dipole forces of attraction.[53] Interactions were formerly described as polar and nonpolar, however, it has been recognised that polar interactions occur only between the acidic and basic sites of interacting materials.[54] Dipole-dipole interactions are now characterised as part of "nonpolar" van der Waals interactions.[55] "Polar" interactions, including hydrogen bonds, are considered to be electron donor-acceptor (Lewis acid-base) interactions.[56]

In this section we shall discuss the contact angle of liquids on solid surfaces and the adsorption of surfactants at an interface. A surfactant (or surface active agent) is a molecule which demonstrates surface activity,[57] i.e. it adsorbs preferentially at interfaces. Such surface activity arises from the molecular structure of surfactants. Surfactants have a characteristic structure consisting of two main structural groups known as "lyophobic" and "lyophilic." Lyophobic groups have little attraction for the solvent and commonly consist of a

hydrocarbon or fluorocarbon chain. Lyophilic groups interact strongly with the solvent and are often polar in nature.[58]

1.7.2 SURFACE ENERGY AND CONTACT ANGLES

The discussion of the excess energy present at solid surfaces is assisted by the consideration of the formation of new surfaces by separating two bulk phases, Figure 1.12.

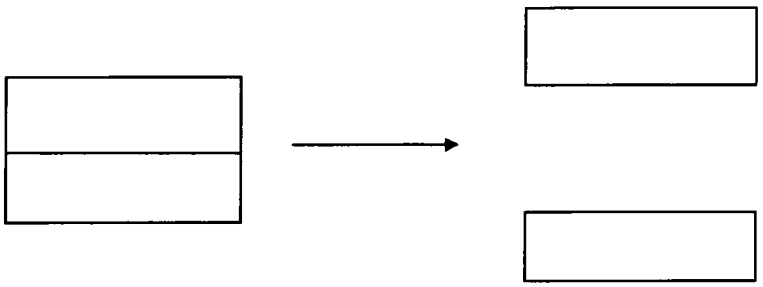

Figure 1.12: The formation of a new surface.[48]

The reversible work required to produce a surface of unit area is the surface energy, Equation 1.5:[48]

$$\gamma = \left(\frac{\delta G}{\delta A}\right)_{T,P,n} \qquad \textbf{Eq. 1.5}$$

where γ is the surface energy, G is the Gibbs free energy, A is the surface area, T is the absolute temperature, P is the pressure and n is the total number of moles in the system. A drop placed on a solid surface changes shape until it reaches an equilibrium, Figure 1.13. The driving force behind this rearrangement is the minimisation of the free energy of the system.[52]

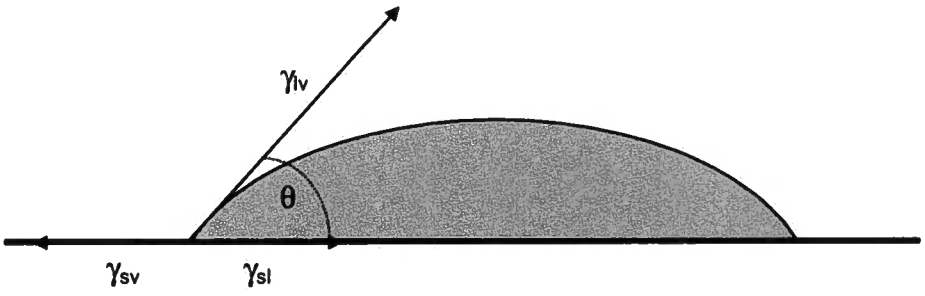

Figure 1.13: A drop on a solid surface.[52]

The equilibrium at the 3 phase boundary (solid, liquid and gas) is described by the Young equation,[59-61] Equation 1.6:

$$\gamma_{sv} - \gamma_{sl} = \gamma_{lv}\cos\theta \qquad \textbf{Eq. 1.6}$$

where γ_{sv} is the surface energy of the solid in equilibrium with the saturated vapour of the liquid; γ_{sl} is the interfacial energy between the solid and the liquid; γ_{lv} is the surface energy of the liquid in equilibrium with its saturated vapour; and θ is the equilibrium contact angle for a drop of the liquid on the surface. This equation forms the basis of a set of arguments which enable the calculation of the surface energy of an ideal solid from the measurement of contact angles.[62] An ideal solid is molecularly smooth and characterised by a well defined value of surface energy. The wetting liquid must be a neutral probe, i.e. it must not interact physically or chemically with the surface.[52] These restraints make the measurement of surface energy in real systems very difficult. Liquid drops can display many different stable contact angles on a real surface and this behaviour is called "contact angle hysteresis."[63,64] The maximum contact angle is often observed when the liquid first wets the solid when it is known as the "advancing angle." The minimum angle, the "receding angle," is observed on removal of the liquid from a previously wet surface.

1.7.3 CONTACT ANGLE HYSTERESIS

When contact angle hysteresis arises from surface roughness or surface heterogeneity it is known as "thermodynamic hysteresis." A type of time dependent hysteresis known as "kinetic hysteresis," arises from non-equilibrium processes. These non-equilibrium processes may result from the fact that real liquids are not neutral probes and may penetrate and/or swell the surface region of the solid. It might also be that polymer surfaces are mobile and may rearrange in response to the environment.[52] These properties of real surfaces produce many closely spaced local energy minima (or metastable states) in place of one energy minimum. This leads to a range of allowed contact angles with energy barriers of varying magnitudes between them.[52]

1.7.3.1 Surface Roughness

On a rough surface there is more surface than is actually measured by the unit area. A new term, known as the roughness factor (r), can be used to modify the Young equation (Equation 1.6),[65] Equation 1.7:

$$r\left(\gamma_{sv} - \gamma_{sl}\right) = \gamma_{lv}\cos\theta_w \qquad \textbf{Eq. 1.7}$$

where the subscript w indicates the contact angle on a rough surface, the Wenzel angle. The roughness factor, r, is defined below,[52] Equation 1.8:

$$r = \frac{\text{actual surface}}{\text{geometric surface}} \qquad \textbf{Eq. 1.8}$$

Wenzel's angle is related to Young's angle (θ_y) as follows,[52] Equation 1.9:

$$\cos\theta_w = r\cos\theta_y \qquad \textbf{Eq. 1.9}$$

The roughness factor is always greater than 1 for rough surfaces and equal to 1 for flat surfaces. If the Young angle is greater than 90° the roughness factor increases the contact angle and decreases the angle if it is less than 90°. This treatment is valid in the case of one defined energy minimum but does not include the effect of metastable states on the contact angle.[52] Further treatments which consider the angle of the rough surface at individual points predict the existence of a large number of metastable configurations separated by energy barriers.[66-68]

1.7.3.2 Surface Heterogeneity

Usually real surfaces display some degree of heterogeneity, that is the surface molecular composition is not uniform across the entire surface region. This results in various regions on a sample surface possessing different wetting properties.[52,69] A basic equation to account for surface heterogeneity has been proposed,[70] Equation 1.10:

$$\cos\theta_c = Q_1 \cos\theta_1 + Q_2 \cos\theta_2 \qquad \textbf{Eq. 1.10}$$

where subscripts 1 and 2 refer to two different surface components, Q is the fractional coverage of each component, θ is the Young angle and θ_c is Cassie's angle, the equilibrium contact angle measured on a heterogeneous surface. This treatment is again concerned with the idealised situation of one energy minimum. Further work was required to predict the metastable states thought to be responsible for the range of contact angles experimentally observed.[71]

1.7.3.3 Kinetic Contact Angle Hysteresis

Kinetic contact angle hysteresis is time dependent and arises from the modification of the liquid drop towards a more stable state.[52] Such hysteresis can be caused by penetration of the test liquid into the solid surface. This has

been observed by water on polystyrene thin films.[72] A further cause of time dependent contact angle hysteresis on polymer surfaces is change in the molecular structure in response to the nature of the test liquid.[73] For example, hydrophilic groups in poly(2-hydroxyethyl methacrylate) can reorientate towards water.[74,75]

1.7.4 POLYMER SURFACES IN SOLUTION

An unequal charge distribution always exists at an interface between two bulk phases.[58] One side of the interface develops a net positive charge while the other side becomes negatively charged. A potential is therefore present across the interface with is termed an "electrical double layer."[58] Overall neutrality is maintained as the net charge on one side of the interface is equal and opposite to the charge on the other side. The distribution of neutralising charges around a surface in solution is important as this distribution determines how the electrical potential varies with distance from the surface. Initial theories on this distribution of neutralising charges envisaged an ordered, parallel arrangement of counterions but this was soon superseded by a model which suggested a more diffuse layer of neutralising charges.[76-78] However, this model proved incorrect for surfaces with a high charge density and small distances because it did not take into account the ionic radii of the counterions. A new theory proposes that the solution phase portion of the interface should be separated into two different regions.[79] Close to the solid surface a layer of tightly bound counterions adsorbed onto defined sites is envisaged. Further from the surface a more diffuse layer of counterions exists,[58] Figure 1.14:

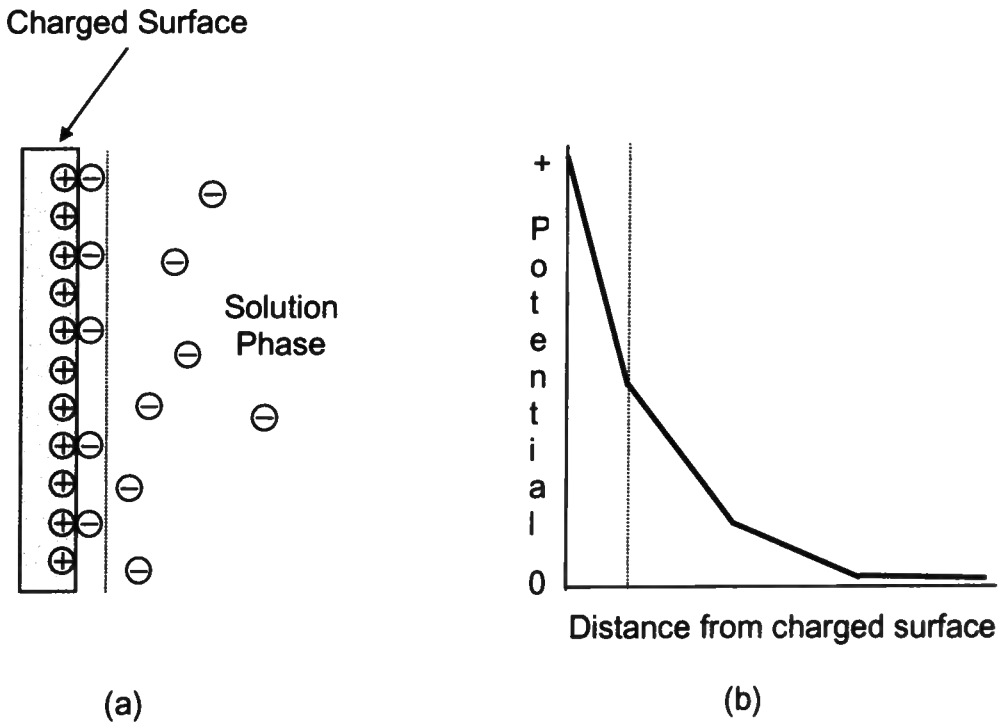

Figure 1.14: The stern electrical double layer: (a) schematic representation of the counterion distribution; and (b) variation in the electrical potential with distance from charged surface.[58]

The potential is predicted to initially decrease quickly with increasing distance from the charged surface and then falls more gradually, Figure 1.14(b). It may even be possible for the adsorbed counterions to change the sign of the surface.[58] The effective thickness ($1/\kappa$) of the diffuse region can be calculated,[80] Equation 1.11:

$$\frac{1}{\kappa} = \left(\frac{\varepsilon_r \varepsilon_0 RT}{4\pi F^2 \sum_i C_i Z_i^2} \right)^{\frac{1}{2}} \qquad \textbf{Eq. 1.11}$$

where ε_r ($= \varepsilon/\varepsilon_0$) is the relative static permittivity or dielectric constant of the solution (ε is the static permittivity of the solution and ε_0 is the permittivity of a vacuum); R is the gas constant; T is the absolute temperature; F is the Faraday

constant; Z is the valence of the ion; and C_i is the molar concentration of any ion in the solution. This thickness is a measure of how far from the surface into the solution phase the electrical potential has an effect. There are several conclusions which may be drawn from Equation 1.11:[58]

- This distance is inversely proportional to the valence of the counterion (Z) and the square root of their concentration;
- The distance will be increased as the temperature is raised;
- The distance will also increase with increasing permittivity of the solution and since water has a high dielectric constant, electrical effects will be more important in aqueous systems than in organic solvents.

1.7.5 SURFACTANT ADSORPTION AT THE SOLID-LIQUID INTERFACE

The adsorption of surfactants at the solid-liquid interface is controlled by the following factors:[58,81-90] the chemical nature of the structural groups on the solid surface; the molecular structure of the surfactant (ionic or nonionic, hydrophobic tail length, etc.); and the environment of the aqueous phase (pH, electrolyte concentration, temperature, etc.). Generally, the adsorption of surfactant involves single surfactant ions rather than micelles.[91,92] There are a number of mechanisms by which surfactants may adsorb onto solid surfaces:[58]

1. Ion Exchange, counterions adsorbed onto the solid from solution are replaced by surfactant ions,[58,93-95] Figure 1.15:

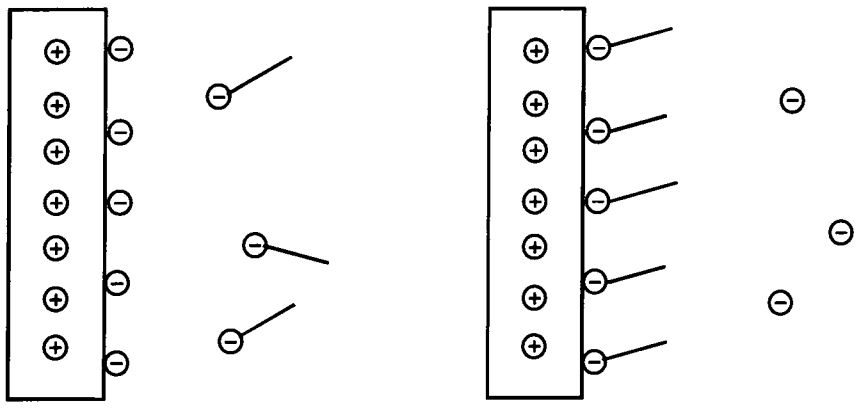

Figure 1.15: Ion exchange.[58]

2. Ion paring, adsorption of surfactant ions onto unoccupied oppositely charged sites,[58,94,95] Figure 1.16:

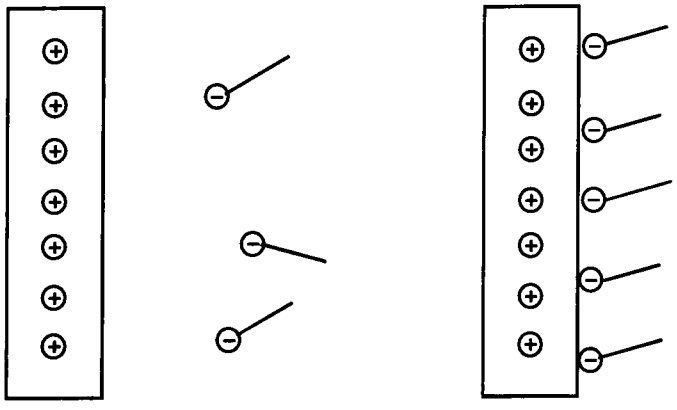

Figure 1.16: Ion pairing.[58]

3. Acid-base interaction[54] via hydrogen bonding[94-96] or Lewis acid-Lewis base reaction, Figures 1.17 and 1.18 respectively:

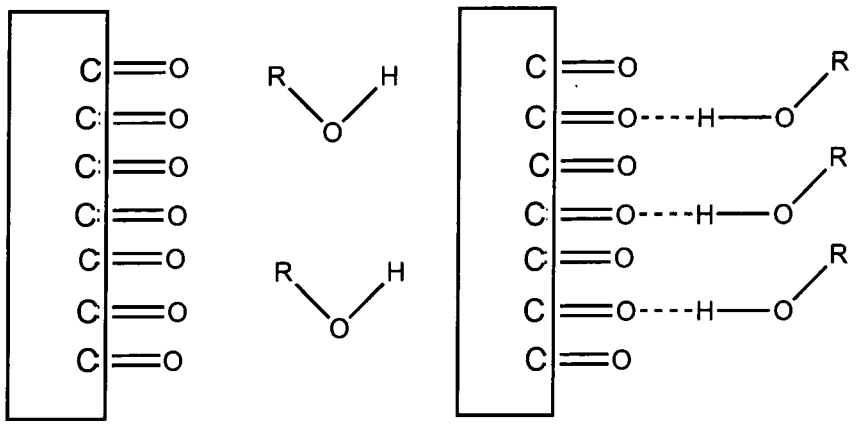

Figure 1.17: Adsorption via hydrogen bonding.[58]

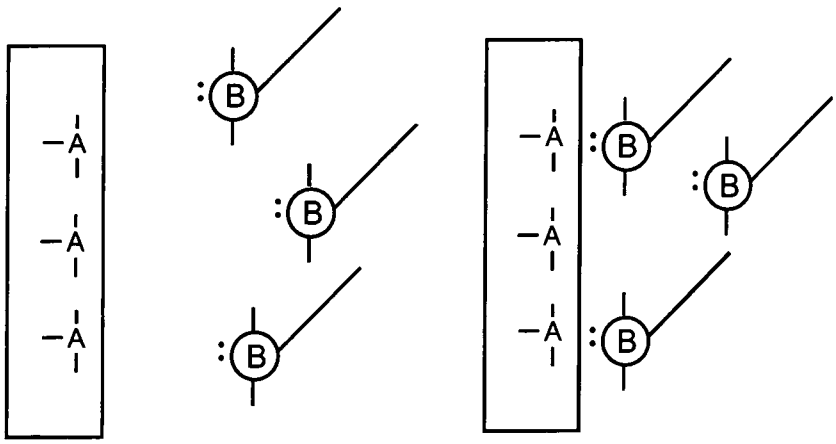

Figure 1.18: Adsorption via Lewis acid - Lewis base interaction.[58]

4. Adsorption by dispersion forces occurs via London-van der Waals dispersion forces. This mechanism of adsorption may supplement all other adsorption types,[58] Figure 1.19:

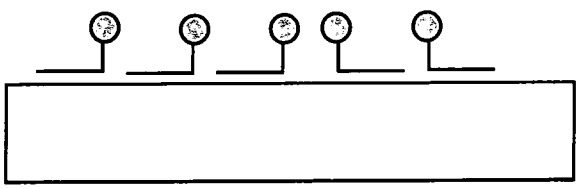

Figure 1.19: Adsorption via dispersion forces.[58]

5. Hydrophobic bonding occurs via attraction between hydrophobic groups on the surfactant molecule adsorbing onto the solid by aggregation of their chains,[58,93,97,98] Figure 1.20:

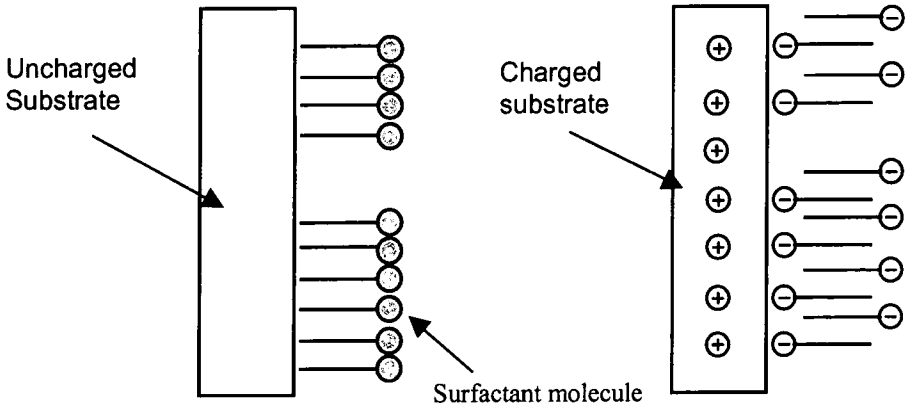

Figure 1.20: Adsorption via hydrophobic bonding on a charged and an uncharged surface.[58]

The mechanism of adsorption of the surfactant at the solid liquid interface and hydrophobic interactions between surfactant tails determine the conformation of the adsorbed surfactant layer. Adsorption of ionic surfactants onto an oppositely charged mineral surfaces has been extensively studied.[83,84,90,93,97,99-102] At low surfactant concentrations, electrostatic interactions between the ionic surfactant species and the oppositely charged solid surface dominate the adsorption. As the surfactant concentration is increased there is a marked increase in surfactant adsorption due to the onset of surfactant aggregation at the surface through lateral interactions between hydrocarbon chains.[83] Eventually, at high surfactant concentrations, a plateau region is reached corresponding to maximum surface coverage. Due to electrostatic repulsion, further increases in the surfactant concentration do not lead to an increase in adsorption.

1.8 CHARACTERISATION TECHNIQUES

1.8.1 PHOTOELECTRON SPECTROSCOPY

1.8.1.1 Introduction

X-ray Photoelectron Spectroscopy (XPS) has become well established as an invaluable tool for the investigation and characterisation of surfaces. During the period 1955 to 1970 it was realised that the chemical environment of atoms effected the binding energy of core level electrons.[103] The technique provides information about the chemical nature of surfaces and the acronym ESCA (Electron Spectroscopy for Chemical Analysis) was coined.[104] XPS involves irradiation of a sample with low energy X-rays. These X-rays eject electrons from electronic levels in atoms and molecules.[105,106] The process is known as photoionisation and the electrons produced are termed photoelectrons,[107] Figure 1.21(a).

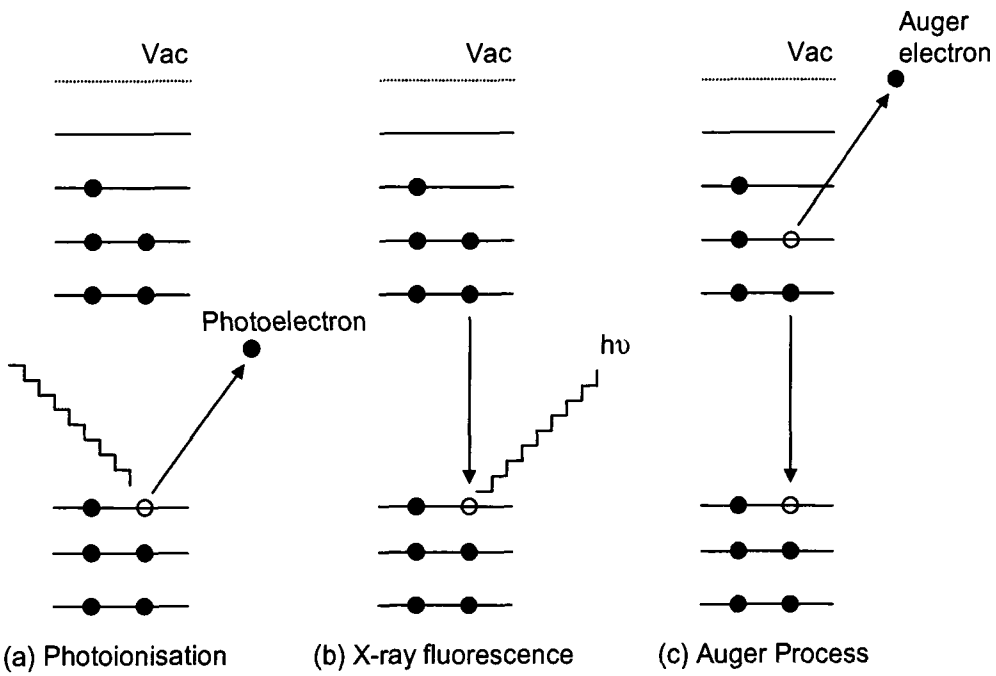

Figure 1.21: Schematic of the photoionisation process.[107]

The removal of a core electron in the photoionisation process leaves a "vacancy." The filling of this vacancy by an electron from a higher energy shell can result in two different processes, X-ray fluorescence and the emission of an Auger electron, Figure 1.21(b) and (c) respectively. X-ray fluorescence results in the emission of an X-ray photon whilst the Auger process leads to the emission of an Auger electron. An energy barrier must be overcome for a photoelectron to be ionised and escape from an atom. This energy barrier is known as the binding energy (BE) of an electron. The BE is characteristic of the element and electronic level from which the electron was ejected. It is the determination of this energy which is the goal of an XPS spectrometer. If the energy of incident photons ($h\upsilon$) used in XPS is greater than the BE of an electron it will be ejected with kinetic energy (KE). It is this kinetic energy which is measured directly in XPS. The binding energy is related to the kinetic energy as shown below, Equation 1.12:[105]

$$BE = h\upsilon - KE \qquad \textbf{Eq. 1.12}$$

$h\upsilon$ is known, but before BE can calculated a further term must be considered, the work function ($e\varnothing$). This is a combination of terms, including the work function of the sample $\varnothing_s$ (the energy required to remove an electron from the highest occupied electronic level inside a solid E_f to the vacuum E_v). It also includes $\varnothing_{sp}$, the work function of the spectrometer. $e\varnothing$ is taken as a constant and the kinetic energy of the photoionsied electron becomes a function of a number of terms, Equation 1.13:[105]

$$KE = h\upsilon - BE - e\varnothing \qquad \textbf{Eq. 1.13}$$

Electrons are emitted with kinetic energies ranging from 0 eV to approximately 1000 eV.[105]

1.8.1.2 Surface Sensitivity

XPS is extremely surface sensitive. It is therefore ideally suited to the study of surface modification and thin film production. The technique is confined to the surface region because only electrons ionised from the surface region can escape to be detected.[108]

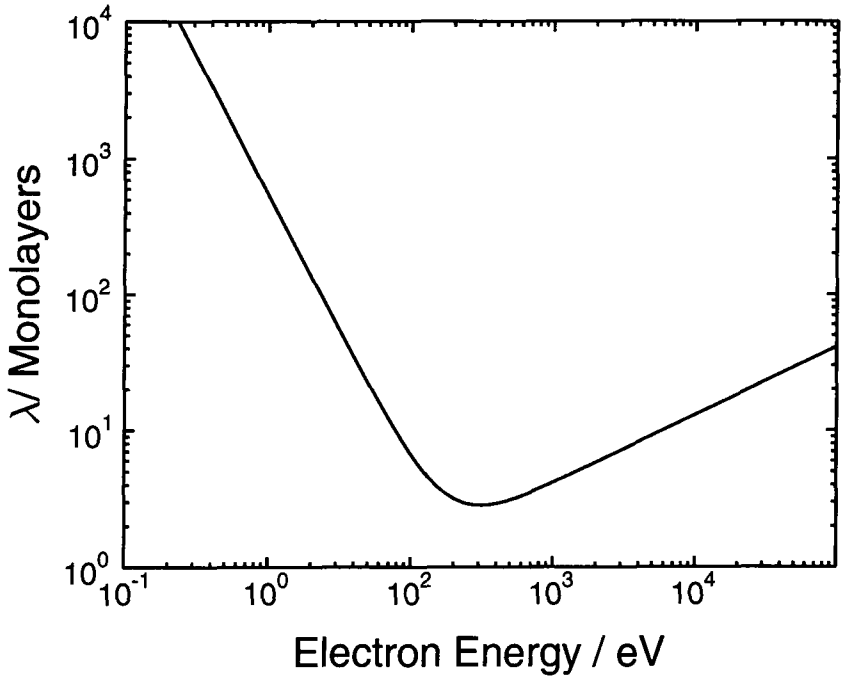

Figure 1.22: The dependence of Attenuation Length on Electron Energy.[105]

The escape depth of an electron is dependent on energy losses from the electron due to excitation of phonons (lattice vibrations) and electron-electron excitations. Therefore the mean free path of an electron in a solid before it undergoes inelastic scattering will depend on its kinetic energy,[109] Figure 1.22. At low kinetic energies there is insufficient energy for the excitation of the loss processes outlined above, so the mean free path is long. At high kinetic energy the mean free path is long, as the probability of excitation is low. The energy range of electrons important to XPS is approximately 100-1000 eV. In this region the mean free paths of electrons in solids are small and electrons escape only from the first few atomic layers.

1.8.1.3 Instrumentation

The heart of an XPS machine consists of three main components:

1) X-ray Source;
2) The electron energy analyser;
3) The electron detector.

The above components and the sample chamber must be maintained in the ultra-high vacuum (UHV) pressure range, ideally below 1 x 10^{-9} mbar.[110] This level of vacuum is required to prevent the scattering of photoelectrons by gas particles prior to detection and contamination of the sample surface. The latter is actually the most stringent, for example at a pressure of 10^{-6} mbar the surface of a sample would be covered with a monolayer of background gas in one second.[110] UHV is achieved and maintained by continually pumping an enclosed stainless steel chamber. Suitable pumps include diffusion and turbomolecular pumps which operate by imparting kinetic energy to gas molecules in the desired direction. The former require liquid nitrogen cold traps to prevent oil contamination and help provide efficient removal of water molecules and other contaminants.

1.8.1.4 X-ray Source

Common X-ray sources operate by bombarding a target material with high energy electrons. Electrons stream from an incandescent filament at ground potential and are accelerated towards the target which is set at a positive potential of several thousand volts. These electrons ionise core electrons from atoms within the target. Relaxation of electrons at high electronic levels within the atom into these "holes" results in the emission of energy as X-rays.[105] The choice of target material is of vital importance. The X-rays produced must be energetic enough to photoionise a sufficient range of core electrons to enable comprehensive elemental characterisation. Furthermore, the spread of photon energy must be narrow enough so as not to limit the resolution of the spectrometer.[105] Electron bombardment will heat the target substantially and it

must therefore be constructed of materials possessing good thermal conductivities. Aluminium and magnesium fulfil all these criteria and are used extensively as anode materials. The most intense X-ray line from a Mg source is the $K\alpha_{1,2}$ line at an energy of 1253.6 eV with a width of 0.7 eV.[111] Emission occurs as a result of electron decay from the $2p_{1/2}$ orbital to the 1s level.[112] A second emission line, due to a doubly ionised transition ($\alpha_{3,4}$), occurs 8 eV higher at approximately 8% of the intensity. Al produces photons with an energy of 1486.6 eV with a line width of 0.85 eV. The photon energy spectrum produced from an unmonochromated source is fairly complex, Figure 1.23:

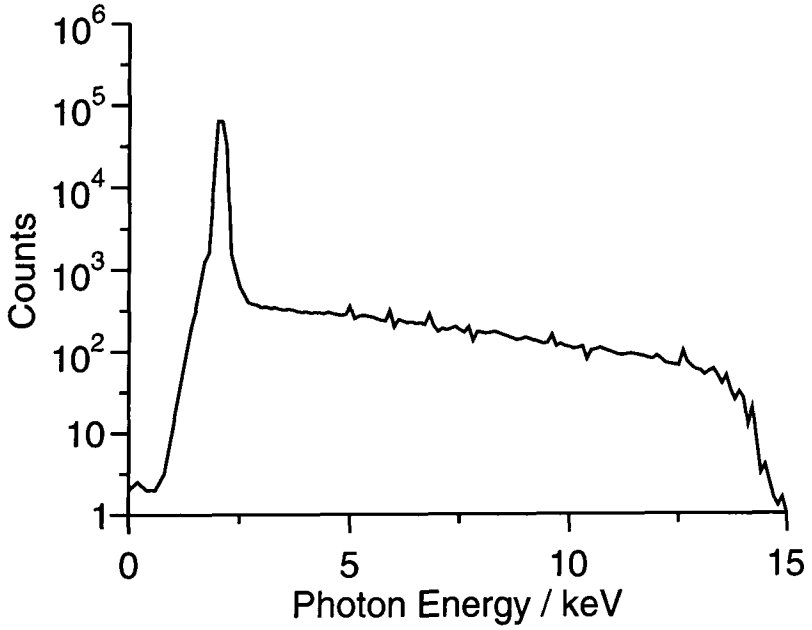

Figure 1.23: X-ray Emission Spectrum in a Logarithmic Intensity Plot from an Aluminium Target Bombarded with Electrons at 15 kV.[105]

There is a continuous background called Bremsstrahlung extending up to the incident electron energy on which the characteristic lines are situated.[105]

1.8.1.5 Electron Energy Analyser

The most commonly used electron energy analyser in XPS is the concentric hemispherical analyser (CHA). This is an electrostatic energy analyser as opposed to designs based on magnetic fields, Figure 1.24:

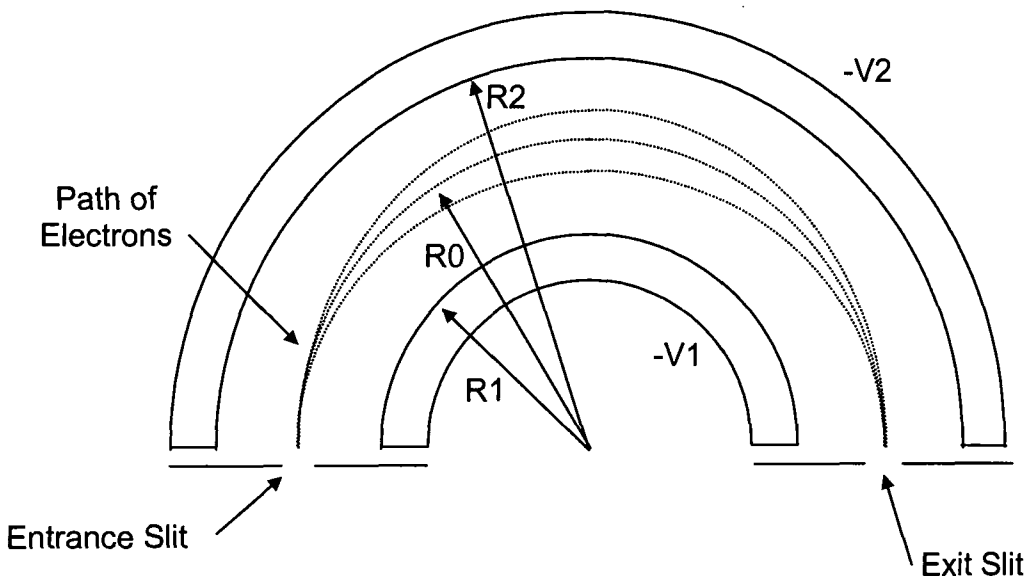

Figure 1.24: Schematic cross-section of a CHA.[105]

The analyser consists of two concentric hemispherical surfaces between which a potential difference is applied.[105] The negative potential V2 is greater than V1, and electrons with the correct energy are forced into a hemispherical path equidistant between the spheres. These electrons are focused at the exit slit. The resolving power is given by the following, Equation 1.14:[105]

$$\frac{\Delta E}{E} \qquad \textbf{Eq. 1.14}$$

where ΔE is the half width and E is the kinetic energy of the electron. Electrostatic lenses are positioned before the sample at the entrance slit. These retard the electrons before they enter the analyser. Two modes of retardation are usually employed, namely CAE, alternatively known as FAT (standing for

Constant Analyser Energy and Fixed Analyser Transmission respectively), and the CRR or FRR mode (Constant Retard Ratio and Fixed Retard Ratio respectively). Both these retardation regimes improve the ultimate resolution by reducing the value of E.

1.8.1.6 Electron Detection

The current of electrons entering the detector from the analyser is very small,[105] approximately 10^{-16} to 10^{-14} A. We therefore need to amplify this current in order to measure it. Many spectrometers use a device known as a channeltron. This consists of a small spiral glass tube coated on the inside with a high resistance material. A high potential of approximately 3 kV is applied to the ends of the tube turning the surface into a continuos dynode. Electrons entering the device collide with the walls which emit a number of secondary electrons. Further collisions produce an avalanche effect giving the channeltron a very high gain. Amplification of between 10^7 and 10^8 is routinely achievable.[105]

1.8.1.7 Spectral Interpretation

Spectra recorded from XPS instruments usually plot counts (or counts per second) against the kinetic or binding energy of electrons. A series of peaks are formed on a background. The background generally increases in intensity towards low kinetic energy. Distinct steps in the background occur to the low kinetic energy side of large peaks. These peaks result from electrons which initially have the same energy as the main peak, but have been inelastically scattered before reaching the analyser. The Bremsstrahlung background from unmonochromated X-ray sources provides the general background detected.[105]

As discussed above, other transitions in the target atoms give rise to spectral features known as satellites. If a Mg anode is used spectral peaks have a small satellite shifted 8.4 eV to higher KE (lower BE) of the principle line. Further additions to the spectra arise due to Auger transitions in ionised atoms.

Electrons from higher energy levels fall down to occupy gaps left by the photoionisation of core electrons in the sample. The excess energy is lost from the atom by ejection of a second electron, the Auger electron, Figure 1.21c. The kinetic energy of this electron is a function of the energy gap between the electronic levels involved.[105] Hence the energies of Auger electrons are characteristic of the elements from which they are emitted and can be used for the determination of elemental composition of the sample.

Of great importance to surface scientists was the discovery that non-equivalent atoms of the same element give rise to core level peaks with resolvable binding energy differences, termed the chemical shift.[105] Elements in different oxidation states and chemical environments can be unambiguously identified. This chemical shift arises from the fact that the electron density around an atom is affected by the nature of the local environment.

1.8.1.8 Sample Charging

A specific problem associated with XPS analysis of polymer surfaces is sample charging. The vast majority of polymer films are electrical insulators. Ionisation during analysis charges the sample surface and this charge cannot be dissipated. The KE of electrons leaving the positively charged surface is reduced as energy is lost to the field and surface charging causes peaks to be shifted to lower KE, i.e. higher BE. Methods for eliminating this problem include flooding the sample with low energy electrons.[105] In practice the charging effect can be accounted for at the data interpretation stage if all BE are compared to a reference peak.

1.8.1.9 Peak Fitting

Often the spectral resolution is inadequate to completely separate atoms in different chemical environments. The observed photoelectron spectrum is a convoluted envelope produced by contributions from several overlapping peaks

from atoms in different chemical environments. After the spectrum is offset to account for sample charging, peaks of the same width are added to the spectrum and a computer attempts to fit the manually added peaks to the acquired data by minimising the square of the difference between them. The factors which affect the peak width are:

- linewidth of the X-ray source (section 1.8.1.4);
- the resolution of the spectrometer (section 1.8.1.5);
- the natural width of the core level under analysis.

The contributions from the above factors result in a peak shape with both Gaussian and Lorentzian contributions. However, it has been demonstrated that the Lorentzian contribution can be ignored without the introduction of significant error.[50]

1.8.2 INFRARED (IR) SPECTROSCOPY

A molecule may absorb a quantum of electromagnetic radiation which leads to an increase in the internal energy of the molecule, Equation 1.15:[113]

$$\Delta E = E_n - E_m = h\nu = \frac{hc}{\lambda} \qquad \textbf{Eq. 1.15}$$

where ΔE is the energy separation between two energy states E_n and E_m in the molecule, h is the Planck constant, ν is the frequency, c is speed of light and λ is the wavelength of the radiation. Electronic, vibrational or rotational energy levels of the molecule may be excited depending on the wavelength of the absorbed radiation. If electromagnetic radiation in the IR region of the spectrum is used then the absorption of that radiation increases the vibrational energy level of molecules. Different molecules absorb IR radiation of different wavelengths due to the excitation of different molecular vibrations. The wavelength of absorption is characteristic of different functional groups present in the molecule.

IR is a very useful technique for the characterisation of polymers. Several attributes of IR spectroscopy make it widely applicable:[114]

- It can differentiate between many different chemical functionalities;
- The so called figure print region may enable confident identification of individual polymer systems;
- If correctly calibrated the technique may be used quantitatively;
- Collection of data is rapid and the components of an IR spectrometer are relatively inexpensive.

However, IR spectroscopy suffers from some important limitations, namely:[114] the signal-to-noise ratio is low; the frequency resolution is poor; and polymer samples have to be light transmitting. These problems have been overcome by the use of Fourier Transform Infrared (FTIR) spectroscopy.

1.8.2.1 FTIR Spectroscopy

At the heart of a FTIR spectrometer is an interferometer, the type most often used is based on the Michelson interferometer,[113] Figure 1.25. The Interferometer splits the source radiation into two equal beams. One beam is reflected by a movable mirror back to the detector while the other beam is reflected by a fixed mirror to the detector. The beams are combined at the detector to produce an interference pattern. This is dependent on the difference between the distance each beam has travelled (δ) which in turn is dependent on the position of the movable mirror. The source produces many wavelengths and the intensity at the detector is therefore a function of many different interference patterns. The interference pattern produced is called an interferogram. A plot of the wavenumber of the radiation against intensity is obtained by the procedure of Fourier transformation of the interferogram in a microcomputer.[113] If a molecule which absorbs at a particular wavenumber is placed in the path of one of the beams then the interference pattern corresponding to this wavenumber is not cancelled out and remains in the interferogram.[113]

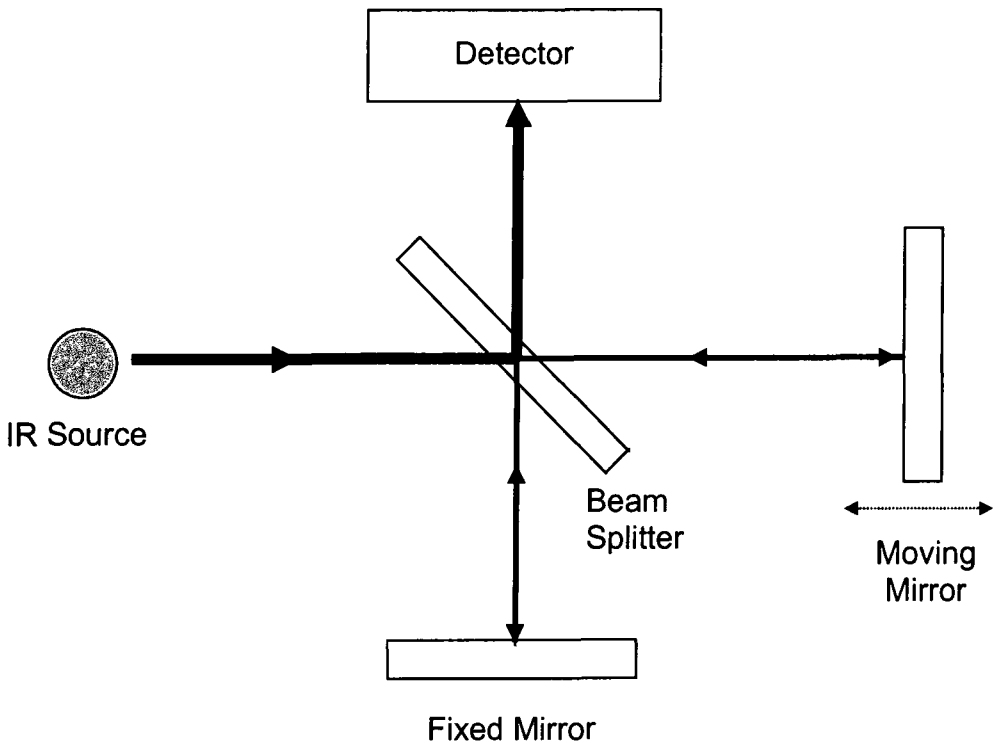

Figure 1.25: Schematic of the Michelson Interferometer.[114]

There are several advantages to FTIR spectroscopy:[114]

- All frequencies are detected simultaneously. This increases the signal-to-noise ratio and decreases the time required to obtain a spectrum compared to standard IR spectrometers.
- No entrance or exit slits are used which might limit the radiation throughput.
- The frequency readings are highly precise as a laser is used to control the position of the movable mirror.

Furthermore, these advantages allow the use of a variety of different sampling techniques. One such technique is attenuated total internal reflectance spectroscopy (ATR).

1.8.2.2 ATR-FTIR Spectroscopy

ATR-FTIR spectroscopy enables the IR analysis of samples which display low radiation transmission without the need for lengthy and potentially destructive sample preparation techniques. The technique involves measuring the radiation specularly reflected from the interface between a sample and a high reflective index optical element (e.g. a diamond),[115] Figure 1.26.

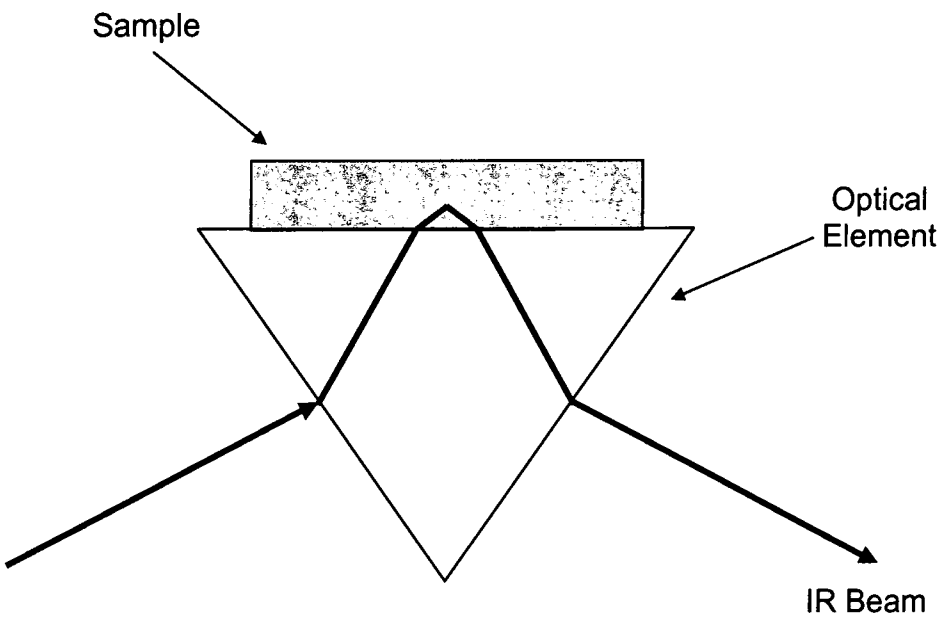

Figure 1.26: ATR Unit.[115]

This technique is especially suited to the analysis of polymer surfaces because the sampling depth is restricted to the first few microns of the sample surface. The actual penetration is governed by several factors such as the angle of incidence between the radiation and the surface, the wavelength of the radiation and the refractive index of the sample.[115] This leads to the following observations:[115]

- The depth of penetration increases with wavelength and bands become more intense as the wavelength increases;

- The depth of penetration decreases as the angle of incidence and the refractive index of the optical element increase.
- The depth of penetration also decreases as the refractive index of the sample falls.

These factors all affect the intensity of the spectra obtained.

1.8.3 DEPOSITION RATE MEASUREMENT

The deposition rate of thin films can be measured using an oscillating quartz crystal. The technique generally involves using the oscillating frequency decrease on mass deposition to determine the weight of a coating on a quartz crystal.[116-119] The AT-cut crystal oscillating in a thickness shear mode was found to produce the most accurate results, Figure 1.27.

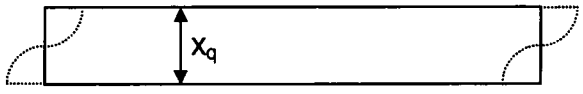

Figure 1.27: Schematic of a quartz crystal oscillating in the thickness shear mode.[116]

The thickness (x_q) of an infinite quartz plate is directly related to the wavelength λ of the continuous elastic transverse wave, the phase velocity (v_q) of that wave and the frequency (ν_q) of the oscillating crystal,[116] Equation 1.16:

$$x_q = \frac{1}{2}\lambda = \frac{1}{2}\left(\frac{v_q}{\nu_q}\right) = \frac{1}{2} v_q \tau_q \qquad \textbf{Eq. 1.16}$$

where τ_q is the period. If we now consider the area mass density (m_q) of the quartz crystal and the density (ρ_q) the thickness is related by the following,[116] Equation 1.17:

$$m_q = \rho_q x_q \qquad \textbf{Eq. 1.17}$$

A change in the area mass density will therefore change the frequency, Equation 1.18:

$$\frac{\Delta \upsilon_q}{\upsilon_q} \approx - \frac{\Delta m_q}{m_q} \qquad \textbf{Eq. 1.18}$$

If the area mass density change of the quartz crystal is substituted by the deposition of foreign material (m_f), assuming that (for small mass changes) the foreign mass is equivalent to a corresponding change in the mass of the crystal, then we now have the following,[117,118] Equation 1.19:

$$\frac{\Delta v_q}{\upsilon} \approx - \frac{m_f}{m_q} \qquad \textbf{Eq. 1.19}$$

which can be used to calculate the mass of the foreign deposit if the following limitations are noted:[116]

- The relation is an approximation;
- The elastic properties of the deposited material will be different from the quartz crystal;
- Experimentally the crystal is of finite size.

Experimental data suggests that this technique is reasonably accurate when the mass of the deposit is less than 2% of the mass of the quartz crystal.[120] In many modern instruments the change in the period of oscillation is measured as this is linearly related to the change in mass,[121] Equation 1.20:

$$\Delta \tau = \frac{2}{v_q \rho_q} m_f = \frac{2 \rho_f}{v_q \rho_q} \qquad \textbf{Eq. 1.20}$$

The density of the foreign material can therefore be found from the change in the period of oscillation. If the density of the foreign material is known the changing thickness of the deposit can be monitored by digital equipment.

1.8.4 VIDEO CONTACT ANGLE (VCA) ANALYSIS

The VCA apparatus employs the sessile drop technique for the determination of the contact angles of liquid drops placed on solid surfaces. A droplet of known volume is dispensed by a motorised syringe and placed on the surface of the sample, Figure 1.28. A closed circuit television (CCT) camera captures an image of the droplet on the sample surface and displays it in real time on a monitor. A snap shot of the image is then taken and a personal computer (PC) calculates the angle the droplet makes with the sample surface.

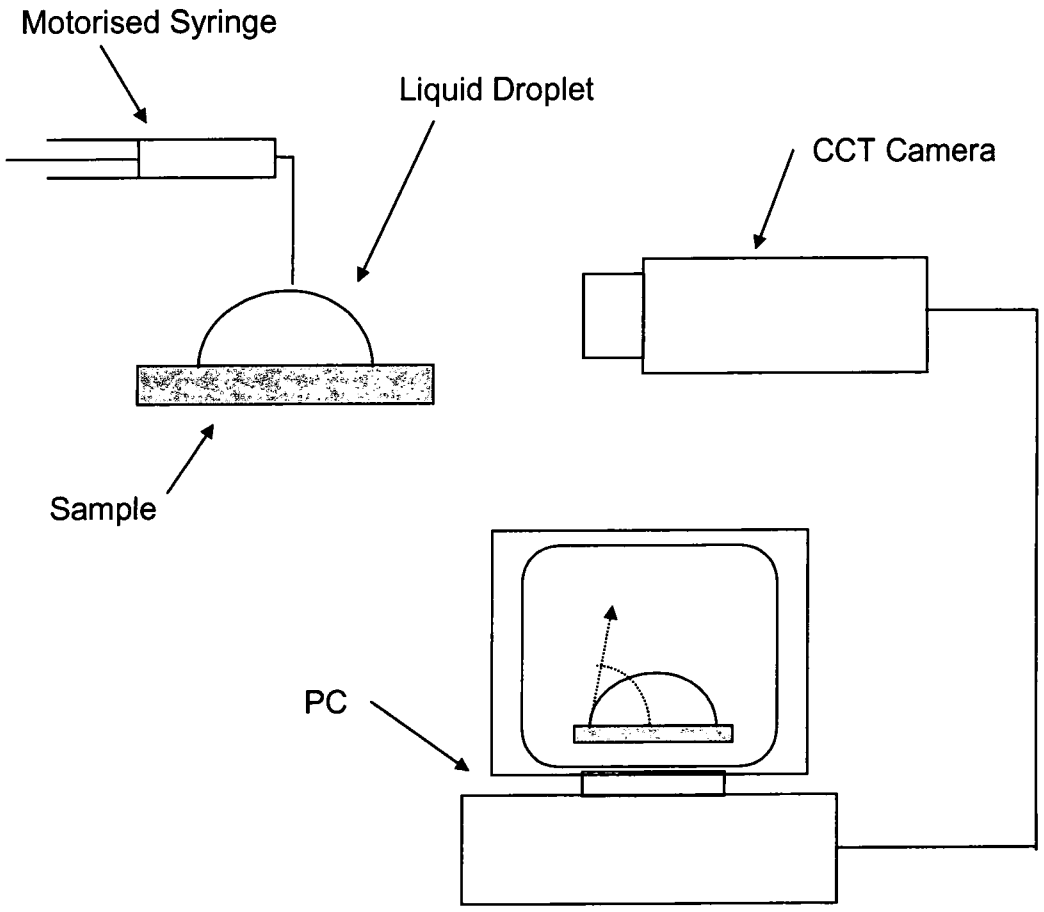

Figure 1.28: Schematic of the VCA apparatus.

Care must be taken when analysing the results of such experiments. The angle recorded by this technique is known as a static angle.[50] The droplet may not be in equilibrium (section 1.7.3) and no information on contact angle hysteresis can be obtained.

1.8.5 DYNAMIC CONTACT ANGLE (DCA) ANALYSIS

The dynamic contact angle apparatus (often known as the Wilhelmy plate method)[122] measures the advancing, receding and dynamic contact angles of flat surfaces and filaments.[48] The sample often takes the form of a thin plate. It is held vertically and partially immersed in a test liquid, Figure 1.29:

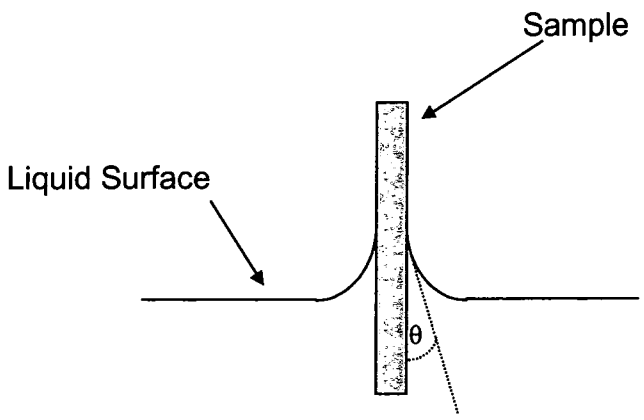

Figure 1.29: Profile of a vertical plate partially immersed in liquid.[48]

The force acting on the plate (F) is,[48] Equation 1.21:

$$F = p\gamma\cos\theta - \rho gAd \qquad \textbf{Eq. 1.21}$$

Where p is the plate perimeter, γ is the liquid surface energy, θ is the contact angle, ρ is the liquid density, g is the gravitational acceleration, A is the cross-section area of the plate and d is the immersion depth. A plot of F verses d

should give a straight line from which θ can be found.[48] The experimental apparatus consists of a microbalance from which the plate is suspended and a motorised stage is used to move a beaker containing the test liquid over the plate, Figure 1.30:

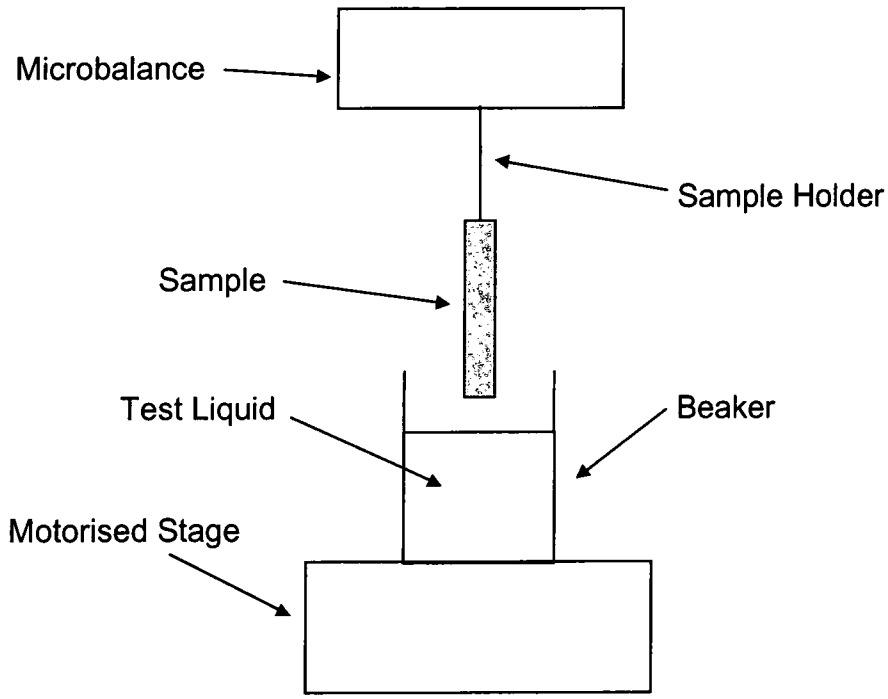

Figure 1.30: Schematic of the Wilhelmy plate apparatus.[50]

Advancing contact angles are obtained by immersing the plate in the liquid and receding angles are measured when the plate is withdrawn.[48] The advantages of this type of measurement technique are as follows:

- Advancing and receding angles are measured so any contact angle hysteresis will be found;
- The whole surface of the plate is used for the calculation of the contact angle.

1.9 REFERENCES

1. Hollahan, J. R.; Bell, A. T., Eds. *Techniques and Applications of Plasma Chemistry*; Wiley: New York, 1974.
2. Hudis, M. In *Techniques and Applications of Plasma Chemistry*; Hollahan, J. R.; Bell, A. T., Eds.; J. Wiley & Sons: London, 1974; pp. 113-147.
3. Gerenser, L. *J. Adhesion Sci. Technol.* **1987**, *4*, 303.
4. Dynes, P. J.; Kaelbe, D. H. *J. Macromol. Sci. Chem.* **1976**, *A10*, 535.
5. Rossmann, K. *J. Polymer Sci.* **1956**, *19*, 141.
6. Hansen, R. H.; Schonhorn, H. *J. Polym. Sci.: Part B: Polym. Phys.* **1966**, *4*, 203.
7. Coburn, J. W. *IEEE Trans. on Plasma Science* **1991**, *19*, 1048.
8. Garbassi, F.; Morra, M. *Surface and Interface Analysis* **1989**, *17*, 585.
9. Egitto, F. D.; Matienzo, L. J.; Blackwell, K. J.; Knoll, A. R. *J. Adhesion Sci. Technol.* **1994**, *8*, 411.
10. Khairallah, Y.; Arefi, F.; Amouroux, J.; Leonard, D.; Bertrard, P. *J. Adhesion Sci. Technol.* **1994**, *8*, 363.
11. Hansen, R. H.; Pascale, J. V.; Benedictis, T. D.; Rentzepis, P. M. *J. Polym. Sci.: Part A: Polymer Chemistry* **1965**, *3*, 2205.
12. Tobin, J. A.; Denton, D. D. *Appl. Phys. Lett.* **1992**, *60*(21, 25 May), 2595.
13. Berger, J. M.; Ferraton, J. P.; Yous, B.; Donnadieu, A. *Thin Solid Films* **1981**, *86*, 337.
14. Wells, R. K.; Badyal, J. P. S.; Drummond, I. V. V.; Robinson, K. S.; Street, F. J. *J. Chem. Soc., Chem. Commun.* **1991**, *6*, 549.
15. Flamm, D. L. In *Plasma Etching: An Introduction*; Manos, D. M.; Flamm, D. L., Eds.; Academic Press, Inc.: London, 1989; pp. 91-184.
16. Yasuda, H. *Plasma Polymerization*; Academic Press, Inc.: London, 1985.
17. Langmuir, I. *Phys. Rev.* **1929**, *33*(June), 954.
18. Chen, F. F. *Introduction to Plasma Physics*; Plenum: New York, 1974.
19. Riley, P. E. *J. Electrochem. Soc.* **1993**, *140*(5, May), 1518.
20. Penning, F. M. *Electrical Discharges in Gases*; Cleaver-Hume: London, 1957.
21. Brovetto, P.; Maxia, V. *Nuovo Ciments Della Societa Italiana di Fisica D - Condensed Matter Atomi Molecular and Chemical Physics Fluid Plasma Biophysis* **1995**, *17*, 169.
22. Chapman, B. *Glow Discharge Processes*; John Wiley & Sons: Chichester, 1980.
23. Atkins, P. W. *Physical Chemistry*; Oxford University Press: Oxford, 1990.
24. Elliasson, B.; Kogelschates, U. *IEEE Trans. on Plasma Science* **1991**, *19*, 6.
25. Bell, A. *Topics in Current Chemistry, Plasma Chemistry*, III ed.; John Wiley & Sons: Chichester, 1980.
26. Yasuda, H. *J. Polym. Sci., Macro. Rev.* **1981**, *16*, 199.
27. Grill, A. *Cold Plasmas in Materials Technology*; IEEE Press: New Jersey, 1994.
28. McMurry, J. *Organic Chemistry*, 3rd ed.; Brooks/Cole: California, 1992.
29. Poll, H. U.; Artz, M.; Wickleder, K. H. *Eur. Polym. J.* **1970**, *12*, 505.

30. Smith, E. B. *Basic Chemical Thermodynamics*, 4th ed.; Clarendon Press: Oxford, 1992.
31. Kobayashi, H.; Shen, M.; Bell, A. T. *J. Macromol. Sci. Chem.* **1974**, *A8*(8), 1345.
32. Beck, A. J.; O'Toole, L.; Short, R. D.; Ameen, A. P.; Jones, F. R. *J. Chem. Soc., Chem. Commun.* **1995**, *10*, 1053.
33. Yasuda, H.; Wang, C. R. *J. Polym. Sci.: Polym. Chem. Ed.* **1985**, *23*, 87.
34. Morosoff, N.; Yasuda, H.; Brandt, E. S.; Reilley, C. N. *J. Appl. Polym. Sci.* **1979**, *23*, 3449.
35. Yasuda, H.; Hirotsu, T. *J. Polym. Sci.: Polym. Chem. Ed.* **1978**, *16*, 743.
36. Yeh, Y. S.; Shyy, I. N.; Yasuda, H. *J. Appl. Polym. Sci.: Appl. Polym. Sym* **1988**, *42*, 1.
37. Bell, A. T.; Nakajima, K.; Shen, M. *J. Appl. Polym. Sci.* **1979**, *23*, 2627.
38. Panchalingam, V.; Chen, X.; Savage, C. R.; Timmons, R. B.; Eberhart, C. *J. Appl. Polym. Sci.: Appl. Polym. Sym* **1994**, *54*, 123.
39. Panchalingham, V.; Chen, X.; Savage, C. R.; Timmons, R. B.; Huo, H.-H.; Eberhart, R. C. *ASAIO Journal* **1993**, M305.
40. Anandan, C.; Mukherjee, C.; Seth, T.; Dixit, P. N.; Bhattacharyya, R. *Appl. Phys. Lett.* **1995**, *66*(1, January), 85.
41. Ryan, M. E.; Hynes, A. M.; Badyal, J. P. S. *Chem. Mater.* **1996**, *8*, 37.
42. Timmons, R. B.; Savage, C. R. *Chem. Mater.* **1991**, *3*(4), 575.
43. Badyal, J. P. S.; Hynes, A. M. *Chem. Mater.* **1998**, *10*, 2177.
44. Hynes, A. M.; Shenton, M. J.; Badyal, J. P. S. *Macromolecules* **1996**, *29*, 4220.
45. Hashimoto, K.; Hikosaka, Y.; Hasegawa, A.; Nakamura, M. *Jpn. J. Appl. Phys., Part 1* **1996**, *35*(6A), 3363.
46. Rinsch, C. L.; Chen, X.; Panchalingam, V.; Eberhart, C.; Wang, J.-H.; Timmons, R. B. *Langmuir* **1996**, *12*, 2995.
47. Uchida, T.; Senda, K.; Vinogradov, G. K.; Morita, S. *Thin Solid Films* **1996**, *281-282*, 536.
48. Wu, S. *Polymer Interface and Adhesion*; Marcel Dekker: New York, 1982.
49. Cherry, B. W. *Polymer Surfaces*; Cambridge University Press: Cambridge, 1981.
50. Garbassi, F.; Morra, M.; Occhiello, E. *Polymer Surfaces: From Physics to Technology*; Wiley: Chichester, 1994.
51. Adamson, A. W. *Physical Chemistry of Surfaces*, 5th ed.; Wiley: Chichester, 1991.
52. Morra, M.; Occhiello, E.; Garbassi, F. *Adv. Colloid Interface Sci.* **1990**, *32*, 76.
53. Good, R. J. In *Advances in Chemistry Series No. 43*; American Chemical Society: Washington DC, 1964; p. 74.
54. Fowkes, F. M. *J. Adhesion Sci. Technol.* **1987**, *1*, 7.
55. Oss, v; Good, R. J.; Chaudhury, M. K. *Langmuir* **1988**, *4*, 884.
56. Fowkes, F. M.; Kaczinski, M. B.; Dwight, D. W. *Langmuir* **1991**, *7*(11), 2464.
57. Hiemenz, P. C. *Principles of Colloid and Surface Chemistry*; Marcel Dekker: New York, 1977.
58. Rosen, M. J. *Surfactants and Interfacial Phenomena*, 2nd ed.; John Wiley & Sons: New York, 1989.

59. Young, T. *Phil. Trans.* **1805**, *95*, 65.
60. Young, T. *Phil. Trans.* **1805**, *95*, 82.
61. Chaudhury, M. K.; Whitesides, G. M. *Science* **1992**, *255*(6 March), 1230.
62. Good, R. J. In *Contact Angle, Wettability and Adhesion*; Mittal, K. L., Ed.; VSP: Utrecht, 1993; pp. 3-36.
63. Rayleigh, L. *Phil. Mag.* **1890**, *30*, 397.
64. Sulman, H. L. *Trans. Inst. Mining and Metallurgy* **1920**, *29*, 44.
65. Wenzel, R. N. *Ind. Eng. Chem.* **1936**, *28*, 988.
66. Johnson, R. E.; Dettre, R. H. In *Adv. Chem. Ser. 43*; Fowkes, F. M., Ed.; American Chemical Society: Washington DC, 1964; pp. 112-135.
67. Neumann, A. W.; Good, R. J. *J. Colloid Interface Sci.* **1972**, *38*, 341.
68. Eick, J. D.; Good, R. J.; Neumann, A. W. *J. Colloid Interface Sci.* **1975**, *53*, 235.
69. Drelich, J.; Wilbur, J. L.; Miller, J. D.; Whitesides, G. M. *Langmuir* **1996**, *12*(7), 1913.
70. Cassie, A. B. D. *Discuss. Faraday Soc.* **1948**, *3*, 11.
71. Johnson, R. E., Jr.; Dettre, R. H. *J. Phys. Chem.* **1964**, *68*(7, July), 1744.
72. Andrade, J. D.; Smith, L. M.; Gregmis, D. E. In *Surface and Interfacial Aspects of Biomedical Polymers*; Andrade, J. D., Ed.; Plenum: New York, 1985; Vol. 1, p. 281.
73. Chen, Y.-L.; Helm, C. A.; Israelachvili, J. N. *J. Phys. Chem.* **1991**, *95*(26), 10736.
74. Holly, F. J.; Refojo, M. F. *J. Biomed. Mater. Res.* **1975**, *9*, 1975.
75. Holly, F. J.; Refojo, M. F. In *Adv. Chem. Ser. 31*; Andrade, J. D., Ed.; American Chemical Society: Washington D.C., 1976; pp. 252-266.
76. Gouy, G. J. *J. Phys. Chem.* **1910**, *9*, 457.
77. Gouy, G. J. *Ann. Phys.* **1917**, *7*, 129.
78. Chapman, D. L. *Phil. Mag.* **1913**, *25*, 475.
79. Stern, O. *Z. Electrochem.* **1924**, *30*, 508.
80. Adamson, A. W. *Physical Chemisty of Surfaces*, 3rd ed.; Interscience: New York, 1976.
81. Myers, D. *Surfactant Science and Technology*; VCH: New York, 1988.
82. Lens, J. P.; Terlingen, J. A. C.; Engbers, G. H. M.; Feijen, J. *Langmuir* **1998**, *14*, 3214.
83. Somasundaran, P.; Krishnakumar, S. *Colloids Surfaces A: Physicochem. Eng. Aspects* **1994**, *93*, 79.
84. Biswas, S. C.; Chattoraj, D. K. *J. Colloid Interface Sci.* **1998**, *205*, 12.
85. Esumi, K.; Iitaka, M.; Koide, Y. *J. Colloid Interface Sci.* **1998**, *208*, 178.
86. Yamada, S.; Israelachvili, J. *J. Phys. Chem. B.* **1998**, *102*(1), 234.
87. Waltermo, Å.; Sjöberg, M.; Anhede, B.; Claesson, P. M. *J. Colloid Interface Sci.* **1993**, *156*, 365.
88. Claesson, P. M.; Herder, P. C.; Berg, J. M.; Christenson, H. K. *J. Colloid Interface Sci.* **1990**, *136*(2), 541.
89. Christenson, H. K.; Claesson, P. M.; Berg, J.; Herder, P. C. *J. Phys. Chem.* **1989**, *93*(4), 1472.
90. Otsuka, H.; Esumi, K. *Langmuir* **1994**, *10*(1), 45.
91. Kölbel, H.; Hörig, K. *Angew. Chem.* **1959**, *71*, 691.
92. Kölbel, H.; Kuhn, P. *Angew. Chem.* **1959**, *71*, 211.
93. Wakamatsu, T.; Fuerstenau, D. W. In *Adsorption from Aqueous Solution;*

Advances in Chemistry 79; Weber, J. W. J.; Matijevic, E., Eds.; American Chemical Society: Washington DC, 1968; pp. 161-172.
94. Rupprecht, H.; Liebl, H. *Kolloid Z. Z. Polym.* **1972**, *250*, 719.
95. Law, J. P. J.; Kunze, G. W. *Soil Sci. Soc. Am. Proc.* **1966**, *30*, 321.
96. Snyder, L. R. *J. Phys. Chem.* **1968**, *72*(2, February), 489.
97. Dick, S. G.; Fuerstenau, D. W.; Healy, T. W. *J. Colloid Interface Sci.* **1971**, *37*, 595.
98. Giles, C. H.; D'Silva, A. P.; Easton, I. A. *J. Colloid Interface Sci.* **1974**, *47*, 766.
99. Somasundaran, P.; Fuerstenau, D. W. *J. Phys. Chem.* **1966**, *70*(1, January), 90.
100. Kjellin, U. R. M.; Claesson, P. M.; Audebert, R. *J. Colloid Interface Sci.* **1997**, *190*, 476.
101. Lai, C.-L.; Harwell, J. H.; O'Rear, E. A.; Komatsuzaki, S.; Arai, J.; Nakakawaji, T.; Ito, Y. *Colloids Surfaces A: Physicochem. Eng. Aspects* **1995**, *104*, 231.
102. Scamehorn, J. F.; Schechter, R. S.; Wade, W. H. *J. Colloid Interface Sci.* **1983**, *85*, 463.
103. Siegbahn, K.; Nordling, L. N.; Fahlman, A.; Nordberg, R.; Hamrin, K.; Hedman, J.; Johansson, G.; Bermark, T.; Karlsson, S. E.; Lindgren, I.; Lindberg, B. *ESCA: Atomic Molecular and Solid State Structure Studied by Means of Electron Spectroscopy*; Almqvist and Wiksells: Uppsala, 1967.
104. Wertheim, G. K. *J. Franklin Institute* **1974**, *298*, 289.
105. Briggs, D.; Seah, M. P., Eds. *Practical Surface Analysis*, 2nd ed.; J. Wiley & Sons: Chichester, 1990; Vol. 1.
106. Woodruff, D. P.; Delchar, T. A. *Modern Techniques of Surface Science*; Cambridge University Press: Cambridge, 1990.
107. Hollas, J. *Modern Spectroscopy*; J. Wiley & Sons: Chichester, 1988.
108. Smith, G. C. *Surface Analysis by Electron Spectroscopy*; Plenum Press: London, 1994.
109. Prutton, M. *Surface Physics*; Claredon: Cambridge, 1984.
110. O'Hanlon. *A User's Guide to Vacuum Technology*, 2nd ed.; J. Wiley & Sons: Chichester, 1989.
111. Sabbatini, L.; Zambini, P. G. *Surface Characterisation of Advanced Polymer*; VCH: Cambridge, 1993.
112. Woodruff, D. P.; Delchar, T. A., Eds. *Modern Techniques of Surface Science*; Cambridge University Press: Cambridge, 1986.
113. Hollas, J. M. *Modern Spectroscopy*, 2nd ed.; J. Wiley & Sons: Chichester, 1992.
114. Koenig, J. L. In *Optical Techniques to Characterize Polymer Systems*; Bässler, H., Ed.; Elsevier: Oxford, 1989; pp. 1-40.
115. Willis, H. A.; Zichy, V. J. I. In *Polymer Surfaces*; Clark, D. T.; Feast, W. J., Eds.; J. Wiley & Sons: Chichester, 1978; pp. 287-307.
116. Pulker, H. K. *Thin Films and Technology*; Elsevier: Oxford, 1984; Vol. 6 Coatings on Glass.
117. Sauerbrey, G. *Physikal. Verhandl.* **1957**, *8*, 113.
118. Sauerbrey, G. *Z. Phys.* **1955**, *155*, 206.
119. Lostis, P. *Rev. Optique* **1959**, 38.
120. Pulker, H. K. *Z. Angew. Phys.* **1966**, *20*, 537.
121. Behrndt, K. H. *J. Vac. Sci. Technol. A* **1971**, *8*, 622.

122. Wilhelmy, L. *Ann. Phys.* **1863**, *119*, 177.

CHAPTER TWO

PULSED PLASMA POLYMERISATION OF ACRYLIC ACID

2.1 INTRODUCTION

Low temperature plasma polymerisation is well established as a versatile, economic route for the deposition of polymeric coatings.[1] It is a clean, solvent-free technique, able to deposit coatings onto a wide range of substrate materials. The plasma process is not thermal and the dynamics of film formation are not described by equilibrium thermodynamics.[2] Polymerisation occurs via activation and reaction of organic molecules in an electrical discharge.[1] One of the limitations of the plasma polymerisation technique is that reactive processes such as ion bombardment, UV damage, and cross-linking reactions[3] in the plasma produce polymer networks with complex structures which often bear little resemblance to the precursor molecule. Therefore, one of the challenges has been to produce films containing high levels of chemical specificity. Variation of experimental parameters (e.g. input power,[4,5] gas composition and pressure,[6,7] substrate temperature,[7-10] substrate position,[11] nature of substrate,[4,6] reactor dimensions[12] etc.) offers some degree of control over the stoichiometry. For example, it has been found that reducing the power supplied to the plasma increases the retention of functional groups in many of the systems studied.[4] However, the overall selectivity tends to remain fairly poor. More recently it has been demonstrated that pulsing of the excitation power source can reduce cross-linking and functional group diversity during plasma polymerisation.[13-30] This has been attributed to attenuated damage of the growing plasma film as a result of the curtailed excitation and ionisation of molecules during the off-period of the voltage pulse cycle.[15] Furthermore, in some cases, it has been shown that conventional polymerisation mechanisms can proceed during the off-time at reactive sites generated within the on-period of the pulse cycle.[14,16,31] Examples of structural retention during electrically pulsed plasma polymerisation include deposition from silicon containing monomers,[16,17,32] halocarbons,[13,14,16,17,31] tin containing precursors,[15,33] alcohols[18] and other reactive molecules.[26]

This chapter describes a further advancement on the theme of pulsed plasma polymerisation where both the electrical field and co-reactant gas were pulse modulated. The aim was the production of a plasma polymer surface with a high density of acid groups. Acrylic acid (AA) was chosen as the monomer since it

contains an acid group and an unsaturated carbon-carbon double bond, Structure 2.1. This double bond is susceptible to conventional polymerisation reaction pathways during the duty cycle off-period.[31] The formation of thin films by continuous wave (CW) plasma polymerisation of AA is well documented.[5,34-44] These plasma polymers have found use in many surface-related applications such as: control of substrate wettability;[34] protein adsorption;[45] modification of adhesion;[46,47] interaction with biological species;[38] and ultrafiltration.[39] In many of these applications sufficient density of functional groups on the polymer surface is vital. However, the incorporation of carboxylic acid groups at the surface under CW conditions is fairly low (20 %). It has previously been demonstrated that the wettability of AA plasma polymerised thin films can be enhanced by pulsing the electrical discharge.[48] Here we investigate the influence of electrical pulsing and oxygen gas injection during AA plasma polymerisation. Oxygen introduction into polymer forming plasma reactions has been shown to have a marked effect on the chemistry of deposits thus formed.[7,49]

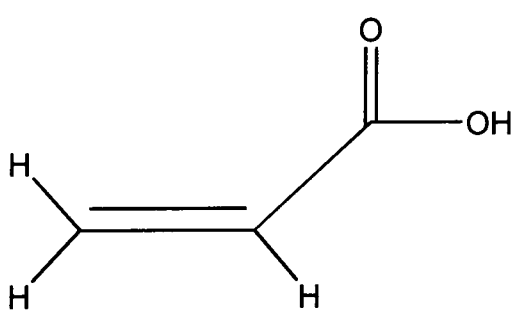

Structure 2.1: Acrylic acid.

2.2 EXPERIMENTAL APPARATUS AND PROCEDURE

All plasma polymerisation reactions were performed in an electrodeless cylindrical glass reactor (internal diameter of 52 mm and length of 320 mm). The reactor was continuously pumped by a two stage rotary pump (Edwards E2M2) via a liquid nitrogen cold trap. The base pressure ultimately achievable in the reactor was 5 x 10^{-3} mbar measured at the reactor outlet by a Pirani pressure

gauge (Edwards PR10-k). Gas was emitted into the chamber via a leak valve (Edwards CV10K), Figure 2.1.

Radio frequency (rf) power was provided by a copper coil wrapped around the circumference of the reactor eleven times. A home-made LC matching network inductively coupled the coils to a home-made radio frequency power generator. The generator operated at 13.56 MHz with a maximum power output of approximately 70 Watts. The network matched the output impedance of the partially ionised gas to that of the generator (50 Ohms) by minimising the standing wave ratio (SWR). The SWR (i.e. total power generated/power transmitted to the plasma) was measured by a SWR power meter (RS) in series. The SWR was minimised by adjusting the inductance and capacitance of the LC circuit after rf power had been switched on. The glass reactor and copper coils were completely contained in a Faraday cage to prevent rf leakage.

Six main types of experiment were carried out: CW plasma polymerisation of AA; electrically pulsed plasma polymerisation of AA; CW plasma polymerisation of AA with oxygen gas; electrically pulsed plasma polymerisation of AA with oxygen gas; CW plasma polymerisation of AA with simultaneous pulsed gas injection; and electrically pulsed plasma polymerisation of AA with simultaneous pulsed gas injection. The experimental procedure and apparatus for each set of experiments differed in detail but some basic routines were the same in all cases. The basic procedure is presented below, followed by a more detailed description of the individual experiments.

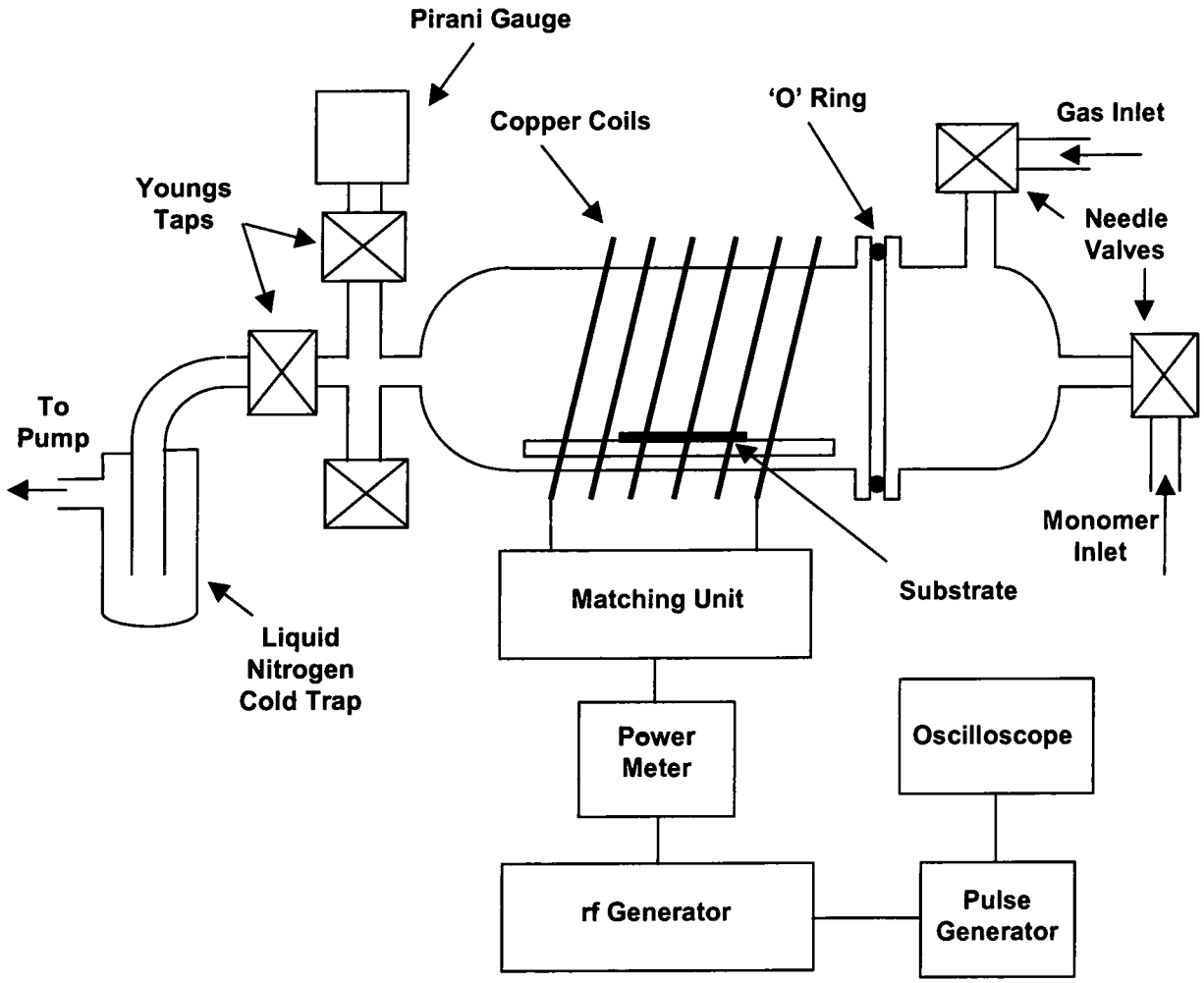

Figure 2.1: Schematic Diagram of the Experimental Apparatus.

2.2.1 EXPERIMENTAL PROCEDURE

AA monomer (Aldrich, 99% purity) was further purified by several freeze-thaw cycles. The cycle involved placing the monomer into a glass tube fitted with a Young's tap (monomer tube) and attaching the tube via the leak valve to the reactor chamber. The monomer was frozen with liquid nitrogen and the monomer tube was evacuated then allowed to thaw. This method relies on the principle that the solubility of a gas in a liquid is dependent on the vapour pressure above the liquid. Reducing this vapour pressure reduces the solubility of dissolved gases.[50] The freeze-thaw cycles were continued until no pressure

rise in the reactor system was observed on evacuation of the monomer tube (typically three cycles). This indicated that the majority of the dissolved gas had been removed. Gases (Argon, Helium, Nitrogen, Oxygen, Hydrogen, Neon and Carbon Dioxide, BOC Gases) were used without further purification.

Prior to each experiment the reactor was scrubbed clean with detergent and scouring powder, rinsed with copious amounts of water and isopropyl alcohol (IPA) before finally being oven dried. Before polymerisation air was emitted into the reactor and a 50 W air cleaning plasma ignited at a pressure of 0.2 mbar for 30 minutes. The reactor was pumped down to base pressure following air plasma cleaning, isolated from the pump and opened up to the atmosphere to allow insertion of a previously prepared glass slide. The slides were ultrasonically cleaned in detergent and water for 30 minutes followed by a one hour cleaning in 1:1 cyclohexane and IPA. The slides were then stored in fresh IPA until required. Once inserted into the reactor the slide was positioned at the centre of the copper coils and the system was pumped back down to base pressure. At this stage the leak rate of the reactor was determined (Section 2.2.2.1). The monomer was then introduced into the reactor at a set pressure, typically 0.2 mbar, via the leak valve five minutes prior to polymerisation. The flow rate of monomer into the plasma chamber was then calculated (Section 2.2.2.2). The glow discharge was then ignited and immediately balanced manually using the matching network. After the treatment time had elapsed the plasma was extinguished and the monomer was purged through the system for a further two minutes.

2.2.1.1 CW Plasma Polymerisation

CW plasma polymerisation of AA was carried out as described above. Following ignition of the plasma the discharge power was set according to the power meter and the plasma balanced. The treatment time was typically ten minutes followed by a further two minutes of purging with monomer vapour. The reactor was then evacuated to base pressure, vented to atmosphere and the slides were removed

and affixed to probe tips using double sided adhesive tape for immediate characterisation.

2.2.1.2 Electrically Pulsed Plasma Polymerisation of AA

For electrically pulsed plasma experiments a pulse generator supplied a pulse of 5 V amplitude to the rf generator. The pulse duration (known as on-time) and frequency could be varied over a wide range (1 μs-10 s and 1000 MHz - 0.1 Hz respectively). This pulse input was used to modulate the output of the rf generator, with power being supplied to the coils only during the pulse on-time. The actual minimum pulse duration achievable was limited to 5 μs by the rise and fall times of the rf generator which were approximately 1 and 2 μs respectively. The pulse output from the pulse generator was monitored by an oscilloscope via a standard coaxial cable. A probe consisting of a wire connected to the oscilloscope was placed inside the Faraday cage adjacent to the reactor. This probe monitored the output performance of the rf generator by detecting the rf signal radiated by the copper coil antenna.

It was necessary to set the pulsing conditions prior to the insertion of the glass substrate as the plasma had to be balanced under CW conditions. Therefore, following the air cleaning plasma, air was emitted into the reactor via the leak valve. A plasma was ignited and the power set at the desired value. Pulsing of the discharge was then switched on. The overall average power (<P>) supplied to the system was calculated using the following equation, Equation 2.1:[27]

$$\langle P \rangle = P_p \times \left(\frac{t_{on}}{t_{on} + t_{off}} \right) \qquad \textbf{Eq. 2.1}$$

where t_{on} is the plasma on-time; t_{off} is the off-time; and P_p is the peak power. The on-time and off-time were varied between 5-10000 μs and 0.05-64 ms respectively. The peak power could be set between 1.5 and 70 W. After the reactor had been set up it was vented to the atmosphere to allow insertion of the glass substrates. From this point the experimental procedure was essentially the

same as that for CW plasma polymerisation (Section 2.2.1.1) except that the plasma discharge conditions had already been determined.

2.2.1.3 CW Plasma Polymerisation of AA with Oxygen Gas

The reaction procedure was analogous to the CW polymerisation of AA up to the point of deposition (Section 2.2.1.1). The pressure of the monomer was set at 0.2 mbar and the flow rate was measured. Oxygen was then allowed to enter the reactor via a second needle valve to make the total pressure up to a new value. The reactant mixture was purged through the system for five minutes and then the plasma was ignited at the required discharge power. After ten minutes the plasma was extinguished and the reactor purged for a further two minutes with the reactant mix.

2.2.1.4 Electrically Pulsed Plasma Polymerisation of AA with Oxygen Gas

The pulsing conditions were set up as described above (Section 2.2.1.2) and the desired reactant mixture was obtained (Section 2.2.1.3). For these experiments the AA pressure was maintained at 0.2 mbar but the total pressure in the reactor was made up to a new value with oxygen gas.

2.2.1.5 CW Plasma Polymerisation of AA with Pulsed Gas Injection

For the gas pulsing experiments a gas pulsing valve was driven by a dedicated pulse driver (General Valve Corporation). The gas pulsing valve was connected directly to the plasma reactor with an upstream gas pressure of 0.2 bar above atmospheric pressure. The gas pulsing valve consisted of a PEEK stopper (known as a "poppet") mechanically pressed shut by the action of a spring, Figure 2.2. Pulses arriving from the pulse driver energised an electromagnet creating a magnetic field which pulled the armature up against the end plate, thus opening the valve. The valve remained open while power was applied.[51] The gas pulsing

duty cycle was expressed as a percentage and calculated as follows, Equation 2.2:

$$\text{Gas Pulsing Duty Cycle} = \left(\frac{\text{on - time}}{\text{on - time + off - time}}\right) \times 100 \quad \textbf{Eq. 2.2}$$

The minimum on-time which could be set on the gas pulsing driver was 5 μs but the duty cycle had to be less than 50% and the maximum frequency at which the valve could operate was 250 Hz. The maximum error in the electrical pulse was 2 μs or 0.001%, whichever was greater.[52]

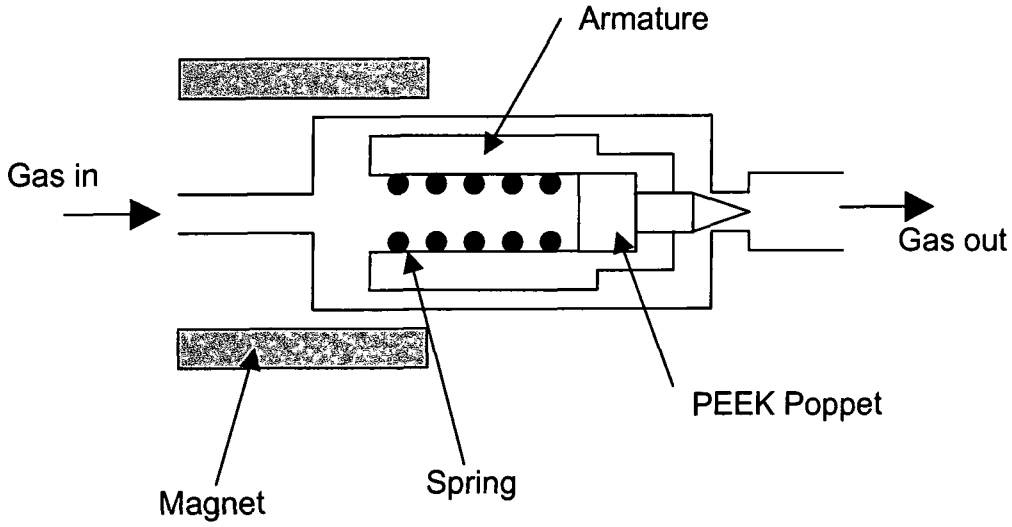

Figure 2.2: Schematic of the Iota One Gas Pulsing Valve.[51]

The AA pressure was set at 0.2 mbar and the gas pulsing valve was activated with the required on-time and off-times. The gas pulsing valve driver's output was monitored on the oscilloscope via a coaxial cable connected to an auxiliary BNC output on the driver. The plasma was then switched on in the usual fashion (Section 2.2.1.1).

2.2.1.6 Electrically Pulsed Plasma Polymerisation of AA with Simultaneous Pulsed Gas Injection

For combined gas and electrical pulsing the reaction conditions were set up prior to insertion of the glass substrates, as described above (Section 2.2.1.2). The gas pulsing driver's auxiliary output was used to modulate the rf generator instead of the usual pulse generator. This ensured synchronous gas and electrical pulsing as confirmed by the oscilloscope.

2.2.2 FLOW AND LEAK RATE DETERMINATION

The calculation of leak rates and gas flow rates for plasma reactor systems is important as a knowledge of the impurities present in the reactor volume and the flow rate of monomer molecules will help in the interpretation of results. Indeed, the composition and deposition rates of plasma polymers are often a function of monomer flow rates.[1] The unit used for the flow rate (Qm) is mol s^{-1}. This quantity is often confused with the throughput (Q) which is the rate of change with time of the product of the pressure of a gas and the volume in which it is contained.[53] Frequently used units for this quantity are atm cm^3 s^{-1} and Pa m^3 s^{-1}. The number of moles of gas passing through an orifice per unit time (Qm) is a function of the gas temperature but the throughput is not.[53] The gas is assumed to behave ideally and the ideal gas law is applied, Equation 2.3:

$$PV = nRT \qquad \textbf{Eq. 2.3}$$

where P is the pressure (Pa), V is the volume (m^3), n is the amount of gas (moles), R is the gas constant (J K^{-1} mol^{-1}), and T is the absolute temperature (K). The volume of the reaction chamber was estimated by attaching a small vile at atmospheric pressure to the chamber. The chamber was then pumped to base pressure, isolated from the pump and the small volume opened to the chamber. The volume of the reaction chamber could now be calculated using Equation 2.3.[54] This method ignored the leak rate of the reactor, which was a reasonable

omission, as the leak rate was low, the time of measurement was fast (<30 s) and the pressure rise was comparatively large.

2.2.2.1 Leak Rate

To measure the leak rate, the reactor chamber was pumped down to base pressure, allowed at least 5 minutes to equilibrate and isolated from the pump. The rise in pressure with time over a relatively narrow pressure range was measured. The temperature of the lab was taken and all apparatus and materials were assumed to be in thermal equilibrium. Differentiation of the ideal gas law, Equation 2.3, with respect to time at constant temperature yields an expression that may be used to evaluate the molar leakage rate (Qm_l),[53] Equation 2.4:

$$Qm_l = \frac{dN}{dt} = \frac{\left[P\left(\frac{dV}{dt}\right) + V\left(\frac{dP}{dt}\right)\right]}{RT} \qquad \textbf{Eq. 2.4}$$

As the volume is constant the first term is zero, thereby simplifying the expression, Equation 2.5:

$$Qm_l = \frac{\left(\frac{\Delta P}{\Delta t}\right)V}{RT} \qquad \textbf{Eq. 2.5}$$

where Δt is the time required for the pressure to rise over the pressure range ΔP. Note that the time interval Δt was small to ensure that the pressure rise was linear. Typical leak rates were approximately 1×10^{-9} mol s^{-1}.

2.2.2.2 Flow Rate and Percentage Purity

To measure the molecular flow rate of monomer into the reactor the system was initially pumped down to base pressure. At this point the leak rate of the chamber was measured as described above (Section 2.2.2.1). The chamber was again pumped down to base pressure and monomer gas was allowed to enter the chamber at the required pressure (the pressure used for plasma polymerisations). The system was allowed to equilibrate for five minutes. This was to allow time for all components of the system to reach thermal equilibrium and for adsorption and desorption of monomer from the inside of the reactor chamber to equilibrate. At this point the temperature of the lab was measured and the reaction chamber isolated from the pump. The pressure rise over a small pressure range was measured as a function of time. Equation 2.5 was then used to calculate the molecular flow rate (Qm), after one small alteration,[53] Equation 2.6:

$$Qm = \frac{\left[\left(\frac{\Delta P}{\Delta t}\right) - \left(\frac{\Delta P_0}{\Delta t}\right)\right]V}{RT} \qquad \textbf{Eq. 2.6}$$

where $\Delta P_0/\Delta t$ is the change in pressure when the chamber is isolated from the pump without monomer flow (i.e. the leak rate measurement). The percentage monomer in the reaction chamber, with respect to other gases present due to leaks, could then be found,[53] Equation 2.7:

$$\% \text{ Monomer} = \frac{\text{Flow Rate}}{(\text{Flow Rate} + \text{Leak Rate})} \times 100 \qquad \textbf{Eq. 2.7}$$

Flow rates were kept constant at approximately 5×10^{-6} mol s^{-1}. Measurement error was approximately 10% due to the difficulties in measuring the rapid pressure rise on isolation of the rotary pump. This meant that the AA vapour in the reactor was more than 99.9% pure (except when oxygen was deliberately added).

2.2.3 CHARACTERISATION TECHNIQUES

Samples were characterised immediately following plasma polymerisation by X-ray Photoelectron Spectroscopy and transmission FTIR spectroscopy. Plasma deposition rate measurements were performed to aid in the interpretation of results.

2.2.3.1 XPS Characterisation

The glass slides were attached to a stainless steel probe stud using double sided adhesive tape and inserted into a VG ESCA Lab Mk II photoelectron spectrometer. The spectrometer was fitted with an unmonochromated magnesium X-ray source (Mg $K\alpha_{1,2}$ = 1253.6 eV) and operated in the constant analyser energy mode (CAE = 20 eV for high resolution spectra, 50 eV for survey scans). Photoelectrons emitted from the substrate were collected at a 30° take-off angle with respect to the substrate normal. The spectrometer calibration was routinely checked using the gold $4f_{7/2}$ and silver $3d_{5/2}$ peaks at 83.8 and 368.3 eV respectively.[55] Elemental sensitivity factors were determined experimentally relative to the carbon 1s (C(1s)) peak (285.0 eV) using standard compounds. These were taken as C(1s) : O(1s) : N(1s) : Si(2p) = 1.00 : 0.39 : 0.65 : 1.00 respectively. The absence of any Si(2p) XPS feature following plasma polymerisation was indicative of complete coverage of the glass substrate.

2.2.3.2 FTIR Characterisation

An FTIR Mattson Polaris spectrometer was used for transmission IR analysis of the plasma polymers. The substrate used for transmission experiments was a polished sodium chloride plate. A spectrum of the disk was recorded prior to its insertion into the plasma reactor to ensure that the disk was free from contamination. Typically 100 scans were recorded at a resolution of 4 cm^{-1}.

2.2.3.3 Deposition Rate Measurements

Plasma polymer deposition rates were measured with an oscillating AT cut quartz crystal (Kronos, Inc. QM-331 Film Thickness Monitor) placed at the centre of the plasma reactor (Section 1.8.3). The thickness monitor employed the principle of period measurements to ensure linearity, accuracy, and resolution.[56] Film deposition rates were measured in nanograms (ng) to avoid any assumptions about the density of the plasma polymer deposited. Routinely, measurements were not taken until 10 minutes after the plasma was ignited to allow time for the apparatus to reach thermal equilibrium. The change in mass of the quartz crystal was then recorded every minute for 10 minutes and the average mass change (due to the deposition of plasma polymer) per second calculated. Subsequently, the plasma was extinguished, vented to the atmosphere, and the crystal removed to allow cleaning of the reactor prior to the next set of measurements. Crystals were cleaned with methanol and their operational state tested as instructed[56] between each deposition. All deposition experiments were performed at least 3 times to enable the estimation of errors. The error calculated in this manner was assumed to be larger than the intrinsic error in the measurement equipment (0.1 ng at low deposition rates).[56]

2.3 RESULTS

High resolution XPS envelopes were fitted using a Marquardt minimisation routine.[57] The peak shape was assumed to be Gaussian with a fixed relative full width at half maximum. The C(1s) region of a typical AA plasma polymer layer was fitted with five different carbon functionalities[58] (using the hydrocarbon peak at 285.0 eV as a reference offset): $\underline{C}_xH_y$ (285.0 eV); $\underline{C}$-C(=O)-O (285.7 eV); $\underline{C}$-O (286.6 eV); O-$\underline{C}$-O / $\underline{C}$=O (287.9 eV); and $\underline{C}$(=O)-O (289.3 eV), Figure 2.3. The relative amount of $\underline{C}$(=O)-O group incorporation into the plasma polymer was calculated in terms of its percentage contribution to the overall C(1s) envelope and the O/C ratio was found from the O(1s) and C(1s) peak areas (after correction for sensitivity).

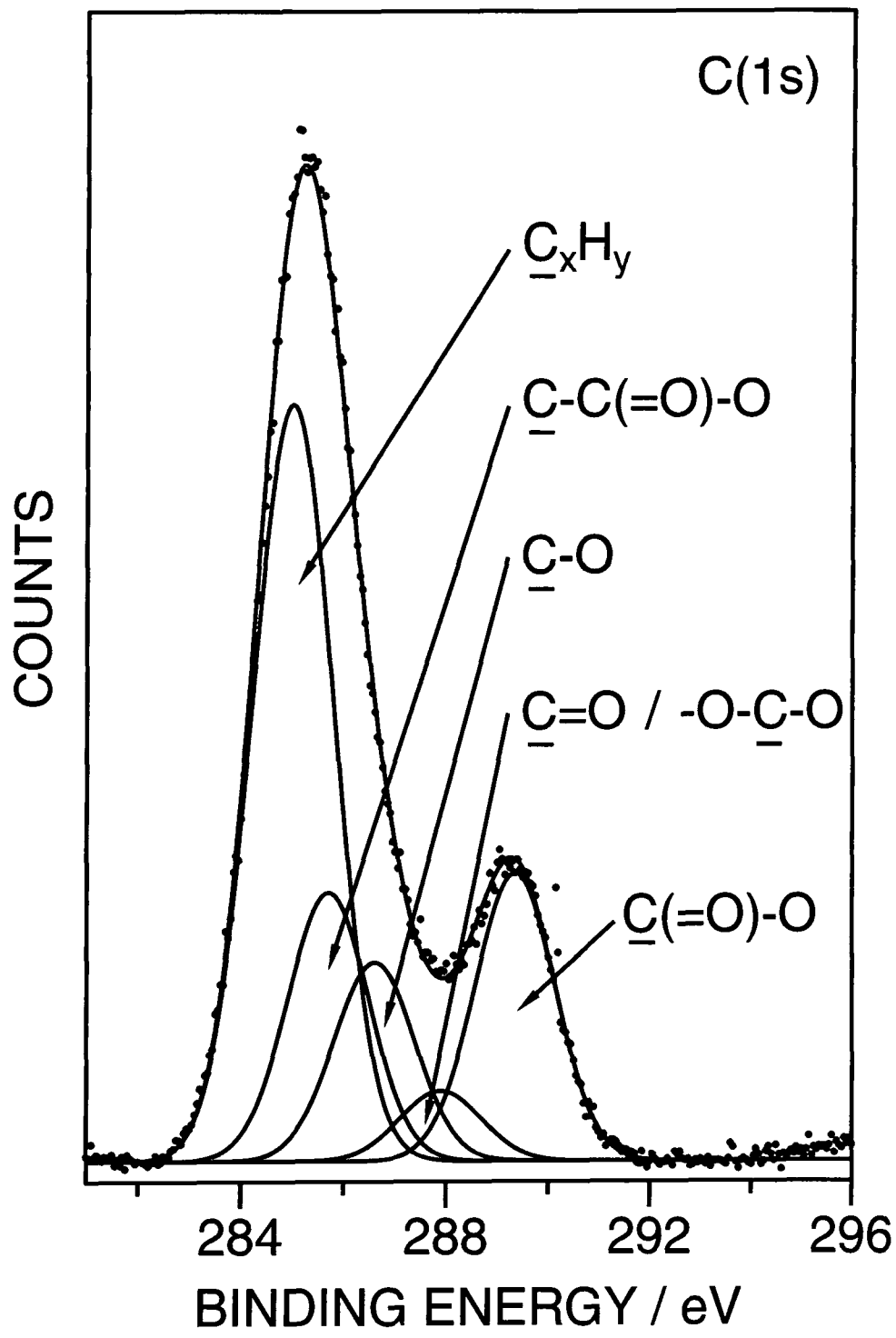

Figure 2.3: C(1s) XPS peak fit for a 2 W CW AA plasma polymer.

2.3.1 CW PLASMA POLYMERISATION

The C(1s) XPS spectra of the CW AA plasma polymer changed appearance with discharge power, Figure 2.4. The thin films produced under the lowest discharge powers bore a greater resemblance to the theoretically expected spectrum than the films deposited at higher powers. This dependence on discharge power has been previously reported in earlier studies.[5,34,37,38,40,42,48,59] The C(=O)-O group became less well defined and the relative intensities of the C-O and O-C-O / C=O groups increased with increasing discharge power. Therefore, a greater degree of monomer break up and film cross-linking occurred in higher power plasmas. The O/C ratio reached 0.52 ± 0.02 and the C(=O)-O group retention was 18% ± 1, at a discharge power of 1.5 W, Figure 2.5. This was considerably less than the theoretically expected O/C ratio of 0.67 and 33% C(=O)-O group content, assuming no monomer break up. Below 1.5 W the CW plasma became unstable and no deposition occurred.

The deposition rate decreased with a concomitant increase in discharge power, Figure 2.6. This observation was consistent with the detection of a silicon (Si(2p)) signal for electrical discharge powers greater than 7 W. Indeed, at higher powers the mass of the quartz crystal was seen to decrease indicating that etching processes in the plasma were becoming dominant. To factor out the effect of the change in power, the deposition rate per Joule was considered.[14,16,19] This is known as the deposition efficiency,[14] Equation 2.8:

$$\text{Deposition Efficiency} = \frac{\text{Deposition Rate}}{\text{Average Power}} \qquad \textbf{Eq. 2.8}$$

The deposition efficiency rose with decreasing discharge power, Figure 2.6. This was further evidence for film forming reactions becoming progressively dominant over film ablation processes at lower powers.[16]

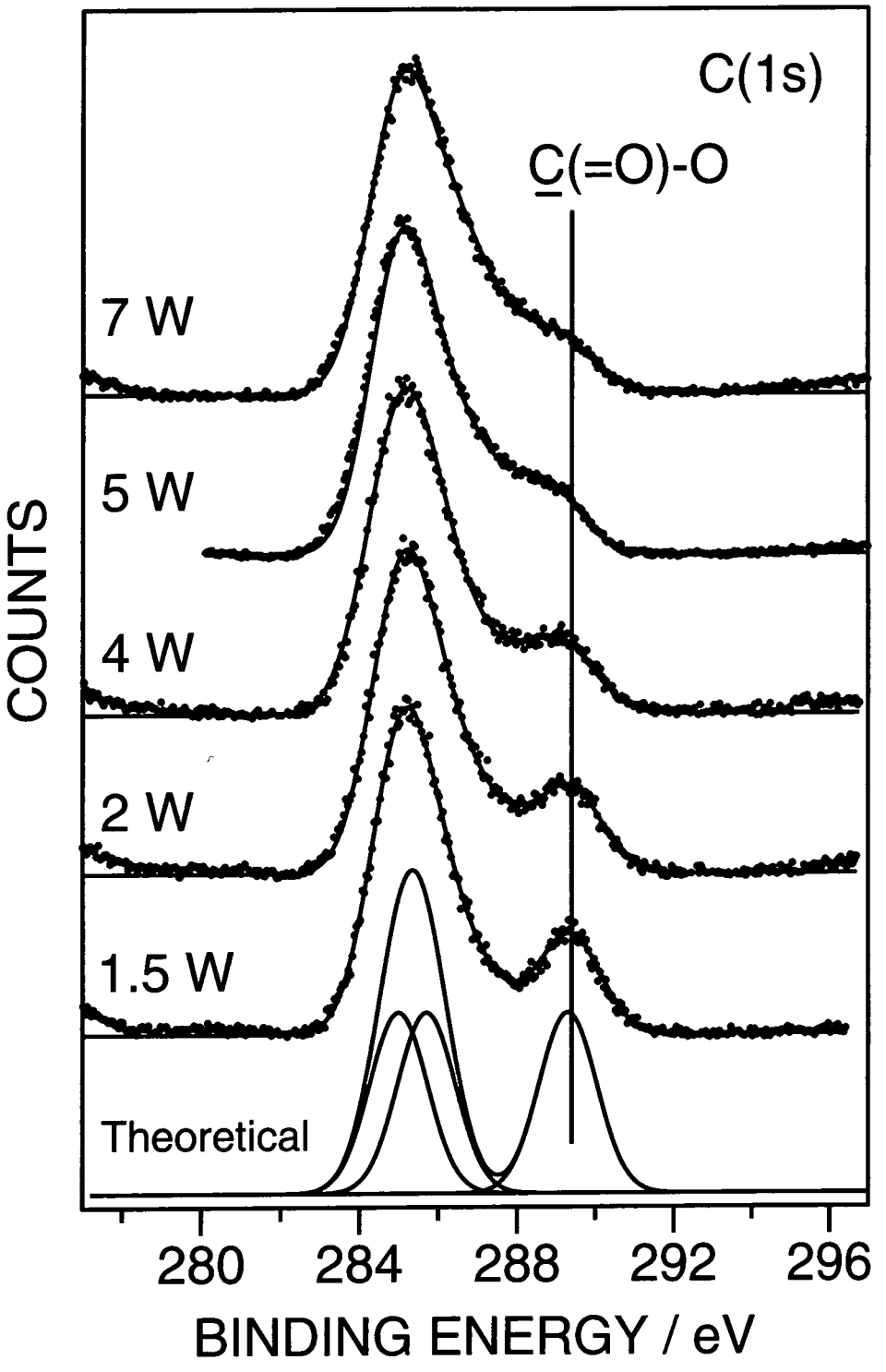

Figure 2.4: C(1s) XPS spectra of CW AA plasma polymer deposited as a function of discharge power.

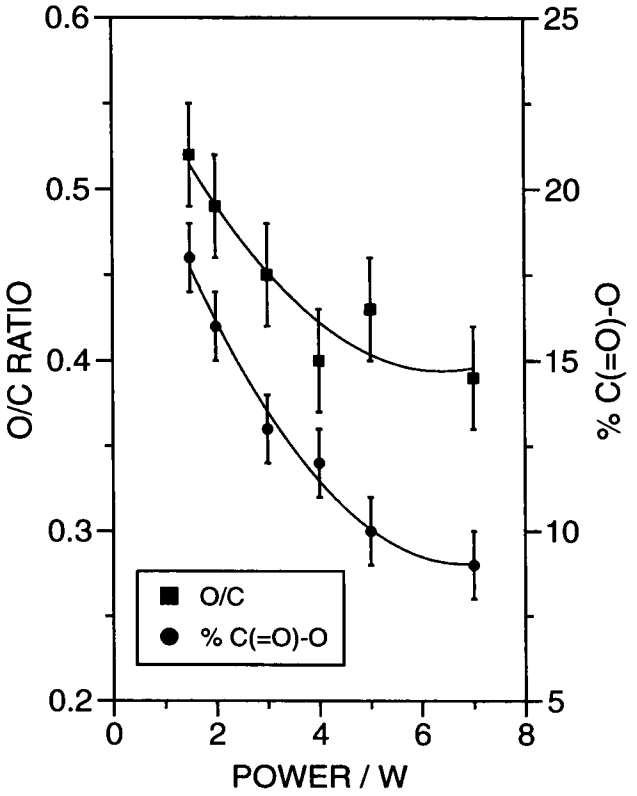

Figure 2.5: Variation in the O/C ratio and percentage C(=O)-O group as a function of discharge power for CW AA plasma polymer.

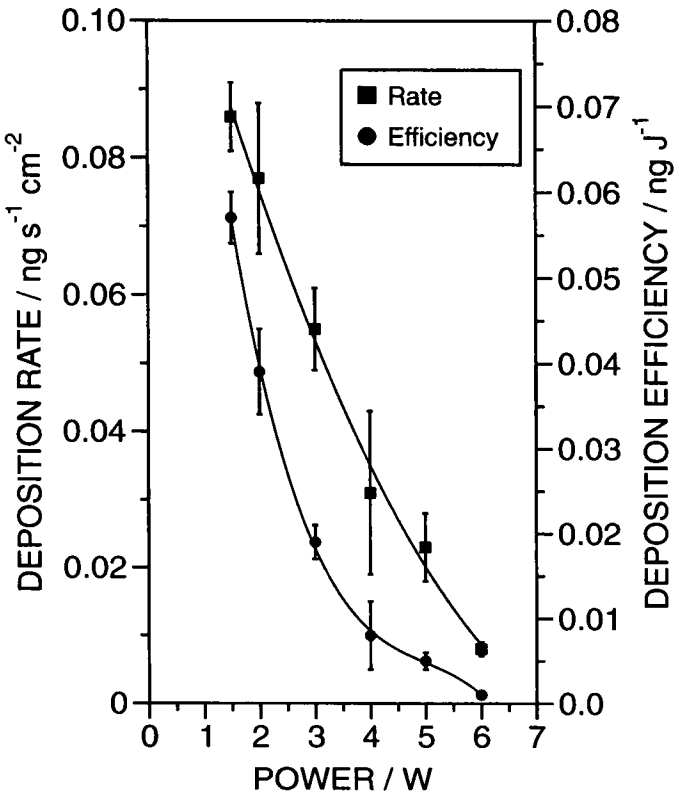

Figure 2.6: Variation in the deposition rate and deposition efficiency as a function of discharge power for CW AA plasma polymer.

2.3.2 ELECTRICALLY PULSED PLASMA POLYMERISATION

The average power could be reduced further by pulsing the electrical discharge. Low duty cycles (shorter on-times or longer off-times) enhanced oxygen and C(=O)-O group incorporation into the deposited plasma polymer. Systematically decreasing the plasma on-time (with a constant off-time of 4 ms and peak power of 5 W) or increasing the off-time (with a constant on-time of 180 μs and peak power of 5 W) increased the intensity of the C(=O)-O peak at the expense of the other oxygenated functionalities, Figures 2.7 and 2.8. Optimum conditions at the lowest average powers yielded O/C ratios as high as 0.72 ± 0.03 and C(=O)-O group concentrations of 30 % ± 1, Figures 2.9 and 2.10. This was significantly better than anything achieved during CW plasma polymerisation in this study. The glow discharge became unstable at very low duty cycles. For a given average power, increasing the peak power to 70 W from 5 W during electrically pulsed plasma polymerisation (with a constant off-time of 4ms) reduced the O/C ratio and C(=O)-O group retention of the plasma polymer, Figures 2.9 and 2.10. Thus the peak power supplied to the pulsed plasma was a factor in determining the functionalisation of the resultant film.

During pulsed plasma polymerisation the deposition rate reached a maximum of 0.1 ng s^{-1} cm^{-2} at 0.1 W average power, Figure 2.11. Shorter duty cycles resulted in a decrease in the deposition rate. The deposition efficiency per Joule was again considered to factor out the effect of average power, Figure 2.12. The deposition efficiency rose with decreasing average power, indicating that film forming reactions had become progressively dominant over film ablation and termination processes at lower average powers.[16] A decrease in the efficiency at very low powers may have been indicative of a lack of reactive film forming species at these extremely low duty cycles.

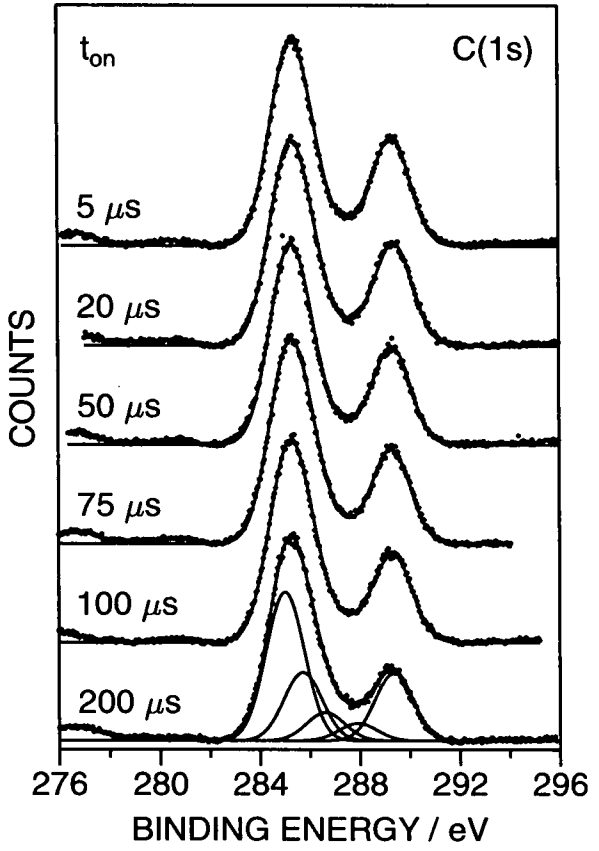

Figure 2.7: C(1s) XPS spectra of AA electrically pulsed plasma polymer deposited as a function of t_{on} (t_{off} = 4 ms, P_p = 5 W).

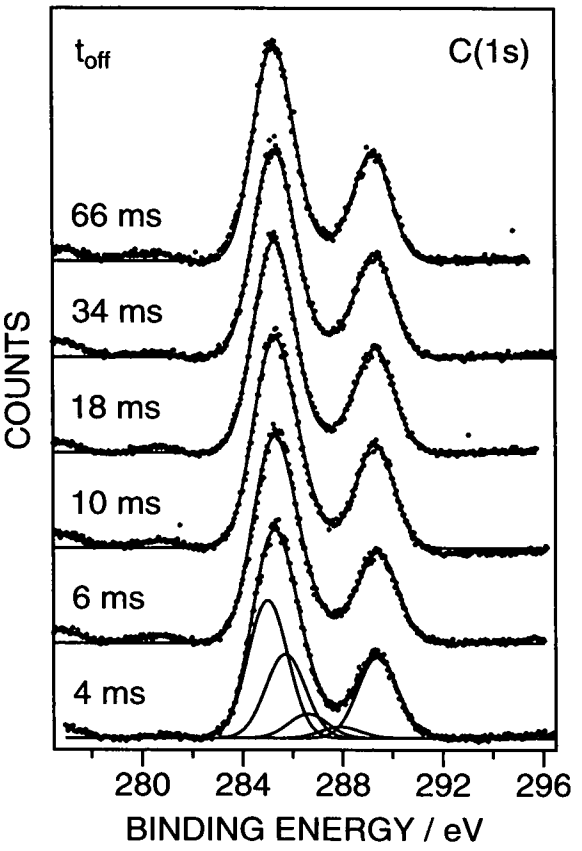

Figure 2.8: C(1s) XPS spectra of AA electrically pulsed plasma polymer deposited as a function of t_{off} (t_{on} = 180 μs, P_p = 5W).

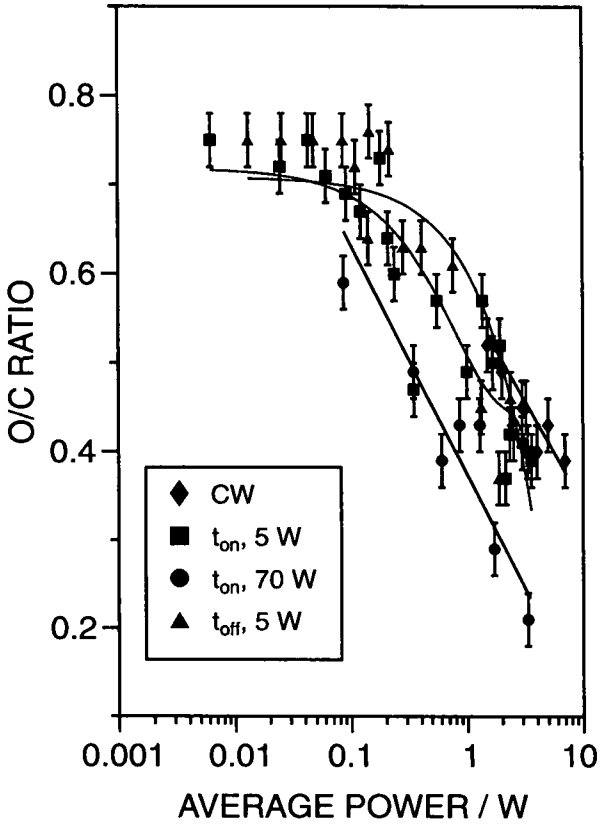

Figure 2.9: Variation in the O/C ratio as a function of average power for AA CW and electrically pulsed plasma polymer.

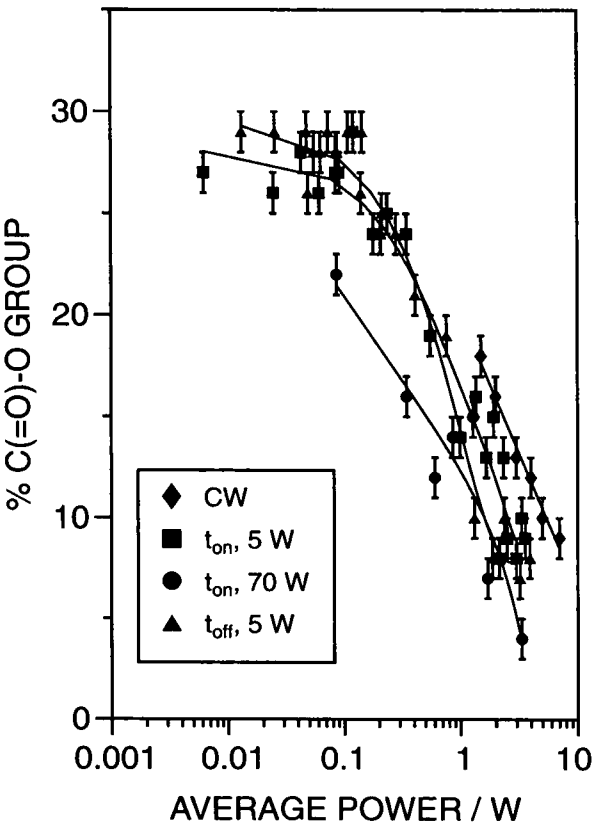

Figure 2.10: Variation in the percentage C(=O)-O group as a function of average power for AA CW and electrically pulsed plasma polymer.

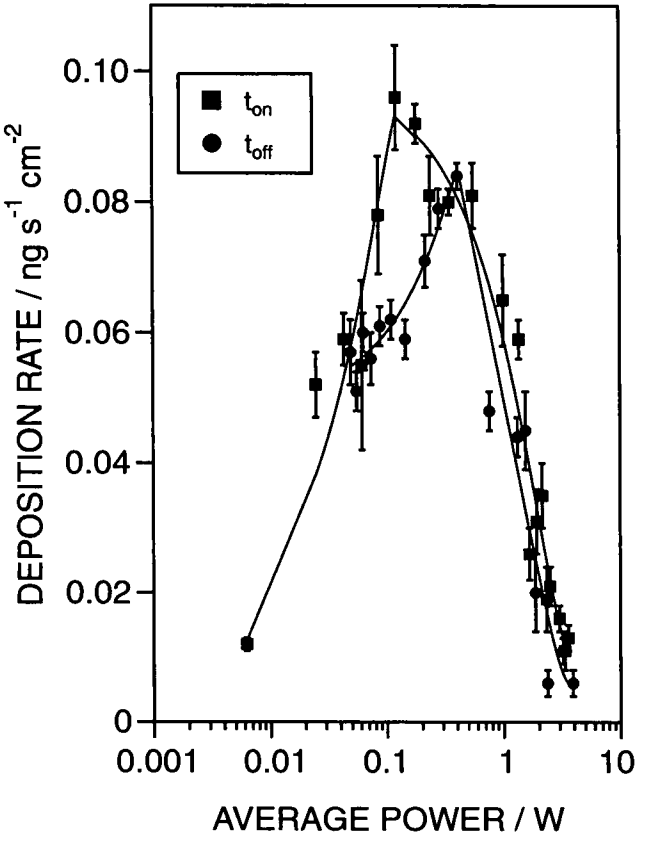

Figure 2.11: Variation in the deposition rate as a function of average power for AA electrically pulsed plasma polymer.

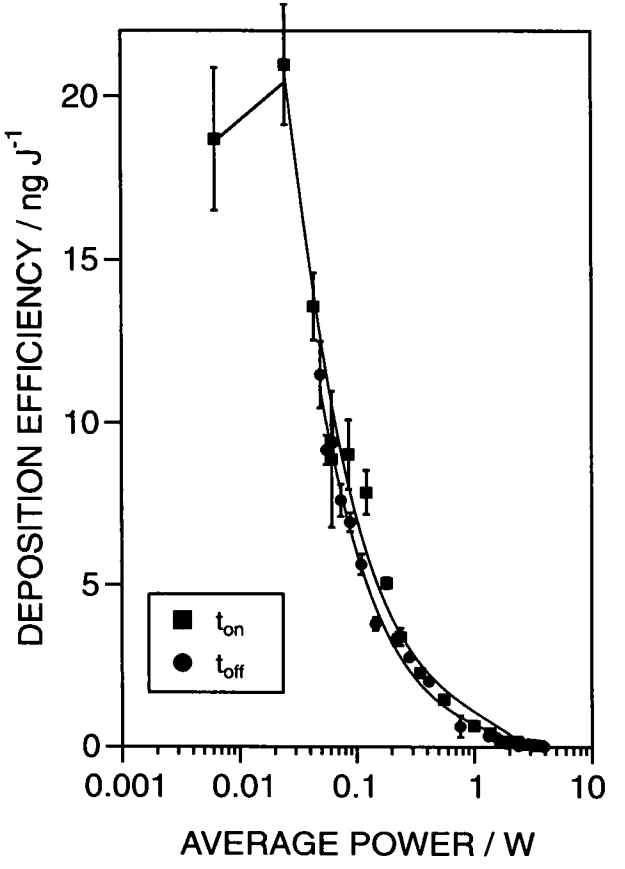

Figure 2.12: Variation in the deposition efficiency as a function of average power for AA electrically pulsed plasma polymer.

2.3.3 CW PLASMA POLYMERISATION WITH OXYGEN GAS

A substantial increase in the oxygen content of the CW plasma polymerised AA films was achieved by adding oxygen to the AA feed during CW plasma polymerisation (2 W), Figure 2.13. The AA pressure was first set at 0.2 mbar by adjustment of the needle valve and the flow rate was measured (Section 2.2.2.2). Oxygen gas was then introduced via a second needle valve and the total pressure was set at the required value. The O/C ratio reached 0.62 $\pm$ 0.03 and the C(=O)-O group retention was 25% $\pm$ 1, at a total pressure of 0.4 mbar, Figure 2.14. However, functional group incorporation appeared to be non-selective and the concentration of all oxygenated functionalities increased with oxygen partial pressure.

The deposition rate and efficiency decreased rapidly with increasing oxygen concentration, Figure 2.15. No evidence for polymer formation was found above a total pressure of 0.4 mbar, supported by the detection of a Si(2p) signal during XPS analysis. At these higher pressures the quartz crystal decreased in mass indicating that etching of the crystal was taking place at total pressures above 0.4 mbar.

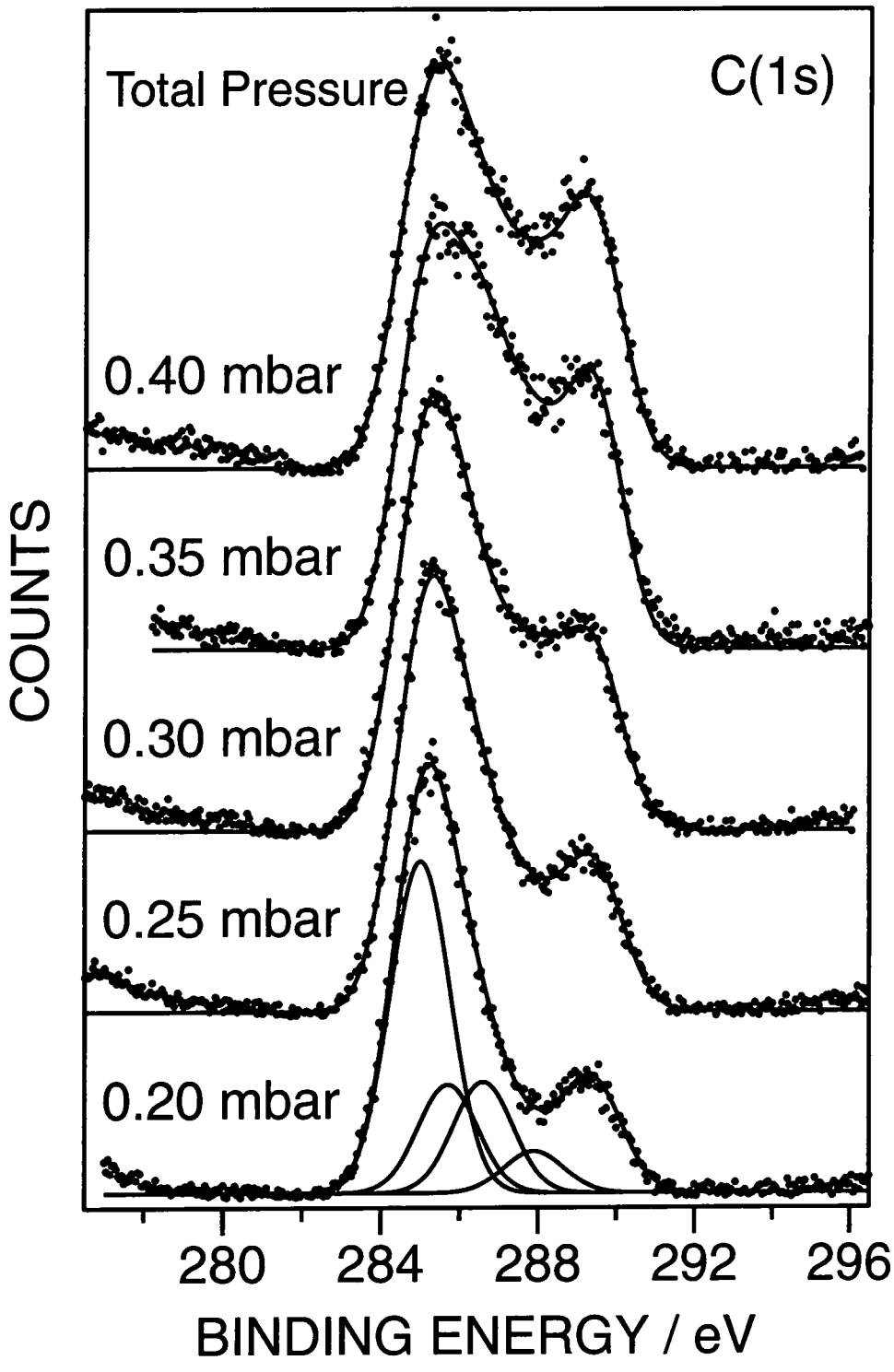

Figure 2.13: C(1s) XPS spectra of 2 W CW AA plasma polymer deposited as a function of added oxygen.

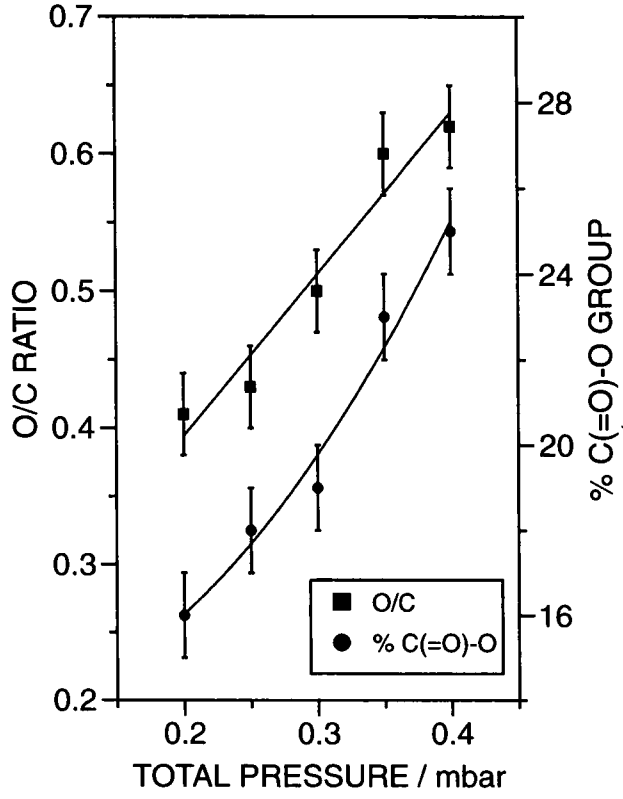

Figure 2.14: Variation in the O/C ratio and percentage C(=O)-O group as a function of added oxygen for 2 W CW AA plasma polymer.

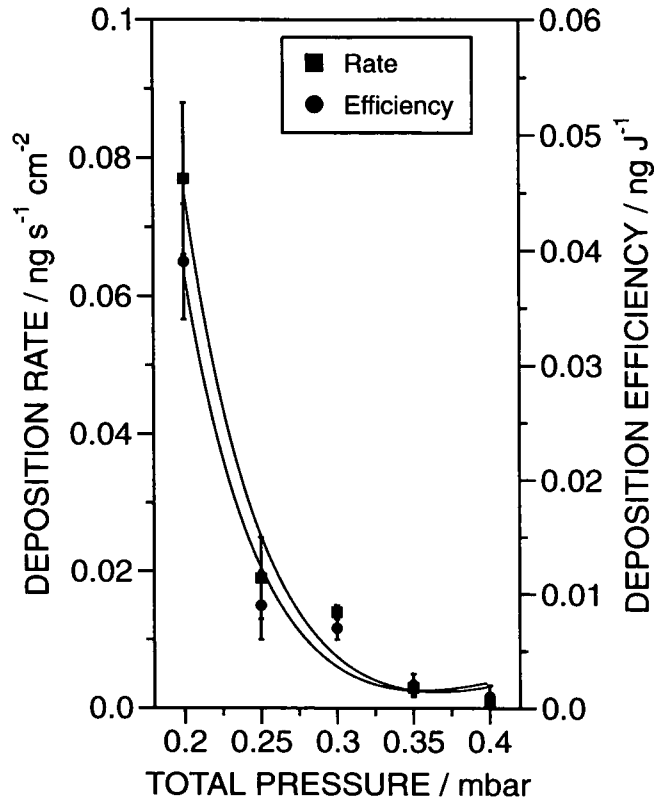

Figure 2.15: Variation in the deposition rate and deposition efficiency as a function of added oxygen for 2 W CW AA plasma polymer.

2.3.4 ELECTRICALLY PULSED PLASMA POLYMERISATION WITH OXYGEN GAS

At high oxygen partial pressures the extensively oxygenated polymer surfaces observed during CW conditions were further enhanced by electrically pulsing the plasma, Figure 2.16. The proportion of oxygenated groups formed increased with oxygen partial pressure (at constant electrical pulsing conditions of t_{on} = 180 μs, t_{off} = 4 ms and P_p = 5 W), Figure 2.17. At a total pressure of 0.6 mbar the O/C ratio was 1.31 ± 0.04 and the percentage C(=O)-O group incorporation reached 42 % ± 1. As before, the deposition rate and efficiency decreased as the amount of oxygen introduced into the discharge rose, Figure 2.18. However, film formation was still evident at a total pressure of 0.6 mbar, significantly higher than CW plasma polymerisation. After a total pressure of 0.6 mbar no film formation could be detected and the mass of the crystal began to decrease.

It was found that reducing the electrical pulse on-time at high oxygen partial pressures reduced the oxygen content and C(=O)-O group incorporation of the plasma polymer, Figure 2.19. Maximum oxygen incorporation was observed at 190 μs t_{on}, where the O/C ratio was measured to be 1.30 ± 0.04 and the percentage C(=O)-O group incorporation was 41 % ± 1, Figure 2.20. Further increasing the plasma t_{on} resulted in incomplete coverage of the substrate. Increasing the electrical pulse off-time decreased the functionalisation of the films produced, Figure 2.21. The O/C ratio and C(=O)-O group incorporation decreased with increasing off-time, Figure 2.22. These trends, observed for the pulsed plasma polymerisation of AA in the presence of added oxygen, were opposite to those found in the absence of oxygen.

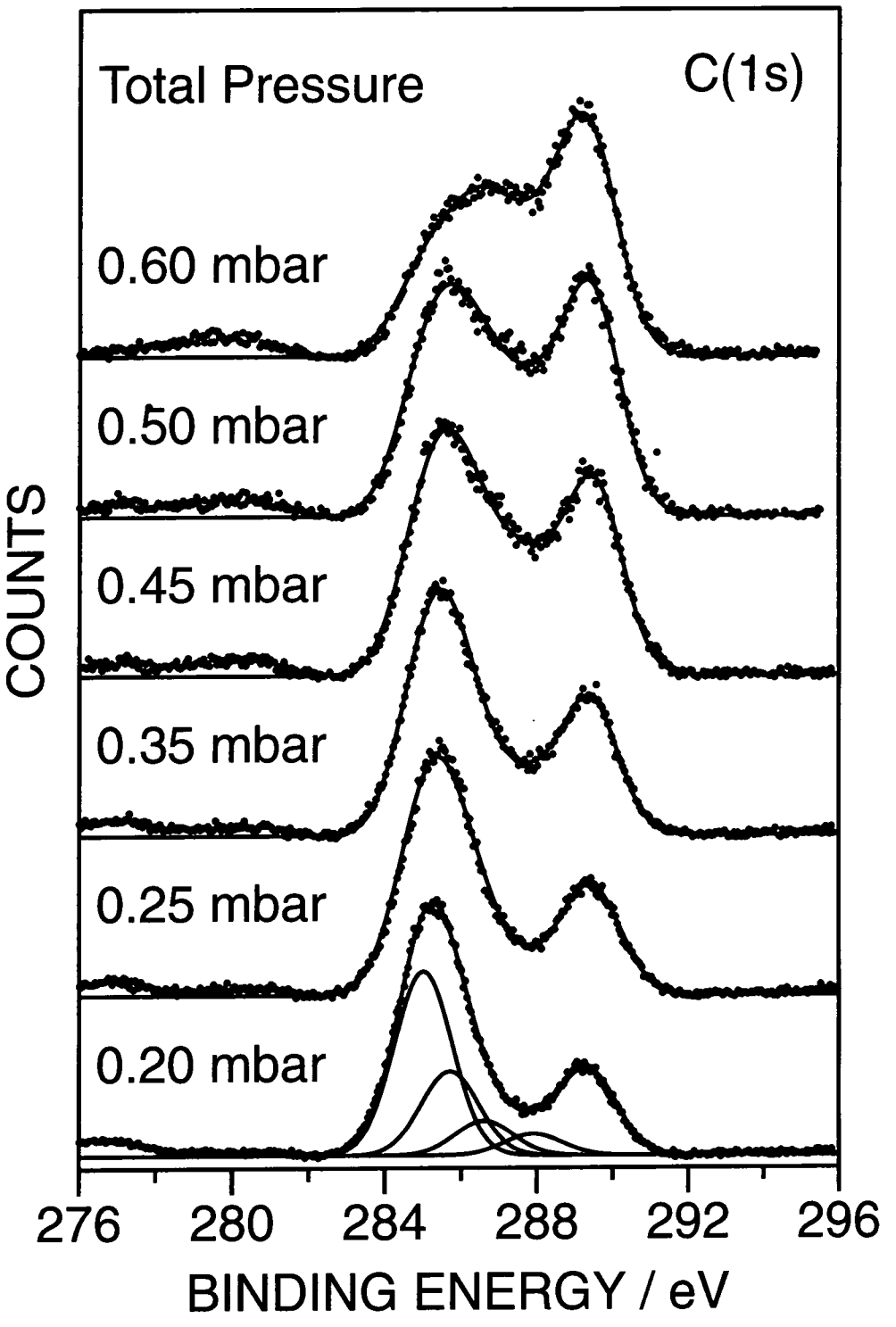

Figure 2.16: C(1s) XPS spectra of AA electrical pulsed plasma polymer (t_{on} = 180 μs, t_{off} = 4 ms and P_p = 5 W) deposited as a function of added oxygen.

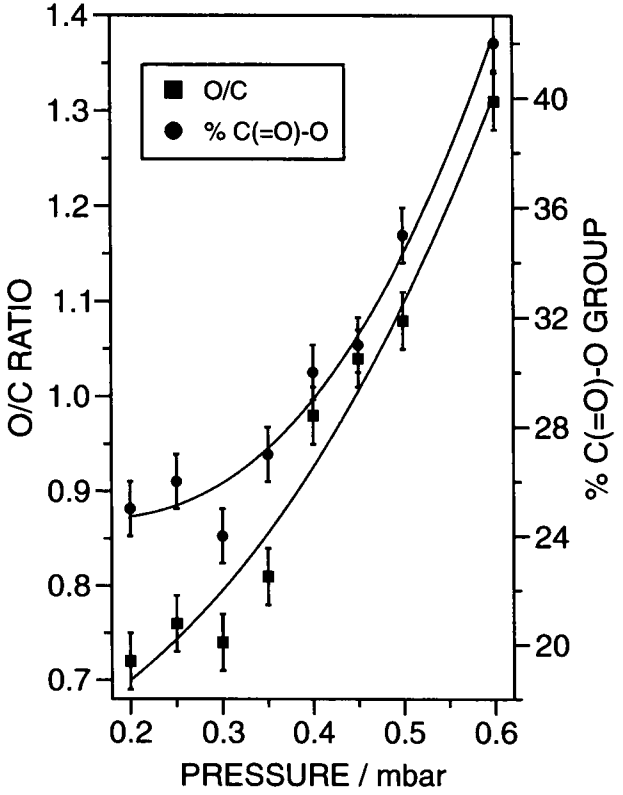

Figure 2.17: Variation in the O/C ratio and percentage C(=O)-O group as a function of added oxygen for AA electrically pulsed plasma polymer (t_{on} = 180 μs, t_{off} = 4 ms and P_p = 5 W).

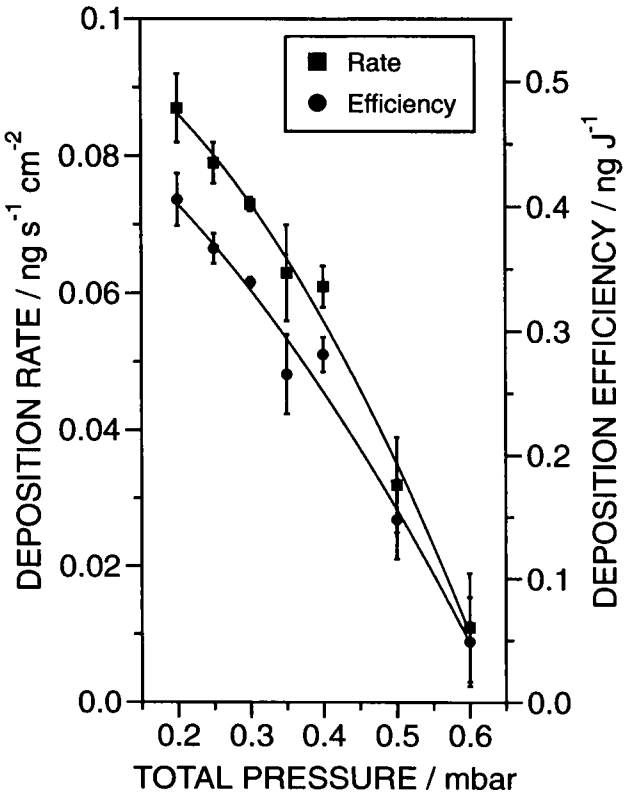

Figure 2.18: Variation in the deposition rate and efficiency as a function of added oxygen for AA electrically pulsed plasma polymer (t_{on} = 180 μs, t_{off} = 4 ms and P_p = 5 W).

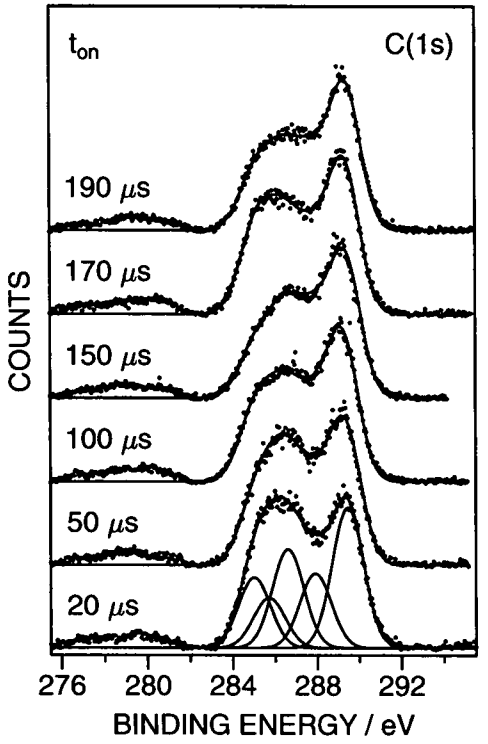

Figure 2.19: C(1s) XPS spectra of AA electrically pulsed plasma polymer with added oxygen deposited as a function of t_{on} (t_{off} = 4 ms, P_p = 5 W, AA pressure = 0.2 mbar and total pressure = 0.6 mbar).

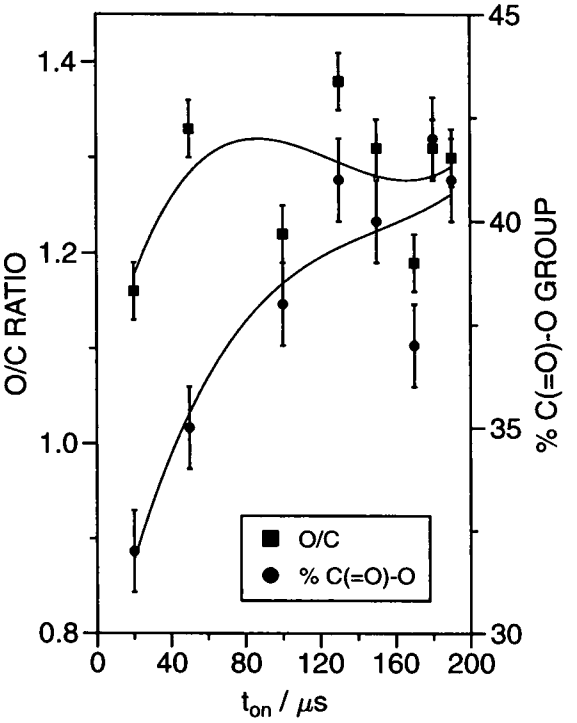

Figure 2.20: Variation in the O/C ratio and percentage C(=O)-O group of AA electrically pulsed plasma polymer with added oxygen deposited as a function of t_{on} (t_{off} = 4 ms, P_p = 5 W, AA pressure = 0.2 mbar and total pressure = 0.6 mbar).

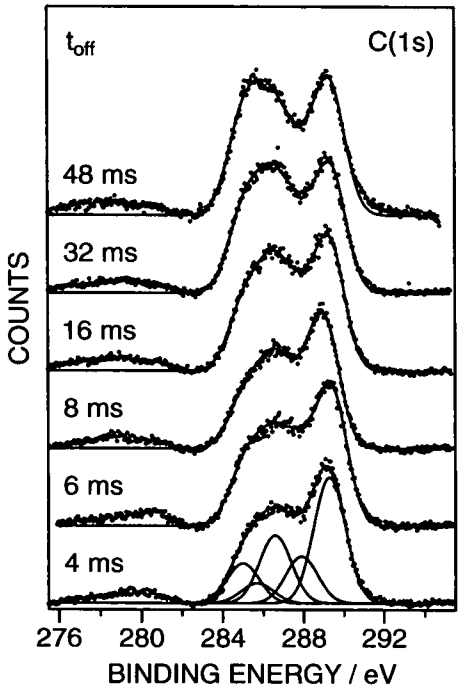

Figure 2.21: C(1s) XPS spectra of AA electrically pulsed plasma polymer with added oxygen deposited as a function of t_{off} (t_{on} = 180 μs, P_p = 5 W, AA pressure = 0.2 mbar and total pressure = 0.6 mbar).

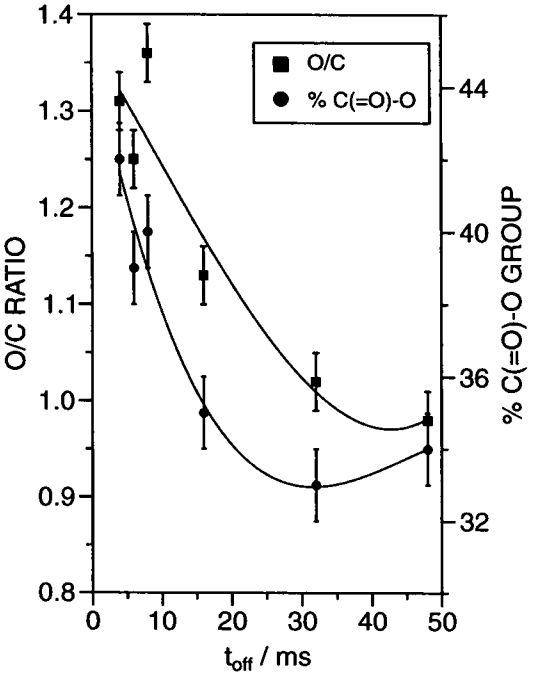

Figure 2.22: Variation in the O/C ratio and percentage C(=O)-O group of AA electrically pulsed plasma polymer with added oxygen deposited as a function of t_{off} (t_{on} = 180 μs, P_p = 5 W, AA pressure = 0.2 mbar and total pressure = 0.6 mbar).

2.3.5 CW PLASMA POLYMERISATION WITH PULSED OXYGEN INJECTION

Greater oxygen incorporation was seen with increasing gas pulse on-times during pulsed oxygen injection into a 2 W CW AA plasma, Figure 2.23. The AA pressure was first set at 0.2 mbar by adjustment of the needle valve and the flow rate was then measured (Section 2.2.2.2). Oxygen (at a pressure of 1.2 bar before the valve) was then injected into the plasma reactor via a gas pulsing valve (Section 2.2.1.5). The O/C ratio reached 0.72 ± 0.02 and the C(=O)-O group retention was 25% ± 1, Figure 2.24. Below 150 μs no evidence for added molecular oxygen could be detected. It is possible that pulses below this value are of insufficient duration to open the gas pulsing valve.[51] The deposition rate and efficiency decreased markedly on oxygen addition, Figure 2.25. After 165 μs polymer production appeared to cease and the Si(2p) XPS substrate feature was evident.

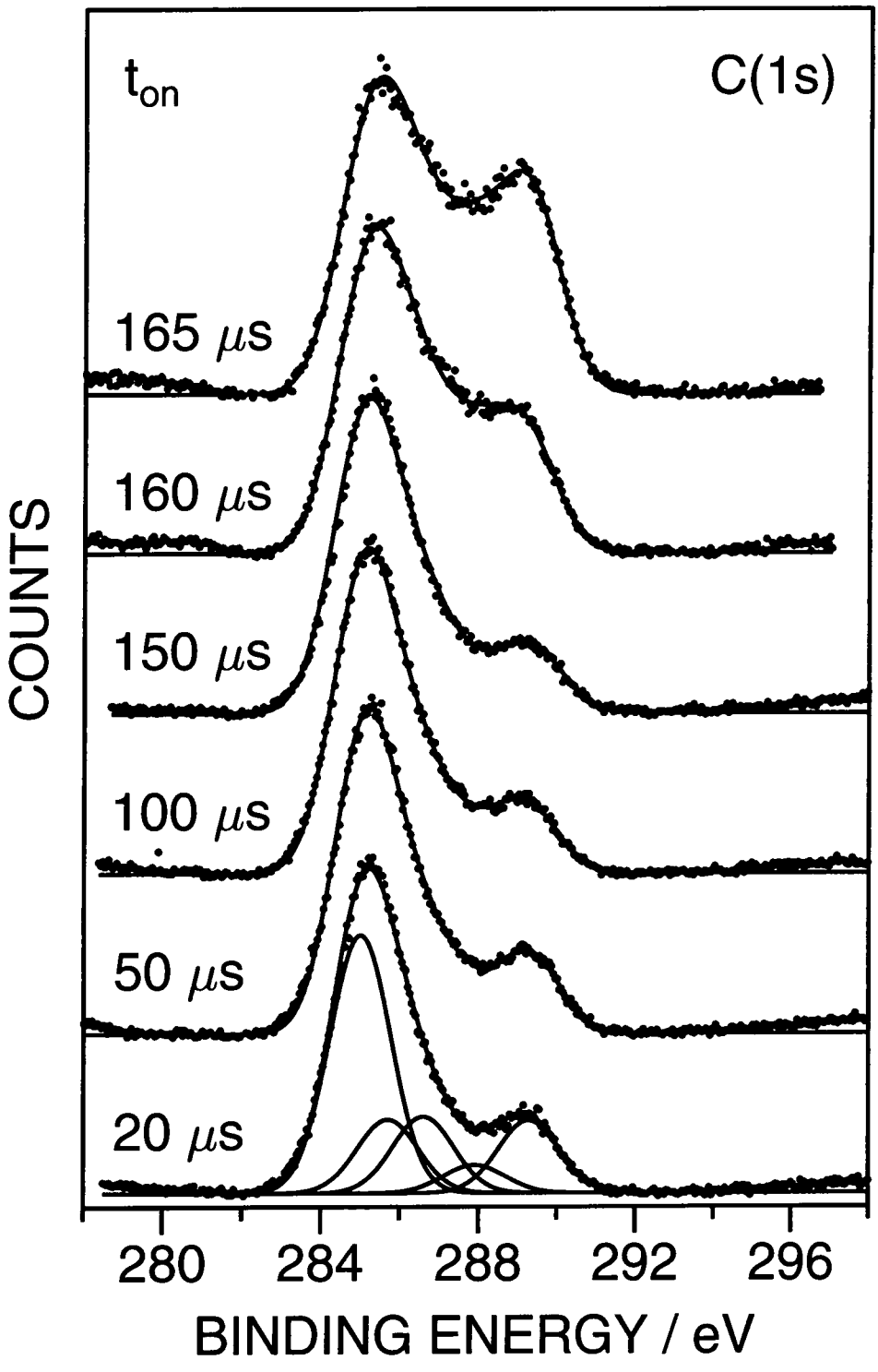

Figure 2.23: C(1s) XPS spectra of 2 W CW AA plasma polymer with pulsed oxygen injection deposited as a function of gas t_{on} (t_{off} = 4 ms).

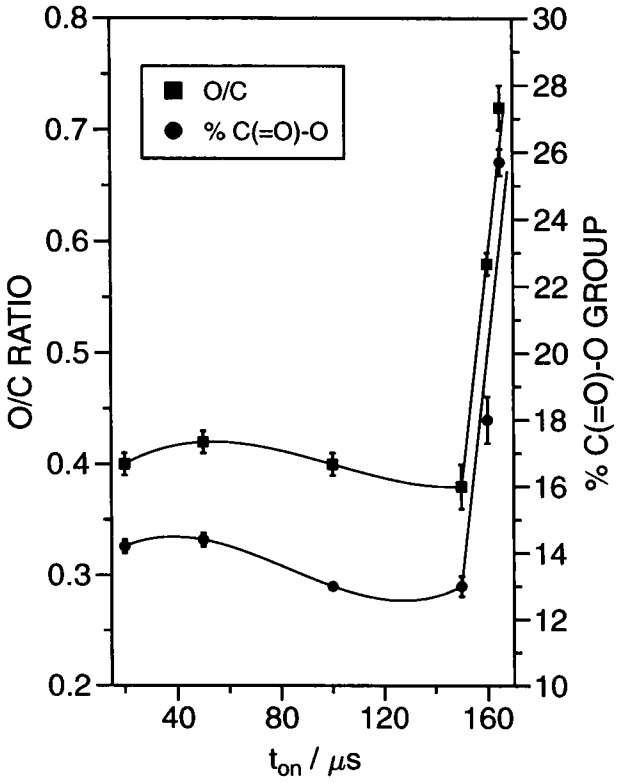

Figure 2.24: Variation in the O/C ratio and percentage C(=O)-O group as a function of oxygen gas pulse t_{on} (t_{off} = 4 ms) for 2 W CW AA plasma polymer.

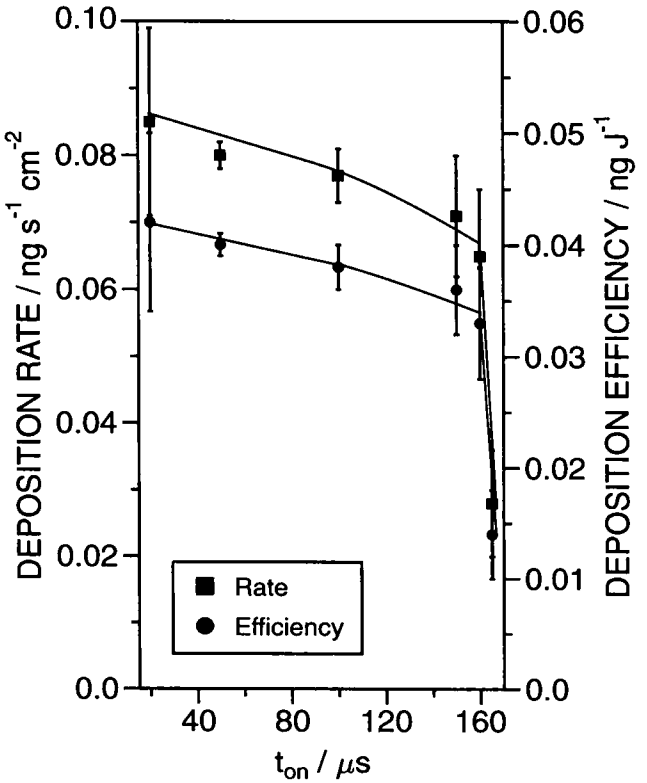

Figure 2.25: Variation in the deposition rate and deposition efficiency as a function of oxygen gas pulse t_{on} (t_{off} = 4 ms) for 2 W CW AA plasma polymer.

2.3.6 SYNCHRONISED PULSED GAS AND ELECTRICAL PLASMA POLYMERISATION

Simultaneous pulsing of various gases during electrical pulsed plasma polymerisation showed that the addition of molecular oxygen produced the most oxidation, Figure 2.26. The electrical and gas on-time was 180 μs, off-time was 4 ms and the peak power was 5 W. The simultaneous electrical and oxygen pulse on-time was found to have a large influence on the plasma polymer composition, Figure 2.27. For t_{on} values below approximately 130 μs the electrical power effect of the plasma was dominant, i.e. the influence of oxygen in the system was negligible and decreasing t_{on} increased the C(=O)-O group incorporation into the plasma polymer as noted previously. For t_{on} values greater than approximately 130 μs, the oxygen partial pressure in the system started to play an increasingly important role. The composition of the thin films changed markedly up to a maximum at approximately 175 μs electrical and gas t_{on}, where the O/C ratio was measured to be 1.00 $\pm$ 0.04 and the percentage C(=O)-O group incorporation was 43 % $\pm$ 1, Figure 2.28.

The deposition efficiency increased rapidly with decreasing duty cycle, Figure 2.29. The deposition rate displayed a similar t_{on} trend to that seen for the absence of gas reported earlier in that it passed through a maximum. However, it is interesting to note that the decrease in the deposition rate with increasing duty cycle was far more abrupt. No evidence of polymer formation was observed for on-times longer than approximately 200 μs, even though the average power was still quite modest.

Increasing the electrical and gas off-time during synchronised electrical and oxygen gas pulsed plasma polymerisation of AA decreased the functionalisation of the films produced, Figure 2.30. The O/C ratio and C(=O)-O group incorporation generally decreased as the off-time increased, Figure 2.31. This trend was opposite to that observed for the electrically pulsed polymerisation of AA and may just be a manifestation of the decrease in oxygen concentration within the plasma as the off-time was increased.

The deposition rate passed through a maximum and fell markedly with increasing duty cycle, Figure 2.32. At very low duty cycles the deposition rate decreased to a point where no polymer formation was observed. The deposition efficiency also reached a maximum, increasing as expected with decreasing duty cycle, until at very long off-times the efficiency began to decrease.

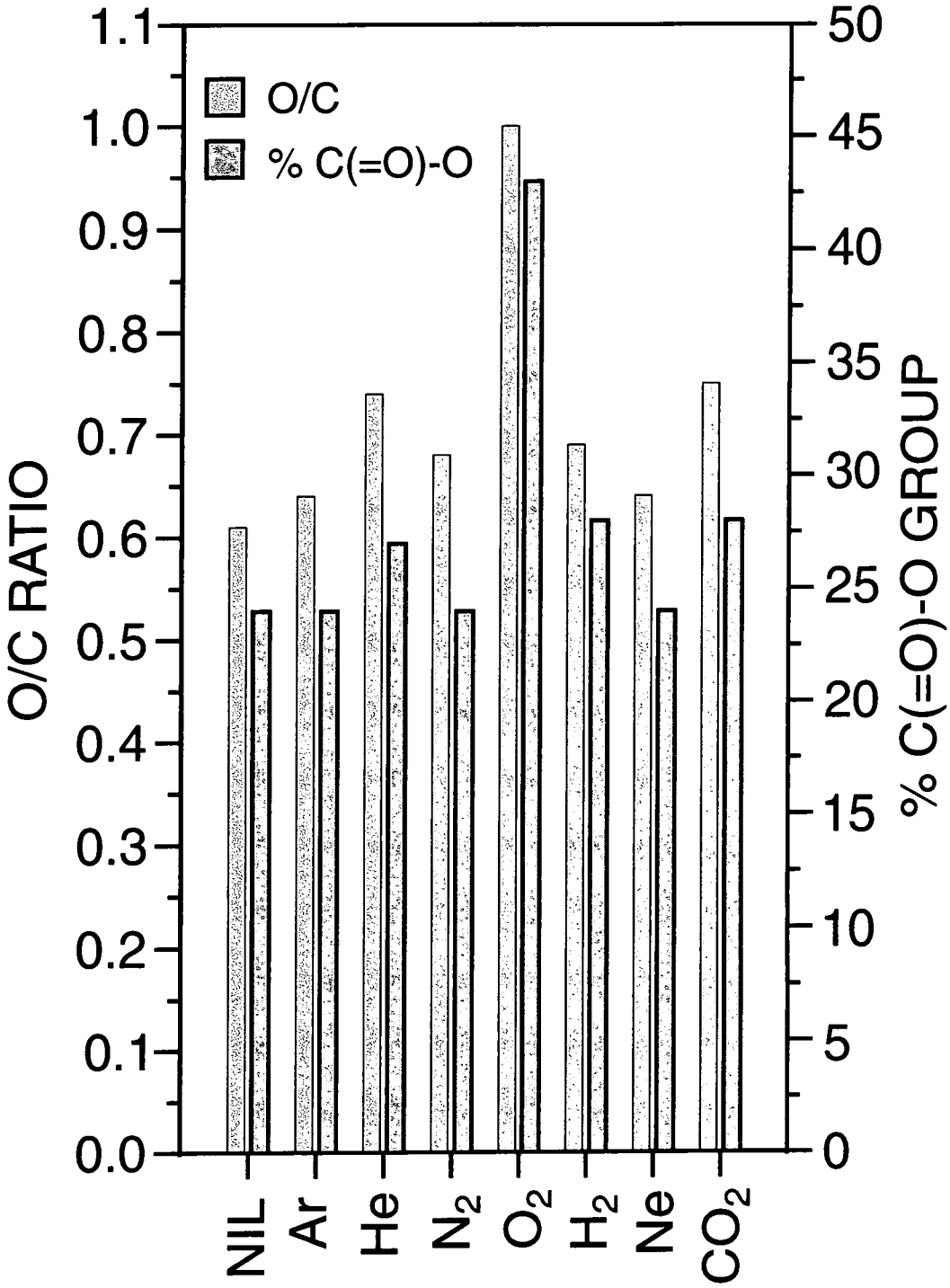

Figure 2.26: Comparison of the O/C ratio and percentage C(=O)-O group incorporation for various gases during synchronised gas and electrical pulsed AA plasma polymerisation (t_{on} = 180 μs, t_{off} = 4 ms and P_p = 5 W).

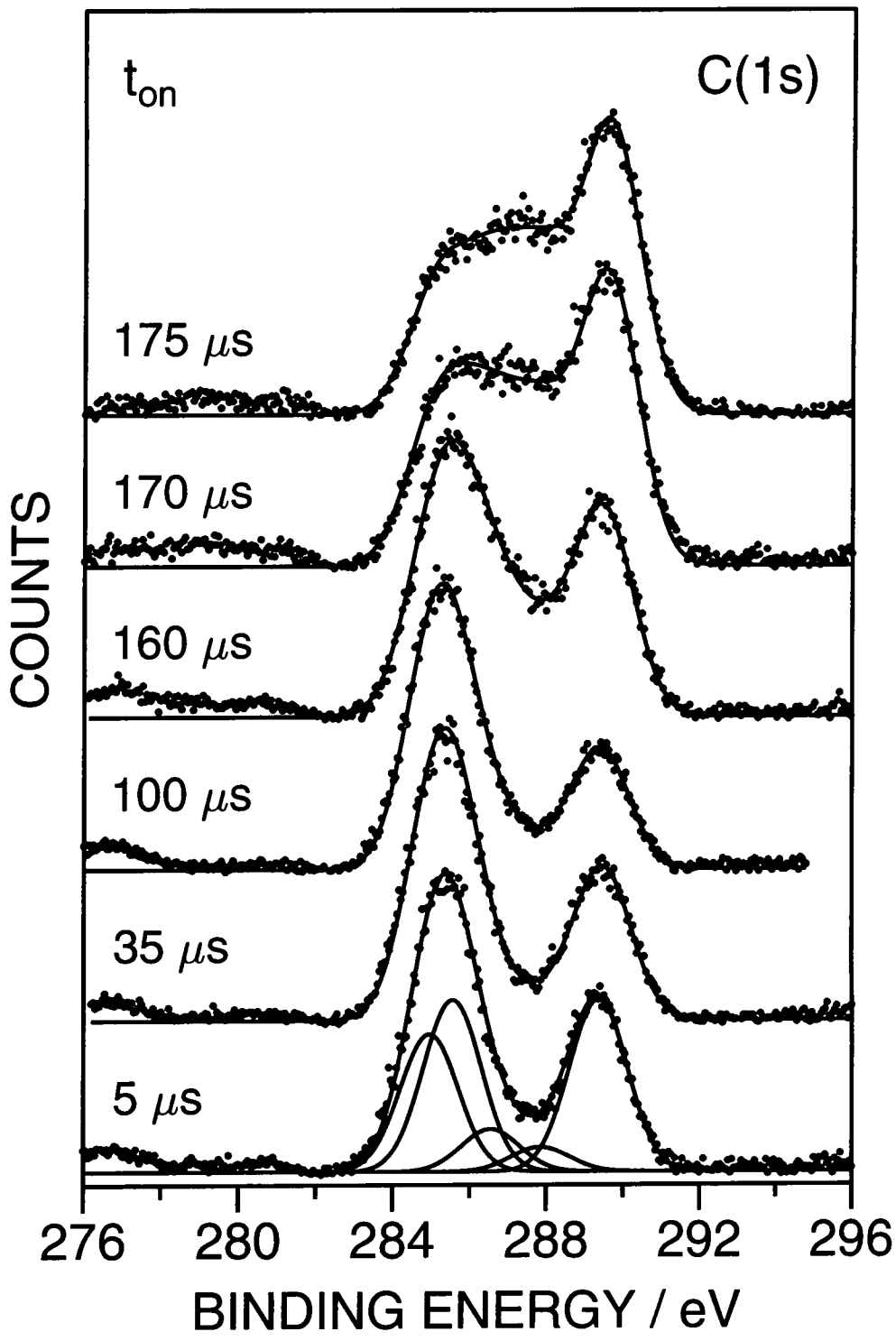

Figure 2.27: C(1s) XPS spectra of AA plasma polymer with synchronised oxygen gas and electrical pulsing deposited as a function of gas and electrical t_{on} (t_{off} = 4 ms and P_p = 5 W).

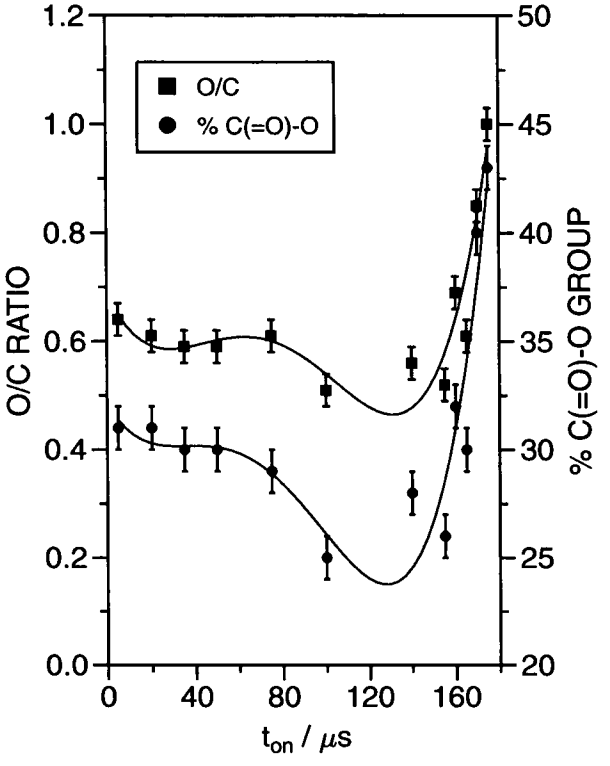

Figure 2.28: Variation in the O/C ratio and percentage C(=O)-O group as a function of synchronised oxygen gas and electrical pulse t_{on} (t_{off} = 4 ms and P_p = 5 W) for AA plasma polymer.

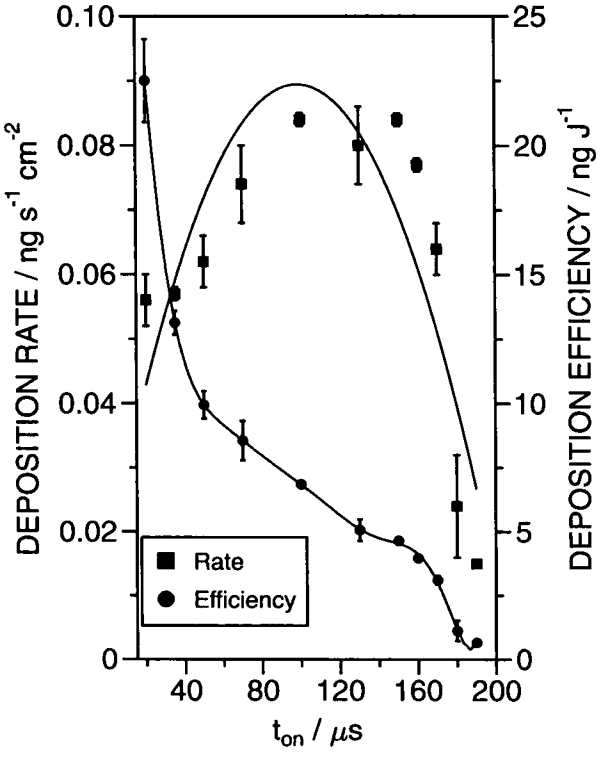

Figure 2.29: Variation in the deposition rate and deposition efficiency as a function of synchronised oxygen gas and electrical pulse t_{on} (t_{off} = 4 ms and P_p = 5 W) for AA plasma polymer.

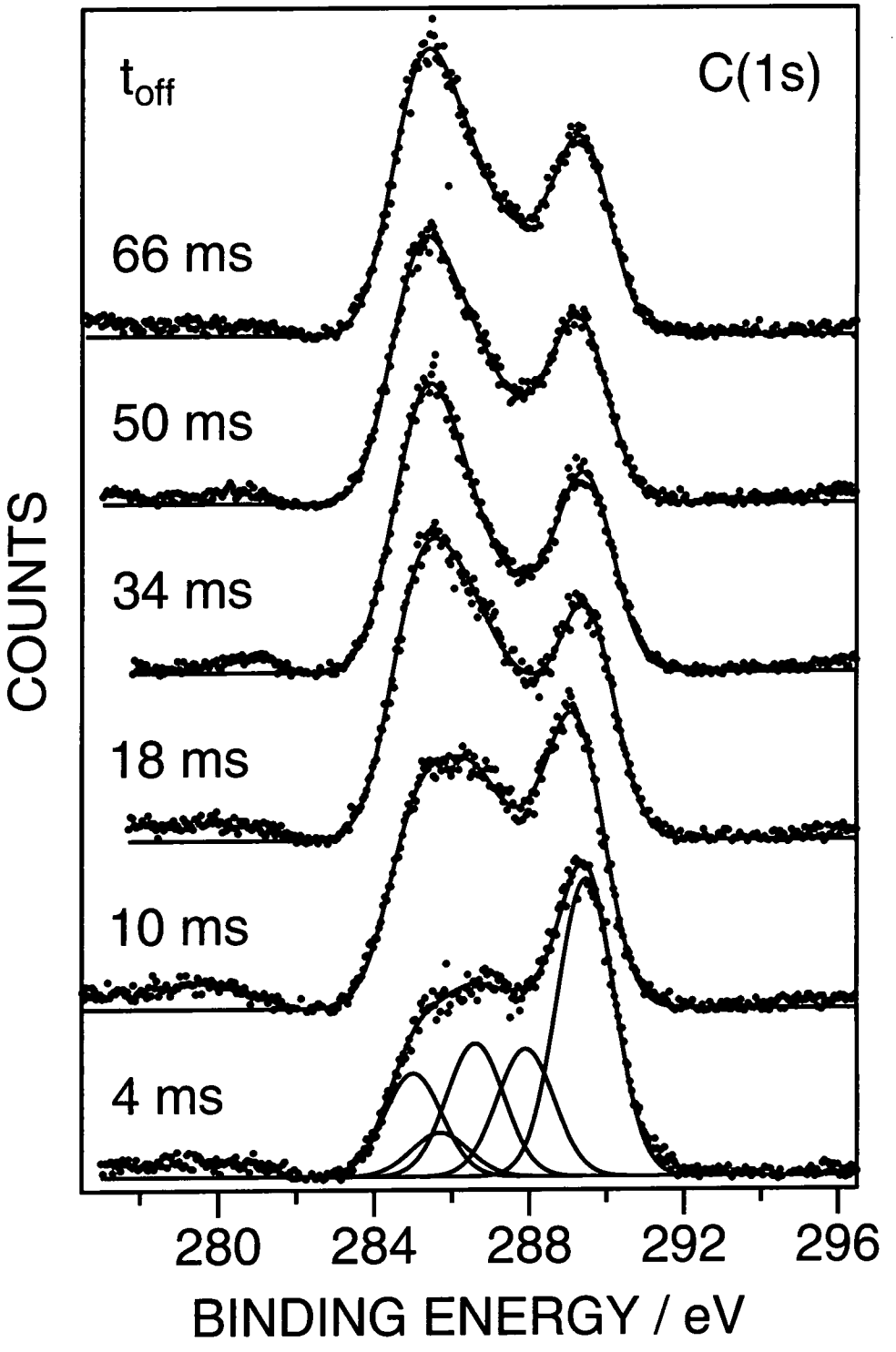

Figure 2.30: C(1s) XPS spectra of AA plasma polymer with synchronised oxygen gas and electrical pulsing deposited as a function of gas and electrical t_{off} (t_{on} = 180 μs and P_p = 5 W).

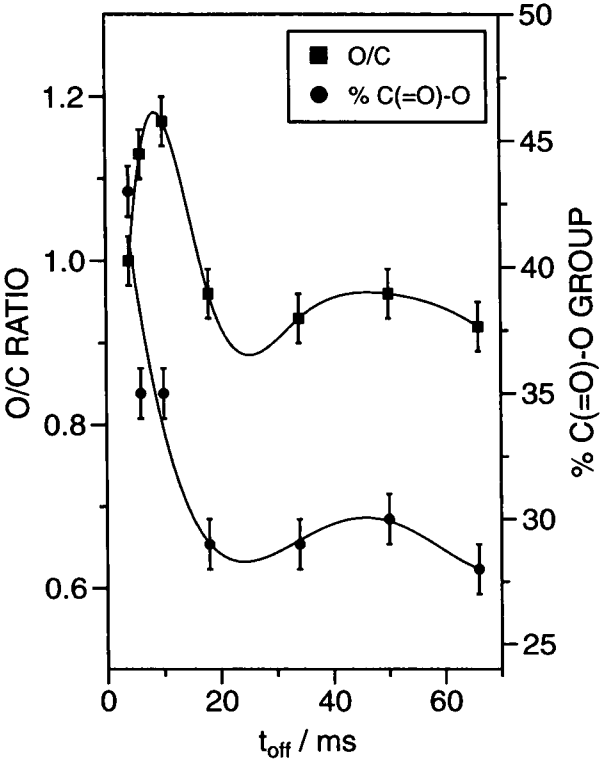

Figure 2.31: Variation in the O/C ratio and percentage C(=O)-O group as a function of synchronised oxygen gas and electrical pulse t_{off} (t_{on} = 180 μs and P_p = 5 W) for AA plasma polymer.

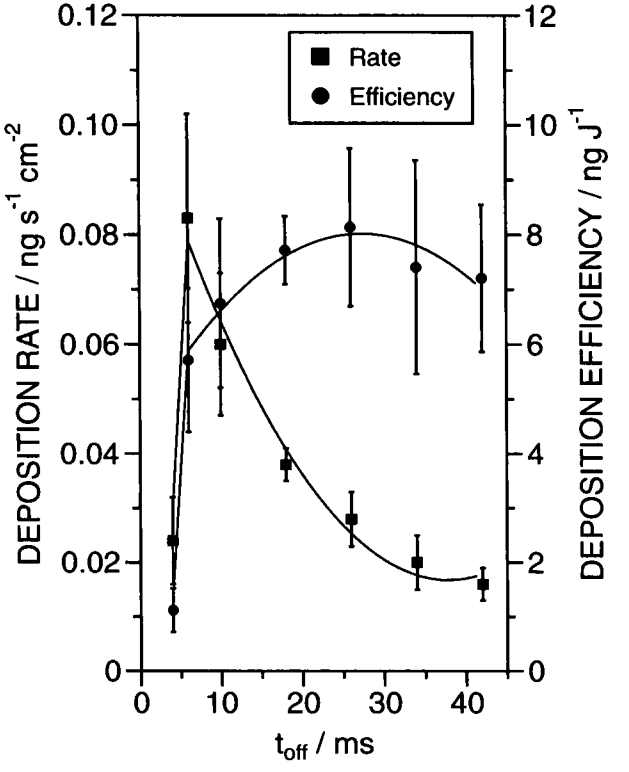

Figure 2.32: Variation in the deposition rate and deposition efficiency as a function of synchronised oxygen gas and electrical pulse t_{off} (t_{on} = 180 μs and P_p = 5 W) for AA plasma polymer.

2.3.7 FTIR RESULTS

The FTIR spectrum of the AA monomer and the AA pulsed plasma polymer were compared, Figure 2.33. The AA monomer had the following absorbencies:[60] (1) carboxylic acid O-H stretching band 3300-2500 cm^{-1}; (2) carboxylic acid C=O stretching band 1694 cm^{-1}; (3) two carbon-carbon double bond C=C stretching bands, typical of unsymmetrical conjugated alkenes, at approximately 1630 cm^{-1}; (4) O-H bending band 1431 cm^{-1}; (5) C-O stretching band doublet 1294 and 1236 cm^{-1}; and (6) O-H out-of-plane bend at approximately 920 cm^{-1}. The AA pulsed plasma polymer had the following absorbencies:[60] (7) O-H stretching band 3500-2500 cm^{-1}; (8) carbon dioxide (from the atmosphere) 2361 cm^{-1}; (9) C=O stretching band 1709 cm^{-1}; (10) O-H bending band 1450 cm^{-1}; and (11) C-O stretching band doublet at approximately 1230 cm^{-1}. Much of the fine structure in the FTIR spectrum of the monomer was lost during plasma polymerisation. The carbon-carbon double bond absorbence was absent from the plasma polymer. Absorbencies arising from the acid group were retained in the plasma polymer indicating that many of these groups were incorporated into the pulsed plasma polymer. In both spectra the C-H stretching bands were hidden beneath the O-H peak.

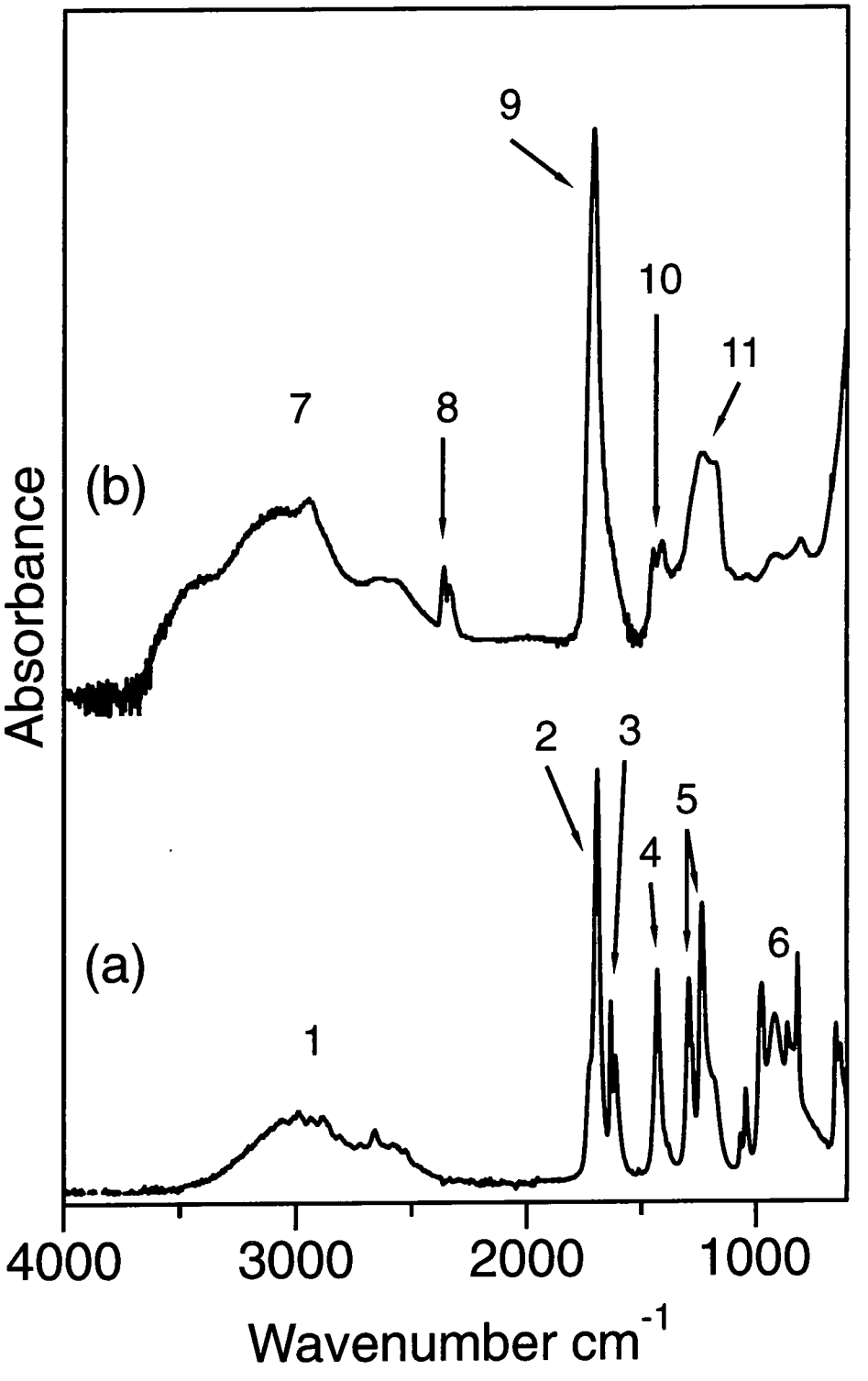

Figure 2.33: Transmission FTIR spectra of (a) AA monomer; and (b) AA pulsed plasma polymer deposited onto a NaCl plate.

2.4 DISCUSSION

Plasma polymerisation of AA produced a highly oxygenated polymeric thin film. At a constant monomer pressure and flow rate, decreasing the CW discharge power produced an XPS spectra that became progressively more like the XPS spectra of conventional poly(acrylic acid), Figure 2.4. This trend appears to be general to a number of different reactor configurations and deposition regimes.[5,34,38-40,43] This behaviour may be attributed to reduced fragmentation of the monomer molecule in the gas phase and within the growing film. The discharge power has a direct influence upon the average electron energy, the electron energy distribution and the density of excited species in the plasma.[61] Opening of the carbon-carbon double bond requires 2.74 eV as opposed to 3.61 eV for carbon-carbon single bond dissociation.[34] A drop in the number of high energy electrons with decreasing average electrical power will consequently favour polymer forming reactions over monomer fragmentation and cross-linking processes.[3] Therefore, as the discharge power is reduced, a greater number of non-fragmented precursor molecules reach the growing plasma polymer surface. It was found that increased incorporation of these non-fragmented molecules into the plasma polymer resulted in the composition of the thin film bearing a greater resemblance to the conventional poly(acrylic acid) polymer. A reduction in the number of high-energy electrons will also lower the rate of molecular excitation and thus the intensity of VUV induced damage of the growing polymeric film.[62] A corresponding reduction in plasma sheath potential (formed around the electrically isolated substrate)[3] will curtail ion induced cross-linking and sputtering of the growing polymer film.[63] Furthermore, a drop in oxygen atom concentration within the plasma, due to reduced monomer fragmentation (carbon-oxygen single bond dissociation energy 3.64 eV and carbon-oxygen double bond dissociation energy 7.55 eV),[64] will reduce atomic oxygen assisted chemical etching of the growing plasma polymer layer.

The deposition rate of the CW AA plasma polymer, measured by the quartz crystal microbalance, decreased rapidly with increasing discharge power. At low discharge powers plasma deposition was expected to have occurred under energy deficient conditions.[1] Under this regime an increase in the discharge

power would increase the deposition rate. Previously, such behaviour has been reported for the CW plasma polymerisation of AA under different deposition conditions.[5,40] The rapid decrease in deposition rate with increasing discharge power observed in this study may be attributed to an increase in etching of the plasma polymer at high powers. A possible cause of this increase in etching with discharge power is chemical etching by oxygen atoms.[7,63] Evidence has been presented which suggests that monomer fragmentation processes, which may yield reactive oxygen atoms, became more prevalent with increasing discharge power. Attack of the growing plasma polymer by oxygen atoms would yield carbon monoxide, carbon dioxide and water.[65,66] Indeed, the plasma polymers formed at the higher discharge powers were oxygen deficient, Figure 2.5. Etching of surfaces exposed to AA plasmas above 7 W was evident from the decrease in mass of the quartz crystal at higher CW powers.

Pulsing the electrical discharge on the ms-μs time scale enabled a further reduction in the average power and a significant enhancement of functional group retention was achieved. The deposition rate reached a maximum of approximately 0.1 ng s^{-1} cm^{-2} at an average power of 0.1 W. At average powers below 0.1 W deposition occurred in the power deficient regime and increased with increasing average power. Above 0.1 W the deposition rate decreased with increasing average power *vis-à-vis* the CW deposition. The deposition efficiency, which is a direct measure of the amount of polymer formed per joule of energy input, increased rapidly with decreasing average power. Film forming reactions became progressively dominant over film ablation and termination processes as the average power was reduced.[16] Furthermore, the rapid increase in deposition efficiency with decreasing duty cycle provided evidence for film forming reactions in the plasma off-time.[14,16,18] Structural retention increased with increasing plasma off-time. Chemistry occurring during the plasma off-time film growth period was more selective and film growth may have taken place through exclusive activation of the carbon-carbon double bond.[18] The increase in structural retention with decreasing plasma on-time was a result of a reduction in monomer fragmentation processes occurring during on-times. Other differences between CW and pulsed plasma deposition may have been important. The negative substrate bias built up during plasma on-times decayed rapidly once the

plasma was extinguished (<1 ms).[18] This minimised bond breaking randomisation and ablation processes by energetic cationic species being accelerated towards the growing polymeric film.[18] Furthermore, excessive heating of the substrate was avoided during low duty-cycle pulsed plasmas. Samples removed immediately from the reactor for rapid analysis following pulsed plasma polymerisation were not heated above room temperature. Cooler substrate temperatures under pulsing conditions will increase film chemistry selectivity during deposition.[18,36]

Addition of molecular oxygen to the plasma during AA deposition increased the oxygen content of the polymeric film formed. O/C ratios increased linearly with the amount of oxygen introduced into the plasma. Oxygen plasmas contain a large number of different species such as atomic oxygen (ground state), metastables, singlet oxygen O_2 ($^1\Delta_g$), a small concentration of ozone, electrons and emitted light.[61,67,68] Previous studies have shown that ground state oxygen atoms, in conjunction with vacuum ultra-violet (VUV) radiation, cause surface activation.[3,37,63,67,69,70] This combination causes extensive unselective oxidation of growing plasma polymers. The oxygen atoms produced also attack organic material.[63] Etching of polymeric material by the reactive oxygen atoms via random chain scissoring[71,72] competes with film forming processes. It was found that the deposition rate of the AA plasma polymer decreased rapidly as the concentration of oxygen in the plasma increased due to attack by atomic oxygen and VUV radiation. Above a total pressure of 0.4 mbar etching processes dominated and the mass of the quartz crystal fell.

Introduction of molecular oxygen during electrical pulsing of the AA plasma increased the oxidation of the plasma polymer. The deposition rate decreased with increased oxygen addition as before. However, at low duty cycles a greater total pressure could be achieved before the onset of plasma etching. At these higher oxygen concentrations a highly oxidised film was formed, reaching an O/C ratio of 1.36. Up to 42 percent of the carbon atoms present were in highly oxidised environments (C(=O)-O). Decreasing the plasma on-time reduced the oxidation, reflecting a decrease in the formation of reactive atomic oxygen and VUV. Increasing the plasma off-time also resulted in a decrease in the oxidation

of the polymeric films. This may be attributed to the absence of oxygen atoms during off-time polymer forming reactions.

Pulsed oxygen injection into a low power CW AA plasma produced a highly oxidised surface when the gas pulse on-time was above a certain threshold (150 μs gas on-time). The deposition rate decreased markedly above this point. On increasing the gas on-time further, the deposition rate fell rapidly and etching of the quartz crystal occurred above 165 μs. From the XPS analysis of the polymeric films formed there appeared to be little difference between constant oxygen addition and pulsed oxygen injection into the CW plasma under the experimental conditions employed.

The effect of simultaneous pulsed gas injection into an electrically pulsed AA plasma was investigated for a variety of different gases as a function of the surface oxygenation of the resultant polymeric thin film. Oxygen gas was seen to cause the greatest oxygenation. Carbon dioxide also increased the surface oxidation of the polymeric film. An increase in the surface oxidation of the AA plasma polymer was also recorded when, most notably, helium, nitrogen and hydrogen were injected into the discharge. Increased oxidation may have been due to VUV free radical formation. Previous studies have shown that significant oxidation of polyethylene and polystyrene can be achieved by a nitrogen glow discharge in the presence of oxygen gas.[73,74] The pulsed injection of oxygen gas, synchronised with electrical pulsing of the AA plasma, revealed similar trends to the pulsed injection of oxygen into a CW plasma. Below approximately 120 μs gas and electrical on-time no evidence for oxygen addition could be found. The O/C ratio and percentage C(=O)-O incorporation mirrored the trend obtained in the absence of gas pulsing. Furthermore, the deposition rate was unaffected by oxygen injection in this regime. It is believed that these short pulses are insufficient to open the gas pulsing valve.[51] Above approximately 120 μs the oxidation of the plasma polymer increased rapidly with a concomitant rapid decrease in deposition rate. Variation in the oxidation of the polymeric film during electrical and gas pulsing was recorded as a function of gas and electrical off-time. An initial increase in the O/C ratio with increasing off-time may have been due to a decrease in the etching of the polymeric film by the added oxygen

species. As the off-time increased the proportion of oxygen in the discharge decreased resulting in a reduction in the oxidation of the polymeric film. The deposition rate, after an initial jump, steadily decreased with increasing off-time. It is proposed that a decrease in oxygen atom etching, on increasing the off-time, was responsible for the initial rapid increase in deposition rate. However, deposition in this region took place according to the power deficient regime.[1] Therefore, a further decrease in the power supplied to the discharge reduced the deposition rate. The deposition efficiency increased due to off-time chemistry. At very long off-times depletion of reactive species reduced the efficiency of deposition.

2.5 CONCLUSION

The pulsed plasma polymerisation of AA produces thin films with a high degree of functional group retention. The oxidation of these films can be enhanced by the addition of molecular oxygen to the plasma. The films thus formed possess an extensively oxidised surface region as concluded from the XPS data. However, the oxidation appears to be unselective with high concentrations of several different oxygenated functionalities.

2.6 REFERENCES

1. Yasuda, H. *Plasma Polymerization*; Academic: London, 1985.
2. Rossnagel, S. M. In *Thin Film Processes II*; Vossen, J. L.; Kern, W., Eds.; Academic: London, 1991.
3. Grill, A. *Cold Plasmas in Materials Technology*; IEEE Press: New Jersey, 1994.
4. d'Agostino, R.; Favia, P.; Fracassi, F. *J. Polym. Sci.: Part A: Polymer Chemistry* **1990**, *28*, 3387.
5. Alexander, M. R.; Duc, T. M. *J. Mater. Chem.* **1998**, *8*(4), 937.
6. Clark, D. T.; Shuttleworth, D. *J. Polym. Sci.: Polym. Chem. Ed.* **1980**, *18*, 27.
7. d'Agostino, R.; Cramarossa, F.; Illuzzi, F. *J. Appl. Phys.* **1987**, *61*(8, 15 April), 2754.
8. López, G. P.; Ratner, B. D. *J. Polym. Sci.: Part A: Polymer Chemistry* **1992**, *30*, 2415.
9. López, G. P.; Ratner, B. D. *J. Appl. Polym. Sci.: Appl. Polym. Sym* **1990**, *46*, 493.
10. Yasuda, H.; Wang, C. R. *J. Polym. Sci.: Polym. Chem. Ed.* **1985**, *23*, 87.
11. Shard, A. G.; Munro, H. S.; Badyal, J. P. S. *Polym. Chem.* **1991**, *31*, 152.
12. Kim, H. Y.; Yasuda, H. K. *J. Vac. Sci. Technol. A* **1997**, *A15(4)*, 1837.
13. Timmons, R. B.; Savage, C. R. *Chem. Mater.* **1991**, *3*(4), 575.
14. Badyal, J. P. S.; Hynes, A. M. *Chem. Mater.* **1998**, *10*, 2177.
15. Llewellyn, I. P.; Rimmer, N.; Scarsbrook, G. A.; Heinecke, R. A. *Thin Solid Films* **1990**, *191*, 135.
16. Panchalingam, V.; Chen, X.; Savage, C. R.; Timmons, R. B.; Eberhart, C. *J. Appl. Polym. Sci.: Appl. Polym. Sym* **1994**, *54*, 123.
17. Panchalingham, V.; Chen, X.; Savage, C. R.; Timmons, R. B.; Huo, H.-H.; Eberhart, R. C. *ASAIO Journal* **1993**, M305.
18. Rinsch, C. L.; Chen, X.; Panchalingam, V.; Eberhart, C.; Wang, J.-H.; Timmons, R. B. *Langmuir* **1996**, *12*, 2995.
19. Chen, X.; Rajeshwar, K.; Timmons, R. B.; Chen, J.-J.; Chyan, O. M. R. *Chem. Mater.* **1996**, *8*(5), 1067.
20. Tang, L.; Wu, Y.; Timmons, R. B. *J. Biomed. Mater. Res.* **1998**, *42*, 156.
21. Han, L. M.; Timmons, R. B. *J. Polym. Sci.: Part A: Polymer Chemistry* **1998**, *36*, 3121.
22. Timmons, R. B.; Wang, J.-H. US Patent WO 97/38801, 1997.
23. Timmons, R. B.; Savage, C. R. *Abs. Pap. Am. Chem. Soc.* **1991**, *201*(2), 53.
24. Panchalingam, V.; Poon, B.; Huo, H.-H.; Savage, C. R.; Timmons, R. B.; Eberhart, R. C. *J. Biomaterials Sci.: Polym. Ed.* **1993**, *5*(1/2), 131.
25. Savage, C. R.; Timmons, R. B.; Lin, J. W. *Adv. Chemsitry Ser.* **1993**, *236*, 745.
26. Uchida, T.; Senda, K.; Vinogradov, G. K.; Morita, S. *Thin Solid Films* **1996**, *281-282*, 536.
27. Bell, A. T.; Nakajima, K.; Shen, M. *J. Appl. Polym. Sci.* **1979**, *23*, 2627.
28. Han, L. M.; Timmons, R. B. *Chem. Mater.* **1998**, *10*(5), 1422.

29. Panchalingam, V.; Chen, X.; Savage, C. R.; Timmons, R. B. *Abs. Pap. Am. Chem. Soc.* **1993**, *205*(2), 228.
30. Panchalingam, V.; Chen, X.; Savage, C. R.; Timmons, R. B. *Abs. Pap. Am. Chem. Soc.* **1992**, *204*(2), 138.
31. Ryan, M. E.; Hynes, A. M.; Badyal, J. P. S. *Chem. Mater.* **1996**, *8*, 37.
32. Anandan, C.; Mukherjee, C.; Seth, T.; Dixit, P. N.; Bhattacharyya, R. *Appl. Phys. Lett.* **1995**, *66*(1, January), 85.
33. Hashimoto, K.; Hikosaka, Y.; Hasegawa, A.; Nakamura, M. *Jpn. J. Appl. Phys., Part 1* **1996**, *35*(6A), 3363.
34. Cho, D. L.; Claesson, P. M.; Gölander, C.-G.; Johansson, K. *J. Appl. Polym. Sci.* **1990**, *41*, 1373.
35. Goldshtein, D. V.; Gilman, A. B.; Shifrina, R. R.; Potapov, V. K. *High Energy Chem.* **1991**, *25*, 303.
36. López, G. P.; Chilkoti, A.; Briggs, D.; Ratner, B. D. *J. Polym. Sci.: Part A: Polymer Chemistry* **1992**, *30*, 2427.
37. Gölander, C.-G.; Lassen, B.; Nilssonekdahl, K.; Nilsson, U. R. *J. Biomaterials Sci.: Polym. Ed.* **1992**, *4*(1), 25.
38. Ko, T. M.; Cooper, S. L. *J. Appl. Polym. Sci.* **1993**, *47*, 1601.
39. Cho, D. L.; Ekengren, Ö. *J. Appl. Polym. Sci.* **1993**, *47*, 2125.
40. O'Toole, L.; Beck, A. J.; Ameen, A. P.; Jones, F. R.; Short, R. D. *J. Chem. Soc. Faraday Trans.* **1995**, *91*(21), 3907.
41. Beck, A. J.; O'Toole, L.; Short, R. D.; Ameen, A. P.; Jones, F. R. *J. Chem. Soc., Chem. Commun.* **1995**, *10*, 1053.
42. O'Toole, L.; Beck, A. J.; Short, R. D. *Macromolecules* **1996**, *29*(15), 5172.
43. Candan, S.; Beck, A. J.; O'Toole, L.; Short, R. D. *J. Vac. Sci. Technol. A* **1998**, *16*(3), 1702.
44. Beck, A. J.; France, R. M.; Leeson, A. M.; Short, R. D.; Goodyear, A.; Braithwaite, N. St. J. *Chem. Commun.* **1998**, 1221.
45. Lassen, B.; Malmsten, M. *J. Mater. Sci. Mater. Med.* **1994**, *5*, 662.
46. Carlsson, C. M. G.; Johansson, K. S. *Surface and Interface Analysis* **1993**, *20*, 441.
47. Novis, Y.; Chtaïb, M.; Caudano, R. *Brit. Polym. J.* **1989**, *21*(2), 171.
48. Yasuda, H.; Hsu, T. *J. Polym. Sci.: Polym. Chem. Ed.* **1977**, *15*, 81.
49. Alexander, M. R.; Short, R. D.; Jones, F. R.; Stollenwerk, M.; Michaeli, W.; Blomfield, C. J. Determination of the Structure of HMDSO / O2 Plasma Deposits Using High Resolution XPS; 43rd AVS National Symposuim, Philadephia.
50. Barrow, G. M. *Physical Chemistry*, 5th ed.; McGraw-Hill: London, 1988.
51. Gibson, D. W.; Parker Hannifin Corporation. Private Communication.
52. General Valve Corporation. Iota One Operating Manual and Set-up Instructions.
53. Ehrlich, C. D.; Basford, J. A. *J. Vac. Sci. Technol. A* **1992**, *10(1)*, 1.
54. Chapman, B. *Glow Discharge Processes*; John Wiley & Sons: Chichester, 1980.
55. Wagner, C. D.; Riggs, W. M.; Davis, L. E.; Moulder, J. F.; Muilenber, G. E. *Handbook of X-Ray Photoelectron Spectroscopy*; Perkin-Elmer: New York, 1978.
56. Kronos, I. *QM-300 Series Film Thickness Monitor*; Operation & Service Manual: California, 1971.

57. Evans, J. F.; Gibson, J. H.; Moulder, J.F.; Hammond, J. S.; Goretzki, H.; Fresenius, Z. *Anal. Chemie.* **1984**, *319*, 841.
58. Beamson, G.; Briggs, D. *High Resolution XPS of Organic Polymers, The Scienta ESCA 300 Database*; John Wiley & Sons: Chichester, 1992.
59. Chilkoti, A.; Ratner, B. D.; Briggs, D. *Chem. Mater.* **1991**, *3*(1), 51.
60. Wilson, M. D.; Whitesides, G. M. *J. Am. Chem. Soc.* **1988**, *110*, 8718.
61. McTaggart, F. K. *Plasma Chemistry in Electrical Discharges*; Elsevier Publishing Company: London, 1967.
62. Hudis, M.; Prescott, L. E. *Polym. Lett.* **1972**, *10*, 179.
63. Flamm, D. L. In *Plasma Etching: An Introduction*; Manos, D. M.; Flamm, D. L., Eds.; Academic Press, Inc.: London, 1989; pp. 91-184.
64. Smith, E. B. *Basic Chemical Thermodynamics*, 4th ed.; Clarendon Press: Oxford, 1992.
65. Bernacki, S. E.; Kosicki, B. B. *J. Electrochem. Soc.* **1984**, *131*(8, August), 1926.
66. Mayoux, C.; Antoniou, A.; Ai, B.; Lacoste, R. *Eur. Polym. J.* **1973**, *9*, 1069.
67. Hollahan, J. R.; Bell, A. T., Eds. *Techniques and Applications of Plasma Chemistry*; Wiley: New York, 1974.
68. Hollahan, J. R. *J. Chem. Ed.* **1966**, *43*, A401.
69. Hopkins, J.; Wheale, S. H.; Badyal, J. P. S. *J. Phys. Chem.* **1996**, *100*, 14062.
70. Cook, J. M.; Benson, B. W. *J. Electrochem. Soc.* **1983**, *130*(12, December), 2459.
71. Wu, B. J.; Hess, D. W.; Soong, D. S.; Bell, A. T. *J. Appl. Phys.* **1993**, *54*(4, April), 1725.
72. Harada, K. *J. Appl. Polym. Sci.* **1981**, *26*, 3395.
73. Shard, A. G.; Badyal, J. P. S. *Polymer Communications* **1991**, *32*, 217.
74. Badyal, J. P. S.; Shard, A. G. *J. Phys. Chem.* **1991**, *95*, 9436.

CHAPTER THREE

SURFACE ATTACHMENT OF FLUOROSURFACTANT MOLECULES

3.1 INTRODUCTION

Polyelectrolytes (PE) can spontaneously interact with oppositely charged surfactants in aqueous solution to produce PE-surfactant complexes.[1] These systems have been extensively studied as a function of many parameters including surfactant tail length,[2-7] nature of the PE,[6-11] density of charges along the PE backbone,[3,9,10,12,13] solution pH[6] and the incorporation of low molecular weight electrolytes.[2,3,6,13-16] Electrostatic attraction between the oppositely charged constituents and interactions between long chain surfactant tails can lead to a highly cooperative binding process and stabilisation of the PE-surfactant complex.[2,3,14,15,17-21] Complexes formed in solution between polyelectrolyte and low concentrations of surfactant can exist in a 'string of pearls' type morphology with micelle like surfactant aggregates adsorbed along the polymer chain.[12,22-24] Such PE-surfactant complexes readily precipitate from water according to a strict 1:1 stoichiometry corresponding to overall charge balance.[1,25,26] In the solid phase these materials tend to display a layered arrangement attributed to demixing of the polar PE backbone and the hydrophobic surfactant tails. The precise structure is governed by a number of factors such as relative volume fractions of ionic and alkyl phases and the molecular geometry of the surfactant molecules.[25] Examples of PE-surfactant complexes with cubic, lamellar and cylindrical morphologies are well known.[1,25,26] These materials are becoming of significant technological interest. For example, PE-fluorosurfactant complexes are potential candidates for ultra-low surface energy applications such as water-repellent fabrics, self-lubricating machine parts, and other non-stick end-uses.[27]

Rather than making the whole PE-surfactant complex in solution, followed by precipitation, a more direct approach comprising coupling surfactants to pre-coated polyelectrolyte plasma polymer surfaces is presented. A major benefit of plasma polymerisation is that a wide range of substrate materials can be employed irrespective of their chemical nature, shape or topography.[28,29] The complexation of a cationic fluorosurfactant (Structure 3.1) with highly functionalised acrylic acid (AA) plasma polymer thin films has been investigated

using XPS and contact angle analysis. Of particular interest is the liquid repellency of these surface PE-fluorosurfactant complexes.

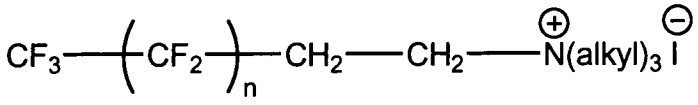

Structure 3.1: Fluorinated Surfactant Molecule.

The structure of the fluorinated surfactant consisted of a trialkyl ammonium ion head group separated by an ethylene spacer from the fluorinated tail.

3.2 EXPERIMENTAL

3.2.1 PULSED PLASMA POLYMERISATION

The experimental apparatus and procedure for pulsed plasma depositions has been described previously (Chapter 2). All pulsed plasma polymerisations were carried out using the monomers AA (Aldrich, 99% purity) or 6-Heptenoic acid (Aldrich, 99% purity). Monomers were further purified with multiple freeze-thaw cycles. After cleaning, the reactor was pumped to base pressure and AA monomer vapour was introduced to a pressure of 0.2 mbar and an approximate flow rate of 5×10^{-6} mol s^{-1}. Under these flow conditions the purity of AA vapour in the reactor was better than 99.9%. 6-Heptenoic acid has a low vapour pressure and was therefore introduced at a pressure of 0.05 mbar with an approximated flow rate of 2×10^{-8} mol s^{-1}. The percentage of monomer in the reactor under these conditions was 95%, the remaining gas being due to air leaks. All plasma polymers were deposited onto ultrasonically cleaned glass substrates under electrical pulsing conditions of 20 μs on-time, 4 ms off-time and 5 W peak-power. The pulsed electrical discharge was maintained for 30 minutes before the rf was switched off. Prior to removing the coated substrates the monomer vapour was purged through the reactor for a further 2 minutes.

3.2.2 AQUEOUS PHASE REACTION OF PULSED PLASMA POLYMERS

Following pulsed plasma polymerisation the coated substrates were immersed in a series of aqueous solutions according to several experimental protocols. Protocol 1, neutralisation of AA groups: pulsed plasma polymerised AA was placed in 1 M sodium hydroxide (NaOH) aqueous solution for varying lengths of time and dried under vacuum. These samples were either characterised using XPS or used in Protocol 2. Protocol 2, treatment with cationic trialkyl ammonium fluorosurfactant ($CF_3(CF_2)_nC_2H_5(alkyl)_3N^+$ Structure 3.1, supplied by Clariant GmbH, trade name Fluowet® NMQ, information about the length of the fluorinated segment was not given): samples neutralised according to Protocol 1 or untreated AA plasma polymer coated substrates were placed into an aqueous solution of $CF_3(CF_2)_nC_2H_5(alkyl)_3N^+$ (10% concentration) for 1 hour. Following surfactant treatment the samples were rinsed in high purity water (B.S. 3978 grade 1) for 10 minutes and dried under vacuum. The samples were then characterised using XPS. Several glass slides were coated on both sides with the AA pulsed plasma polymer and then treated with $CF_3(CF_2)_nC_2H_5(alkyl)_3N^+$ as described above. These samples were then analysed using DCA. Protocol 3, treatment with a second cationic fluorosurfactant ($R_f$alkylN^+R_3 Structure 3.2, supplied by DuPont, trade name Zonyl® FSD, details of the structure of this fluorosurfactant are proprietary): AA pulsed plasma polymer coated substrates were placed into an aqueous solution of $R_f$alkylN^+R_3 (10% concentration) for 1 hour. Following surfactant treatment the samples were rinsed in high purity water for 10 minutes and dried under vacuum. Samples were then characterised using XPS.

$$R_f(C_nH_{2n})_x(alkyl)_3N^{\oplus}\ Cl^{\ominus}$$

Structure 3.2: Zonyl® Cationic Fluorosurfactant.

Protocol 4, treatment of 6-heptenoic acid pulsed plasma polymer with $CF_3(CF_2)_nC_2H_5(alkyl)_3N^+$: 6-heptenoic acid pulsed plasma polymer coated

substrates were placed into an aqueous solution of $CF_3(CF_2)_nC_2H_5(alkyl)_3N^+$ for 1 hour. Following surfactant treatment the samples were rinsed in high purity water for 10 minutes and dried under vacuum. Samples were then characterised using XPS. Protocol 5, treatment with amphoteric fluorosurfactant: AA pulsed plasma polymer coated substrates were placed into an aqueous solution of amphoteric fluorosurfactant $R_f(C_nH_{2n})_x(alkyl)_2N^+\text{-}O^-$ for 1 hour. Following surfactant treatment the samples were rinsed in high purity water for 10 minutes and dried under vacuum. Samples were then characterised using XPS and VCA.

3.2.3 CONVENTIONAL COMPLEX FORMATION

Conventional PE-fluorosurfactant complexes were produced following the procedure outlined in the literature.[27] The poly(acrylic acid)-$CF_3(CF_2)_nC_2H_5(alkyl)_3N^+$ complex precipitated readily from aqueous solution on addition of $CF_3(CF_2)_nC_2H_5(alkyl)_3N^+$ to neutralised poly(acrylic acid) solution. Following further purification with pure water a white gel like material was formed. This precipitate was dissolved in methanol and solvent cast onto a glass substrate. The poly(acrylic acid)-$R_f$alkylN^+R_3 complex was also readily precipitated from aqueous solution on addition of $R_f$alkylN^+R_3 to neutralised poly(acrylic acid) solution. The precipitate, further purified with pure water, was a clear, sticky gel like material. This complex was only sparingly soluble in methanol. However, a sufficient quantity of the complex was solvent cast to completely cover a glass substrate (proven by the absence of a Si(2p) signal in the XPS spectra).

3.2.4 SAMPLE CHARACTERISATION

3.2.4.1 XPS Characterisation

A Vacuum Generators ESCA Lab Mk. II photoelectron spectrometer equipped with an unmonochromated X-ray source (Mg $K\alpha_{1,2}$ = 1253.6 eV) was used for chemical characterisation of the samples. Photoelectrons were collected at a

30° take-off angle from substrate normal and energy filtered by a concentric hemispherical analyser (CHA) operating in constant analyser energy mode (CAE = 20 eV). The spectrometer was calibrated with respect to the gold $4f_{7/2}$ and silver $3d_{5/2}$ peaks at 83.8 and 368.3 eV respectively.[31] Elemental sensitivity factors were determined experimentally relative to the carbon 1s (C(1s)) peak (285.0 eV) using standard compounds. These were taken as F(1s) : Na(1s) : C(1s) : O(1s) : N(1s) : Si(2p) = 0.24 : 0.17 : 1.00 : 0.39 : 0.65 : 1.00 respectively. The absence of any Si(2p) XPS feature following plasma polymerisation was indicative of complete coverage of the glass substrate.

3.2.4.2 DCA Characterisation

Dynamic contact angle characterisation (DCA) was performed on samples to assess the liquid repellency of the fluorinated surfaces formed (Section 1.8.5). Thin glass slides (area 24 mm^2) were coated on both sides with plasma polymer and treated with fluorosurfactant as described above (Section 3.2.2). These samples were placed into the DCA apparatus (CAHN Dynamic Contact Angle Analyzer DCA-322) suspended from the microbalance via a lightweight clip. The sample was allowed five minutes to equilibrate before analysis commenced. Two test liquids (high purity water, B.S. 3978 grade 1 and hexadecane, Aldrich, 99% purity) were moved over the sample at a rate of 154 $\mu m\ s^{-1}$ until a sample submersion depth of 12 mm was reached. At this point the motorised stage paused for 60 seconds before the liquid was removed at the same rate.

3.2.4.3 VCA Characterisation

Due to the technical difficulties in preparing samples coated on both sides the wettability of many of the samples was investigated using the sessile drop technique (Section 1.8.4) employing video contact angle (VCA) apparatus (Instruments S.A. Video Contact Angle System, VCA 2500XE). A known volume of the test liquid, high purity water (B.S. 3978 grade 1) or hexadecane (Aldrich, 99% purity), was dispensed through a motorised micro-syringe and brought into

contact with the surface of the sample. The contact angle of the liquid was calculated by analysis of the shape of the droplet on the sample surface.

3.3 RESULTS

3.3.1 NEUTRALISATION OF AA PLASMA POLYMER

AA plasma polymer was deposited onto glass slides under the electrical pulsing conditions of 20 μs on-time, 4 ms off-time and 5 W peak power for 30 minutes. The highly functionalised surfaces produced were placed into 1 M NaOH solution for varying lengths of time to neutralise the surface carboxylic acid groups. The slides were subsequently dried under vacuum prior to XPS analysis. The elemental composition of the neutralised AA plasma polymers is tabulated below as a function of time in the basic solution, Table 3.1.

Time / s	% Na	% C	% N	% O	% Si
0	0	61	0	29	0
1	6	63	0	29	2
10	6	61	1	28	4
30	9	59	1	30	1
60	10	61	1	27	1
600	9	60	1	28	1
1800	9	60	1	29	1
3600	8	62	1	27	2
21600	6	72	1	22	0

Table 3.1: Elemental composition of NaOH treated AA plasma polymer.

Sodium was detected after only a brief immersion in the NaOH solution. Sodium levels rapidly reached a plateau of approximately 10% before decreasing. The maximum amount of sodium incorporated was approximately half of the anticipated value if all C(=O)-O groups detected by XPS were neutralised by the NaOH solution. It is possible that a proportion of the C(=O)-O groups detected by XPS may have been ester groups or that the neutralisation reaction did not reach completion. Furthermore, the solution may have failed to penetrate the plasma polymer completely over the sampling depth. A further point to note is that silicon from the glass substrate was detected in the majority of samples investigated. This may indicate that the plasma polymer was partially soluble in the basic solution or that low molecular weight material was lost from the surface in solution. Indeed, CW AA plasma polymer was completely removed from the glass substrate on rinsing in aqueous media whereas pulsed plasma derived coatings were more stable.

3.3.2 ADDITION OF CATIONIC FLUOROSURFACTANT

AA pulsed plasma polymer neutralised with 1 M NaOH solution for 30 minutes, as described above, was placed into $CF_3(CF_2)_nC_2H_5(alkyl)_3N^+$ solution for 1 hour, rinsed in pure water for 10 minutes, dried under vacuum and analysed using XPS. The C(1s) XPS envelope of the surfactant treated AA plasma polymer layer was fitted to several different carbon functionalities:[32] C_xH_y (285.0 eV); C-C(=O)-O or C-CF_n (285.7 eV); C-O (286.6 eV); O-C-O, C=O or C-F (287.9 eV); C(=O)-O or CF-CF_n (289.0 eV); CF_2 (291.2 eV); and CF_3 (293.3 eV). Due to the large number of overlapping C(1s) peaks only the CF_2 and the CF_3 functionalities could be identified unambiguously. The CF_2 peak was therefore used as a reference offset. Detection of these fluorinated functionalities provided direct evidence for the surface attachment of surfactant molecules to the AA plasma polymer, Figure 3.1. The percentage of carbon atoms in the CF_2 and CF_3 chemical environments was calculated to be 27% ± 2 and 5% ± 2 respectively. The elemental composition of the surface region of the surfactant treated AA pulsed plasma polymer indicated that surfactant molecules were attached to the

plasma polymer, Table 3.2. A small amount of sodium was detected, suggesting that not all of the acid salt groups in the sampling depth had reacted with the surfactant. The cationic surfactant counterion iodine was not detected.

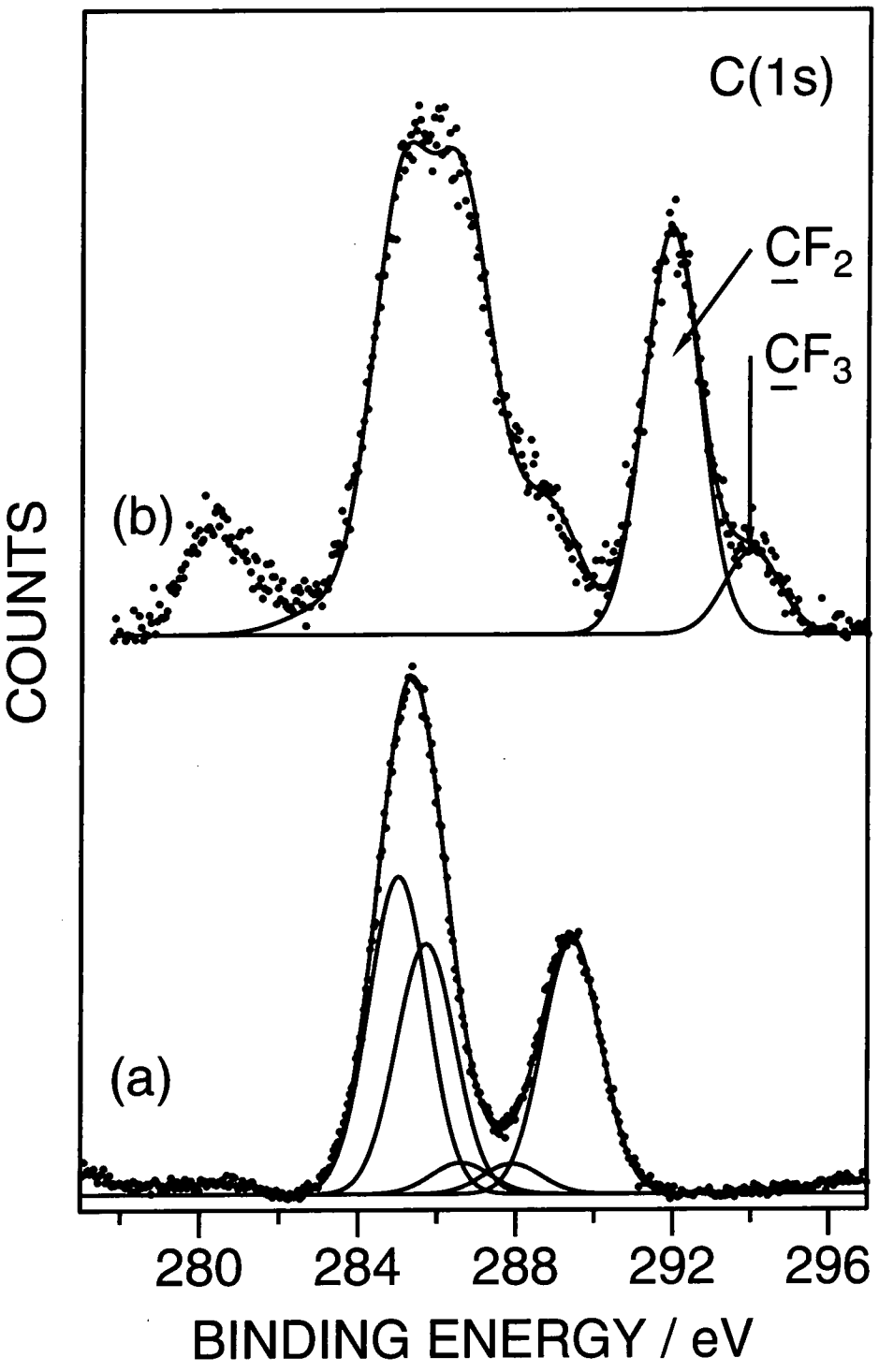

Figure 3.1: C(1s) XPS spectra of (a) AA pulsed plasma polymer (t_{on} = 20 μs, t_{off} = 4 ms, P_p = 5 W); and (b) AA pulsed plasma polymer neutralised with 1 M NaOH solution and treated with $CF_3(CF_2)_nC_2H_5(alkyl)_3N^+$.

Sample	% F	% Na	% C	% N	% O	% Si
AA plasma polymer	0	0	61	0	29	0
NaOH treated	0	9	60	1	28	1
Surfactant treated	37	1	48	1	12	1

Table 3.2: Elemental composition of AA plasma polymer (t_{on} = 20 µs, t_{off} = 4 ms, P_p = 5 W), NaOH treated plasma polymer and surfactant treated neutralised plasma polymer.

3.3.3 DIRECT REACTION OF AA PULSED PLASMA POLYMER WITH CATIONIC FLUOROSURFACTANT

Further investigation into the coupling of surfactant to the AA pulsed plasma surface revealed that similar results could be obtained without the intermediate NaOH neutralisation step. AA pulsed plasma polymer was deposited onto glass substrates (t_{on} = 20 µs, t_{off} = 4 ms, P_p = 5 W, 30 minutes deposition time) and placed directly into an aqueous solution of $CF_3(CF_2)_nC_2H_5(alkyl)_3N^+$. After 1 hour the samples were removed, rinsed for 10 minutes in pure water and dried under vacuum. XPS analysis revealed that a highly fluorinated surface was again produced indicating that fluorinated surfactant was attached to the AA pulsed plasma polymer, Table 3.3.

Sample	% F	% C	% N	% O	% Si
plasma polymer	0	61	0	29	0
Surfactant treated	41	44	3	12	0

Table 3.3: Elemental composition of AA plasma polymer (t_{on} = 20 µs, t_{off} = 4 ms, P_p = 5 W) and $CF_3(CF_2)_nC_2H_5(alkyl)_3N^+$ treated AA plasma polymer.

The C(1s) high resolution XPS spectra of surfactant treated AA pulsed plasma polymer resembled the surface produced from the neutralised surfactant treated plasma polymer, Figure 3.2. Carbon functionalities were fitted to the C(1s) envelope as described in Section 3.3.2 but, again, only the $\underline{C}F_2$ and the $\underline{C}F_3$ peaks could be unambiguously identified. The percentage of carbon atoms in the $\underline{C}F_2$ and $\underline{C}F_3$ chemical environments was calculated to be 29% ± 2 and 7% ± 1 respectively.

3.3.4 ADDITION OF $R_f$alkylN^+R_3 TO AA PULSED PLASMA POLYMER

A second cationic fluorosurfactant, $R_f$alkylN^+R_3, was found to attach to the AA pulsed plasma polymer surface. AA pulsed plasma polymer was deposited onto glass substrates (t_{on} = 20 µs, t_{off} = 4 ms, P_p = 5 W, 30 minutes deposition time) and placed directly into an aqueous solution of $R_f$alkylN^+R_3. After 1 hour the samples were removed, rinsed for 10 minutes in pure water and dried under vacuum. XPS analysis revealed that a highly fluorinated surface was produced indicating that the fluorinated surfactant was attached to the AA pulsed plasma polymer, Table 3.4.

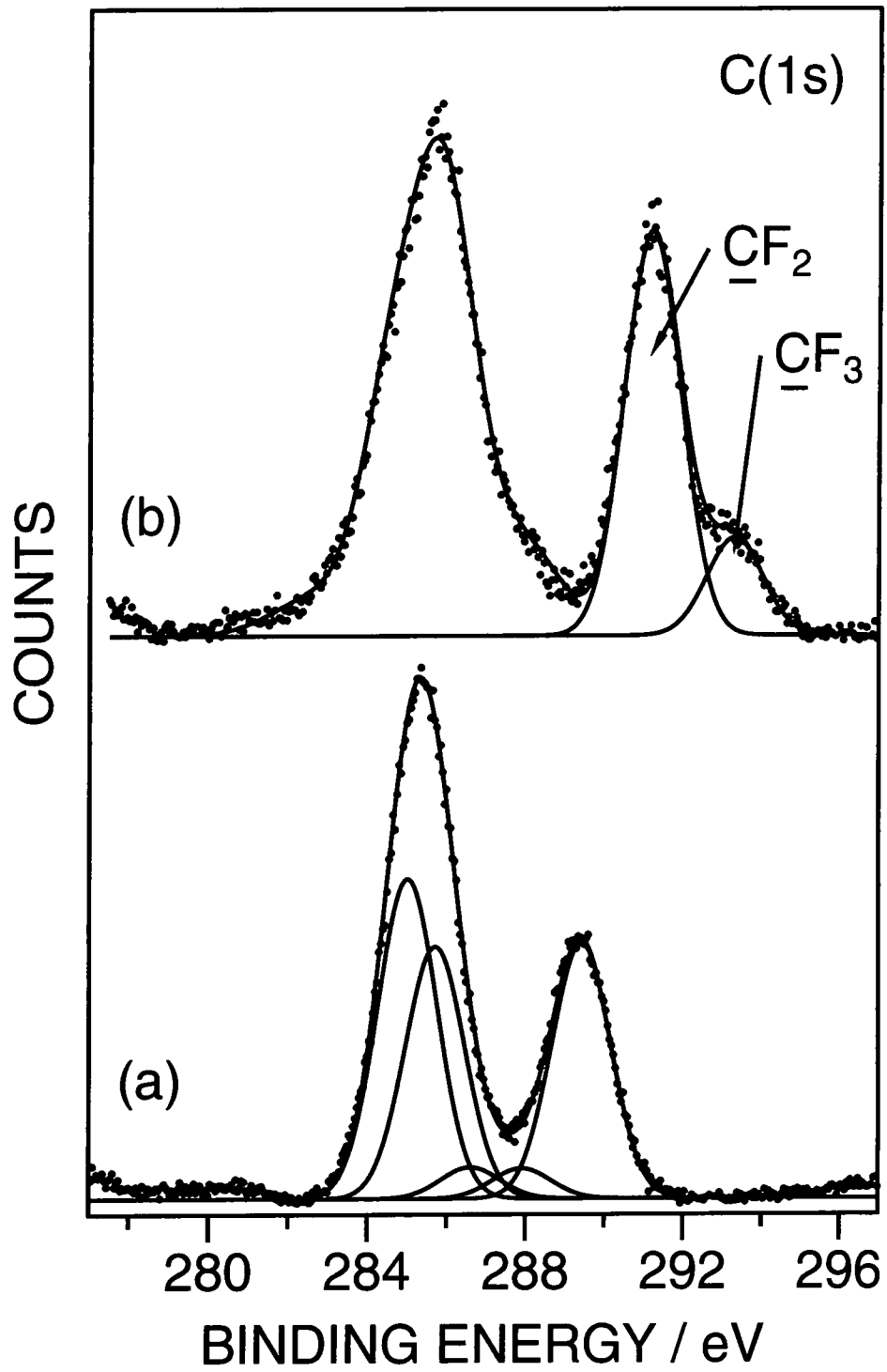

Figure 3.2: C(1s) XPS spectra of (a) AA pulsed plasma polymer (t_{on} = 20 μs, t_{off} = 4 ms, P_p = 5 W); and (b) AA pulsed plasma polymer treated with $CF_3(CF_2)_nC_2H_5(alkyl)_3N^+$.

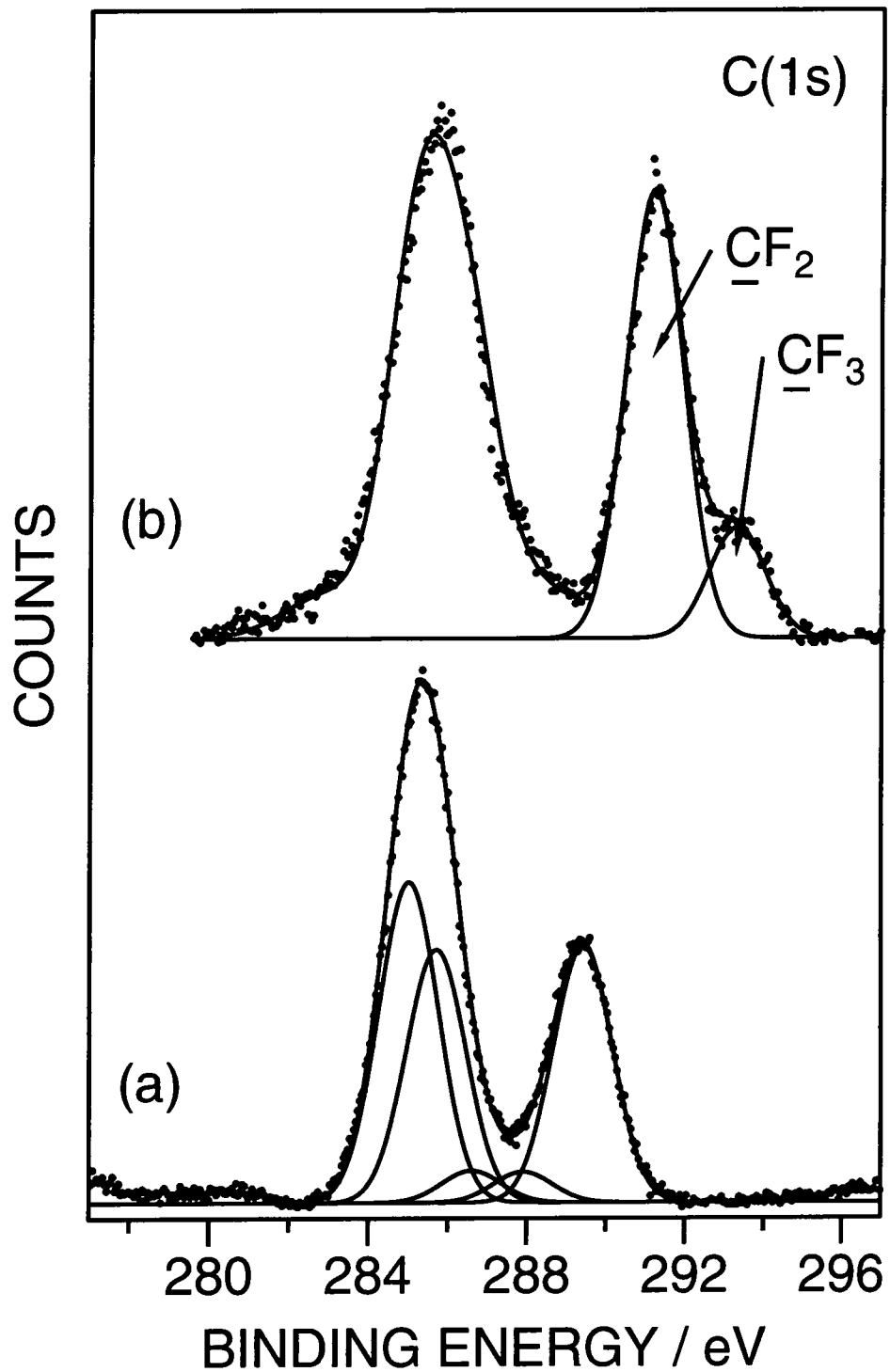

Figure 3.3: C(1s) XPS spectra of (a) AA pulsed plasma polymer (t_{on} = 20 μs, t_{off} = 4 ms, P_p = 5 W); and (b) AA pulsed plasma polymer treated with $R_f$alkylN^+R_3.

Sample	% F	% C	% N	% O	% Si
plasma polymer	0	61	0	29	0
$R_f$alkylN^+R_3 treated	43	45	3	10	0

Table 3.4: Elemental composition of AA plasma polymer (t_{on} = 20 µs, t_{off} = 4 ms, P_p = 5 W) and $R_f$alkylN^+R_3 treated plasma polymer.

The C(1s) high resolution XPS spectra of $R_f$alkylN^+R_3 treated AA pulsed plasma polymer again demonstrated a high percentage of fluorinated carbon environments, Figure 3.3. Carbon functionalities were fitted to the C(1s) envelope as described earlier (Section 3.3.2) but, as before, only the $\underline{C}F_2$ and the $\underline{C}F_3$ peaks could be unambiguously identified. The percentage of carbon atoms in the $\underline{C}F_2$ and $\underline{C}F_3$ chemical environments was calculated to be 33% ± 2 and 8% ± 1 respectively.

3.3.5 CONVENTIONAL COMPLEX FORMATION

The conventional complexes, poly(acrylic acid)-$CF_3(CF_2)_nC_2H_5(alkyl)_3N^+$ and poly(acrylic acid)-$R_f$alkylN^+R_3, solvent cast onto glass slides were analysed by XPS and the surface region elemental composition was calculated, Table 3.5.

Complex	% F	% C	% N	% O	% Si
PAA-$CF_3(CF_2)_nC_2H_5(alkyl)_3N^+$	40	49	2	9	0
PAA-$R_f$alkylN^+R_3	48	44	2	6	0

Table 3.5: Elemental composition of PAA-$CF_3(CF_2)_nC_2H_5(alkyl)_3N^+$ and PAA-$R_f$alkylN^+R_3 solvent cast complex.

The surface region elemental composition of the conventionally produced complexes was similar to the surfactant treated AA pulsed plasma polymer surface. Counterions were not detected in the complexes indicating that a one-to-one stoichiometry with respect to charges has been achieved. High resolution C(1s) XPS spectra of the conventional complex resembled the C(1s) spectra for the AA pulsed plasma polymer surfactant treated surface, Figure 3.4. The percentage of carbon atoms in the $\underline{C}F_2$ and $\underline{C}F_3$ chemical environments was calculated to be 25% ± 1 and 6% ± 1 respectively for the PAA-$CF_3(CF_2)_nC_2H_5(alkyl)_3N^+$ conventional complex and 41% ± 1 and 8% ± 1 respectively for the PAA-$R_f alkyl N^+R_3$ conventional complex.

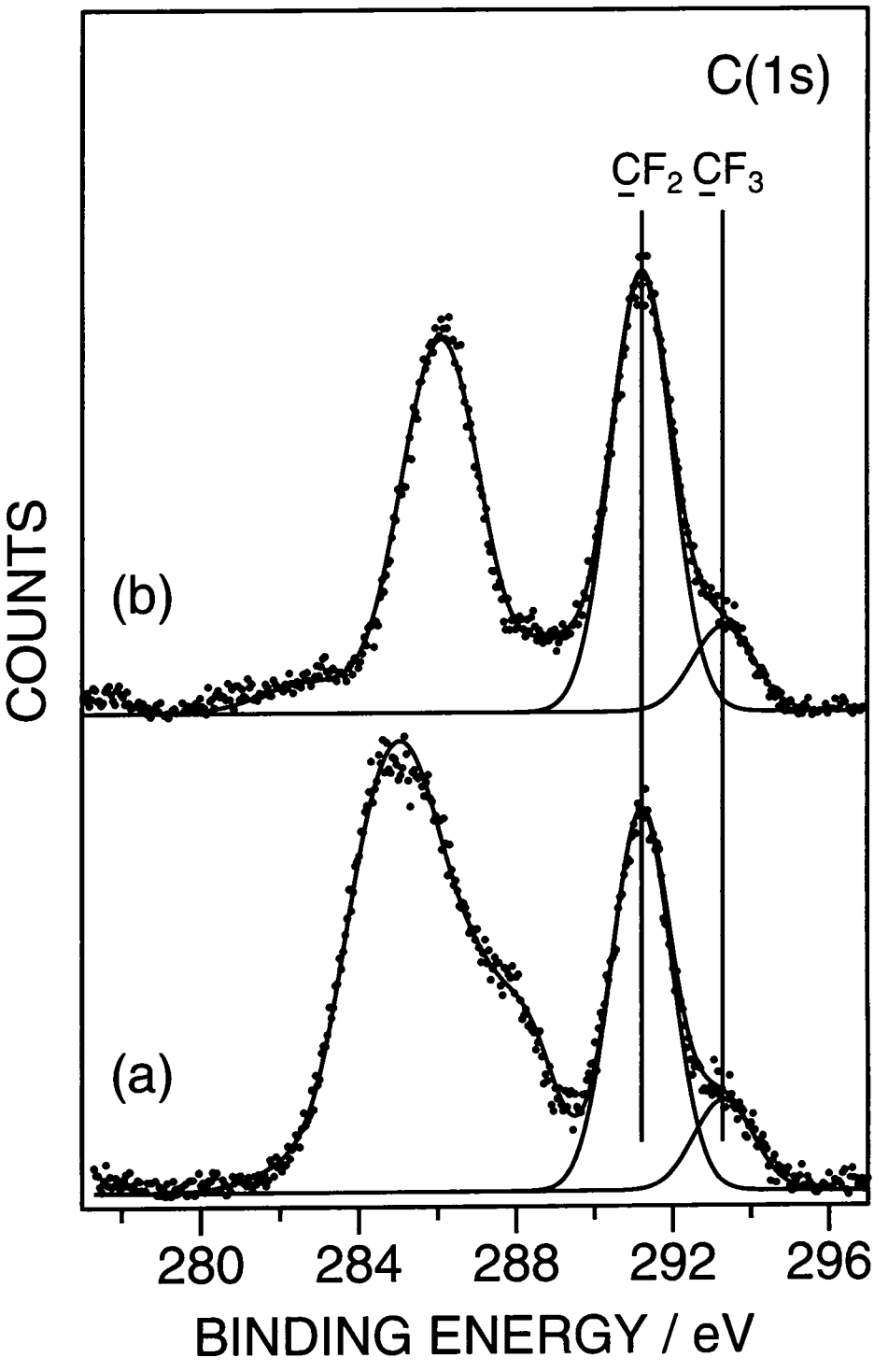

Figure 3.4: C(1s) XPS spectra of (a) PAA-$CF_3(CF_2)_nC_2H_5(alkyl)_3N^+$ conventional solvent cast complex; and (b) PAA-$R_f$alkylN^+R_3 conventional solvent cast complex.

3.3.6 DCA ANALYSIS OF $CF_3(CF_2)_nC_2H_5(alkyl)_3N^+$ TREATED AA PULSED PLASMA POLYMER

The wettability of AA pulsed plasma polymer deposited onto both sides of a glass slide treated with $CF_3(CF_2)_nC_2H_5(alkyl)_3N^+$ was investigated using the DCA apparatus, Table 3.6. Two test liquids were employed, high purity water and hexadecane. DCA analysis enabled both the advancing and receding contact angles to be measured; i.e. the amount of contact angle hysteresis was found.

Sample		Advancing CA	Receding CA	Difference
AA pulsed plasma polymer	Water	39°± 3	37° ± 2	2
	Hexadecane	15° ± 2	14° ± 2	1
plasma polymer with $CF_3(CF_2)_nC_2H_5(alkyl)_3N^+$	Water	64° ± 7	64° ± 3	0
	Hexadecane	102° ± 1	28° ± 3	74
PAA-$CF_3(CF_2)_nC_2H_5(alkyl)_3N^+$ conventional complex	Water	103° ± 1	62° ± 1	41
	Hexadecane	75° ± 3	46° ± 7	29
Solvent cast PAA with $CF_3(CF_2)_nC_2H_5(alkyl)_3N^+$	Water	59° ± 2	51° ± 1	8
	Hexadecane	75° ± 1	57° ± 2	18
Glass slide treated with $CF_3(CF_2)_nC_2H_5(alkyl)_3N^+$	Water	89° ± 1	36° ± 3	53
	Hexadecane	68° ± 5	56° ± 5	12

Table 3.6: Contact angles of conventional and plasma polymerised AA-fluorosurfactant complexes.

It can be seen that the advancing contact angle with both water and hexadecane for the AA pulsed plasma polymer increased on treatment with $CF_3(CF_2)_nC_2H_5(alkyl)_3N^+$. This is consistent with the fluorinated character of the

surface.[33] It is also noteworthy that the advancing contact angle of the surfactant treated AA pulsed plasma polymer was higher for hexadecane than water. This behaviour was unexpected as hexadecane has a lower surface tension than water[34] and should therefore have been harder to repel.[33] The untreated AA pulsed plasma polymer displayed little hysteresis. However, the surfactant treated AA plasma polymer displayed a large hysteresis with hexadecane. The conventionally produced poly(acrylic acid)-$CF_3(CF_2)_nC_2H_5(alkyl)_3N^+$ complex possessed a high advancing contact angle with water and hexadecane in line with the expected behaviour.[27] However, the receding contact angles displayed some hysteresis with both the water and hexadecane test liquids.

Poly(acrylic acid) dissolved in methanol was solvent cast onto both sides of a glass slide for DCA analysis. This sample was then treated with the $CF_3(CF_2)_nC_2H_5(alkyl)_3N^+$ surfactant solution. The complex formed displayed a similar trend to the AA pulsed plasma polymer treated with $CF_3(CF_2)_nC_2H_5(alkyl)_3N^+$, although not to the same extent. The advancing contact angle with hexadecane was again larger than the water contact angle. A hysteresis was evident but it was not as pronounced as in the plasma polymer case. A surfactant treated glass slide was also analysed as a control. Results indicated that some fluorinated surfactant was attached to the glass slide but the water contact angle possessed a large hysteresis.

3.3.7 PULSED PLASMA POLYMERISATION OF 6-HEPTENOIC ACID

To investigate the influence of the concentration of surface acid groups on the surface attachment of $CF_3(CF_2)_nC_2H_5(alkyl)_3N^+$, 6-heptenoic acid was used as the monomer for plasma polymerisation. In theory, the dependence of the surfactant attachment on the density of acid groups could easily be evaluated by altering the pulsing conditions of the AA plasma polymerisation (Chapter 2). However, in practice it was found that only AA pulsed plasma polymers produced under lower duty cycles were stable under the surfactant treatment conditions. Pulsed plasma polymers formed with larger duty cycles were more readily dissolved in the aqueous solution.

Pulsed plasma polymerisation of 6-heptenoic acid was performed under the standard electrical pulsing conditions employed in the above study (t_{on} = 20 μs, t_{off} = 4 ms, P_p = 5 W, 30 minutes deposition time). XPS analysis of the pulsed plasma polymer revealed that the oxygen incorporation and percentage C(=O)-O group detected were much lower than for the AA plasma polymer deposited under similar conditions, Table 3.7, and 3.8. The difference is rationalised by consideration of the monomer structure, Structure 3.3.

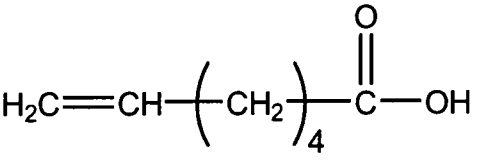

Structure 3.3: 6-Heptenoic acid.

Plasma Polymer	% C	% N	% O	% Si
AA	61 ± 1	0	29 ± 1	0
6-Heptenoic acid	78 ± 1	0	22 ± 1	0
Theoretical	78	0	22	0

Table 3.7: Elemental composition of AA and 6-Heptenoic acid pulsed plasma polymer (t_{on} = 20 μs, t_{off} = 4 ms, P_p = 5 W).

Plasma Polymer	% $\underline{C}_xH_y$	% $\underline{C}$-C(=O)-O	% $\underline{C}$-O	% $\underline{C}$=O / O-$\underline{C}$-O	% $\underline{C}$(=O)-$\underline{O}$
AA	37 ± 1	30 ± 1	2 ± 1	1 ± 1	30 ± 1
6-Heptenoic acid	71 ± 1	13 ± 1	2 ± 1	1 ± 1	13 ± 1
Theoretical	71	14	0	0	14

Table 3.8: Composition of AA and 6-Heptenoic acid pulsed plasma polymer (t_{on} = 20 µs, t_{off} = 4 ms, P_p = 5 W).

The 6-Heptenoic acid pulsed plasma polymer deposited onto glass substrates was treated with $CF_3(CF_2)_nC_2H_5(alkyl)_3N^+$ solution using the procedure outlined above (Section 3.2.2). XPS analysis revealed that a highly fluorinated surface was produced which indicated that fluorinated surfactant was attached to the 6-heptenoic acid pulsed plasma polymer surface, Table 3.9.

Sample	% F	% C	% N	% O	% Si
6-Heptenoic acid pulsed plasma polymer	0	78 ± 1	0	22 ± 1	0
plasma polymer-$CF_3(CF_2)_nC_2H_5(alkyl)_3N^+$	42 ± 1	44 ± 2	3 ± 1	12 ± 2	0

Table 3.9: Elemental composition of 6-Heptenoic acid pulsed plasma polymer (t_{on} = 20 µs, t_{off} = 4 ms, P_p = 5 W) treated with $CF_3(CF_2)_nC_2H_5(alkyl)_3N^+$.

Consideration of the C(1s) XPS spectra of the surfactant treated 6-heptenoic acid pulsed plasma polymer surface region demonstrated that the surface produced resembled the surfactant treated AA pulsed plasma polymer surface, Figure 3.5. The percentage $\underline{C}F_2$ and $\underline{C}F_3$ incorporation was 32% ± 1 and 7% ± 1

respectively which compares favourably to that found for the AA pulsed plasma polymer.

3.3.8 REACTION OF AA PULSED PLASMA POLYMER WITH AMPHOTERIC FLUOROSURFACTANT

The AA pulsed plasma polymer was placed in an aqueous solution of amphoteric fluorosurfactant $R_f(C_nH_{2n})_x(alkyl)_2N^+\text{-}O^-$ for 1 hour, rinsed in pure water for 10 minutes and dried under vacuum. The surfaces formed were analysed using XPS, Table 3.10, and VCA.

Sample	% F	% C	% N	% O	% Si
plasma polymer-$R_f(C_nH_{2n})_x(alkyl)_2N^+\text{-}O^-$	49	43	3	6	0

Table 3.10: Elemental composition of AA pulsed plasma polymer (t_{on} = 20 µs, t_{off} = 4 ms, P_p = 5 W) treated with fluorosurfactant $R_f(C_nH_{2n})_x(alkyl)_2N^+\text{-}O^-$.

A highly fluorinated surface was again formed which indicated that the surfactant had been attached to the AA pulsed plasma polymer. Fitting of the C(1s) spectra allowed calculation of the percentage of carbon atoms in the $\underline{C}F_2$ and $\underline{C}F_3$ chemical environments which were 37% ± 2 and 8% ± 2 respectively, Figure 3.6. VCA analysis was performed using two test liquids, water and hexadecane. The contact angles measured for water and hexadecane were 56° ± 4 and 88° ± 2 respectively. Once more the surface appeared to repel hexadecane to a greater extent than water.

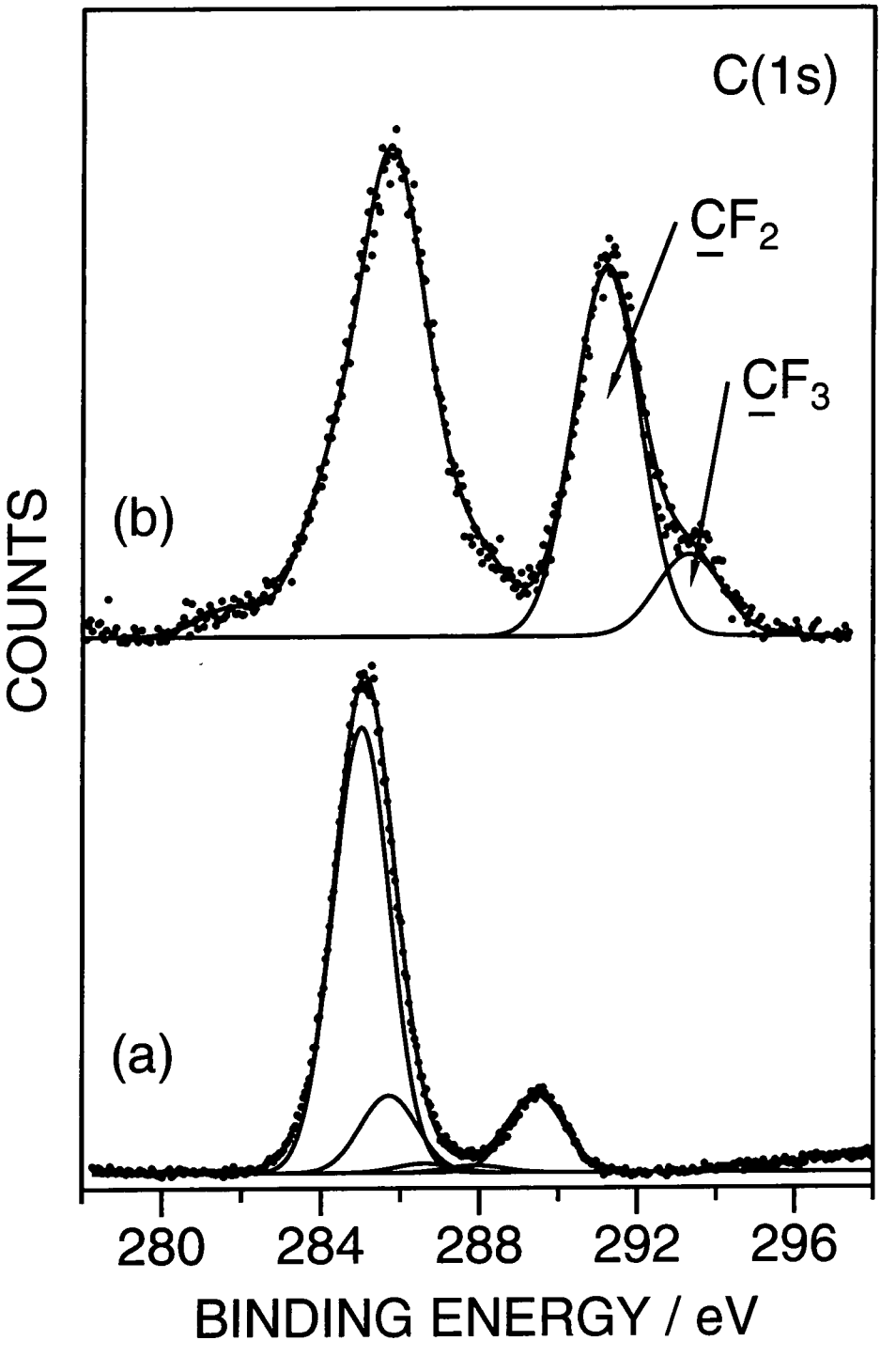

Figure 3.5: C(1s) XPS spectra of (a) 6-Heptenoic acid pulsed plasma polymer (t_{on} = 20 μs, t_{off} = 4 ms, P_p = 5 W); and (b) 6-Heptenoic acid pulsed plasma polymer treated with $CF_3(CF_2)_nC_2H_5(alkyl)_3N^+$.

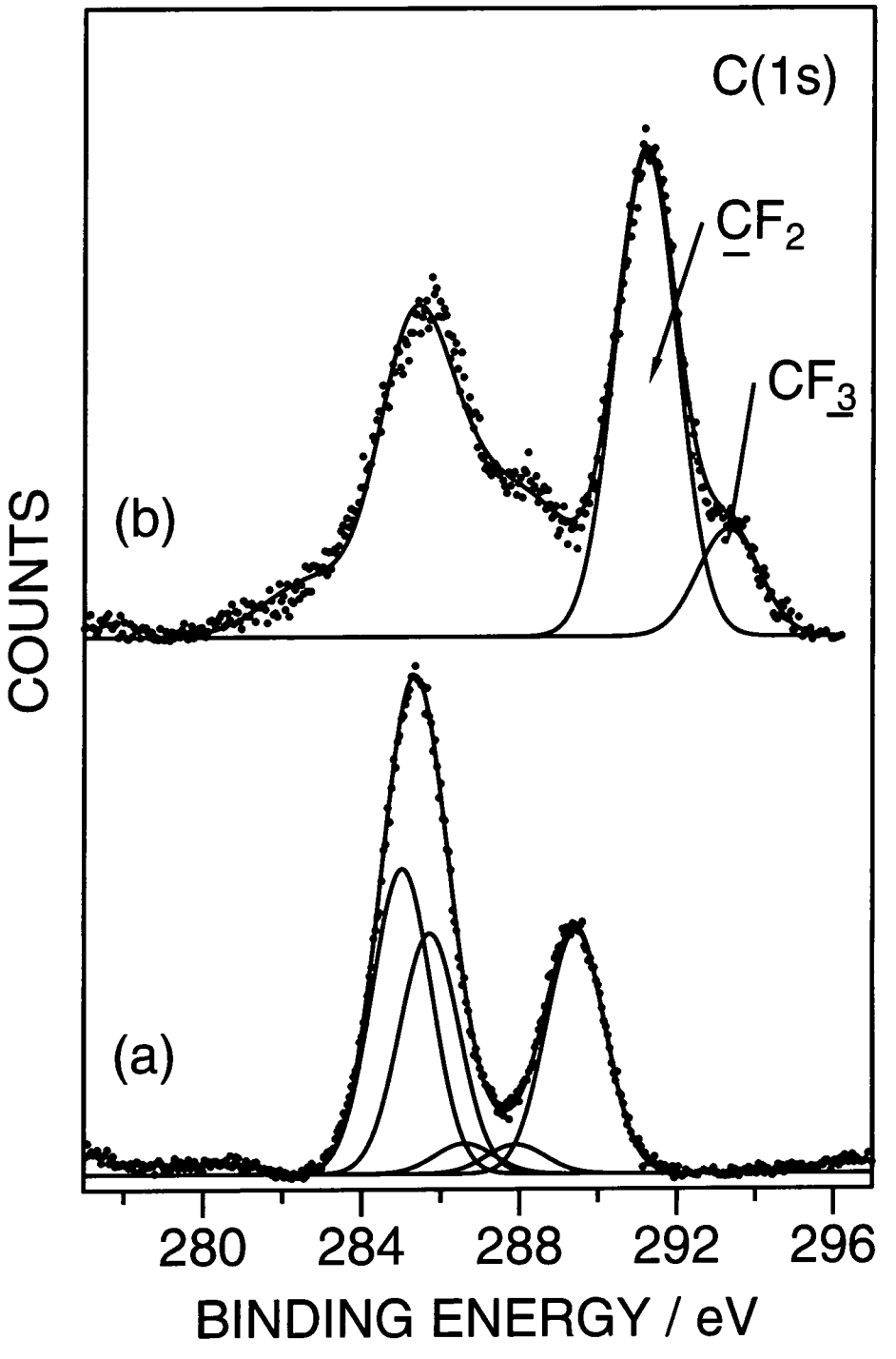

Figure 3.6: C(1s) XPS spectra of (a) AA pulsed plasma polymer (t_{on} = 20 μs, t_{off} = 4 ms, P_p = 5 W); and (b) AA pulsed plasma polymer treated with $R_f(C_nH_{2n})_x(alkyl)_2N^+\text{-}O^-$.

3.4 DISCUSSION

These highly functionalised acrylic acid plasma polymer surfaces were found to readily undergo complexation with the cationic fluorosurfactant solution. A number of factors are known to govern the adsorption of surfactants onto solid surfaces: the chemical nature of the solid surface; the molecular structure of the surfactant; and the solvent environment.[34-44] Generally, surfactant adsorption at low concentrations involves single surfactant ions rather than micelles.[44-46] Adsorption of fluorocarbon surfactant onto hydrophobic groups on polyethylene has been described.[36] However, on removal of the polyethylene from solution the adsorption was shown not to be site specific. Any adsorption due to interactions between hydrophobic groups and the cationic fluorosurfactant used in this study was proved to be reversible by the analysis of $CF_3(CF_2)_nC_2H_5(alkyl)_3N^+$ treated and rinsed polyethylene samples, Figure 3.7. No evidence for surfactant adsorption on polyethylene could be found from the C(1s) XPS spectrum. The shoulder to low binding energy of the hydrocarbon peak was not at a fixed binding energy (its position changed, with respect to the hydrocarbon peak, between separate analysis runs of the same sample). It may have been due to differential surface charging effects,[47] or be a sodium KLL auger line superimposed on the photoelectron spectrum.[30] Such peaks were also noted when the AA plasma polymer samples were neutralised in the NaOH solution, Figure 3.1. Therefore, adsorption at hydrophobic sites on the AA plasma polymer surface was unlikely to be an important mechanism of surfactant attachment. The carboxylic acid groups at the surface of the plasma polymer layer will be expected to become weakly ionised in water (the degree of ionisation of poly(acrylic acid) in aqueous solution is 0.026)[12] and this will lead to a favourable electrostatic attraction between the ionised acid groups and oppositely charged fluorosurfactant ions.[34,35] Such interactions will orientate the charged surfactant head group towards the plasma polymer surface, and leave the fluorinated tail segment extended away towards the air-solid interface. The high contact angle measured for hexadecane is consistent with the aforementioned description. However, the observed wettability towards water is indicative of a polar component at the surface, something which is absent for conventional bulk polyelectrolyte-surfactant complexes,[27] where perfluoroalkyl

chains remain orientated outwards in the presence of both polar and non-polar probe liquids.[43] One possible explanation for the observed switching in liquid repellency could be that the adsorbed fluorosurfactant species form a partly intercalated heterogeneous structure with some of the surfactant hydrophilic polar groups orientated away from the substrate (e.g. a bilayer).[14,36,42,48-50] The driving force for such behaviour would be a balance between attraction of the cationic surfactant head group towards the partially ionised polyelectrolyte surface and the unfavourable surface tension between the fluorocarbon tails and water.[42] However, this is unlikely due to the absence of any XPS signal from the I^- counterion. A more plausible scenario is that the surfactant-polyelectrolyte monolayer is able to reorganise in such a way so as to allow water molecules to interact with the hydrophilic sub-surface of the acrylic acid plasma polymer. Any plasma induced crosslinking during deposition of the acrylic acid plasma polymer layer should restrict sub-surface swelling, and therefore prevent accessibility for the fluorosurfactant moieties to below the surface, in turn this will suppress interdigitation, cooperative binding, and layering of the perfluoroalkyl tails.[14,51] Such oleophobicity/hydrophilicity behaviour is potentially attractive for anti-fogging applications, where the spreading of water droplets in combination with a hindrance towards oily substances is highly sought after.[52] Another area of interest is soil-release, where the substrate is required to repel oily substances in the dry state whilst allowing solvent molecules access to the surface in the wet state in order to assist with the removal of any adhered soil moieties.[53,54]

Complexing of other types of cationic fluorosurfactants to anionic pulsed plasma polymers prepared from acrylic acid and related monomers, e.g. 6-heptenoic acid, were also found to display similar liquid wetting behaviour towards hexadecane and water (i.e. switching). Many of the systems tested demonstrated a large hysteresis between the advancing and receding contact angles. This hysteresis may be due to kinetic or thermodynamic factors (Section 1.7.3).[55] Kinetic hysteresis arises from time dependent surface modifications upon wetting of the substrate by the test liquid. Possible modifications include swelling, penetration of the surface by the test liquid and surface group reorientation.[56-59] Thermodynamic hysteresis could be due to surface roughness or surface heterogeneity.[60]

The amphoteric fluorinated surfactant $R_f(C_nH_{2n})_x(alkyl)_2N^+\text{-}O^-$ was also attached to the plasma polymer surface. The greater fluorinated surface functionalities produced may be indicative of the increased levels of fluorination in the surfactant structure.

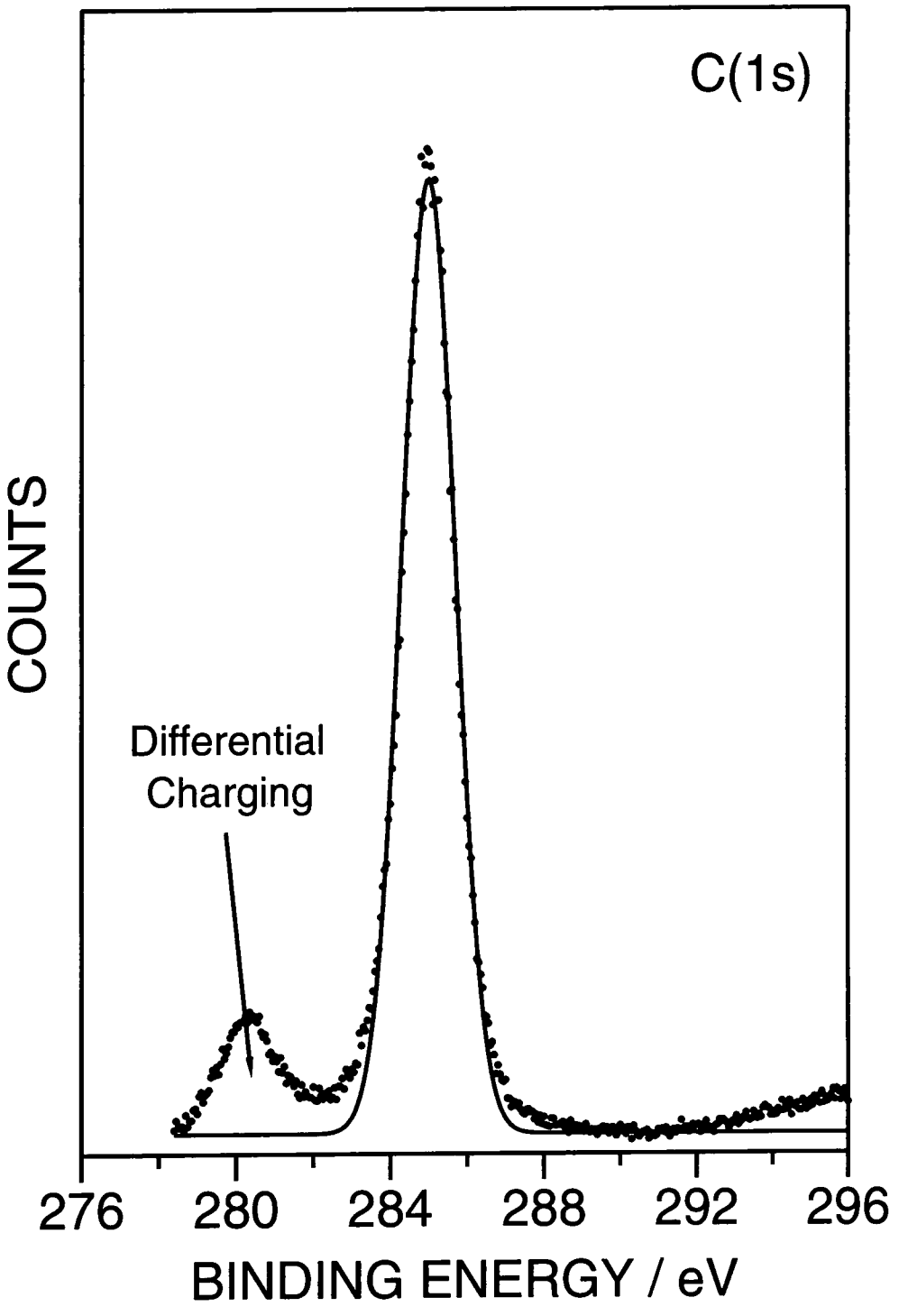

Figure 3.7: C(1s) XPS spectra of $CF_3(CF_2)_nC_2H_5(alkyl)_3N^+$ treated polyethylene.

3.5 CONCLUSION

Fluorinated surfactant was attached to the plasma polymer surface. However, the liquid repellent behaviour expected of a fluorinated surface was only partially evident. In reality the surface produced displayed rather complicated wetting properties which were only partially eluded. The mechanism of surfactant attachment could only be hypothesized from the end product. Further work, such as the construction of an adsorption isotherm,[34] would be required to unambiguously identify the method of adsorption. Such techniques present technical difficulties when applied to plasma systems.

3.6 REFERENCES

1. Antonietti, M.; Burger, C.; Effing, J. *Adv. Mater.* **1995**, *7*(8), 751.
2. Goddard, E. D. *Coll. Surf.* **1986**, *19*, 301.
3. Lindman, B.; Thalberg, K. In *Interactions of Surfactants with Polymers and Proteins*; Goddard, E. D.; Ananthapadmanabhan, K. P., Eds.; CRC Press: Boca Raton, 1993.
4. Okuzaki, H.; Osada, Y. *Macromolecules* **1994**, *27*(2), 502.
5. Okuzaki, H.; Eguchi, Y.; Osada, Y. *Chem. Mater.* **1994**, *6(10)*, 1651.
6. Zezin, A. B.; Izumrudov, V. A.; Kabanov, V. A. *Macromol. Symp.* **1996**, *106*, 397.
7. Thalberg, K.; Lindman, B.; Karlström, G. *J. Phys. Chem.* **1991**, *95*(8), 3370.
8. Shimizu, T.; Seki, M.; Kwak, J. C. T. *Coll. Surf.* **1986**, *20*, 289.
9. Shimizu, T. *Colloids Surfaces A: Physicochem. Eng. Aspects* **1995**, *94*, 115.
10. Okuzaki, H.; Osada, Y. *Macromolecules* **1995**, *28*(13), 4554.
11. Macdonald, P. M.; Tang, A. J. *Langmuir* **1997**, *13*(8), 2259.
12. Fundin, J.; Hansson, P.; Brown, W.; Lidegran, I. *Macromolecules* **1997**, *30*(4), 1118.
13. Thalberg, K.; Lindman, B.; Bergfeldt, K. *Langmuir* **1991**, *7*(12), 2893.
14. Hayakawa, K.; Kwak, J. C. T. In *Cationic Surfactants: Physical Chemistry*; Rubingh, D. N.; Holland, P. M., Eds.; Marcel Dekker: New York, 1991; Vol. 37, pp. 189-248.
15. Hayakawa, K.; Kwak, J. C. T. *J. Phys. Chem.* **1982**, *86*(19), 3866.
16. Herslöf, Å.; Sundelöf, L.-O.; Edsman, K. *J. Phys. Chem.* **1992**, *96*(5), 2345.
17. Hayakawa, K.; Kwak, J. C. T. *J. Phys. Chem.* **1983**, *87*(3), 506.
18. Hayakawa, K.; Santerre, J. P.; Kwak, J. C. T. *Macromolecules* **1983**, *16*(10), 1642.
19. Santerre, J. P.; Hayakawa, K.; Kwak, J. C. T. *Coll. Surf.* **1985**, *13*, 35.
20. Shirahama, K.; Musaki, T.; Takashima, K. In *Microdomains in Polymer Solutions*; Dubin, P., Ed.; Plenum: New York, 1985; Vol. 30, pp. 299-309.
21. Li, Y.; Dubin, P. L. *ACS Symposium Ser.* **1994**, *578*, 320.
22. Abuin, E. B.; Scaiano, J. C. *J. Am. Chem. Soc.* **1984**, *106*(21), 6274.
23. Chu, D.; Thomas, J. K. *J. Am. Chem. Soc.* **1986**, *108*(20), 6270.
24. Chandar, P.; Somasundaran, P.; Turro, N. J. *Macromolecules* **1988**, *21*(4), 950.
25. Antonietti, M.; Burger, C.; Conrad, J.; Kaul, A. *Macromol. Symp.* **1996**, *106*, 1.
26. Antonietti, M.; Conrad, J.; Thünemann, A. *Macromolecules* **1994**, *27*(21), 6007.
27. Antonietti, M.; Henke, S.; Thünemann, A. *Adv. Mater.* **1996**, *8*(1), 41.
28. Yasuda, H. *Plasma Polymerization*; Academic: London, 1985.
29. Morosoff, N. In *Plasma Deposition, Treatment, and Etching*; d'Agostino, R., Ed.; Acdemic: London, 1990; p. 1.
30. Wagner, C. D.; Riggs, W. M.; Davis, L. E.; Moulder, J. F.; Muilenber, G. E.

Handbook of X-Ray Photoelectron Spectroscopy; Perkin-Elmer: New York, 1978.
31. Beamson, G.; Briggs, D. *High Resolution XPS of Organic Polymers, The Scienta ESCA 300 Database*; John Wiley & Sons: Chichester, 1992.
32. Kissa, E. In *Handbook of Fibre Science and Technology*, Part B ed.; Lewin, M.; Sells, S. B., Eds.; Marcel Dekker Inc.: New York, 1984; Vol. II, pp. 143-209.
33. Jasper, J. J. *J. Phys. Chem. Ref. Data* **1972**, *1*(4), 841.
34. Rosen, M. J. *Surfactants and Interfacial Phenomena*, 2nd ed.; John Wiley & Sons: New York, 1989.
35. Myers, D. *Surfactant Science and Technology*; VCH: New York, 1988.
36. Lens, J. P.; Terlingen, J. A. C.; Engbers, G. H. M.; Feijen, J. *Langmuir* **1998**, *14*, 3214.
37. Somasundaran, P.; Krishnakumar, S. *Colloids Surfaces A: Physicochem. Eng. Aspects* **1994**, *93*, 79.
38. Biswas, S. C.; Chattoraj, D. K. *J. Colloid Interface Sci.* **1998**, *205*, 12.
39. Esumi, K.; Iitaka, M.; Koide, Y. *J. Colloid Interface Sci.* **1998**, *208*, 178.
40. Yamada, S.; Israelachvili, J. *J. Phys. Chem. B.* **1998**, *102*(1), 234.
41. Waltermo, Å.; Sjöberg, M.; Anhede, B.; Claesson, P. M. *J. Colloid Interface Sci.* **1993**, *156*, 365.
42. Claesson, P. M.; Herder, P. C.; Berg, J. M.; Christenson, H. K. *J. Colloid Interface Sci.* **1990**, *136*(2), 541.
43. Christenson, H. K.; Claesson, P. M.; Berg, J.; Herder, P. C. *J. Phys. Chem.* **1989**, *93*(4), 1472.
44. Otsuka, H.; Esumi, K. *Langmuir* **1994**, *10*(1), 45.
45. Kölbel, H.; Hörig, K. *Angew. Chem.* **1959**, *71*, 691.
46. Kölbel, H.; Kuhn, P. *Angew. Chem.* **1959**, *71*, 211.
47. Barr, T. L. In *Practical Surface Analysis*, 2nd ed.; Briggs, D.; Sean, M. P., Eds.; J. Wiley & Sons: Chichester, 1990; Vol. Volume 1 Auger and X-ray Photoelectron Spectroscopy, p. 370.
48. McGuiggan, P. M.; Pashley, R. M. *Coll. Surf.* **1987**, *27*, 277.
49. Pashley, R. M.; McGuiggan, P. M.; Horn, R. G.; Ninham, B. W. *J. Colloid Interface Sci.* **1988**, *126*(2, December), 569.
50. Lai, C.-L.; Harwell, J. H.; O'Rear, E. A.; Komatsuzaki, S.; Arai, J.; Nakakawaji, T.; Ito, Y. *Colloids Surfaces A: Physicochem. Eng. Aspects* **1995**, *104*, 231.
51. Ober, C. K.; Wegner, G. *Adv. Mater.* **1997**, *9*(1), 17.
52. Ueno, M.; Ugajin, Y.; Horie, K.; Nishimura, T. *J. Appl. Polym. Sci.* **1990**, *39*, 967.
53. Sherman, P. O.; Smith, S.; Johannessen, B. *Textile Res. Jnl.* **1969**, *39*, 449.
54. Ellzey, S. E.; Connick, W. J.; Drake, G. L.; Reeves, W. A. *Textile Res. Jnl.* **1969**, *39*, 809.
55. Andrade, J. D.; Chen, W.-Y. *Surface and Interface Analysis* **1986**, *8*, 253.
56. Chen, Y.-L.; Helm, C. A.; Israelachvili, J. N. *J. Phys. Chem.* **1991**, *95*(26), 10736.
57. Chen, Y. L. E.; Gee, M. L.; Helm, C. A.; Israelachvili, J. N.; McGuiggan, P. M. *J. Phys. Chem.* **1989**, *93*(20), 7057.
58. Yasuda, H.; Sharma, A. K.; Yasuda, T. *J. Polym. Sci.: Polym. Phys. Ed.*

1981, *19*, 1285.
59. Fowkes, F. M.; Kaczinski, M. B.; Dwight, D. W. *Langmuir* **1991**, *7*(11), 2464.
60. Drelich, J.; Wilbur, J. L.; Miller, J. D.; Whitesides, G. M. *Langmuir* **1996**, *12*(7), 1913.

CHAPTER FOUR

SURFACE ATTACHMENT OF FLUOROSURFACTANT MOLECULES TO ALLYL AMINE PLASMA POLYMERS

4.1 INTRODUCTION

Allyl amine possesses an amine group and a double bond, Structure 4.1, making it an ideal candidate for the fabrication of amine rich surfaces via plasma polymerisation. Examples of the formation of allyl amine plasma polymers have previously been reported in the literature.[1-5] Potential uses for allyl amine plasma polymer surfaces include initial substrates for multilayer assemblies[2] and surfaces for cell growth and protein attachment.[4-7] Below plasma polymerised allyl amine surfaces are utilised for the attachment of an amphoteric fluorocarbon surfactant, Structure 4.2.

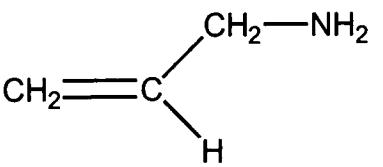

Structure 4.1: Allyl Amine.

Structure 4.2: Amphoteric Fluorosurfactant.

The allyl amine plasma polymer coating presents a solid polyelectrolyte (PE) surface to bulk phases. The attachment of fluorosurfactant molecules to this PE surface may be a new route to the formation of liquid repellent surfaces. Complexes between PE and surfactant molecules are well known.[8-21] Several features appear to be common to many of these systems:

- Complexation reactions are almost always performed in aqueous solution;[8,22,23]
- Many parameters affect the complexation reactions including surfactant tail length,[9-14] nature of the PE,[13-18] density of charges along the PE

backbone,[10,16,17,19,20] solution pH,[13] and the incorporation of low molecular weight electrolytes;[9,10,13,20,21,24,25]

- Solid PE-surfactant complexes can be easily precipitated from aqueous solution;[8,22,23]
- Such complexes are formed according to a strict 1:1 stoichiometry with respect to the charges.[8,22,23]

PE-fluorosurfactant complexes have been precipitated from aqueous solution and this new class of solid compounds displays liquid repellent properties.[26]

4.2 EXPERIMENTAL PROCEDURE

4.2.1 APPARATUS AND PROCEDURE

The experimental apparatus and procedure for plasma depositions was described previously (Chapter 2). Allyl amine monomer (Aldrich, 99% purity) was further purified by multiple freeze-thaw cycles. Prior to each experiment the reactor was scrubbed clean with detergent and scouring powder, rinsed with copious amounts of water and isopropyl alcohol (IPA) before finally being oven dried. Before polymerisation, air was emitted into the reactor and a 50 W air cleaning plasma was ignited at a pressure of 0.2 mbar for 30 minutes. The reactor was pumped down to base pressure following air plasma cleaning, isolated from the pump and opened up to the atmosphere to allow insertion of the substrate. Glass slides cleaned as previously described (Section 2.2) were used as the substrate for XPS analysis and further reaction. Polished sodium chloride plates were used as substrates for ATR-FTIR analysis. The substrate was positioned at the centre of the copper coils and the system was pumped back down to base pressure. At this stage the leak rate of the reactor was determined (Section 2.2.2.1). Acceptable leak rates were below 1×10^{-9} mol s^{-1}. Allyl amine vapour was then introduced into the reactor at a pressure of 0.2 mbar and the flow rate was calculated (Section 2.2.2.2). The flow rate was kept constant at approximately 1.5×10^{-6} mol s^{-1}. This resulted in a monomer purity in the reactor of above 99.9%. The glow discharge was then ignited and immediately balanced using the matching network. After the treatment time of 30 minutes had elapsed

the plasma was extinguished and the monomer was purged through the system for a further two minutes.

4.2.2 CONTINUOUS WAVE (CW) PLASMA POLYMERISATION

CW plasma polymerisation of allyl amine was carried out as described above. The discharge power was set according to the power meter and the plasma balanced. After plasma polymerisation the sample was removed from the reactor and immediately analysed by XPS or ATR-FTIR.

4.2.3 ELECTRICALLY PULSED PLASMA POLYMERISATION

For electrically pulsed plasma experiments a pulse generator supplied a pulse of 5 V amplitude to modulate the rf generator as previously described (Section 2.2.1.2). It was necessary to set up the reaction conditions prior to the insertion of the substrate as the plasma had to be balanced under CW conditions. Therefore, following the air cleaning plasma, air was emitted into the reactor via the leak valve. A plasma was ignited, the power set and the pulsing was switched on. The overall average power (<P>) supplied to the system was calculated (Equation 2.1, Section 2.2.1.2).[27] After the reactor had been prepared it was vented to the atmosphere to allow insertion of the substrates. From this point the experimental procedure was essentially the same as that for CW plasma polymerisation (Section 4.2.2), except that the plasma discharge conditions had already been determined.

4.2.4 TREATMENT WITH AMPHOTERIC FLUORINATED SURFACTANT

Allyl amine pulsed plasma polymer layers were deposited onto glass substrates under the pulsing conditions of t_{on} = 20 μs, t_{off} = 1000 μs and P_p = 5 W for 30 minutes. These substrates were subsequently placed in an aqueous solution of the amphoteric fluorinated amine oxide surfactant ($R_f(C_nH_{2n})_x(alkyl)_2N^+$-$O^-$

Structure 4.1, supplied by Clariant GmbH, trade name Fluowet® OX, details of the structure of this fluorosurfactant were not given by the supplier) at various concentrations for 1 hour, rinsed in pure water for 10 minutes, and dried under vacuum. Following fluorosurfactant treatment the samples were analysed by XPS and VCA.

4.2.5 SAMPLE CHARACTERISATION

4.2.5.1 XPS Characterisation

Samples were characterised immediately following plasma polymerisation by XPS spectroscopy. The glass slides were attached to a stainless steel probe stud using double sided adhesive tape and inserted into a Vacuum Generators ESCA Lab Mk. II photoelectron spectrometer. The spectrometer was fitted with an unmonochromated magnesium X-ray source (Mg $K\alpha_{1,2}$ = 1253.6 eV) and operated in the constant analyser energy mode (CAE = 20 eV for high resolution spectra, 50 eV for survey scans). Photoelectrons emitted from the substrate were collected at a 30° take-off angle with respect to the substrate normal. The spectrometer calibration was routinely checked using the gold $4f_{7/2}$ and silver $3d_{5/2}$ peaks at 83.8 and 368.3 eV respectively.[28] Elemental sensitivity factors were determined experimentally relative to the carbon 1s (C(1s)) peak (285.0 eV) using standard compounds. These were taken as C(1s) : F(1s) : O(1s) : N(1s) : Si(2p) = 1.00 : 0.24 : 0.39 : 0.65 : 1.00 respectively. The absence of any Si(2p) XPS feature following plasma polymerisation was indicative of complete coverage of the glass substrate.

4.2.5.2 ATR-FTIR Characterisation

A FTIR Mattson Polaris instrument fitted with a golden gate apparatus for attenuated total reflection (ATR) spectroscopy was used for infrared analysis of plasma polymers deposited onto polished sodium chloride plates. Typically 128 scans were acquired at a resolution of 4 cm^{-1}.

4.2.5.3 VCA Characterisation

The wettability of the samples was investigated using the sessile drop technique (Section 1.8.4) employing video contact angle (VCA) apparatus (Instruments S.A. Video Contact Angle System, VCA 2500XE). A known volume of the test liquid, high purity water (B.S. 3978 grade 1) or hexadecane (Aldrich, 99% purity), was dispensed through a motorised micro-syringe and brought into contact with the surface of the sample. The contact angle of the liquid was calculated by analysis of the shape of the droplet on the sample surface.

4.3 RESULTS

High resolution XPS envelopes were fitted using a Marquardt minimisation routine. The peak shape was assumed to be Gaussian with a fixed relative full width at half maximum.[29] Using the hydrocarbon peak at 285.0 eV as a reference offset the C(1s) region of a typical allyl amine plasma polymer layer was fitted with four different carbon functionalities:[1,30,31] an unfunctionalised hydrocarbon group ($\underline{C}_xH_y$ at 285.0 eV); a carbon singly bonded to nitrogen functionality ($\underline{C}$-NH_2, $\underline{C}$-NH-$\underline{C}$, $\underline{C}$-N=C at 285.9 eV); an imine group ($\underline{C}$=N 286.8 eV); and an amide or carbonyl group (C(N)=O, C=O 288.0 eV), Figure 4.1. Oxygen may have been incorporated into the plasma polymer due to post polymerisation reactions of trapped radicals in the plasma polymer with atmospheric oxygen following removal of the sample. Alternatively direct oxidation during plasma polymerisation by water desorbed from the reactor walls could also have been responsible.[7] A small signal was present towards the high binding energy end of the C(1s) spectrum. This signal arose from fluorinated carbon impurities. The N(1s) region was fitted with one peak at approximately 399.5 eV for nitrogen singly bonded to carbon,[30] Figure 4.2. The FWHM of this peak was large (approximately 2.8 eV) which indicated the presence of nitrogen atoms in different chemical environments.[1] The N/C ratio was found from the N(1s) and C(1s) peak areas (after correction for sensitivity).

The IR spectra of the allyl amine monomer was compared with the 2 W CW allyl amine plasma polymer deposited onto a NaCl plate, Figure 4.3. The peaks were identified with reference to the literature:[1,32,33] (1) asymmetrical and symmetrical primary amine N-H stretch double absorption bands at 3370 and 3288 cm^{-1} respectively; (2) C-H stretching vibrations for $=CH_2$ and =CH- groups at 3079 and 2978 cm^{-1} respectively;[33] (3) aliphatic C-H stretch 2914 and 2850 cm^{-1}; (4) CH_2 out of plane deformation bending absorption for $=CH_2$ 1800 cm^{-1}; (5) C=C stretching vibration 1642 cm^{-1}; (6) N-H primary bend absorption 1600 cm^{-1}; (7) aliphatic CH_2 scissoring vibration 1451 cm^{-1} and CH_2 in plane deformation for $=CH_2$ 1422 cm^{-1}; (8) C-H in plane deformation for $=CH_2$ and =CH- 1284 cm^{-1}; (9) C-N stretching vibration 1073 cm^{-1}; (10) C-H out of plane deformation for $=CH_2$ and =CH- 996 cm^{-1}; (11) CH_2 out of plane deformation for $=CH_2$ and =CH- 920 cm^{-1} and N-H bending absorption 826 cm^{-1}; (12) primary amine N-H stretch double absorption band in the monomer replaced by wide absorption band from primary, secondary and imine N-H stretches 3350 to 3200 cm^{-1}; (13) multiple C-H absorption bands of aliphatic groups 2960, 2940 and 2880 cm^{-1}; (14) CO_2 absorption from atmosphere with possibly a small contribution from a nitrile (C≡N) group 2184 cm^{-1}; (15) N-H primary bending absorption considerably broadened by a C=N imine stretch 1632 cm^{-1}; (16) aliphatic CH_2 scissoring band 1454 cm^{-1} and aliphatic C-H symmetrical bending absorption 1379 cm^{-1}.

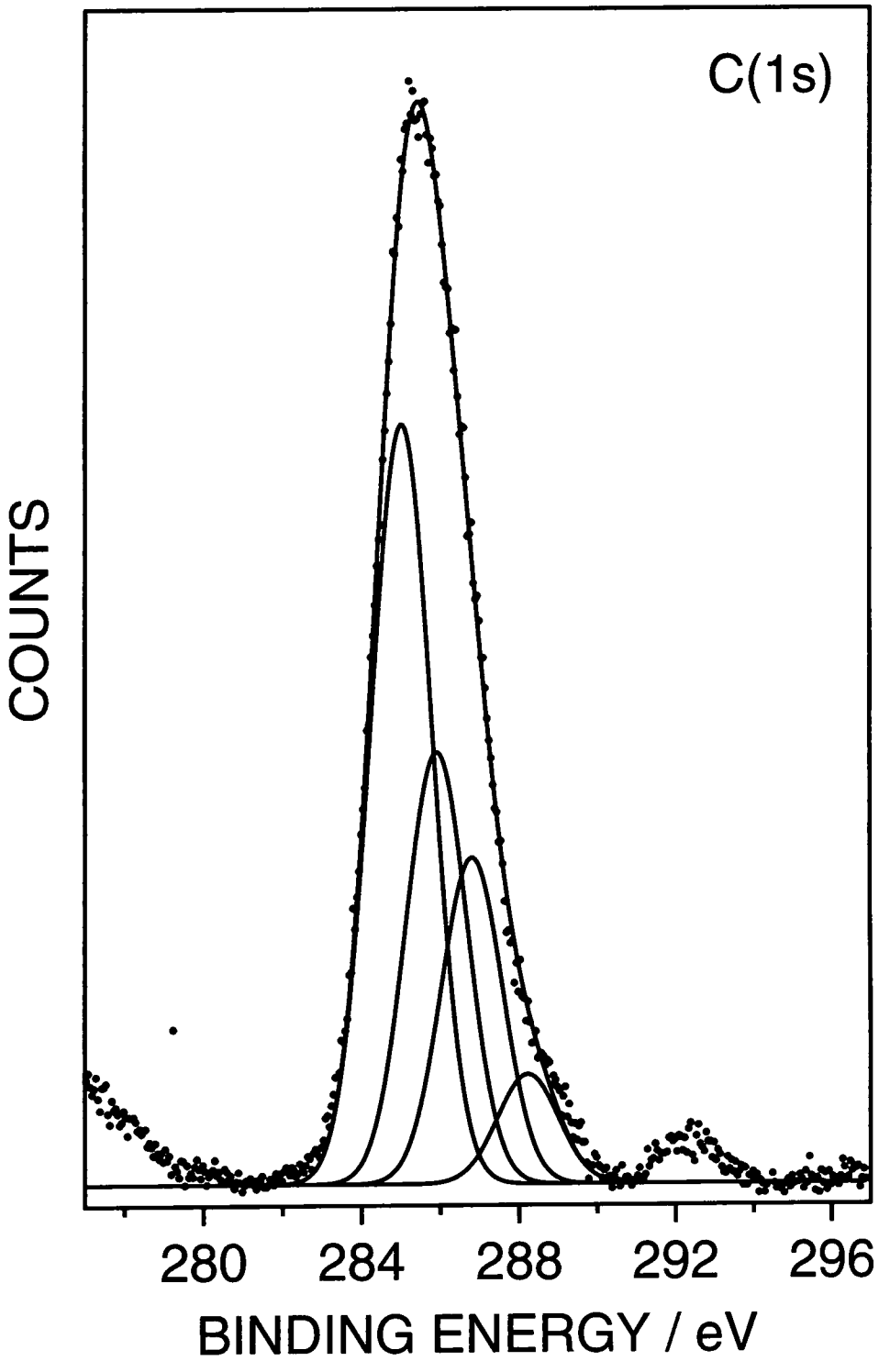

Figure 4.1: C(1s) XPS spectra of 2 W CW allyl amine plasma polymer.

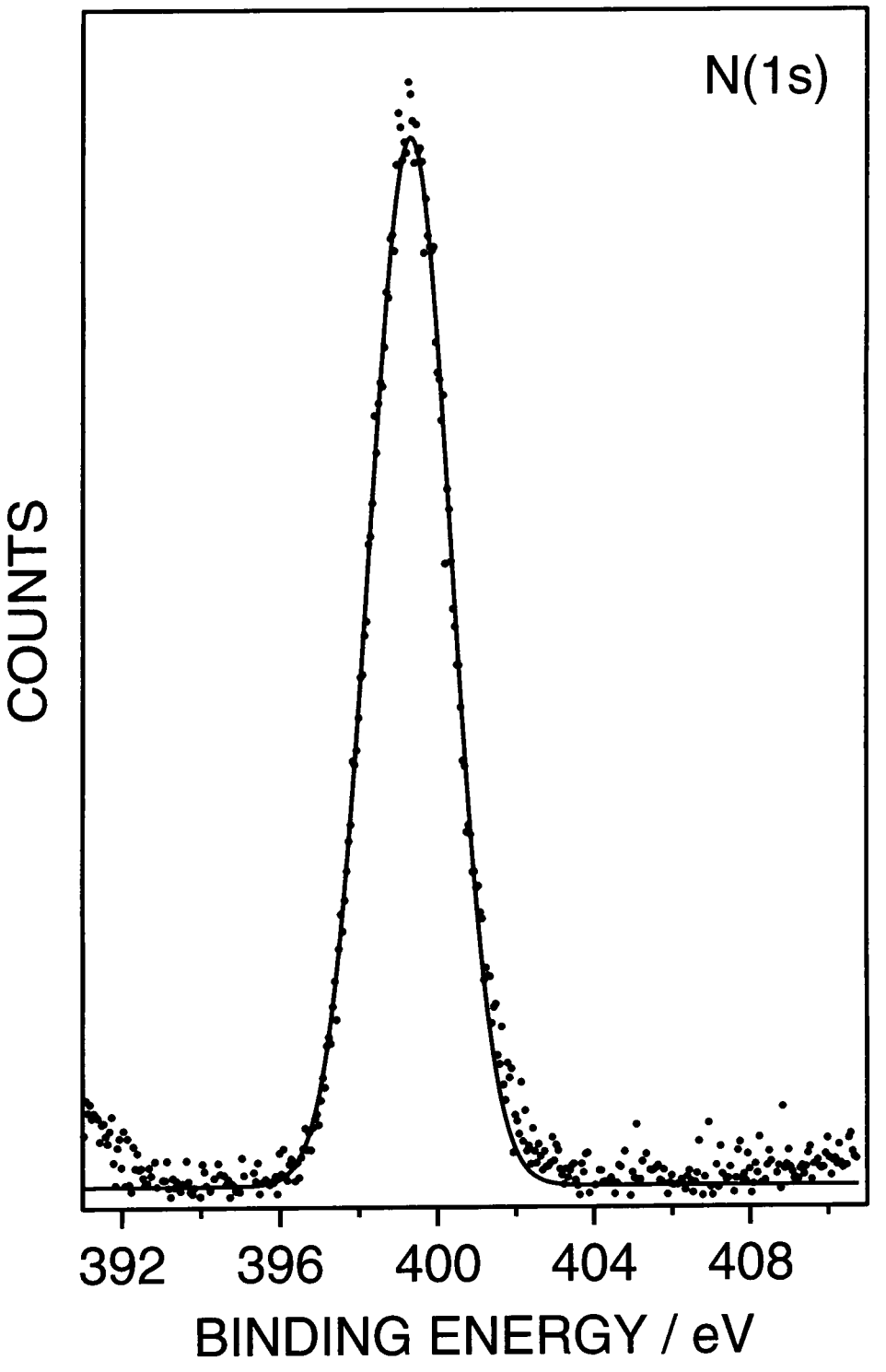

Figure 4.2: N(1s) XPS spectra of 2 W CW allyl amine plasma polymer.

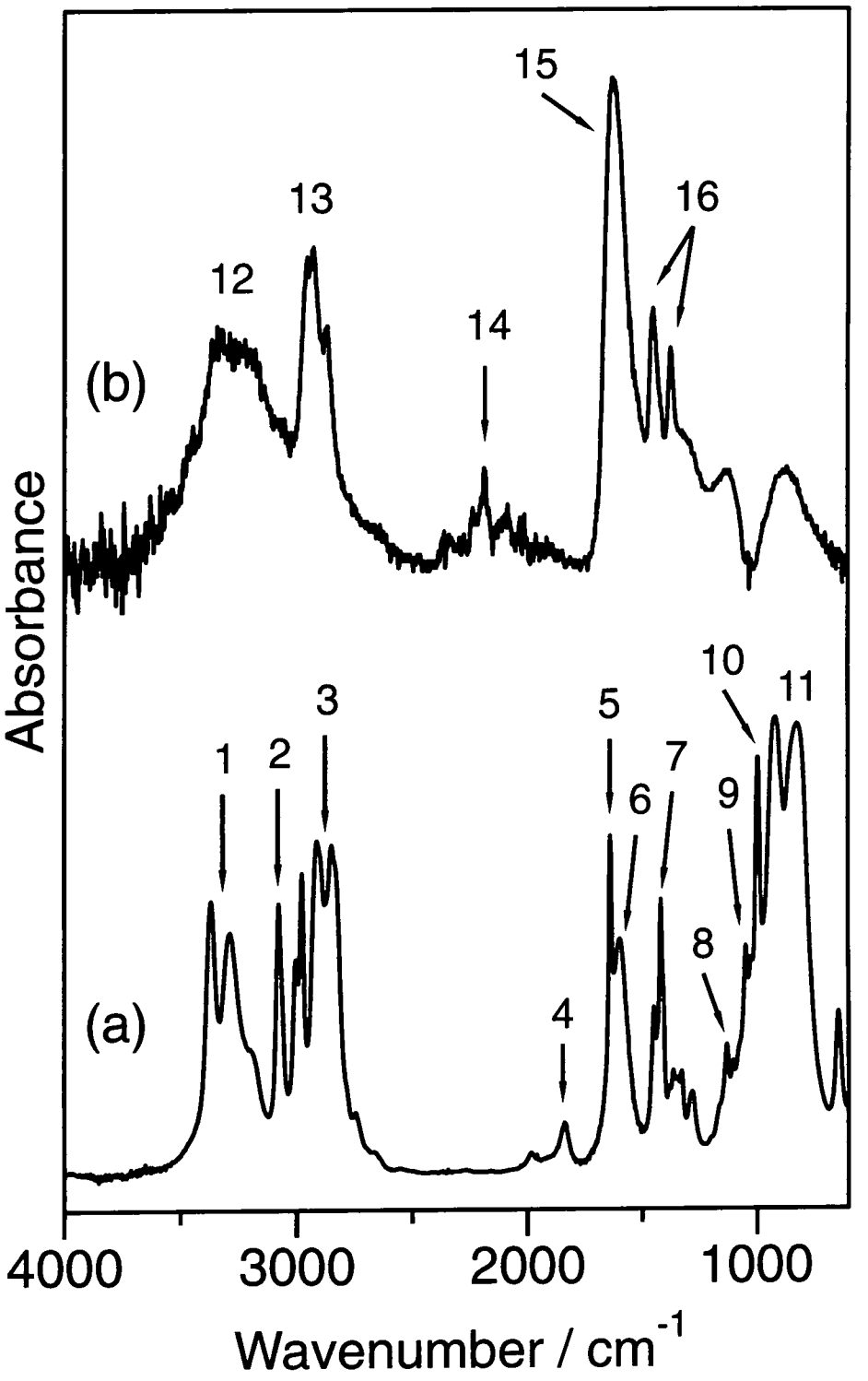

Figure 4.3: ATR-FTIR spectra of (a) allyl amine monomer; and (b) 2 W CW allyl amine plasma polymer.

4.3.1 CW PLASMA POLYMERISATION OF ALLYL AMINE

The C(1s) and N(1s) spectra of the CW allyl amine plasma polymer appeared to vary little with discharge power, Figure 4.4 and 4.5. The N/C ratio reached a maximum value of 0.37 at a discharge power of 2 W, Figure 4.6. Below this power the electrical discharge became unstable. The N/C ratio passed through a minimum at approximately 20 W but recovered slightly as the power was increased. Deconvolution of the C(1s) spectra of allyl amine plasma polymer, deposited as a function of CW discharge power, aided quantification of the effect of power on the chemical composition of the plasma polymers, Figure 4.7. The percentage of unfunctionalised hydrocarbon and imine groups tended to decrease with decreasing discharge power. The opposite trend was observed for carbon atoms singly bonded to nitrogen and the oxygenated carbon functionalities. These groups were seen to increase with decreasing discharge power, reaching a maximum of 29% ± 2 and 7% ± 1 respectively at the lowest discharge power (2 W).

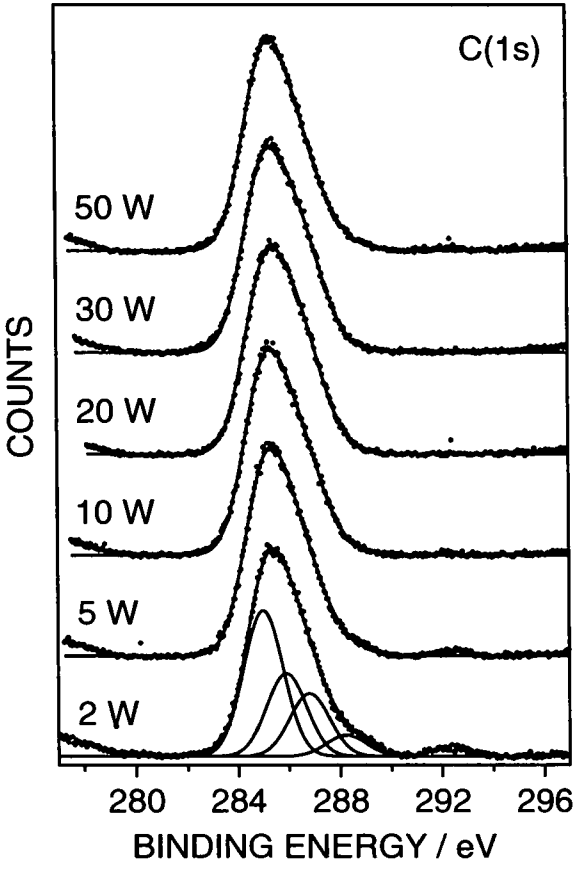

Figure 4.4: C(1s) XPS spectra of CW allyl amine plasma polymers deposited as a function of discharge power.

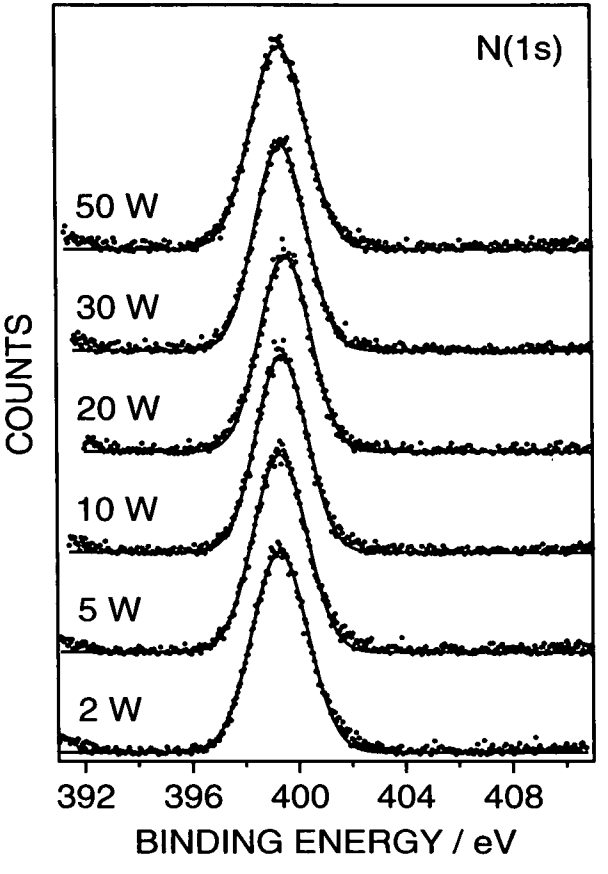

Figure 4.5: N(1s) XPS spectra of CW allyl amine plasma polymers deposited as a function of discharge power.

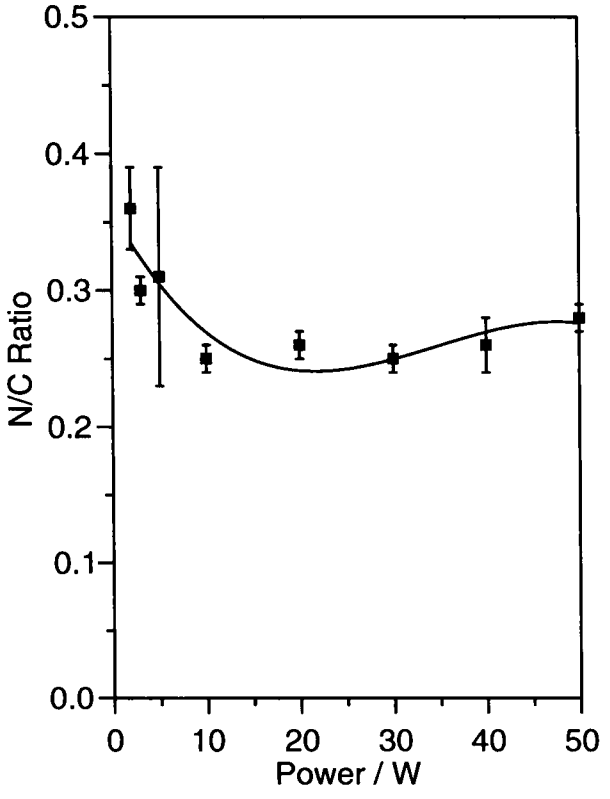

Figure 4.6: Variation in the N/C ratio as a function of discharge power for CW allyl amine plasma polymers.

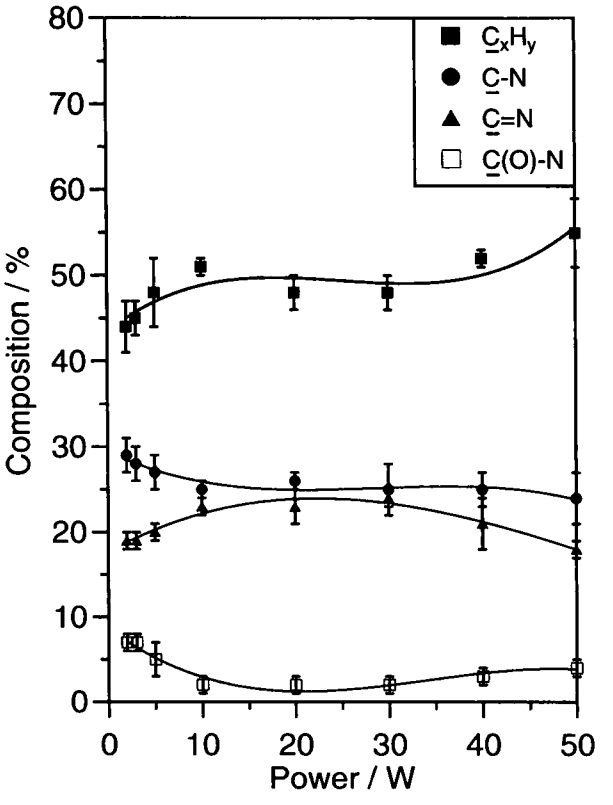

Figure 4.7: Comparison of the percentage carbon functionalities in allyl amine plasma polymer as a function of discharge power.

4.3.2 EVALUATION OF PULSE PLASMA PARAMETERS

From consideration of Equation 2.1 (Section 2.2.1.2), the average power delivered to the plasma (<P>) is a function of three variables:[27] on-time (t_{on}); off-time (t_{off}); and peak power (P_p). To efficiently investigate how these variables affected the percentage of the C-N group incorporated into the plasma polymer a set of eight experiments were planned. Two values (known as levels) were chosen for each of the three variables (known as factors) in order to ascertain which factors, or combination of factors, had the greatest influence on the percentage of the C-N group incorporated into the plasma polymer (known as the response).[34] The choice of level for each factor was partly governed by previous experience and the limitations of the equipment (the rf generator could not deliver reliable pulses shorter than 20 μs and its maximum power output was 70 W). The choice of experimental parameters, the experiments performed and the responses recorded are presented below, Table 4.1, and 4.2.

	Factors		
Levels	**t_{on}**	**t_{off}**	**P_p**
+	1000 μs	5000 μs	50 W
-	20 μs	500 μs	5 W

Table 4.1: Levels for each experimental factor.

Expt.	t_{on}	t_{off}	P_p	Response
1	+	+	+	26
2	-	+	+	30
3	+	-	+	23
4	+	+	-	27
5	+	-	-	28
6	-	+	-	30
7	-	-	+	31
8	-	-	-	32

Table 4.2: Experiments and their responses (percentage C-N group incorporated).

From these results a table was constructed to evaluate the effect of each factor and combination of factors.[34]

Expt	t_{on}	t_{off}	P_p	t_{on}/P_p	t_{off}/P_p	t_{on}/t_{off}	$t_{on}/t_{off}/P_p$
1	+26	+26	+26	+26	+26	+26	+26
2	-30	+30	+30	-30	+30	-30	-30
3	+23	-23	+23	+23	-23	-23	-23
4	+27	+27	-27	-27	-27	+27	-27
5	+28	-28	-28	-28	+28	-28	+28
6	-30	+30	-30	+30	-30	-30	+30
7	-31	-31	+31	-31	-31	+31	+31
8	-32	-32	-32	+32	+32	+32	-32
Total	**-19**	**-1**	**-7**	**-5**	**5**	**5**	**3**

Table 4.3: Evaluation of factors.

The relative importance of each factor on the response was measured by the modulus of the total found in the above table, Table 4.3. The sign of each total dictates whether increasing the value of a factor had a positive or negative effect on the response. From these results it is clear that the t_{on} had the greatest influence on the response. Decreasing t_{on} and P_p increased the percentage of C-N groups retained in the plasma polymer. The combined factors and the plasma t_{off} did not have a large influence on the response over the range studied. In light of these results it was decided to investigate the effect of t_{on} over the plasma polymerisation of allyl amine.

4.3.3 INFLUENCE OF PLASMA ON-TIME

The pulsed plasma polymerisation of allyl amine was investigated as a function of electrical plasma t_{on} (with a constant t_{off} = 1000 μs and P_p = 5 W). The C(1s) and N(1s) high resolution spectra appeared to vary little with t_{on}, Figures 4.8 and 4.9. However, the N/C ratio increased rapidly as the t_{on} was decreased, Figure 4.10. Comparison with the CW results, Figure 4.6, showed that the N/C ratio was enhanced at low t_{on}. The percentage composition of the carbon functionalities for the allyl amine pulsed plasma polymer appeared to follow a similar trend with decreasing average power (i.e. decreasing t_{on}) as in the CW experiments, Figure 4.11. The percentage of C-N functionality reached a maximum, at the lowest t_{on}, while the fraction of hydrocarbon and C=N reached a minimum. The percentage of oxygenated groups again increased towards low average powers.

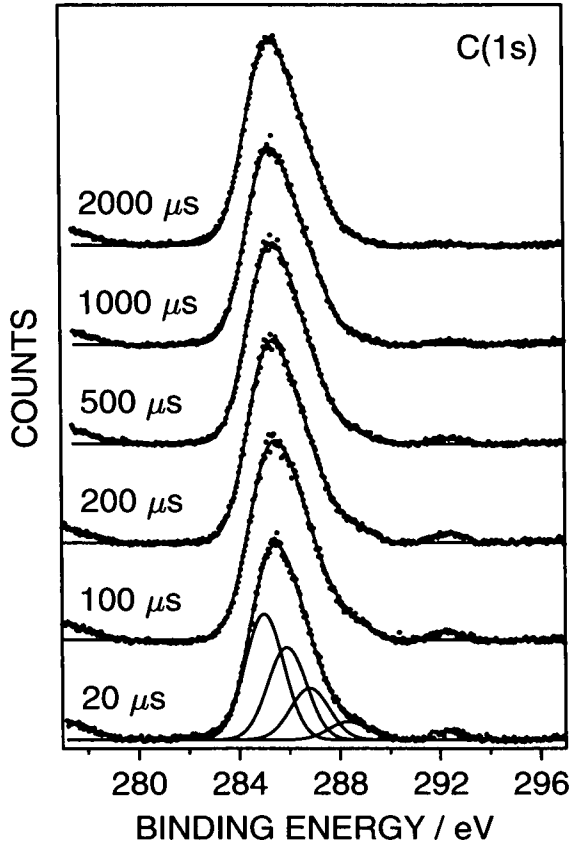

Figure 4.8: C(1s) XPS spectra of allyl amine pulsed plasma polymers deposited as a function of t_{on} (t_{off} = 1000 μs, P_p = 5 W).

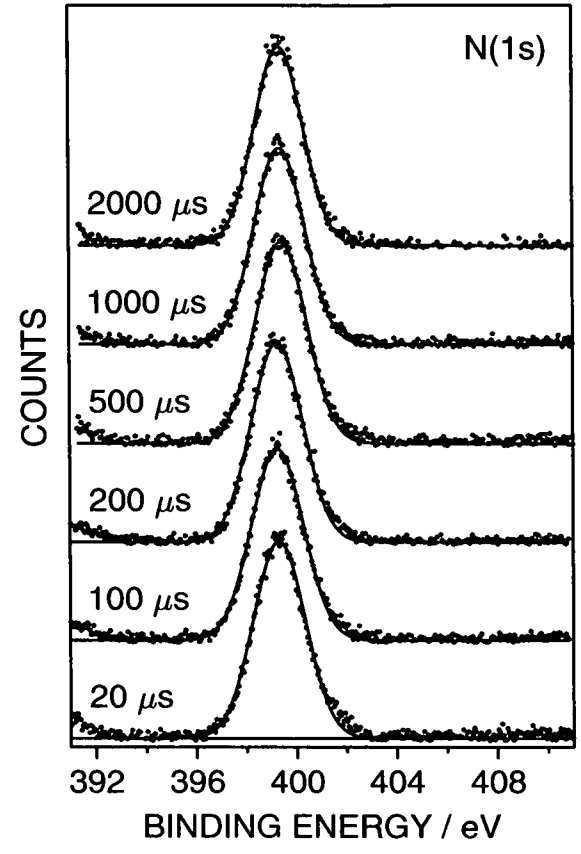

Figure 4.9: N(1s) XPS spectra of allyl amine pulsed plasma polymers deposited as a function of t_{on} (t_{off} = 1000 μs(t_{off} = 1000 μs, P_p = 5 W), P_p = 5 W).

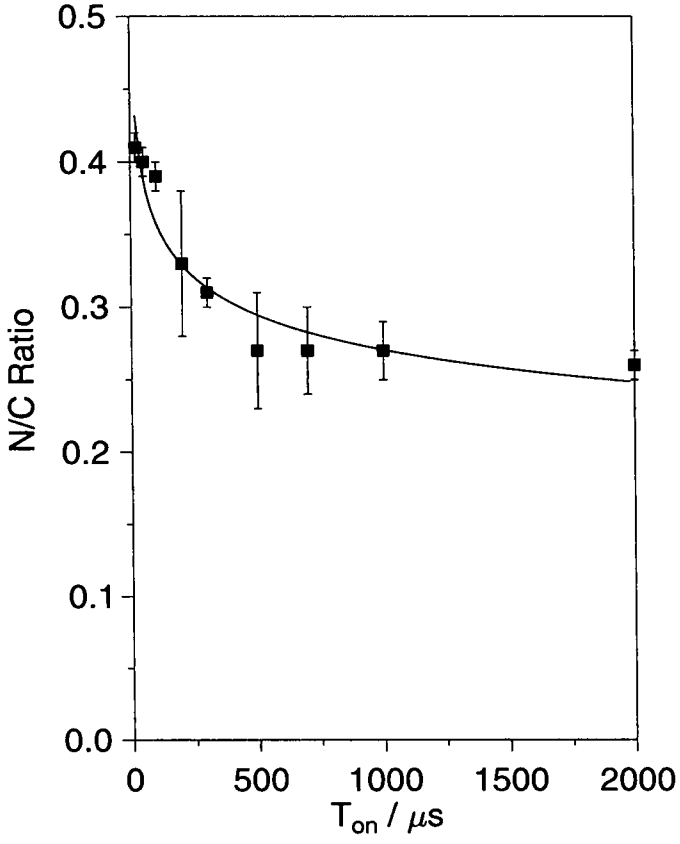

Figure 4.10: Variation in the N/C ratio as a function of t_{on} (t_{off} = 1000 μs, P_p = 5 W) for allyl amine pulsed plasma polymers.

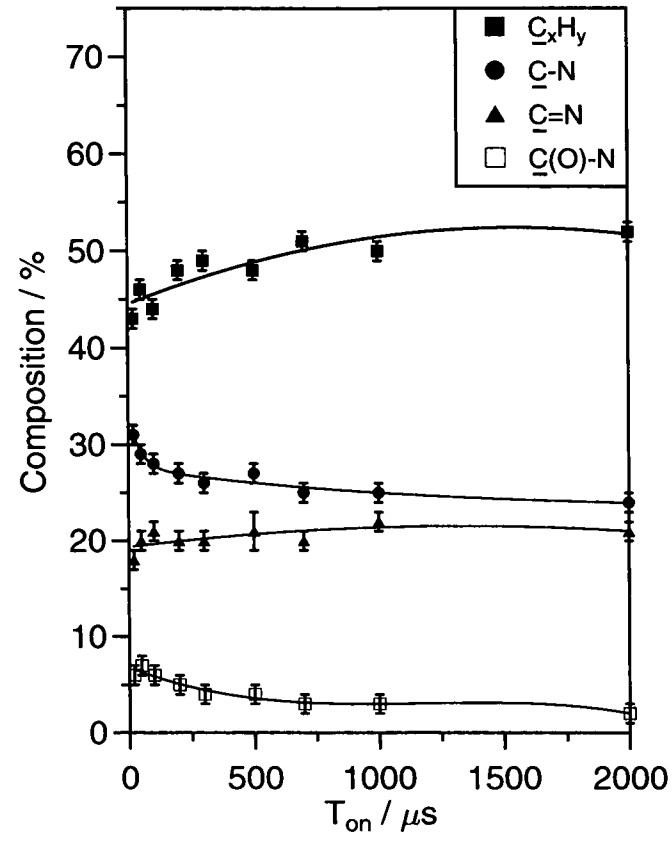

Figure 4.11: Comparison of the percentage carbon functionalities in allyl amine pulsed plasma polymer as a function of t_{on} (t_{off} = 1000 μs, P_p = 5 W).

4.3.4 TREATMENT OF ALLYL AMINE PULSED PLASMA POLYMER WITH AMPHOTERIC FLUOROSURFACTANT

Allyl amine pulsed plasma polymer layers were deposited onto glass substrates (t_{on} = 20 μs, t_{off} = 1000 μs, P_p = 5 W for 30 minutes). These substrates were subsequently placed in $R_f(C_nH_{2n})_x(alkyl)_2N^+$-$O^-$ aqueous solution for 1 hour, rinsed in pure water for 10 minutes and dried under vacuum. Following drying, the samples were characterised using XPS and VCA. A high resolution C(1s) peak fit revealed that surfactant had indeed been attached to the pulsed plasma polymer surface, Figure 4.12. A second high intensity nitrogen peak, corresponding to the N^+ group was evident at approximately 403 eV, Figure 4.13. Using the sessile drop method, contact angle measurements were taken of samples and controls. Water and hexadecane were employed as test liquids, Table 4.4. VCA results indicated that the fluorinated surfactant was attached to the plasma polymer surface which produced a high contact angle with hexadecane. However, the surfactant treated plasma polymer was found to interact strongly with water. This result was not expected in view of the surface fluorination detected by XPS and the oil repellent properties.[35]

Sample	**Test Liquid**	
	Water	**Hexadecane**
Clean Glass	38° ± 3	20° ± 3
Allyl Amine Plasma Polymer (t_{on} = 20 μs, t_{off} = 1 ms, P_p = 10 W)	46° ± 2	<20°
Clean Glass 10% $R_f(C_nH_{2n})_x(alkyl)_2N^+$-$O^-$ 1 hour	50° ± 4	35° ± 3
Allyl Amine Plasma Polymer 10% $R_f(C_nH_{2n})_x(alkyl)_2N^+$-$O^-$ 1 hour	<20°	82° ± 2

Table 4.4: Contact angle measurements of fluorosurfactant treated allyl amine plasma polymer and control samples.

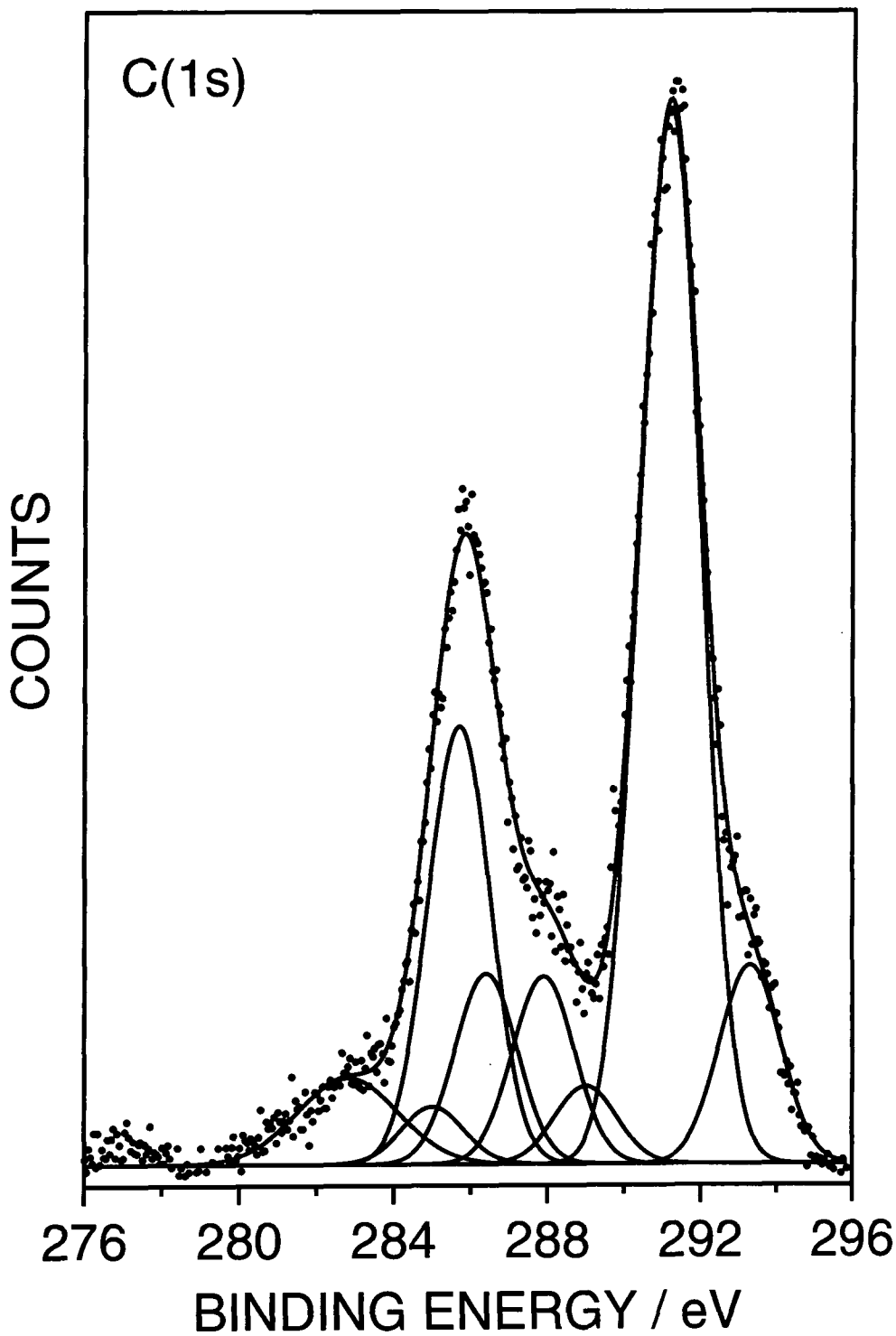

Figure 4.12: C(1s) XPS spectra of allyl amine pulsed plasma polymer (t_{on} = 20 μs, t_{off} = 1000 μs, P_p = 5 W) treated with $R_f(C_nH_{2n})_x(alkyl)_2N^+\text{-}O^-$.

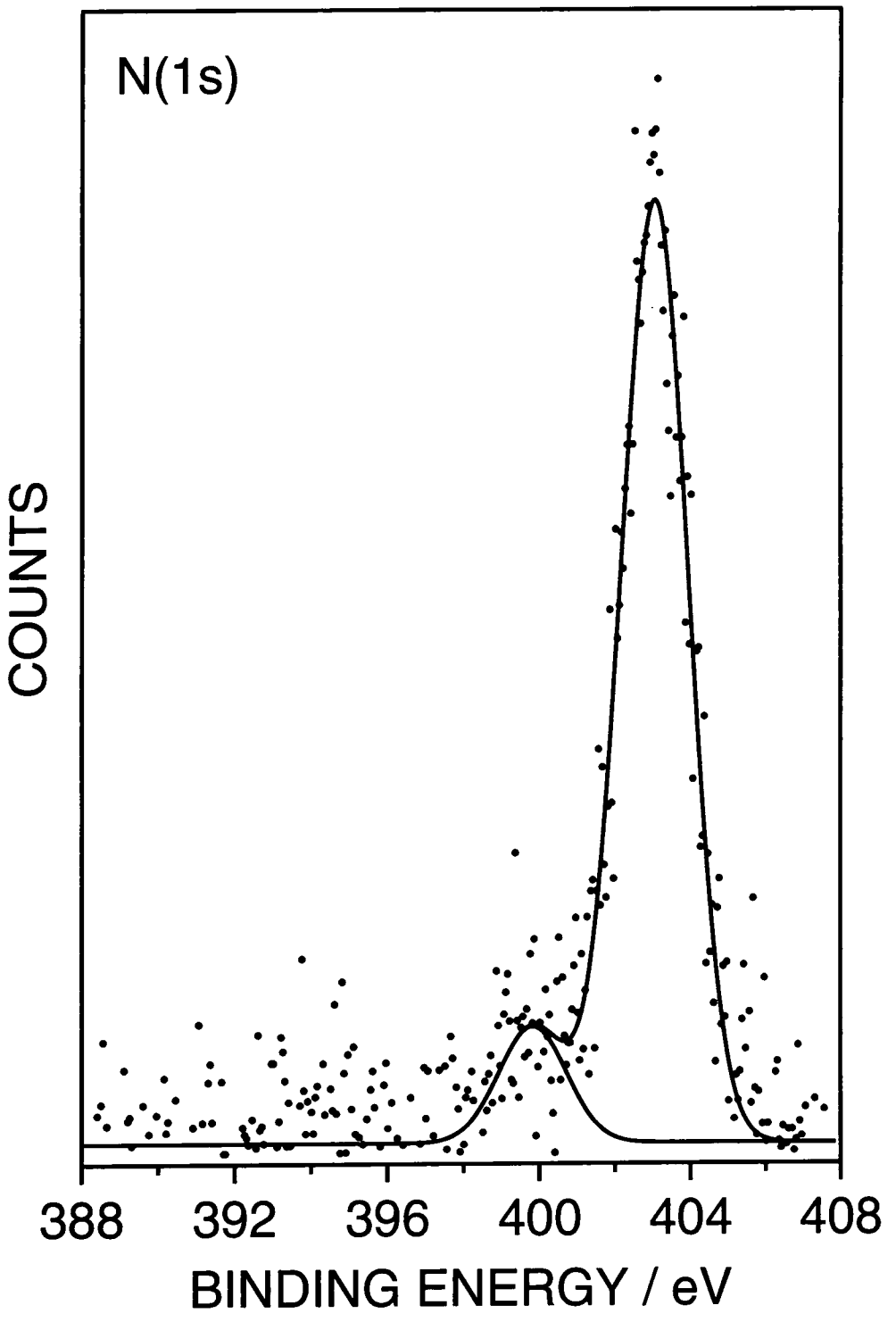

Figure 4.13: N(1s) XPS spectra of allyl amine pulsed plasma polymer (t_{on} = 20 μs, t_{off} = 1000 μs, P_p = 5 W) treated with $R_f(C_nH_{2n})_x(alkyl)_2N^+$-$O^-$.

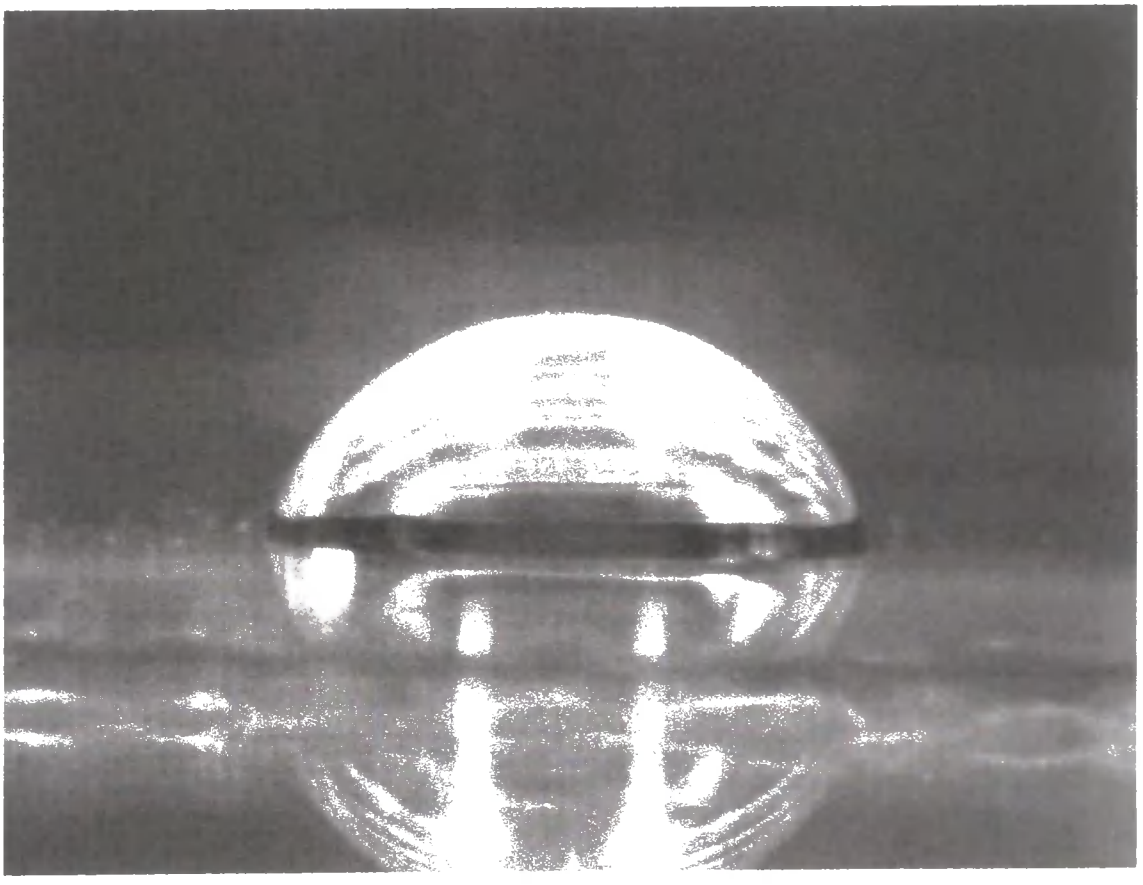

Figure 4.14: Hexadecane on the surface of $R_f(C_nH_{2n})_x(alkyl)_2N^+$-$O^-$treated allyl amine pulsed plasma polymer.

The attachment of fluorosurfactant to the allyl pulsed plasma polymer surface was investigated as a function of bulk solution surfactant concentration. Allyl amine pulsed plasma polymer was deposited onto glass substrates under the same deposition conditions. These samples were placed in various aqueous solutions of different bulk solution $R_f(C_nH_{2n})_x(alkyl)_2N^+$-$O^-$ concentrations and rinsed and dried following the above procedure (Section 4.2.4). High resolution XPS spectra of the C(1s) and N(1s) regions showed that the surface functionalisation varied little above a bulk solution $R_f(C_nH_{2n})_x(alkyl)_2N^+$-$O^-$ concentration of 2%, Figures 4.15 and 4.16. The fluorine to carbon (F/C) ratio of the pulsed plasma polymer, measured by XPS, demonstrated this trend further, Figure 4.17.

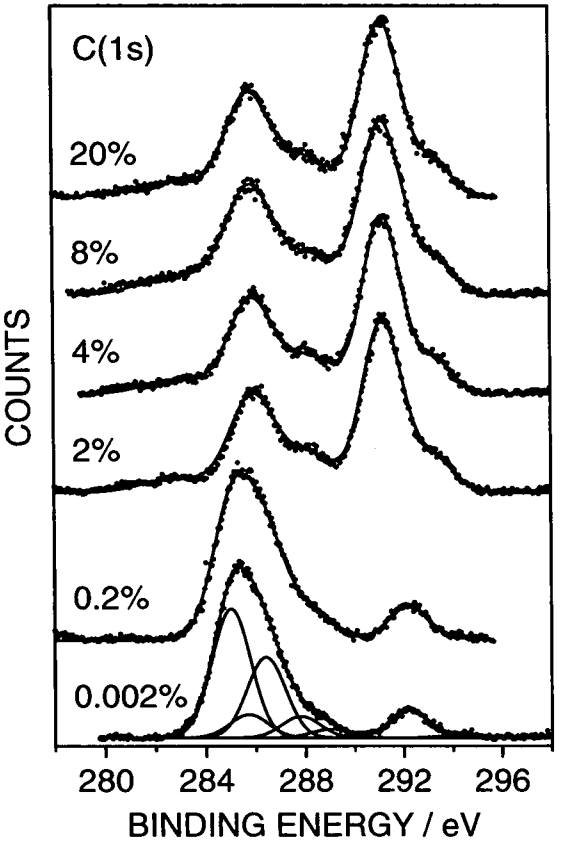

Figure 4.15: C(1s) XPS spectra of allyl amine pulsed plasma polymer treated with $R_f(C_nH_{2n})_x(alkyl)_2N^+\text{-}O^-$ as a function of bulk solution $R_f(C_nH_{2n})_x(alkyl)_2N^+\text{-}O^-$ concentration.

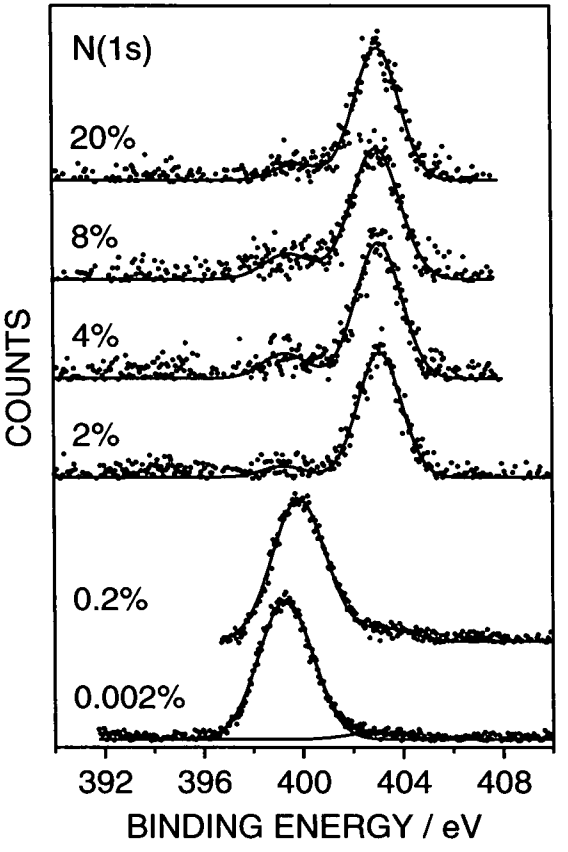

Figure 4.16: N(1s) XPS spectra of allyl amine pulsed plasma polymer treated with $R_f(C_nH_{2n})_x(alkyl)_2N^+\text{-}O^-$ as a function of bulk solution $R_f(C_nH_{2n})_x(alkyl)_2N^+\text{-}O^-$ concentration.

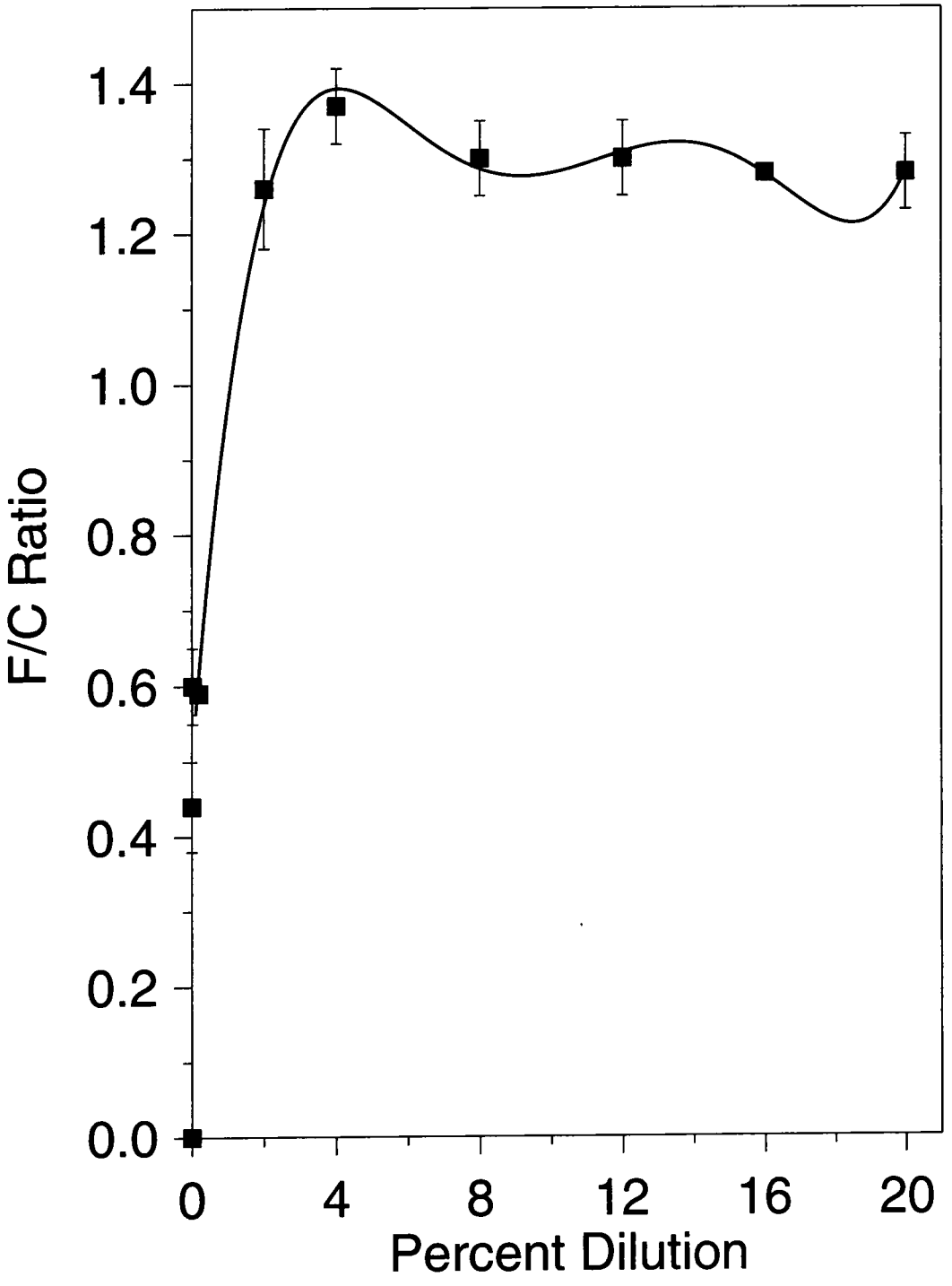

Figure 4.17: Graph of the F/C ratio of $R_f(C_nH_{2n})_x(alkyl)_2N^+$-$O^-$- treated allyl amine pulsed plasma polymer layers as a function of bulk solution $R_f(C_nH_{2n})_x(alkyl)_2N^+$-$O^-$ concentration.

4.4 DISCUSSION

Comparison of the FTIR spectra for the allyl amine monomer and its plasma polymer showed that during plasma polymerisation rearrangement of the monomer molecules had taken place. Bands present in the monomer spectrum were considerably broadened or even lost completely in the spectrum of the plasma polymer. The primary amine stretch double absorption band (1) in the monomer spectrum was broadened in the plasma polymer and may have arisen from several different nitrogen functionalities such as primary and secondary amines and imine groups.[1] Furthermore, the primary N-H bending absorption (6) was considerably broadened in the plasma polymer and may have contained contributions from a carbon-carbon (C=C) double bond stretch, an imine stretch (C=N), a carbonyl stretch (C=O) or an amide stretch (C(-N)=O). However, absorption due to C-H stretching vibrations (2) from alkene groups (=CH_2 and =CH) and other C-H bending absorptions characteristic of alkenes (4,7,8 and 10) were not retained in the plasma polymer. This is strong evidence that the alkene (C=C) double bond was lost during plasma polymerisation.[33] A carbon dioxide stretching absorption from the atmosphere was also detected in the plasma polymer spectrum (14). This may have contained a small contribution from the nitrile (C≡N) absorption. From examination of the IR results it can be concluded that double bonds were lost and new groups such as secondary amines, imines, carbonyls and amides were formed during plasma polymerisation of allyl amine.

The high resolution C(1s) spectra were peak fitted with four different carbon functionalities by reference to literature[1,30,31] and the IR spectra. XPS spectroscopy cannot distinguish between primary and secondary amines. The imine functionality was fitted at 286.8 eV but this may also have included a very small contribution from the nitrile group.[1,30] The peak at 288.0 eV arose from carbon doubly bonded to an oxygen atom, either as a carbonyl group or as an amide (C(-N)=O) functionality. From XPS analysis of the allyl amine plasma polymer it was evident that nitrogen elimination in the plasma increased with increasing discharge power. At low discharge powers, the main route for plasma polymer formation was expected to be via opening of the double bond,[1] reaction (7), Figure 4.18. However, even at the lowest CW power sustainable, IR and

XPS results showed that a high proportion of other functionalities such as secondary amines, imines and amides had been incorporated into the plasma polymer. These functionalities must have been present as a result of monomer fragmentation and reorganisations (Figure 4.18).[1] Reactions (1) to (4) (Figure 4.18) lead to the formation of carbon-nitrogen multiple bonds via hydrogen radical abstraction due to electron bombardment of species in the glow discharge. The enhancement of these processes, which led to an increase in the percentage of hydrocarbon and imine groups with increasing discharge power, was due to an increase in the electron energy in the plasma. The discharge power affects the electron energy distribution within the reactor.[36] Increasing the power increases the number of high energy electrons with sufficient energy to cause monomer fragmentation and cross-linking processes.[37] Increasing the population of high energy electrons promotes the rate of molecular excitement and, therefore, the intensity of VUV induced damage of the growing polymeric film.[38] Increasing the discharge power will also produce a corresponding increase in the plasma sheath potential formed around electrically isolated surfaces in contact with the plasma.[37] This will increase the energy at which ions formed in the gas discharge bombard the growing film.[39] Such ion bombardment will affect the chemical nature of the plasma polymer. An interesting finding is that the oxygenated functionality detected in the XPS spectra decreased with increasing average power. This may indicate that plasma polymers formed by low power discharges were more reactive and retained a greater proportion of intact amine functionalities than polymers produced under more energetic conditions.

Reactions leading to the formation of imine or nitrile functions:

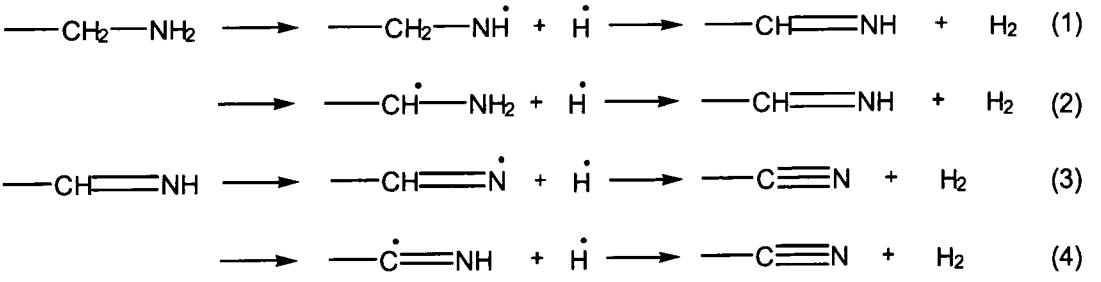

Initiation reactions via the multiple bonds:

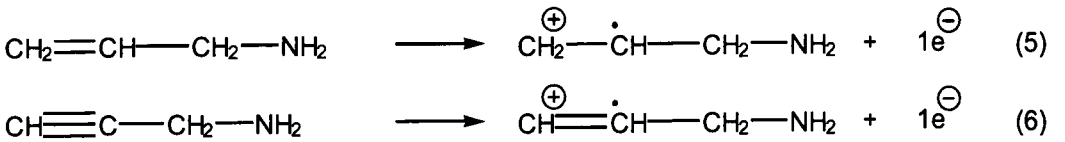

Propagation reactions via the multiple bonds:

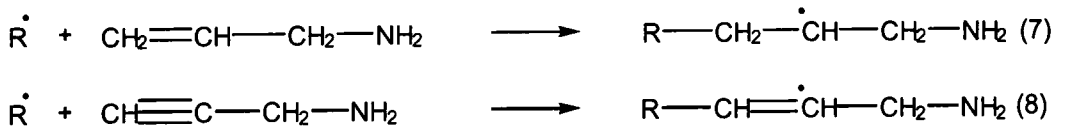

Reactions of the primary amine with radicals:

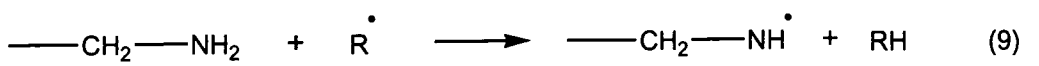

Figure 4.18: Possible reactions in the allyl amine glow discharge.[1]

In an effort to increase the amine group retention in the plasma polymer the average power during plasma polymerisation was decreased further by electrically pulsing the discharge. Evaluation of the pulsing parameters found that a number of factors affected the C-N group retention. However, the plasma on-time was shown to have by far the greatest influence on the response. It was therefore decided to investigate the pulsed plasma polymerisation of allyl amine as a function of on-time. Enhancement of functional group retention of allyl

amine plasma polymers by pulsing the discharge has been reported.[3] The highly functionalised thin films formed were used to investigate the adsorption and denaturation of fibrinogen.[4] An increase in structural retention with decreasing on-time was evident from the increased proportion of C-N groups at the lowest on-times. Furthermore, at these short plasma on-times the proportion of C=N groups reached a minimum of approximately 17%. The increase in structural retention with decreasing plasma on-time was a result of a reduction in monomer fragmentation processes which occurred during the on-time. Propagation reactions via activation of the double bond (reactions 7 and 8, Figure 4.18) may also have occurred in the plasma off-time.[40-42] In the off-time reactions only proceed via addition of unfragmented monomer molecules to active species formed in the plasma on-time (reaction 7, Figure 4.18). Such processes would tend to increase the proportion of amine functionalities included in the plasma polymer. However, even at the lowest on-times, the incorporation of imine groups into the plasma polymer provided evidence for continued monomer fragmentation and rearrangement reactions. Comparison of the N/C ratio and the percentage contribution of the different carbon functionalities showed that the relative increase in the nitrogen content must have been due to an increase in the incorporation of unfragmented monomer molecules. An increase in the percentage of carbonyl or amide groups with decreasing average power, as seen for the CW plasma polymerisation of allyl amine, could indicate an increase in the amine content of the plasma polymer. Amines are powerful nucleophiles and may have reacted with oxygenated species within the glow discharge or carbon dioxide in the atmosphere on venting of the reactor.[43]

The allyl amine pulsed plasma polymer was found to be fairly stable in aqueous solution.[4] The amphoteric fluorosurfactant $R_f(C_nH_{2n})_x(alkyl)_2N^+\text{-}O^-$, dissolved in an aqueous solution, was readily attached to the plasma polymer surface. XPS analysis of the N(1s) region revealed that the nitrogen group ($\text{-}(alkyl)_2N^+\text{-}O^-$) of the surfactant was present on the plasma polymer surface. Consideration of the F/C ratio, as a function of surfactant concentration in the bulk solution, revealed a rapid increase in surfactant adsorption at the plasma polymer-solution interface on increasing the bulk surfactant concentration from 0.2 to 2%. Such a rapid increase of surfactant adsorption over this bulk solution surfactant concentration

range may have been due to the onset of cooperative binding of the surfactant molecules at the plasma polymer surface (Section 1.7.5).[44,45] Above this bulk solution surfactant concentration, the F/C ratio reached a plateau value indicative of surfactant saturation at the plasma polymer surface. The mechanism of surfactant adsorption to the allyl amine plasma polymer surface was difficult to ascertain. Treatment of the allyl amine pulsed plasma polymer with the cationic fluorosurfactant $CF_3(CF_2)_nC_2H_5(alkyl)_3N^+$ resulted in a low amount of surfactant adsorption, Figure 4.19. Therefore, nucleophilic attack by the amine functionality cannot explain the high levels of adsorption displayed by the amphoteric fluorosurfactant $R_f(C_nH_{2n})_x(alkyl)_2N^+\text{-}O^-$. The satellites from the fluorinated carbon peaks were of insufficient area to account for the shoulder observed to low binding energy of the hydrocarbon peak in Figure 4.19. Therefore, this shoulder was attributed to differential surface charging effects.[46] The differential charging was often observed when non-conducting polymeric samples were treated in ionic solutions. Under the slightly acidic conditions of the aqueous $R_f(C_nH_{2n})_x(alkyl)_2N^+\text{-}O^-$ solution (pH 6 at 20°C)[47] the amine functionalities were likely to be positively charged.[2] Therefore, some kind of electrostatic interaction between the cationic plasma polymer and the amphoteric surfactant molecule could be envisaged.[48]

The wettability of the fluorosurfactant coated plasma polymer samples was investigated using the video contact angle apparatus (Section 1.8.4). Surfactant treatment lowered the water contact angle of the allyl amine plasma polymer. This result was not expected as fluorocarbon surfaces typically increase the water contact angle due to their low surface energies[35] (CF_2 dominated surfaces have approximate advancing and receding water contact angles of 116° and 92° respectively).[49] Furthermore, the hexadecane contact angle was significantly increased which is symptomatic of the formation of a low energy fluorinated surface.[35] Water should possess a higher contact angle on a given surface than hexadecane because it has a higher surface tension than hexadecane and is therefore easier to repel.[31] These apparently contradictory results were mirrored in Chapter 3 and similar behaviour has been demonstrated by adsorbed ionic fluorosurfactant on oppositely charged mica surfaces.[50]

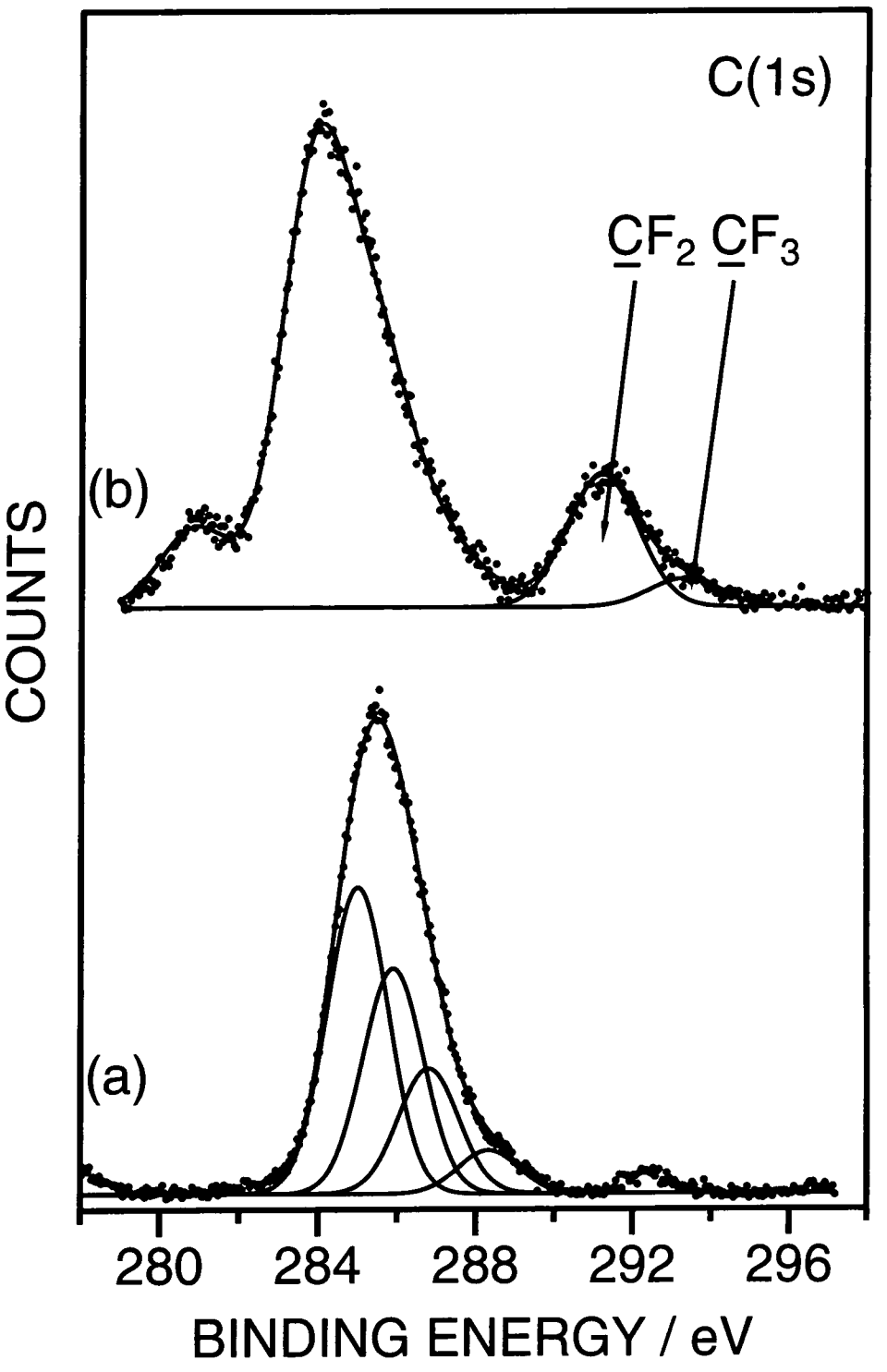

Figure 4.19: C(1s) XPS spectra of (a) allyl amine pulsed plasma polymer (t_{on} = 20 μs, t_{off} = 4 ms and P_p = 5 W); and (b) $CF_3(CF_2)_nC_2H_5(alkyl)_3N^+$ treated allyl amine pulsed plasma polymer.

4.5 CONCLUSION

Fluorosurfactant was again attached to the plasma polymer surface. The mechanism of surfactant adsorption is tentatively suggested to be electrostatic interaction between positively charged amine groups on the plasma polymer surface and the amphoteric surfactant head group. Low amounts of cationic fluorosurfactant adsorption on the allyl amine plasma polymer surface may be a result of electrostatic repulsion between like charges. The fluorinated surfaces produced displayed a complicated wetting behaviour symptomatic of a heterogeneous or mobile surface structure.

4.6 REFERENCES

1. Fally, F.; Doneux, C.; Riga, J.; Verbist, J. J. *J. Appl. Polym. Sci.* **1995**, *56*, 597.
2. Hsieh, M. C.; Farris, R. J.; McCarthy, T. J. *Macromolecules* **1997**, *30*(26), 8453.
3. Rinsch, C. L.; Chen, X.; Panchalingam, V.; Savage, C. R.; Wang, Y. H.; Eberhart, R. C.; Timmons, R. B. *Abs. Pap. Am. Chem. Soc.* **1995**, *209*(2), 141.
4. Tang, L.; Wu, Y.; Timmons, R. B. *J. Biomed. Mater. Res.* **1998**, *42*, 156.
5. Ko, T. M.; Cooper, S. L. *J. Appl. Polym. Sci.* **1993**, *47*, 1601.
6. Beck, A. J.; Short, R. D.; Jones, F. R. *Polymer* **1996**, *37*(24), 5537.
7. France, R. M.; Short, R. D.; Dawson, R. A.; MacNeil, S. *J. Mater. Chem.* **1998**, *8*(1), 37.
8. Antonietti, M.; Burger, C.; Effing, J. *Adv. Mater.* **1995**, *7*(8), 751.
9. Goddard, E. D. *Coll. Surf.* **1986**, *19*, 301.
10. Lindman, B.; Thalberg, K. In *Interactions of Surfactants with Polymers and Proteins*; Goddard, E. D.; Ananthapadmanabhan, K. P., Eds.; CRC Press: Boca Raton, 1993.
11. Okuzaki, H.; Osada, Y. *Macromolecules* **1994**, *27*(2), 502.
12. Okuzaki, H.; Eguchi, Y.; Osada, Y. *Chem. Mater.* **1994**, *6(10)*, 1651.
13. Zezin, A. B.; Izumrudov, V. A.; Kabanov, V. A. *Macromol. Symp.* **1996**, *106*, 397.
14. Thalberg, K.; Lindman, B.; Karlström, G. *J. Phys. Chem.* **1991**, *95*(8), 3370.
15. Shimizu, T.; Seki, M.; Kwak, J. C. T. *Coll. Surf.* **1986**, *20*, 289.
16. Shimizu, T. *Colloids Surfaces A: Physicochem. Eng. Aspects* **1995**, *94*, 115.
17. Okuzaki, H.; Osada, Y. *Macromolecules* **1995**, *28*(13), 4554.
18. Macdonald, P. M.; Tang, A. J. *Langmuir* **1997**, *13*(8), 2259.
19. Fundin, J.; Hansson, P.; Brown, W.; Lidegran, I. *Macromolecules* **1997**, *30*(4), 1118.
20. Thalberg, K.; Lindman, B.; Bergfeldt, K. *Langmuir* **1991**, *7*(12), 2893.
21. Herslöf, Å.; Sundelöf, L.-O.; Edsman, K. *J. Phys. Chem.* **1992**, *96*(5), 2345.
22. Antonietti, M.; Burger, C.; Conrad, J.; Kaul, A. *Macromol. Symp.* **1996**, *106*, 1.
23. Antonietti, M.; Conrad, J.; Thünemann, A. *Macromolecules* **1994**, *27*(21), 6007.
24. Hayakawa, K.; Kwak, J. C. T. In *Cationic Surfactants: Physical Chemistry*; Rubingh, D. N.; Holland, P. M., Eds.; Marcel Dekker: New York, 1991; Vol. 37, pp. 189-248.
25. Hayakawa, K.; Kwak, J. C. T. *J. Phys. Chem.* **1982**, *86*(19), 3866.
26. Antonietti, M.; Henke, S.; Thünemann, A. *Adv. Mater.* **1996**, *8*(1), 41.
27. Bell, A. T.; Nakajima, K.; Shen, M. *J. Appl. Polym. Sci.* **1979**, *23*, 2627.
28. Wagner, C. D.; Riggs, W. M.; Davis, L. E.; Moulder, J. F.; Muilenber, G. E. *Handbook of X-Ray Photoelectron Spectroscopy*; Perkin-Elmer: New

York, 1978.
29. Wells, R. K.; Ryan, M. E.; Badyal, J. P. S. *J. Phys. Chem.* **1993**, *97*, 12879.
30. Beamson, G.; Briggs, D. *High Resolution XPS of Organic Polymers, The Scienta ESCA 300 Database*; John Wiley & Sons: Chichester, 1992.
31. Jasper, J. J. *J. Phys. Chem. Ref. Data* **1972**, *1*(4), 841.
32. Silverstein, R. M.; Bassler, G. C.; Morrill, T. C. *Spectrometric Identification of Organic Compounds*; John Wiley & Sons: Chichester, 1993.
33. Krishnamurthy, V.; Kamel, I. L. *J. Polym. Sci.: Part A: Polymer Chemistry* **1989**, *27*, 1211.
34. Morgan, E. *Chemometrics: Experimental Design*; John Wiley & Sons: Chichester, 1991.
35. Kissa, E. In *Handbook of Fibre Science and Technology*, Part B ed.; Lewin, M.; Sells, S. B., Eds.; Marcel Dekker Inc.: New York, 1984; Vol. II, pp. 143-209.
36. McTaggart, F. K. *Plasma Chemistry in Electrical Discharges*; Elsevier Publishing Company: London, 1967.
37. Grill, A. *Cold Plasmas in Materials Technology*; IEEE Press: New Jersey, 1994.
38. Hudis, M.; Prescott, L. E. *Polym. Lett.* **1972**, *10*, 179.
39. Flamm, D. L. In *Plasma Etching: An Introduction*; Manos, D. M.; Flamm, D. L., Eds.; Academic Press, Inc.: London, 1989; pp. 91-184.
40. Panchalingam, V.; Chen, X.; Savage, C. R.; Timmons, R. B.; Eberhart, C. *J. Appl. Polym. Sci.: Appl. Polym. Sym* **1994**, *54*, 123.
41. Badyal, J. P. S.; Hynes, A. M. *Chem. Mater.* **1998**, *10*, 2177.
42. Rinsch, C. L.; Chen, X.; Panchalingam, V.; Eberhart, C.; Wang, J.-H.; Timmons, R. B. *Langmuir* **1996**, *12*, 2995.
43. Challis, B. C.; Butler, A. R. In *The Chemistry of the Amino Group*; Patai, S., Ed.; Interscience: London, 1968; p. 278.
44. Rosen, M. J. *Surfactants and Interfacial Phenomena*, 2nd ed.; John Wiley & Sons: New York, 1989.
45. Myers, D. *Surfactant Science and Technology*; VCH: New York, 1988.
46. Barr, T. L. In *Practical Surface Analysis*, 2nd ed.; Briggs, D.; Sean, M. P., Eds.; J. Wiley & Sons: Chichester, 1990; Vol. Volume 1 Auger and X-ray Photoelectron Spectroscopy, p. 370.
47. Clariant GmbH, D. P. P. P., BU Textile Chemicals. Private Communication.
48. Lee, L.-H. In *Contact Angle, Wettability and Adhesion*; Mittal, K. L., Ed.; VSP: Utrecht, 1993; pp. 45-96.
49. Brandrup, J.; Immergut, E. H., Eds. *Polymer Handbook*, 2nd ed.; J. Wiley & Sons: London, 1975.
50. Claesson, P. M.; Herder, P. C.; Berg, J. M.; Christenson, H. K. *J. Colloid Interface Sci.* **1990**, *136*(2), 541.

CHAPTER FIVE

SURFACE REACTIONS OF PLASMA POLYMERISED ALLYL ALCOHOL

5.1 INTRODUCTION

Allyl alcohol possesses an alcohol group and a double bond, Structure 5.1, making it an ideal candidate for the fabrication of a hydroxyl rich surface via plasma polymerisation. Plasma polymers formed from allyl alcohol have been described in the literature[1,2] and applications have been found in protein and cell adsorption.[3,4]

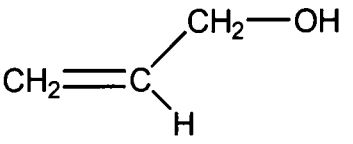

Structure 5.1: Allyl alcohol.

The retention of the hydroxyl functionality in the plasma polymer has been studied as a function of the monomer flow rate (F).[1] It has been found that decreasing the discharge power/monomer flow rate ratio (W/F, where W is the radio frequency (rf) power supplied to the plasma) increases hydroxyl functional group retention.[1,2,5-7] Other deposition parameters such as substrate position[6,8,9] and substrate temperature[10,11] also have had an effect on the hydroxyl group retention. However, these approaches suffered from several important limitations. If the W/F parameter is varied over too large a range then problems due to powdery or oily films and poor substrate adhesion were often encountered.[5] Furthermore, controlling substrate temperature and position had only a limited effect on functional group retention.[5] These problems are addressed by the use of pulsed rf discharges.[3,5,12-24] Pulsed plasmas have been shown to provide a high degree of control over thin film chemistry without the problems associated with the variation of other plasma parameters. Examples of the formation of allyl alcohol pulsed plasma polymers have demonstrated the applicability of this approach to increasing the hydroxyl group retention in allyl alcohol plasma polymerisations.[5,25]

This Chapter reports a further investigation into the continuous wave (CW) and pulsed plasma deposition of allyl alcohol and the subsequent reaction of the thin films thus formed. The plasma polymerised allyl alcohol thin films were characterised by XPS spectroscopy. However, this technique was limited by the relatively small difference in carbon 1s (C1s) chemical shifts observed in the core level binding energies of the C-O-H and C-O-C groups.[1] These groups cannot be unambiguously identified by XPS without further derivatisation reactions. The aim of such reactions is the chemical "tagging" of specific functional groups by the incorporation of new atoms which can be easily identified by XPS analysis.[1,5,26-31] Several stringent standards must be met for the successful derivatisation and unambiguous identification of surface functional groups:[1,30]

- The reaction must be specific to one functional group;
- A new easily identifiable chemical species must be introduced into the surface region;
- The reaction must proceed to completion rapidly and under mild conditions;
- Any solvents used must be able to penetrate the surface of the thin film at least to the XPS sampling depth to ensure complete reaction of the functional groups over the whole sampling range;
- Any solvent must be benign and not react with or damage the polymer layer.

The above criteria is difficult to meet for solvent based techniques because solvents often cause swelling of the polymer layer, reorganisation and loss of low molecular weight oligomers.[30] For these reasons vapour phase labelling reactions are preferred. Trifluoroacetic anhydride (TFAA) has been used extensively for the vapour phase labelling of hydroxyl groups and can be easily identified using XPS[1,2,29,31-33] due to the incorporation of a $\underline{C}F_3$ group which possesses a large chemical shift.[34] This reaction was therefore used for the quantitative identification of hydroxyl groups formed by the plasma polymerisation of allyl alcohol. The reaction generates a volatile by-product which is easily removed.[29] TFAA also reacts readily with epoxide groups[35] but the characteristic epoxide infrared adsorption between 1280 and 1260 cm^{-1} was not observed in the plasma polymer thin films formed and therefore this reaction was not considered important.[5]

The hydroxyl group derivatised thin films produced were reacted with tertra(*tert*-butoxy)zirconium to produce a surface which was reactive towards further derivatisation. Surface bound alkoxyzirconium species were formed by the covalent attachment of tertra(*tert*-butoxy)zirconium to hydroxylated metal oxide surfaces.[36,37] These surfaces were further derivatised with poly(acrylic acid).[37] It was hoped that the technique could be successfully applied to hydroxyl functionalised plasma polymer surfaces to increase the applicability and utility of the process. Such surface bound poly(acrylic acid) complexes are candidates for layer-by-layer deposition of polyelectrolytes to form complexes with novel surface properties.[38-50]

5.2 EXPERIMENTAL PROCEDURE

5.2.1 APPARATUS AND PROCEDURE

The experimental apparatus and procedure for plasma depositions has been described above (Chapter 2). Allyl alcohol monomer (Aldrich, 99% purity) was further purified by multiple freeze-thaw cycles. Prior to each experiment the reactor was scrubbed clean with detergent and scouring powder, rinsed with copious amounts of water and isopropyl alcohol (IPA) before being oven dried. Before polymerisation, air was emitted into the reactor and a 50 W air cleaning plasma was ignited at a pressure of 0.2 mbar for 30 minutes. The reactor was pumped down to base pressure following air plasma cleaning, isolated from the pump and opened up to the atmosphere to allow insertion of the substrate. Glass slides cleaned as described above (Section 2.2) were used as the substrate for XPS analysis and further reaction. Polished sodium chloride plates were used as substrates for ATR-FTIR analysis. The substrate was positioned at the centre of the copper coils and the system pumped back down to base pressure. At this stage the leak rate of the reactor was determined (Section 2.2.2.1). Acceptable leak rates were below 1×10^{-9} mol s^{-1}. Allyl alcohol vapour was then introduced into the reactor at a pressure of 0.2 mbar and the flow rate was calculated (Section 2.2.2.2). The flow rate was kept constant at approximately 8.1×10^{-7} mol

s^{-1}. This resulted in a monomer purity in the reactor of 99.9%. The glow discharge was ignited and immediately balanced using the matching network. After the treatment time of 10 minutes had elapsed the plasma was extinguished and the monomer was purged through the system for a further two minutes.

5.2.2 CW PLASMA POLYMERISATION

CW plasma polymerisation of allyl alcohol was carried out as described above. Following ignition of the plasma the discharge power was set according to the power meter and the plasma balanced. After plasma polymerisation the sample was removed from the reactor and immediately analysed by XPS and ATR-FTIR.

5.2.3 ELECTRICALLY PULSED PLASMA POLYMERISATION

For electrically pulsed plasma experiments a pulse generator supplied a pulse of 5 V amplitude to modulate the RF generator as described earlier (Section 2.2.1.2). It was necessary to set up the reaction conditions prior to the insertion of the substrate as the plasma had to be balanced under CW conditions. Therefore, following the air cleaning plasma, air was emitted into the reactor via the leak valve. A plasma was ignited, the power set and the pulsing was switched on. The overall average power (<P>) supplied to the system was calculated (Equation 2.1, Section 2.2.1.2).[24] After the reactor had been prepared it was vented to the atmosphere to allow insertion of the substrates. From this point the experimental procedure was essentially the same as that for CW plasma polymerisation (Section 5.2.2) except that the plasma discharge conditions had already been determined.

5.2.4 TFAA LABELLING OF ALLYL ALCOHOL CW PLASMA POLYMER

Allyl alcohol CW plasma polymer deposited onto glass substrates at a discharge power of 5 W for 10 minutes was placed in a glass tube and evacuated. The

sample was then isolated from the pump and exposed to TFAA vapour at a reduced pressure for 30 minutes. Following TFAA exposure the sample was pumped down to base pressure and then vented to air. These samples were subsequently analysed by XPS.

5.2.5 REACTION WITH TERTRA(*TERT*-BUTOXY)ZIRCONIUM ($Zr(OC(CH_3)_3)_4$) AND POLY(ACRYLIC ACID)

Allyl alcohol plasma polymers deposited under a variety of discharge conditions were placed into a tube and evacuated to a base pressure of 5×10^{-3} mbar. A second monomer tube containing $Zr(OC(CH_3)_3)_4$ liquid (Aldrich, 99% purity) was opened to the vacuum exposing the sample to $Zr(OC(CH_3)_3)_4$ vapour at a pressure of approximately 0.2 mbar, with constant pumping, for 1 hour. Subsequently the $Zr(OC(CH_3)_3)_4$ liquid was isolated from the system and the sample was evacuated to base pressure for a further hour to remove any unreacted $Zr(OC(CH_3)_3)_4$ vapour physisorbed onto the polymeric surface. The apparatus was then vented to atmosphere and the sample was analysed by XPS. Some samples treated with $Zr(OC(CH_3)_3)_4$ vapour were placed in 1% poly(acrylic acid) dissolved in dioxane for 1 hour. Following treatment the samples were removed from the poly(acrylic acid) solution, rinsed in fresh dioxane for 10 minutes, dried under vacuum and analysed by XPS.

5.2.6 SAMPLE CHARACTERISATION

5.2.6.1 XPS Characterisation

Samples were characterised immediately following plasma polymerisation by XPS spectroscopy. The glass slides were attached to a stainless steel probe stud using double sided adhesive tape and inserted into a Vacuum Generators ESCA Lab Mk II photoelectron spectrometer. The spectrometer was fitted with an unmonochromated magnesium X-ray source (Mg $K\alpha_{1,2}$ = 1253.6 eV) and operated in the constant analyser energy mode (CAE = 20 eV for high resolution spectra, 50 eV for survey scans). Photoelectrons emitted from the substrate

were collected at a 30° take-off angle with respect to the substrate normal. The spectrometer calibration was routinely checked using the gold $4f_{7/2}$ and silver $3d_{5/2}$ peaks at 83.8 and 368.3 eV respectively.[51] Elemental sensitivity factors were determined experimentally relative to the carbon 1s (C(1s)) peak (285.0 eV) using standard compounds. These were taken as C(1s) : F(1s) : O(1s) : N(1s) : Si(2p) = 1.00 : 0.24 : 0.39 : 0.65 : 1.00 respectively. The absence of any Si(2p) XPS feature following plasma polymerisation was indicative of complete coverage of the glass substrate.

5.2.6.2 ATR-FTIR Characterisation

An FTIR Mattson Polaris instrument fitted with a golden gate apparatus for attenuated total reflection (ATR) spectroscopy was used for infrared analysis of plasma polymers deposited onto polished sodium chloride plates. Typically 128 scans were acquired at a resolution of 4 cm^{-1}.

5.3 RESULTS

High resolution XPS envelopes were fitted using a Marquardt minimisation routine. The peak shape was assumed to be Gaussian with a fixed relative full width at half maximum.[52] The C(1s) region of a typical allyl alcohol plasma polymer layer was fitted with three different carbon functionalities[5,34] (using the hydrocarbon peak at 285.0 eV as a reference offset): an unfunctionalised hydrocarbon group ($\underline{C}_xH_y$ at 285.0 eV); a carbon singly bonded to an oxygen function ($\underline{C}$-O 286.6 eV); and a carbonyl group ($\underline{C}$=O 288.0 eV), Figure 5.1. The O(1s) region was fitted with one oxygen peak,[34] Figure 5.2. The O/C ratio was found from the O(1s) and C(1s) peak areas (after correction for sensitivity).

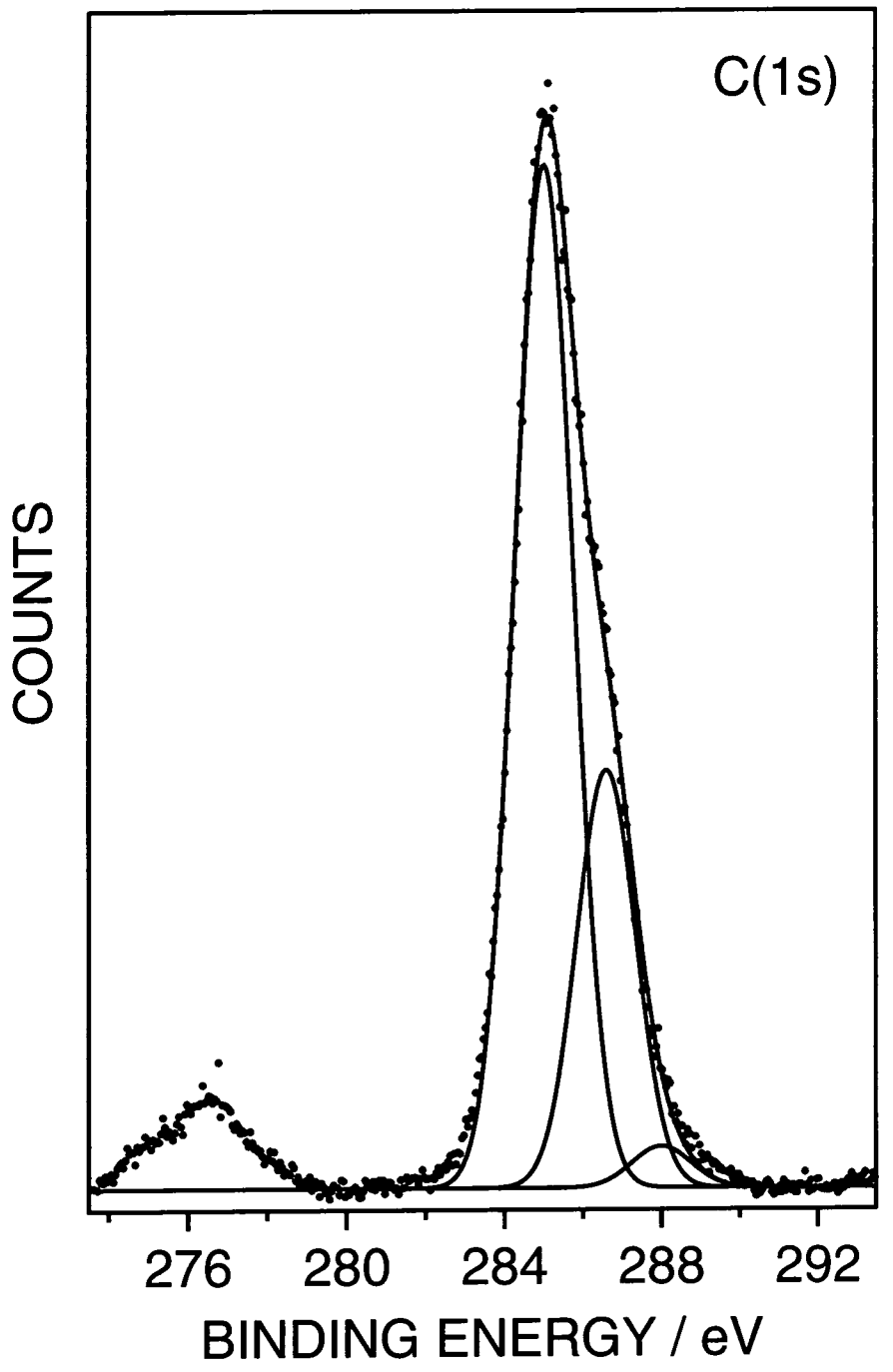

Figure 5.1: C(1s) XPS spectra of 2 W CW allyl alcohol plasma polymer.

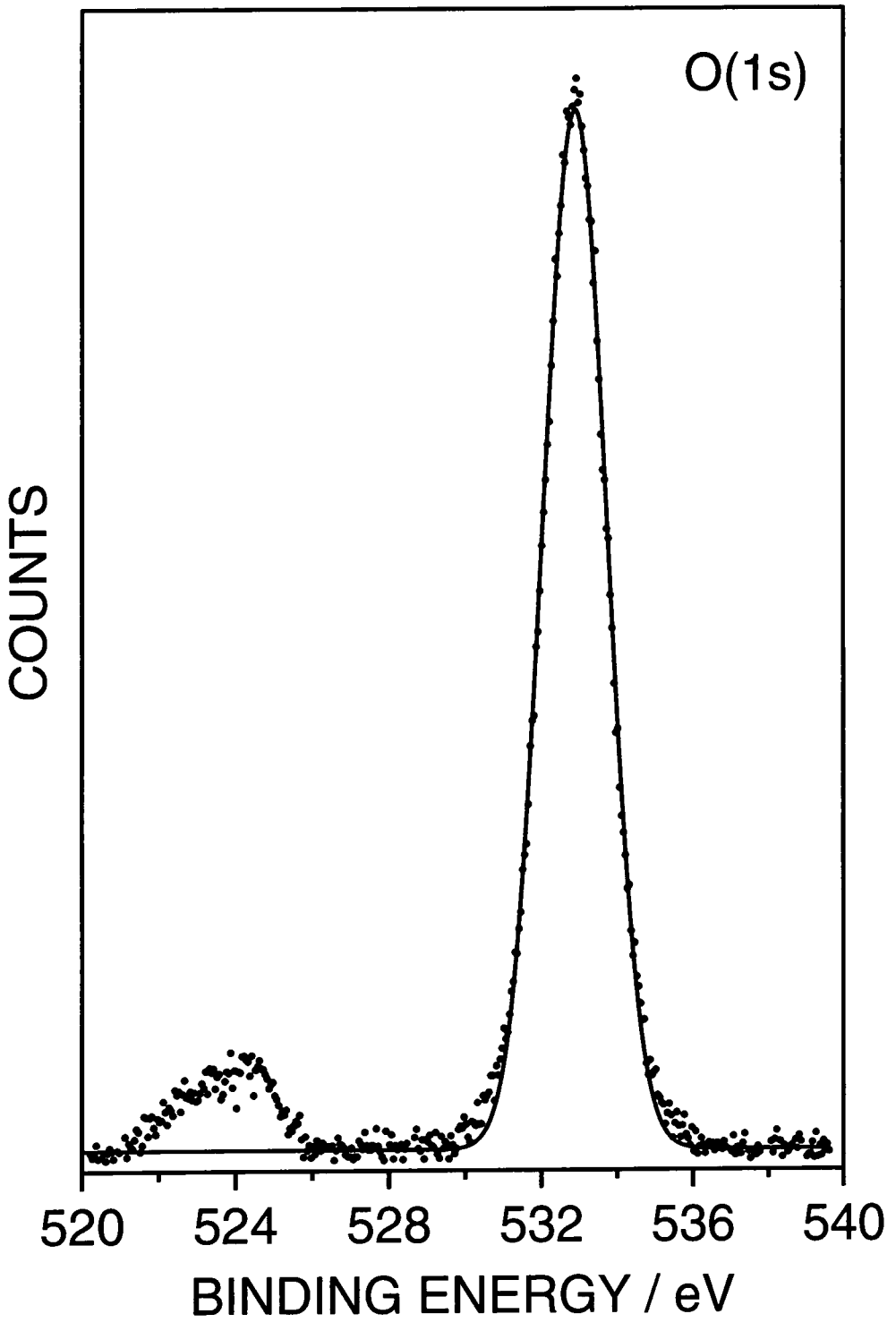

Figure 5.2: O(1s) XPS spectra of 2 W CW allyl alcohol plasma polymer.

5.3.1 CW PLASMA POLYMERISATION OF ALLYL ALCOHOL

IR absorption peaks present in the ATR-FTIR spectrum of the allyl alcohol monomer were identified with reference to the literature,[5,53] Figure 5.3: O-H stretching vibration with intermolecular hydrogen bonding 3310 cm^{-1}; C-H stretching vibrations for $=CH_2$ and =CH- groups at 3010 and 2989 cm^{-1} respectively; aliphatic C-H stretches at 2910 and 2860 cm^{-1}; C=C stretching vibration 1645 cm^{-1}; O-H in plane bending absorption and CH_2 in plane deformation for $=CH_2$ 1424 cm^{-1}; C-O stretching absorption 1113 cm^{-1}; C-H out of plane deformations for $=CH_2$ and =CH- 991 cm^{-1}; and CH_2 out of plane deformation for $=CH_2$ and =CH- 914 cm^{-1}. The ATR-FTIR spectra of the CW allyl alcohol plasma polymer deposited onto NaCl plates showed that many characteristic absorbencies of the monomer molecule were broadened, shifted in position or lost altogether during plasma polymerisation, Figure 5.3. Furthermore, new peaks not present in the monomer spectrum were evident in the plasma polymer. The ATR-FTIR spectrum of the allyl alcohol 2 W CW plasma polymer had the following absorption peaks: O-H stretching vibration with intermolecular hydrogen bonding 3327 cm^{-1}; aliphatic C-H stretches at 2935 and 2880 cm^{-1}; C=O stretching vibration 1705 cm^{-1}; aliphatic CH_2 scissoring band 1458 cm^{-1}; O-H in plane bending absorption 1379 cm^{-1}; and C-O stretching absorption 1038 cm^{-1}. Bands arising from the unsaturated carbon functionality in the monomer molecule were absent from the plasma polymer spectra. Absorbencies that arose from the O-H and C-O stretching vibrations decreased, relative to other absorbencies, with increasing discharge power. Furthermore, the carbonyl absorption became relatively more intense as the discharge power increased.

The C(1s) XPS spectra of the CW allyl alcohol plasma polymer possessed a shoulder, to the high binding energy side of the hydrocarbon peak, which was identified as the C-O functionality. This shoulder was clearly seen to increase in size, relative to the unfunctionalised hydrocarbon peak, with decreasing CW discharge power, Figure 5.4. The O(1s) XPS spectra of the CW allyl alcohol plasma polymer increased in width with increasing CW discharge power, Figure 5.5. This indicated that at higher CW discharge powers oxygen atoms in a

number of chemically different environments were incorporated into the plasma polymer. The O/C ratio reached a maximum value of 0.29 ± 0.01 (the O/C ratio in the monomer molecule is 0.33) at a discharge power of 2 W, Figure 5.6. Below this power the electrical discharge became unstable. Above this minimum CW discharge power the O/C ratio decreased as the power increased. Deconvolution of the C(1s) spectra of allyl alcohol plasma polymer, deposited as a function of CW discharge power, aided quantification of the effect of power on the chemical composition of the plasma polymers, Figure 5.7. The percentage of unfunctionalised carbon atoms and C=O groups increased with increasing discharge power whereas the percentage of C-O groups decreased. The percentage of C-O groups reached a maximum of 29% ± 2, compared with 33% in the monomer molecule, at the lowest discharge power (2 W).

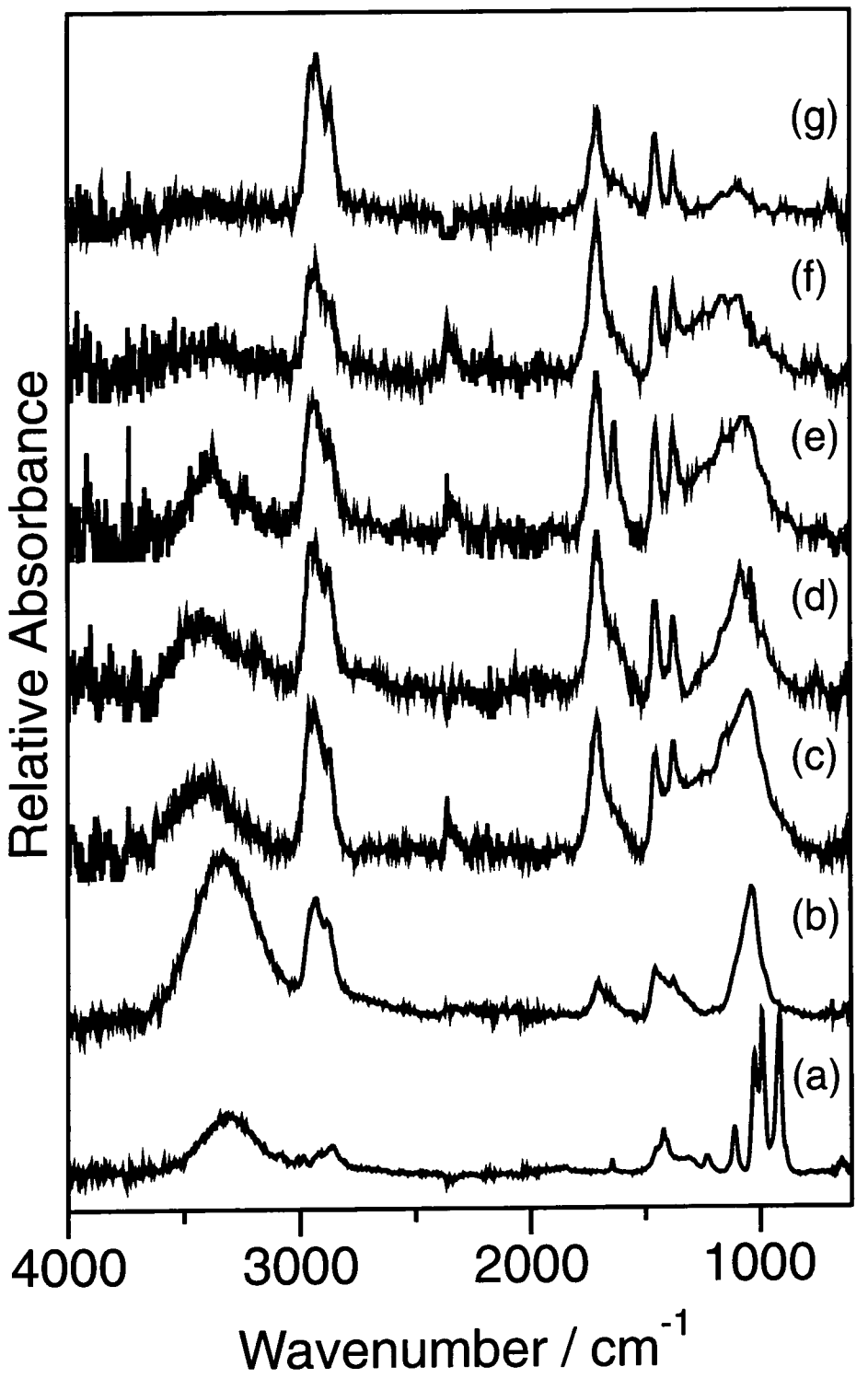

Figure 5.3: ATR-FTIR spectra of (a) allyl alcohol monomer and CW allyl alcohol plasma polymer deposited as a function of power; (b) 2 W; (c) 5 W; (d) 10 W; (e) 20 W; (f) 30 W; (g) 50 W.

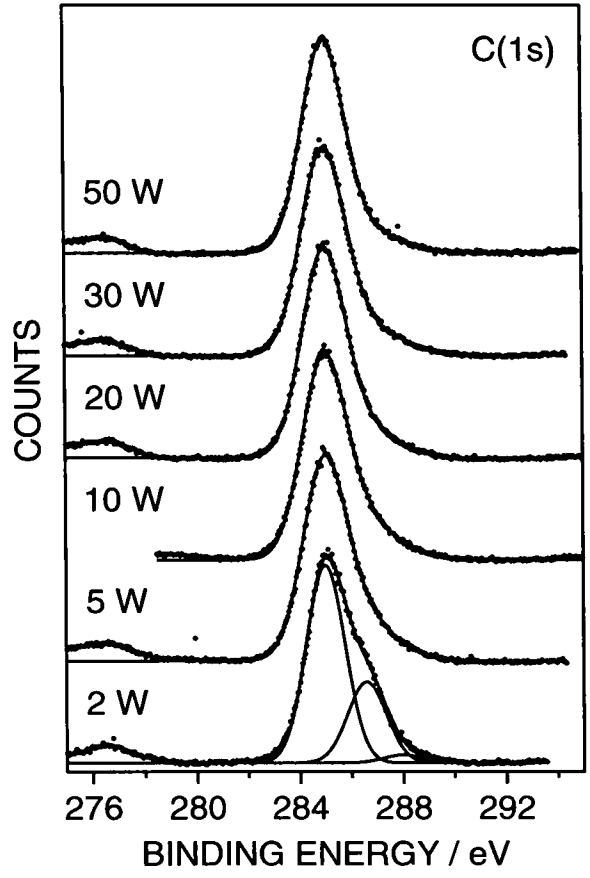

Figure 5.4: C(1s) XPS spectra of CW allyl alcohol plasma polymers deposited as a function of discharge power.

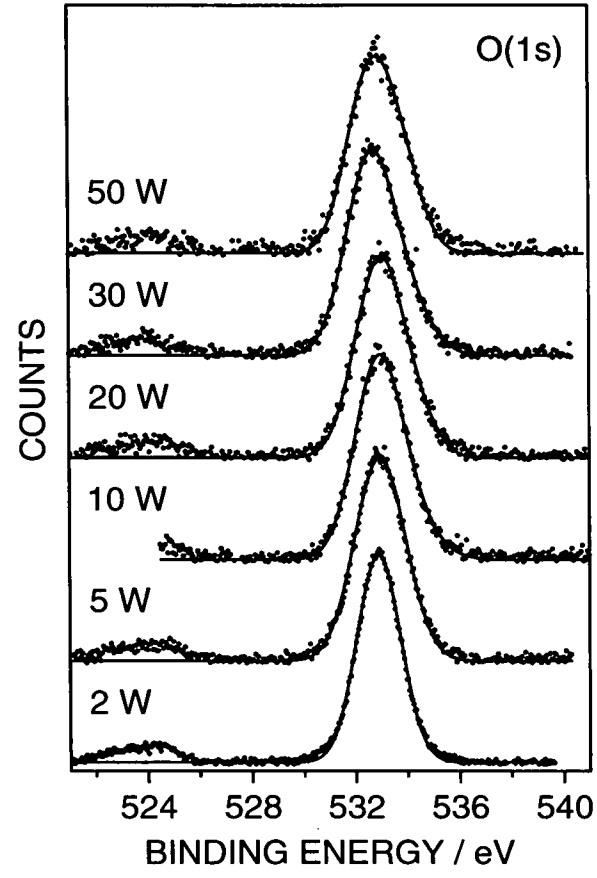

Figure 5.5: O(1s) XPS spectra of CW allyl alcohol plasma polymers deposited as a function of discharge power.

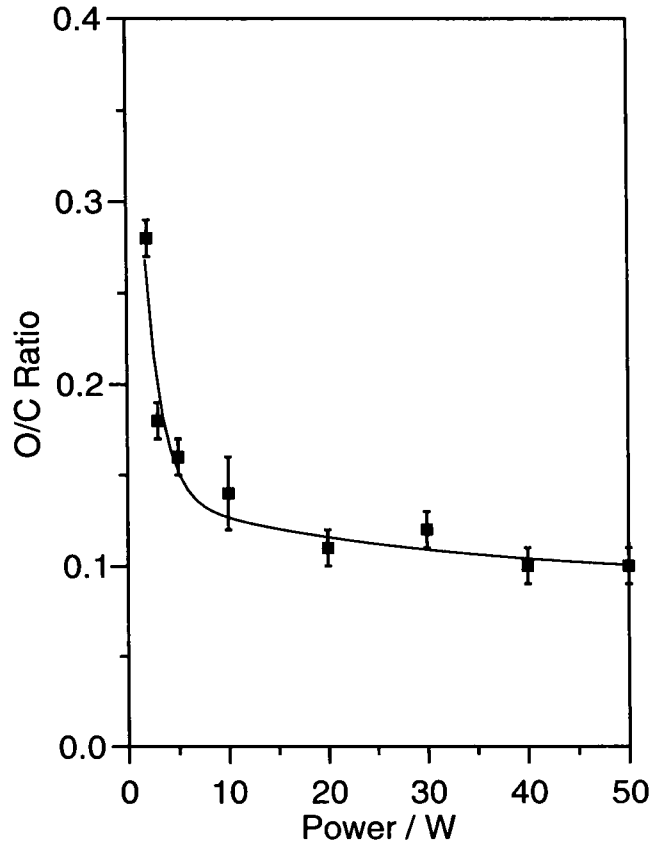

Figure 5.6: Variation in the O/C ratio as a function of discharge power for CW allyl alcohol plasma polymers.

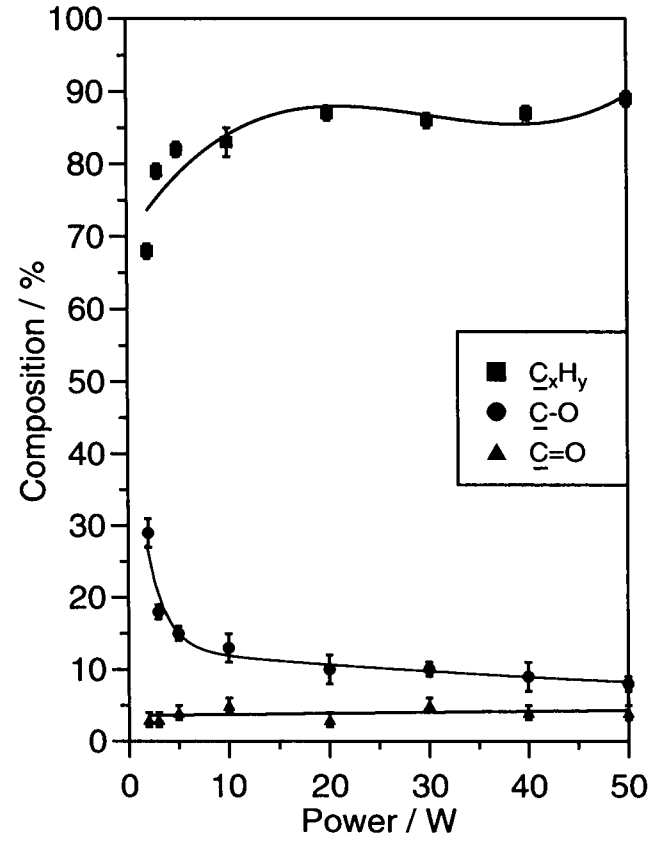

Figure 5.7: Comparison of the percentage carbon functionalities in allyl alcohol plasma polymer as a function of discharge power.

5.3.2 EVALUATION OF PULSE PLASMA PARAMETERS

In an effort to increase the C-O group retention during the plasma polymerisation of allyl alcohol the average power was reduced by electrically pulsing the plasma. From consideration of Equation 2.1 (Section 2.2.1.2) the average power delivered to the plasma (<P>) was a function of three variables:[24] on-time (t_{on}); off-time (t_{off}); and peak power (P_p). To efficiently investigate how these variables affected the percentage of the C-O group incorporated into the plasma polymer a set of eight experiments were planned. Two values (known as levels) were chosen for each of the three variables (known as factors) in order to ascertain which factors, or combination of factors, had the greatest influence on the percentage of C-O group incorporated into the plasma polymer (known as the response).[54] The choice of level for each factor was partly governed by previous experience and the limitations of the equipment (the rf generator could not deliver reliable pulses shorter than 20 μs and its maximum power output was 70 W). The choice of experimental parameters, the experiments performed and the responses recorded are presented below, Table 5.1, and 5.2.

	Factors		
Levels	**t_{on}**	**t_{off}**	**P_p**
+	2000 μs	2000 μs	50 W
-	20 μs	20 μs	5 W

Table 5.1: Levels for each experimental factor.

Expt.	t_{on}	t_{off}	P_p	Response
1	-	+	-	42
2	-	+	+	40
3	-	-	-	30
4	-	-	+	13
5	+	+	-	22
6	+	+	+	13
7	+	-	-	15
8	+	-	+	9

Table 5.2: Experiments and their responses.

From these results a table was constructed to evaluate the effect of each factor and combination of factors.[54]

Expt	t_{on}	t_{off}	P_p	t_{on}/P_p	t_{off}/P_p	t_{on}/t_{off}	$t_{on}/t_{off}/P_p$
1	-42	+42	-42	+42	-42	-42	+42
2	-40	+40	+40	-40	+40	-40	-40
3	-30	-30	-30	+30	+30	+30	-30
4	-13	-13	+13	-13	-13	+13	+13
5	+22	+22	-22	-22	-22	+22	-22
6	+13	+13	+13	+13	+13	+13	+13
7	+15	-15	-15	-15	+15	-15	+15
8	+9	-9	+9	-9	-9	-9	-9
Total	**-16.5**	**12.5**	**-8.5**	**-7**	**1**	**3**	**-4.5**

Table 5.3: Evaluation of factors.

The relative importance of each factor on the response was measured by the modulus of the total found in the above table, Table 5.3. The sign of each total

dictated whether increasing the value of a factor had a positive or negative effect on the response. From these results it was clear that the t_{on} had the greatest influence on the response. Decreasing t_{on} and P_p increased the percentage of C-O groups retained in the plasma polymer. The next most important factor was the t_{off}. Increasing the off-time increased the percentage of C-O groups retained in the plasma polymer. However, the combined factors did not have such an extensive influence on the response. In light of these results it was decided to investigate the effect of t_{on} on the plasma polymerisation of allyl alcohol.

5.3.3 INFLUENCE OF PLASMA ON-TIME

The pulsed plasma polymerisation of allyl alcohol was investigated as a function of electrical plasma t_{on} (with a constant t_{off} = 2000 μs and P_p = 5 W). The ATR-FTIR spectra appeared to vary little with increasing on-time, Figure 5.8. The relative intensity of C-H aliphatic stretching absorbencies generally tended to increase as the on-time was lengthened. In all cases absorbencies which arose from the unsaturated group in the monomer spectrum (C-H stretching and bending absorbencies from $=CH_2$, =CH- groups) were lost during plasma polymerisation. The carbonyl stretch at approximately 1700 cm^{-1} was of low relative intensity in all of the spectra.

The C(1s) XPS high resolution spectra of the allyl alcohol pulsed plasma polymer displayed a large C-O peak at the lowest on-time (20 μs), Figure 5.9. This peak decreased in relative intensity with increasing plasma on-time. The O(1s) XPS high resolution spectra appeared to vary little with t_{on}, Figure 5.10. A graph of the O/C ratio as a function of the plasma on-time showed that the amount of oxygen incorporated into the plasma polymer increased with decreasing plasma on-time, reaching a maximum O/C concentration of 0.44 ± 0.02 at an on-time of 20 μs, Figure 5.11. It is worth noting that this O/C ratio was greater than the O/C ratio present in the monomer molecule (O/C ratio of 0.33). This maximum O/C ratio was considerably greater than that produced during the CW plasma polymerisation of allyl alcohol. The percentage composition of the carbon functionalities for the allyl alcohol pulsed plasma polymer was also calculated

from the XPS C(1s) peak fits, Figure 5.12. The percentage of unfunctionalised carbon atoms increased while the percentage C-O group decreased with increasing discharge power. The maximum C-O group incorporation into the pulsed plasma polymer occurred at an on-time of 20 μs and reached a value of 40%. This was significantly larger than the maximum C-O group detected during CW plasma polymerisation (29%) and the percentage of C-O groups in the monomer molecule (33%). The percentage of carbonyl groups incorporated into the pulsed plasma polymer remained constant over a large range of on-times, only reaching a minimum of 4% at the shortest on-time.

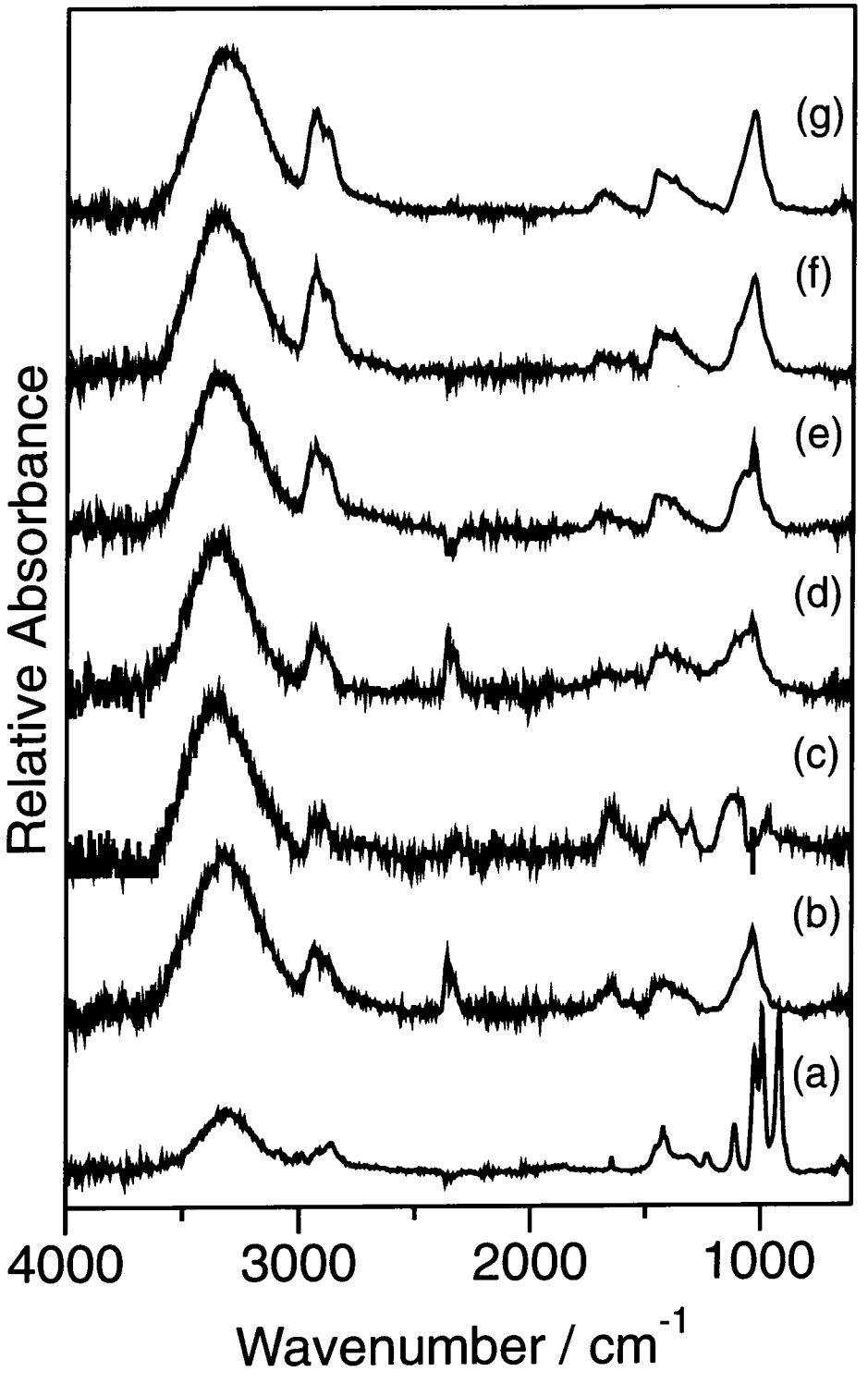

Figure 5.8: ATR-FTIR spectra of (a) allyl alcohol monomer and allyl alcohol pulsed plasma polymer deposited as a function of t_{on} (t_{off} = 2000 μs, P_p = 5 W); (b) 20 μs; (c) 50 μs; (d) 100 μs; (e) 500 μs; (f) 1000 μs; (g) 2000 μs.

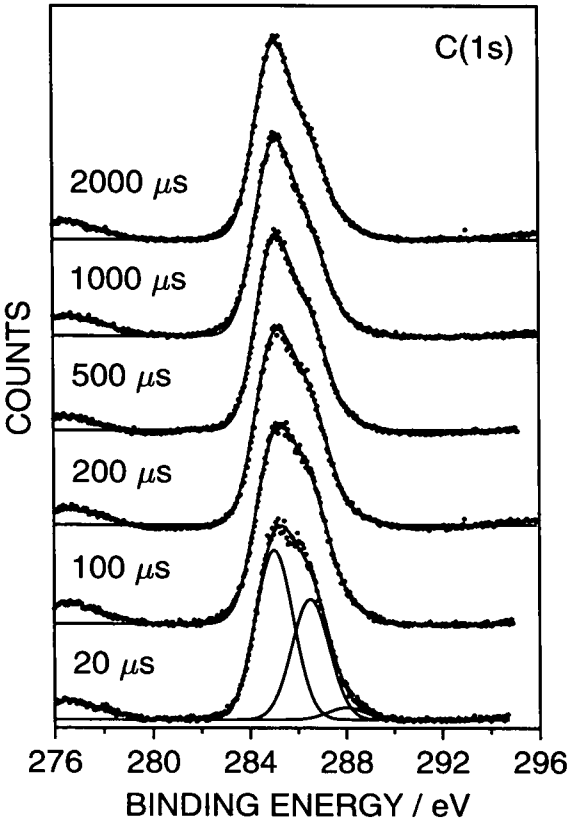

Figure 5.9: C(1s) XPS spectra of allyl alcohol pulsed plasma polymers deposited as a function of t_{on} (t_{off} = 2000 μs, P_p = 5 W).

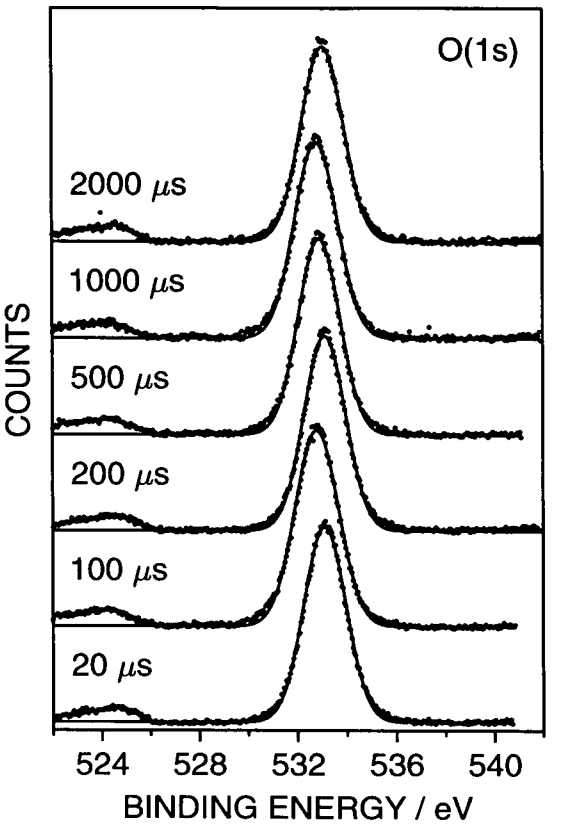

Figure 5.10: O(1s) XPS spectra of allyl alcohol pulsed plasma polymers deposited as a function of t_{on} (t_{off} = 2000 μs, P_p = 5 W).

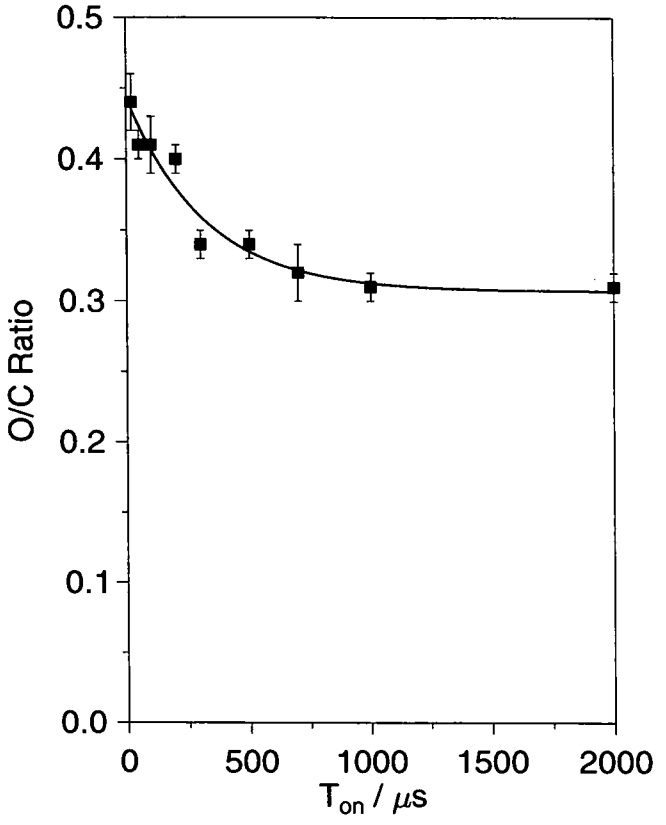

Figure 5.11: Variation in the O/C ratio as a function of t_{on} (t_{off} = 2000 μs, P_p = 5 W) for allyl alcohol pulsed plasma polymers.

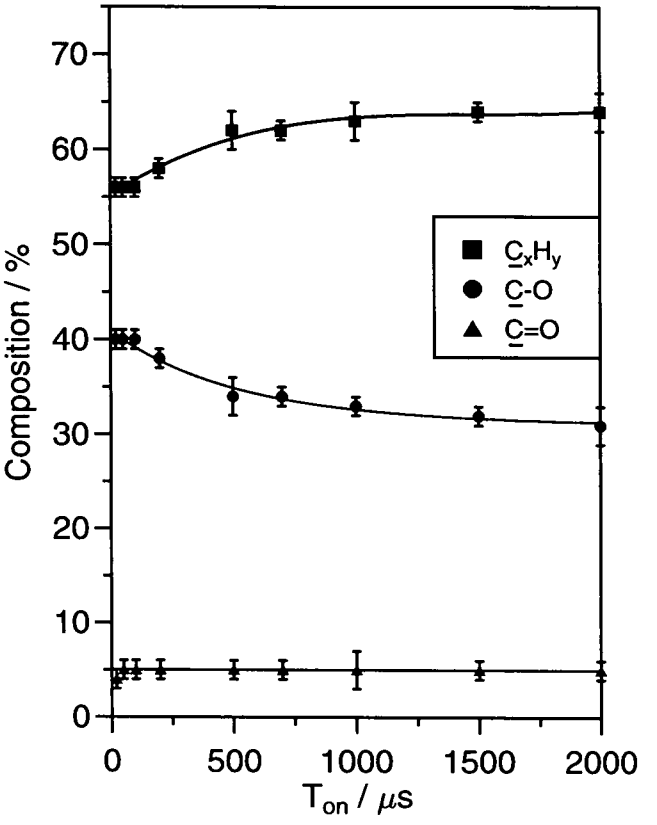

Figure 5.12: Comparison of the percentage carbon functionalities in allyl alcohol pulsed plasma polymer as a function of t_{on} (t_{off} = 2000 μs, P_p = 5 W).

5.3.4 LABELLING OF CW ALLYL ALCOHOL PLASMA POLYMER WITH TFAA

XPS analysis is unable to distinguish between C-O-H and C-O-C carbons because of the very small difference in binding energy between them. Therefore a CW allyl alcohol plasma polymer, deposited at a discharge power of 5 W, was labelled with trifluoroacetic anhydride (TFAA) to enable the quantification of surface hydroxyl groups.[1,5,26] Plasma polymers deposited under 5 W were unstable under the labelling conditions. The hydroxyl groups were selectively converted to $OC(O)CF_3$ functionalities via the reaction shown below, Figure 5.13:

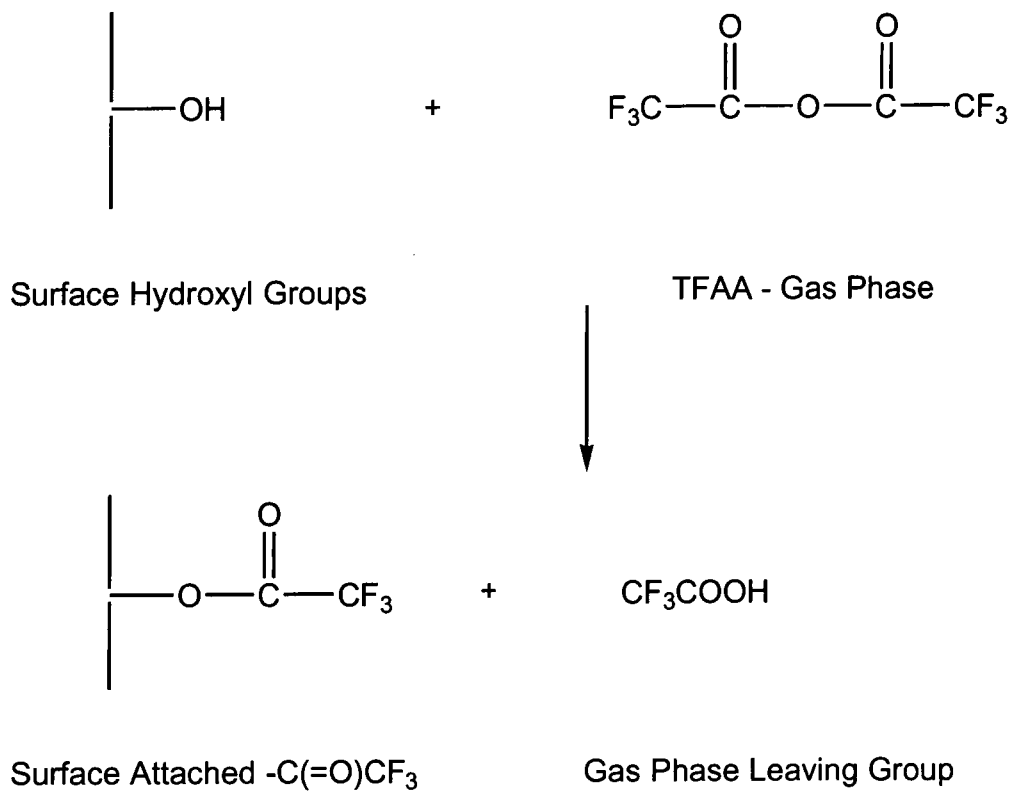

Figure 5.13: Reaction between hydroxyl groups and TFAA.[26]

The amount of TFAA attached to the plasma polymer surface was then easily found using XPS due to the large binding energy shift of the CF_3 group, Figure 5.14. Tables 5.4 and 5.5 give the elemental composition and the percentage of

carbon groups respectively which were incorporated into the TFAA labelled allyl alcohol plasma polymer.

	% F	% C	% N	% O	% Si
5 W CW allyl alcohol plasma polymer	0	87 ± 1	0	14 ± 1	0
TFAA labelled plasma polymer	16 ± 1	69 ± 1	0	15 ± 1	0

Table 5.4: Elemental composition of TFAA labelled CW allyl alcohol plasma polymer.

	% $\underline{C}_xH_y$	% $\underline{C}$-O	% $\underline{C}$-O-C(=O)-CF_3	% $\underline{C}$=O	% $\underline{C}$(=O)-O-CF_3	% $\underline{C}F_3$
5 W CW allyl alcohol plasma polymer	80 ± 1	17 ± 1	0	4 ± 1	0	0
TFAA labelled plasma polymer	66 ± 1	10 ± 1	6 ± 1	4 ± 1	7 ± 1	6 ± 1

Table 5.5: Percentage of carbon groups before and after TFAA labelling of allyl alcohol plasma polymer.

It was clear that a large proportion (over 50%) of the $\underline{C}$-O groups detected in the 5 W CW allyl alcohol plasma polymer did not react with TFAA. This may indicate that many of the $\underline{C}$-O groups detected were ether functionalities ($\underline{C}$-O-C) incorporated into the plasma polymer via monomer fragmentation processes.

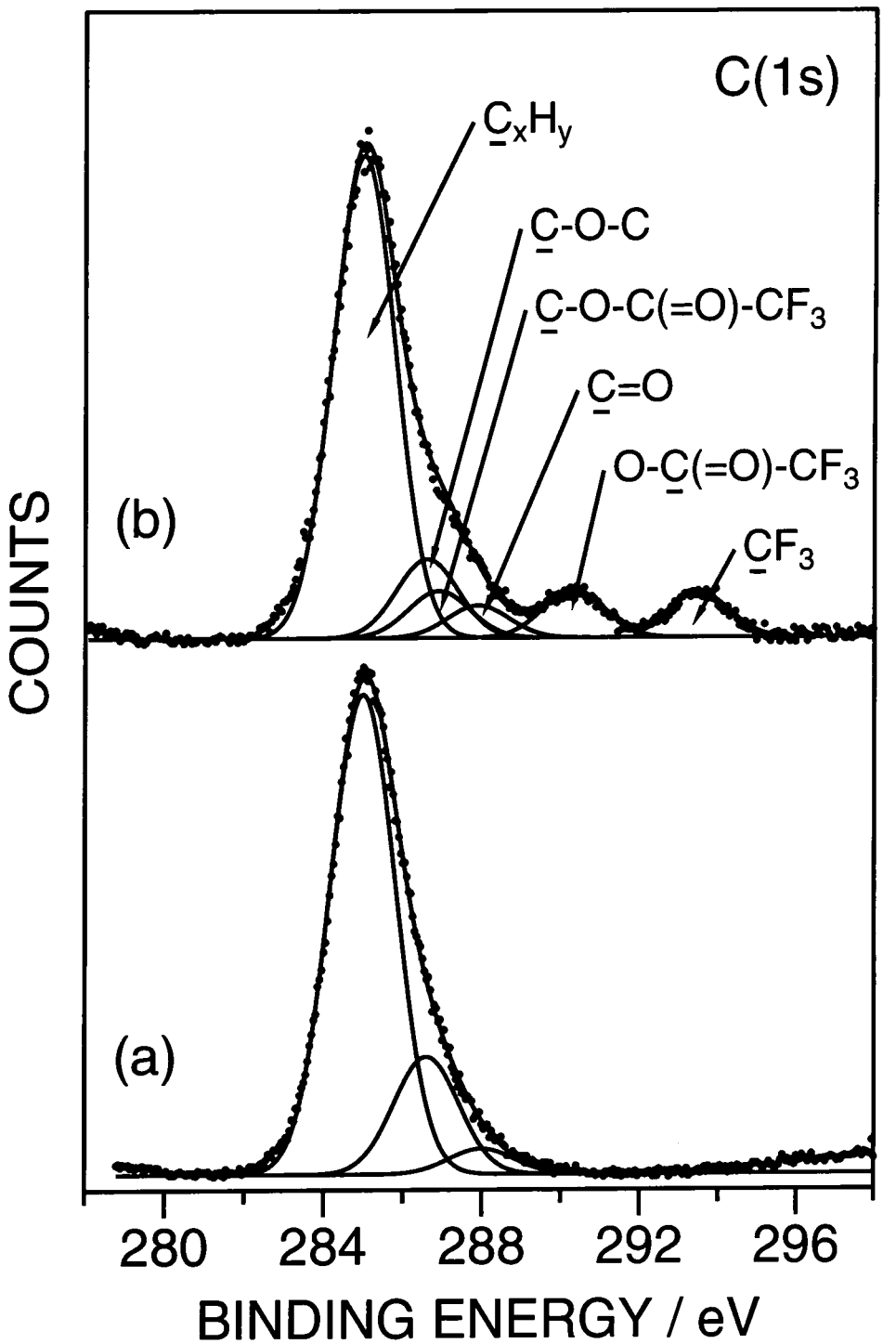

Figure 5.14: C(1s) XPS spectra of (a) 5 W CW allyl alcohol plasma polymer; and (b) 5 W CW allyl alcohol plasma polymer labelled with TFAA.

5.3.5 REACTION OF ALLYL ALCOHOL PLASMA POLYMER WITH $Zr(OC(CH_3)_3)_4$

Allyl alcohol plasma polymers were reacted with tertra(*tert*-butoxy)zirconium ($Zr(OC(CH_3)_3)_4$) to produce a surface bound zirconium compound which was used to bind poly(acrylic acid) to the plasma polymer surface,[37] Figure 5.15. C(1s) XPS analysis of a $Zr(OC(CH_3)_3)_4$ treated 3 W CW allyl alcohol plasma polymer showed a relative increase in the C-O group (including a contribution from $(CH_3)_3$C-O-Zr) from 18% to 24%, Figure 5.16. High resolution XPS spectra of the Zr(3d) and Zr(3p) regions, Figures 5.17 and 5.18 respectively, provided clear evidence that the zirconium complex was indeed attached to the plasma polymer surface. Allyl alcohol pulsed plasma polymer was also treated with $Zr(OC(CH_3)_3)_4$ vapour, Figure 5.19. The percentage C-O group changed from 40% ± 1 to 25% ± 1. The elemental composition was found using a calculated zirconium sensitivity factor[55] of 0.13 for the treated CW and pulsed plasma polymers, Table 5.6.

	% Zr	% C	% N	% O	% Si
3 W CW plasma polymer	0	85 ± 1	0	15 ± 1	0
$Zr(OC(CH_3)_3)_4$ treated CW plasma polymer	5 ± 1	77 ± 2	0	18 ± 2	0
Pulsed plasma polymer	0	69 ± 2	0	31 ± 2	0
$Zr(OC(CH_3)_3)_4$ treated pulsed plasma polymer	6 ± 1	71 ± 2	0	23 ± 2	0

Table 5.6: Elemental composition of 3 W CW allyl alcohol plasma polymer and 3 W CW allyl alcohol plasma polymer treated with $Zr(OC(CH_3)_3)_4$.

The surface bound zirconium compound produced by $Zr(OC(CH_3)_3)_4$ treatment of 3 W CW allyl alcohol plasma polymer was placed into a 1% poly(acrylic acid) solution in dioxane for 1 hour (Plasma polymers produced using average powers below 3 W were not stable in the dioxane solution), rinsed in pure dioxane for 10 minutes, dried under vacuum and then analysed using XPS, Figure 5.20.. Poly(acrylic acid) was attached to the treated plasma polymer. The elemental composition of the surface produced was calculated, Table 5.7. The percentage of the C(=O)-OH group found was 17%.

	% Zr	% C	% N	% O	% Si
3 W CW plasma polymer	0	85 ± 1	0	15 ± 1	0
$Zr(OC(CH_3)_3)_4$ treated CW plasma polymer	5 ± 1	77 ± 2	0	18 ± 2	0
Poly(acrylic acid) treated zirconium complex	1 ± 1	67 ± 1	0	32 ± 2	0

Table 5.7: Elemental composition of 3 W CW allyl alcohol plasma polymer, 3 W CW allyl alcohol plasma polymer treated with $Zr(OC(CH_3)_3)_4$ and a surface bound zirconium compound treated with poly(acrylic acid).

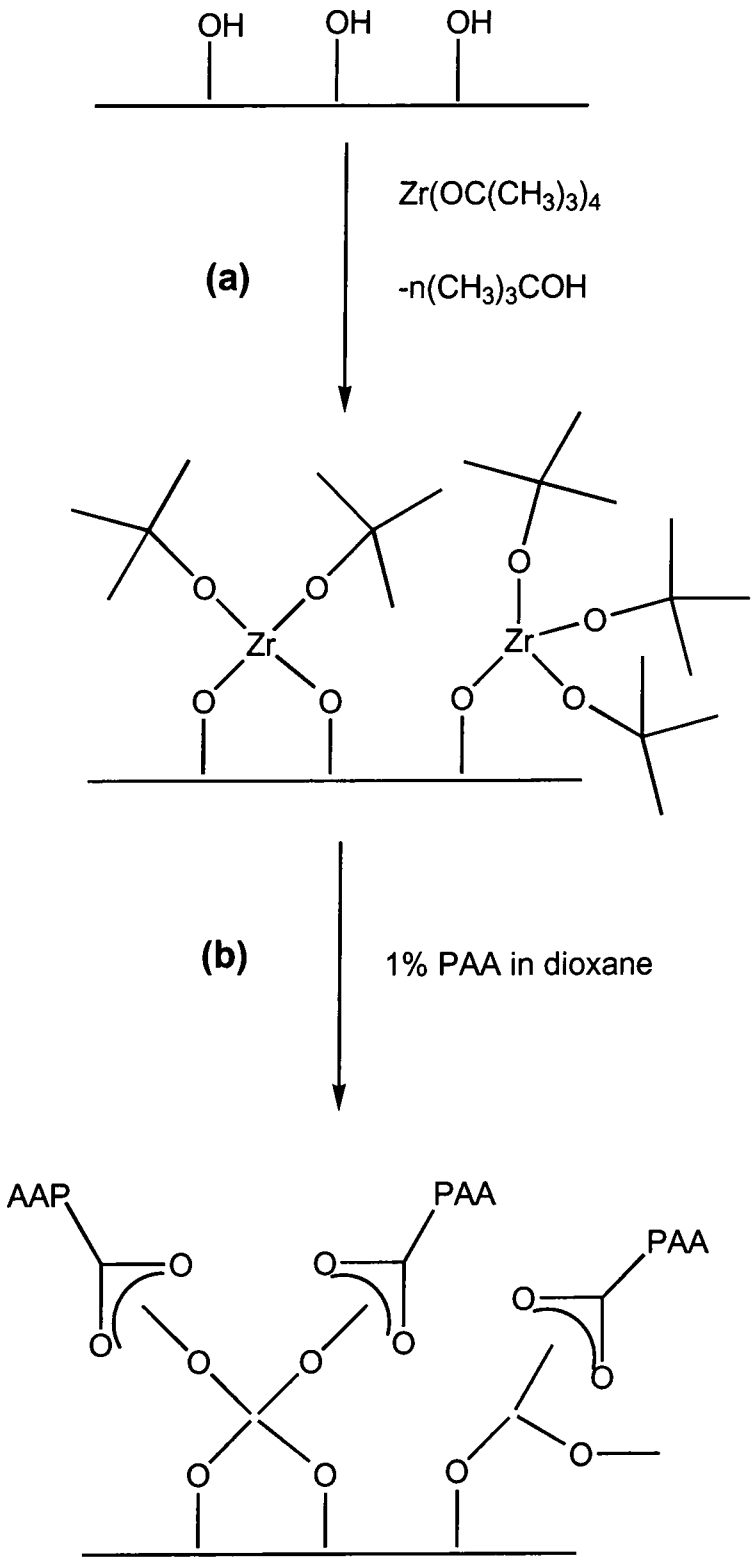

Figure 5.15: Schematic representation of (a) the vapour phase attachment of $Zr(OC(CH_3)_3)_4$ onto an allyl alcohol plasma polymer; and (b) deposition from solution of Poly(acrylic acid) (PAA) onto the treated plasma polymer.[37]

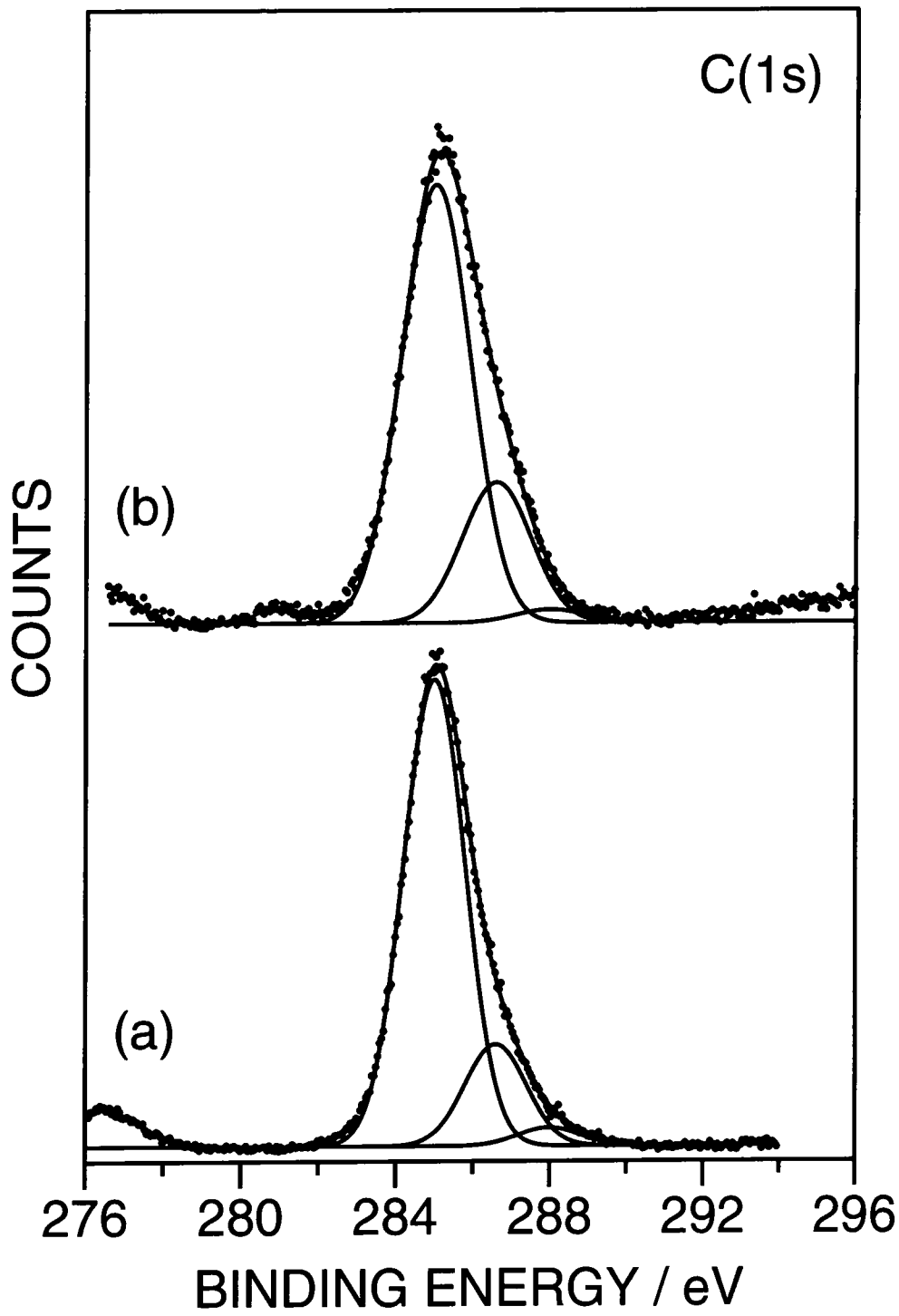

Figure 5.16: C(1s) XPS spectra of (a) 3 W CW allyl alcohol plasma polymer; and (b) 3 W CW allyl alcohol plasma polymer treated with $Zr(OC(CH_3)_3)_4$.

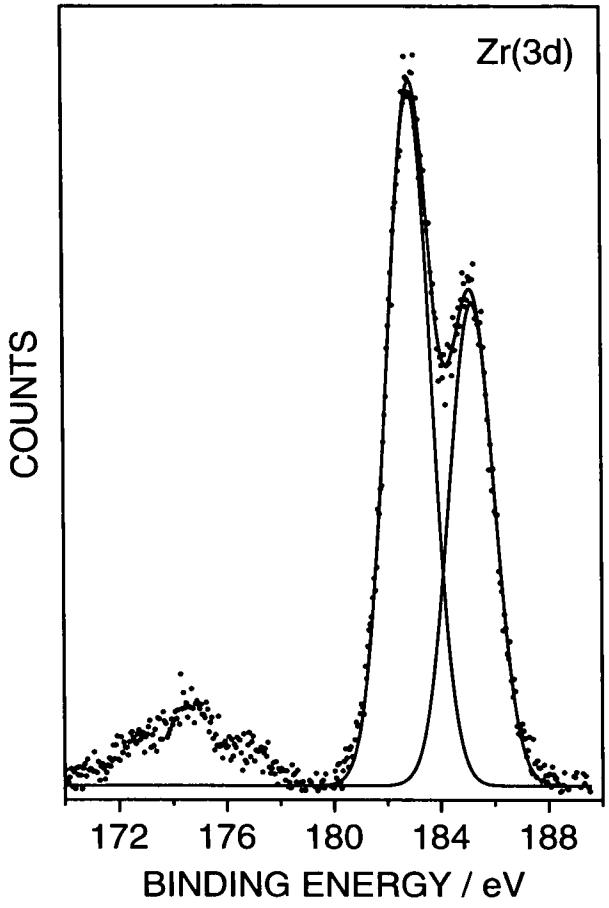

Figure 5.17: Zr(3d) XPS spectra of $Zr(OC(CH_3)_3)_4$ treated 3 W CW plasma polymer.

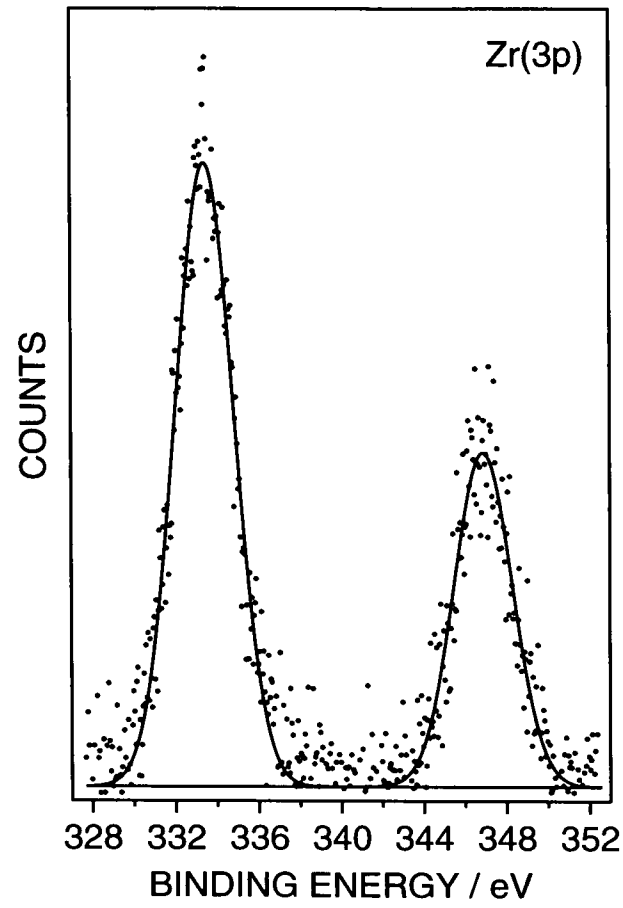

Figure 5.18: Zr(3p) XPS spectra of $Zr(OC(CH_3)_3)_4$ treated 3 W CW plasma polymer.

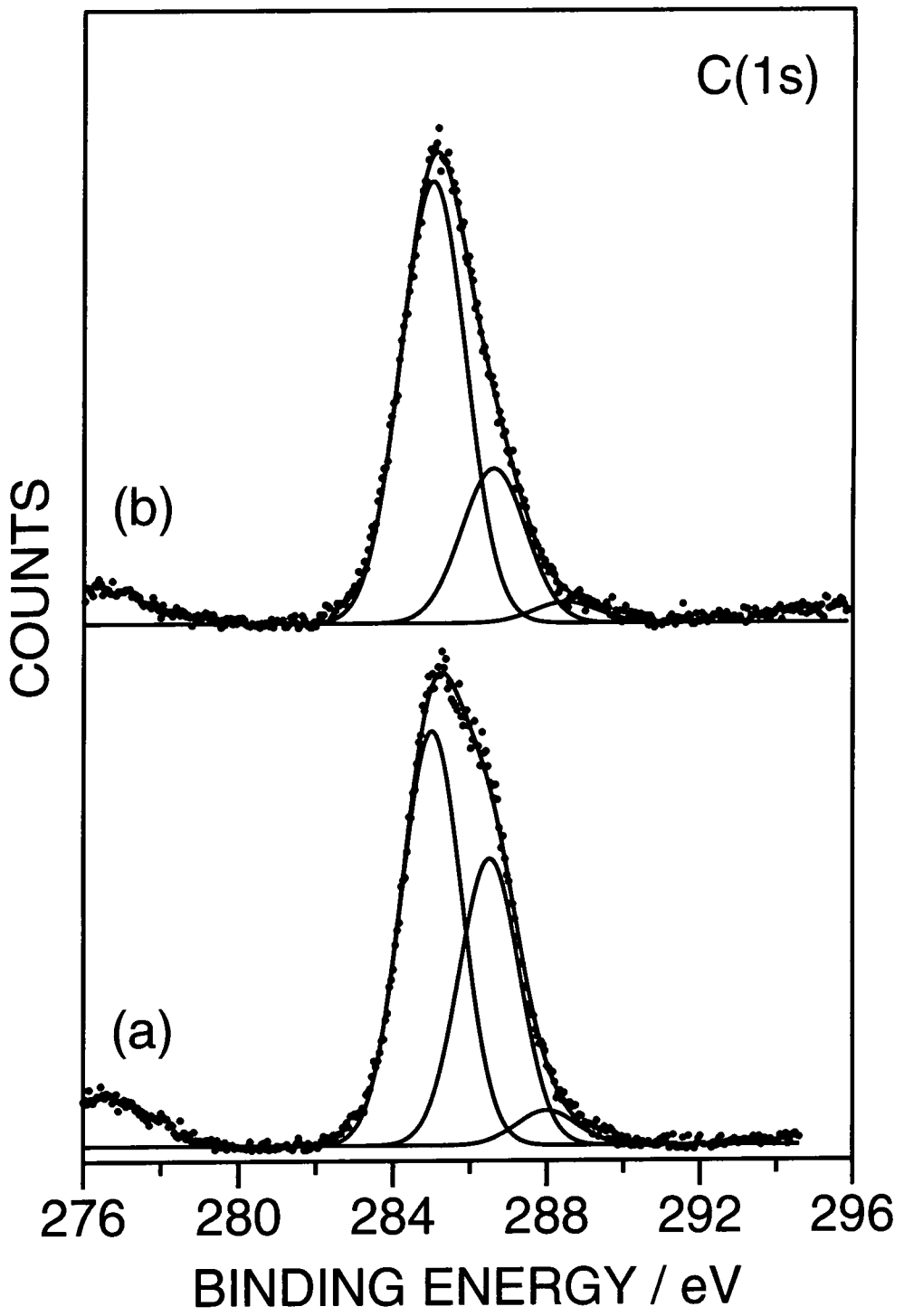

Figure 5.19: C(1s) XPS spectra of (a) pulsed allyl alcohol plasma polymer (t_{on} = 20 μs, t_{off} = 2000 μs and P_p = 5 W); and (b) allyl alcohol pulsed plasma polymer treated with $Zr(OC(CH_3)_3)_4$.

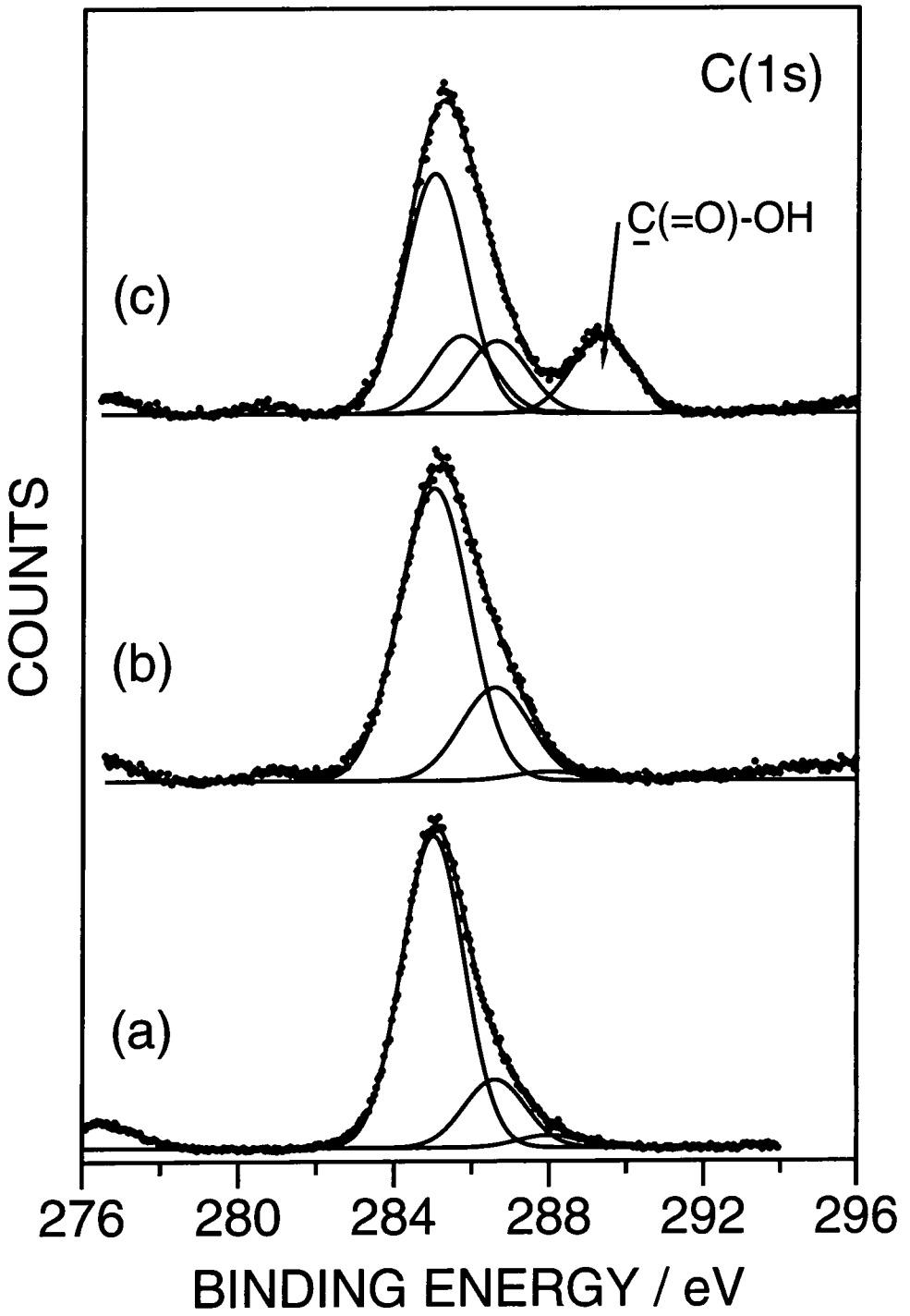

Figure 5.20: : C(1s) XPS spectra of (a) 3 W CW allyl alcohol plasma polymer; (b) 3 W CW allyl alcohol plasma polymer treated with $Zr(OC(CH_3)_3)_4$; and (c) poly(acrylic acid) treated surface bound zirconium compound.

5.4 DISCUSSION

The ATR-FTIR spectra of allyl alcohol, deposited as a function of CW discharge power, provided evidence for an increase in monomer fragmentation processes with increasing discharge power. Peaks due to functionalities present in the monomer molecule (O-H and C-O stretching absorptions) decreased in relative intensity, with respect to aliphatic C-H stretching and bending absorptions, as the discharge power was increased. Furthermore, the carbonyl group absorption, not observed in the monomer spectrum, became more pronounced as the discharge power increased. This increase in monomer fragmentation was due to an increase in the proportion of high energy electrons as the discharge power was increased.[56,57] Comparison of the plasma polymer ATR-FTIR spectra with the monomer spectrum showed that the carbon-carbon double present in the monomer molecule was not retained in the plasma polymer. The intensity of the IR absorption of the plasma polymer thin films deposited onto NaCl disks decreased with increasing discharge power. Such an observation suggested that film deposition rates decreased with increasing discharge power. An increase in the etching effect of species formed by the fragmentation of the monomer molecule may have contributed to the reduction in film production (Section 2.4). XPS results provided further evidence for the increased fragmentation of monomer molecules with increasing discharge power. The retention of oxygen and C-O bonds in the plasma polymer was directly dependent on discharge power. At high powers the proportion of C-O groups in the plasma polymer was at a minimum whereas the concentration of carbonyl groups due to monomer fragmentation and rearrangement processes reached a maximum.

Previous investigations into the pulsed plasma polymerisation of allyl alcohol have concentrated on the effect of the plasma off-time on the retention of the C-O bond in the plasma polymer.[5] However, in this study it was seen that the plasma on-time had the largest influence over the concentration of C-O groups retained. The ATR-FTIR spectra of the allyl amine pulsed plasma polymer, deposited as a function of on-time, showed that peaks due to functionalities present in the monomer molecule (O-H and C-O stretching absorptions) increased in relative intensity as the on-time was decreased. The absence of absorptions arising from

carbon-carbon double bonds in the plasma polymers, together with an increase in functional group retention with decreasing on-time, indicated that polymerisation may have proceeded through reaction of the double bond.[5] At the shortest on-times the percentage of C-O group detected exceeded that present in the monomer molecule. Even at these low average plasma powers carbonyl groups were still observed, indicating that monomer fragmentation processes were still taking place.

Quantification of the hydroxyl group concentration present on the surface of a CW 5 W allyl alcohol plasma polymer was attempted by comparison of the surface elemental concentration of the plasma polymer with the TFAA labelled plasma polymer.[1,5,26] Figure 5.13 suggests that every hydroxyl group present on the plasma polymer surface should have led to the incorporation of one CF_3 functionality. The 5 W CW plasma polymer had an approximate C-O group concentration of 17% which should have resulted in a CF_3 concentration of approximately 13%. The actual CF_3 concentration found was 6%. This indicated that either: not all of the C-O groups detected by XPS were hydroxyl groups and that a large proportion were ether groups;[5] or that there was incomplete reaction over the whole sampling depth of the polymer analysed by XPS.[58] Poor stability of the allyl alcohol film produced at lower average powers, under the labelling conditions, precluded them from this method of quantification.

The vapour phase reaction of $Zr(OC(CH_3)_3)_4$ with allyl alcohol plasma polymer resulted in the attachment of the zirconium compound to the plasma polymer surface. This derivatised surface was able to undergo further reaction in dioxane solution to produce surface bound acid groups.[37]

5.5 CONCLUSION

The Zr compound was irreversibly attached to the allyl alcohol plasma polymer surface via covalent bonds. This complex was able to participate in further surface reactions making it a candidate for layer-by-layer deposition of polymers to produce films with highly controllable structures and thickness (Chapter 6).

5.5 REFERENCES

1. Ameen, A. P.; Short, R. D.; Ward, R. J. *Polymer* **1994**, *35*(20), 4382.
2. Gombotz, W. R.; Hoffman, A. S. *Abs. Pap. Am. Chem. Soc.* **1988**, *193*, 163.
3. Tang, L.; Wu, Y.; Timmons, R. B. *J. Biomed. Mater. Res.* **1998**, *42*, 156.
4. Gombotz, W. R.; Hoffman, A. S.; Guanghui, W. *J. Appl. Polym. Sci.* **1989**, *37*, 91.
5. Rinsch, C. L.; Chen, X.; Panchalingam, V.; Eberhart, C.; Wang, J.-H.; Timmons, R. B. *Langmuir* **1996**, *12*, 2995.
6. Fally, F.; Virlet, L.; Riga, J.; Verbist, J. J. *J. Appl. Polym. Sci.: Appl. Polym. Sym* **1994**, *54*, 41.
7. Fally, F.; Virlet, I.; Riga, J.; Verbist, J. J. *J. Appl. Polym. Sci.: Appl. Polym. Sym* **1996**, *59*, 1569.
8. Yasuda, H. *Plasma Polymerization*; Academic: London, 1985.
9. O'Kane, D. F.; Rice, D. W. *J. Macromol. Sci. Chem.* **1976**, *A10*, 567.
10. López, G. P.; Ratner, B. D. *J. Appl. Polym. Sci.: Appl. Polym. Sym* **1990**, *46*, 493.
11. López, G. P.; Ratner, R. D. *Langmuir* **1991**, *7*(4), 766.
12. Timmons, R. B.; Savage, C. R. *Chem. Mater.* **1991**, *3*(4), 575.
13. Badyal, J. P. S.; Hynes, A. M. *Chem. Mater.* **1998**, *10*, 2177.
14. Llewellyn, I. P.; Rimmer, N.; Scarsbrook, G. A.; Heinecke, R. A. *Thin Solid Films* **1990**, *191*, 135.
15. Panchalingam, V.; Chen, X.; Savage, C. R.; Timmons, R. B.; Eberhart, C. *J. Appl. Polym. Sci.: Appl. Polym. Sym* **1994**, *54*, 123.
16. Panchalingham, V.; Chen, X.; Savage, C. R.; Timmons, R. B.; Huo, H.-H.; Eberhart, R. C. *ASAIO Journal* **1993**, M305.
17. Chen, X.; Rajeshwar, K.; Timmons, R. B.; Chen, J.-J.; Chyan, O. M. R. *Chem. Mater.* **1996**, *8*(5), 1067.
18. Han, L. M.; Timmons, R. B. *J. Polym. Sci.: Part A: Polymer Chemistry* **1998**, *36*, 3121.
19. Timmons, R. B.; Wang, J.-H. US Patent WO 97/38801, 1997.
20. Timmons, R. B.; Savage, C. R. *Abs. Pap. Am. Chem. Soc.* **1991**, *201*(2), 53.
21. Panchalingam, V.; Poon, B.; Huo, H.-H.; Savage, C. R.; Timmons, R. B.; Eberhart, R. C. *J. Biomaterials Sci.: Polym. Ed.* **1993**, *5*(1/2), 131.
22. Savage, C. R.; Timmons, R. B.; Lin, J. W. *Adv. Chemsitry Ser.* **1993**, *236*, 745.
23. Uchida, T.; Senda, K.; Vinogradov, G. K.; Morita, S. *Thin Solid Films* **1996**, *281-282*, 536.
24. Bell, A. T.; Nakajima, K.; Shen, M. *J. Appl. Polym. Sci.* **1979**, *23*, 2627.
25. Rinsch, C. L.; Chen, X.; Panchalingam, V.; Savage, C. R.; Wang, Y. H.; Eberhart, R. C.; Timmons, R. B. *Abs. Pap. Am. Chem. Soc.* **1995**, *209*(2), 141.
26. Tasker, S.; Badyal, J. P. S.; Backson, S. C. E.; Richards, R. W. *Polymer* **1994**, *35*, 4717.
27. Everhart, D. S.; Reilley, C. N. *Anal. Chem.* **1981**, *53*(4, April), 665.

28. Dickie, R. A.; Hammond, J. S.; deVries, J. E.; Holubka, J. W. *Anal. Chem.* **1982**, *54*(12, October), 2045.
29. Gerenser, L. J.; Elman, J. F.; Mason, M. G.; Pochan, J. M. *Polymer* **1985**, *26*(August), 1162.
30. Briggs, D.; Kendall, C. R. *Int. J. Adh. Adhs.* **1982**, *2*, 13.
31. Ameen, A. P.; Ward, R. J.; Short, R. D.; Beamson, G.; Briggs, D. *Polymer* **1993**, *34*(9), 1795.
32. Pochan, J. M.; Gerenser, L. J.; Elman, J. F. *Polymer* **1986**, *27*(July), 1058.
33. Chilkoti, A.; Castner, D. G.; Ratner, B. D.; Briggs, D. *J. Vac. Sci. Technol. A* **1990**, *8*(3, May/June), 2274.
34. Beamson, G.; Briggs, D. *High Resolution XPS of Organic Polymers, The Scienta ESCA 300 Database*; John Wiley & Sons: Chichester, 1992.
35. Chiltoki, A.; Ratner, B. D. *Surface and Interface Analysis* **1991**, *17*, 567.
36. Aronoff, Y. G.; Chen, B.; Lu, G.; Seto, C.; Schwartz, J.; Bernasek, S. L. *J. Am. Chem. Soc.* **1997**, *119*(2), 259.
37. VanderKam, S. K.; Bocarsly, A. B.; Schwartz, J. *Chem. Mater.* **1998**, *10*(3), 685.
38. Phuvanartnuruks, V.; McCarthy, T. J. *Macromolecules* **1998**, *31*, 1906.
39. Hsieh, M. C.; Farris, R. J.; McCarthy, T. J. *Macromolecules* **1997**, *30*(26), 8453.
40. Decher, G.; Hong, J. D.; Schmitt, J. *Thin Solid Films* **1992**, *210/211*, 831.
41. Decher, G. In *Polymeric Materials Encyclopedia: Synthesis, Properties, and Applications*; Salamone, J. C., Ed.; CRC Press: Boca Raton, FL, 1996; Vol. 6, pp. 4540-4546; N.
42. Cheung, J. H.; Fou, A. F.; Rubner, M. F. *Thin Solid Films* **1994**, *244*, 985.
43. Bell, C. M.; Arendt, M. F.; Gomez, L.; Schmehl, R. H.; Mallouk, T. E. *J. Am. Chem. Soc.* **1994**, *116*(18), 8374.
44. Kleinfeld, E. R.; Ferguson, G. S. *Science* **1994**, *265*(15 July), 370.
45. Mao, G.; Tsao, Y.; Tirrell, M.; Davis, H. T. *Langmuir* **1993**, *9*(12), 3461.
46. Ferreira, M.; Rubner, M. F. *Macromolecules* **1995**, *28*(21), 7107.
47. Fou, A. C.; Rubner, M. F. *Macromolecules* **1995**, *28*(21), 7115.
48. Hammond, P. T.; Whitesides, G. M. *Macromolecules* **1995**, *28*(22), 7569.
49. Chen, W.; McCarthy, T. J. *Macromolecules* **1997**, *30*(1), 78.
50. Leväsalmi, J.-M.; McCarthy, T. J. *Macromolecules* **1997**, *30*(6), 1752.
51. Wagner, C. D.; Riggs, W. M.; Davis, L. E.; Moulder, J. F.; Muilenber, G. E. *Handbook of X-Ray Photoelectron Spectroscopy*; Perkin-Elmer: New York, 1978.
52. Evans, J. F.; Gibson, J. H.; Moulder, J.F.; Hammond, J. S.; Goretzki, H.; Fresenius, Z. *Anal. Chemie.* **1984**, *319*, 841.
53. Silverstein, R. M.; Bassler, G. C.; Morrill, T. C. *Spectrometric Identification of Organic Compounds*; John Wiley & Sons: Chichester, 1993.
54. Morgan, E. *Chemometrics: Experimental Design*; John Wiley & Sons: Chichester, 1991.
55. Wagner, C. D.; Davis, L. E.; Zeller, M. V.; Taylor, J. A.; Raymond, R. H.; Gale, L. H. *Surf. Interface Anal.* **1981**, *3*(5), 211.
56. McTaggart, F. K. *Plasma Chemistry in Electrical Discharges*; Elsevier Publishing Company: London, 1967.
57. Grill, A. *Cold Plasmas in Materials Technology*; IEEE Press: New Jersey, 1994.

58. Zeggane, S.; Delamer, M. *Appl. Surf. Sci.* **1988**, *31*, 151.

CHAPTER SIX

LAYER-BY-LAYER POLYELECTROLYTE SURFACE MODIFICATION AND REACTION

6.1 INTRODUCTION

Layer-by-layer deposition of polyelectrolytes (PE) has recently become of interest for the preparation of multilayer films.[1-13] Multilayer films are formed by a simple self-assembly process where charged surfaces are sequentially dipped into aqueous solutions of oppositely charged PE. Sequential adsorption of anionic and cationic PE reverses the surface charge as the PE is typically adsorbed in excess.[1] Adsorption of a charged PE in solution produces a surface with the same charge as the solvated PE. Hence, electrostatic repulsion limits further PE adsorption.[1] Self-assembly by layer-by-layer deposition has several advantages over other forms of multilayer assembly:[2]

- The coating process is simple, taking place in aqueous solution and utilizing basic apparatus;
- An extensive range of polyions can be used as long as they are water soluble, e.g. linear PE,[3,4,14-16] proteins,[17] viruses,[18] dendrimers,[19] clays[7] and silica;[20]
- The overall thickness can be controlled simply by the number of adsorption steps.

Numerous potential applications of these multilayer assemblies have been reported including conducting thin films,[9,10] enzyme reactors,[21] films for nonlinear optics,[22] light-emitting and electrochromic thin films,[23-25] lithographic development[11] and asymmetric gas separation membranes.[13]

Attention has formerly been focused on the adsorption of PE on charged inorganic surfaces. However, modification of organic polymer surfaces with PE assemblies has recently been reported.[1,12,13] In many of the examples quoted in the literature the substrate has been restricted to a narrow range of surface functionalised polymers, for example, chemically modified poly(chlorotrifluoroethylene).[1] However, plasma polymers present an ideal surface for the formation of multilayer assemblies.[2] Advantages of the plasma polymerisation technique are outlined below:[26]

- The choice of substrate material is not limited by the chemical composition of the surface;

- A wide range of precursors and deposition parameters allows extensive control over the nature and density of chemical groups formed on the surface;
- Bulk properties of the substrate are not affected.

From investigations into the adsorption of PE onto organic substrates form dilute aqueous solutions several general features were observed.[1] Firstly, the initial substrate surface chemistry defines the rest of the adsorption process. The assembly process is not independent of the substrate even after a number of layers have been deposited. This observation highlights the applicability of the plasma polymerisation technique to these assemblies. Plasma polymerisation allows surface chemical modification of the substrate. Therefore, the multilayer assembly process will now be governed by the nature of the plasma polymer not the substrate material. Secondly, the assembly process has its own stoichiometry and no specific stoichiometric ratio of PE's is required in the bulk solutions. No limit to the number of layers that could be deposited was found. Thirdly, in the systems studied to date the individual layers deposited were very thin (e.g. 2.0, 2.8 and 4.1 Å).[1] Fourthly, although multilayer assemblies were found to be quite dense, resulting in good gas barrier properties, they were not close packed. It has been suggested that the layers are interdigitated and cross-linked via ionic interactions.[27] Finally, differences in the XPS spectra and contact angles between adsorption stages demonstrate that despite interdigitation the different PE layers are stratified.

This Chapter reports the formation of a multilayer assembly on pulsed plasma polymerised acrylic acid (AA) using the cationic PE poly(diallyldimethylammonium chloride) (PDADMAC), Structure 6.1 and the anionic PE poly(styrene sulfonoate) (PSS), Structure 6.2. PDADMAC is initially adsorbed onto the AA surface and a multilayer assembly is then constructed via electrostatic attraction between oppositely charged PE.

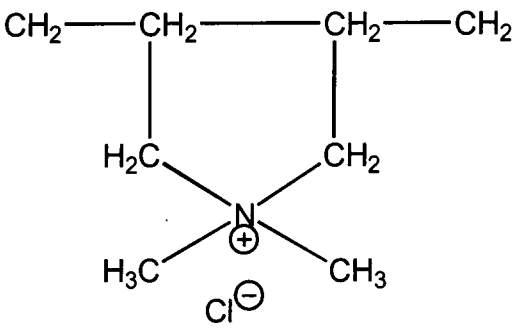

Structure 6.1: PDADMAC Repeat Unit.

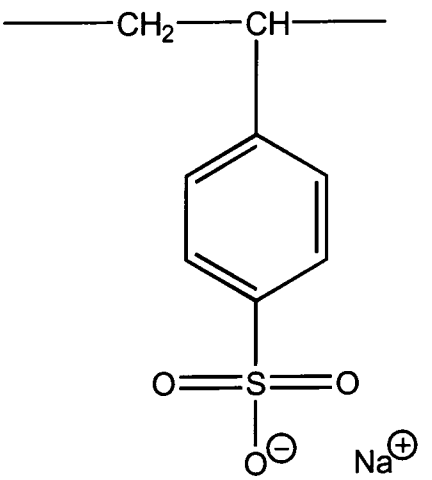

Structure 6.2: PSS Repeat Unit.

6.2 EXPERIMENTAL PROCEDURE

6.2.1 PULSED PLASMA POLYMERISATION

AA pulsed plasma polymer layers were deposited onto glass substrates using the method and apparatus described above (Section 2.2.1.2). The electrical pulsing conditions used in all the plasma polymerisations were kept constant (t_{on} = 20 μs, t_{off} = 4000 μs and P_p = 5 W). Pulsed plasma polymers were deposited

for 30 minutes onto glass substrates to produce a suitable surface for PE adsorption.

6.2.2 MULTILAYER ASSEMBLY

PDADMAC (Aldrich, 99% purity) and PSS (Aldrich, 99% purity) were dissolved in separate aqueous solutions buffered at pH 7 and pH 4 respectively. A 0.2 M (with respect to the repeat unit) PSS solution was used in all assembly experiments. The concentration of the PDADMAC was varied between 0.2 and 20%. Adsorptions were carried out at room temperature in unstirred freshly prepared PE solution. The alternating layers were formed by sequential dipping of the AA plasma polymer into the PE solutions for 1 hour followed by rinsing in pure water (B.S. 3978 grade 1) for 10 minutes, Scheme 6.1. After the required number of layers had been deposited the sample was dried under vacuum for 1 hour prior to analysis by XPS.

6.2.3 FLUOROSURFACTANT ADSORPTION

The layer-by-layer deposition process was halted after PSS adsorption to investigate further reactions of the PE derivatised surface. An AA-PDADMAC-PSS functionalised sample was placed into a 1% cationic fluorosurfactant $CF_3(CF_2)_nC_2H_5(alkyl)_3N^+$ solution for 1 hour, rinsed in pure water (B.S. 3978 grade 1) for 10 minutes, dried under vacuum for 1 hour and analysed using XPS and VCA measurements.

6.2.4 SAMPLE CHARACTERISATION

6.2.4.1 XPS Characterisation

Samples were characterised following drying by XPS spectroscopy. The glass slides were attached to a stainless steel probe stud using double sided adhesive

tape and inserted into a Vacuum Generators ESCA Lab Mk II photoelectron spectrometer. The spectrometer was fitted with an unmonochromated magnesium X-ray source (Mg $K\alpha_{1,2}$ = 1253.6 eV) and operated in the constant analyser energy mode (CAE = 20 eV for high resolution spectra, 50 eV for survey scans). Photoelectrons emitted from the substrate were collected at a 30° take-off angle with respect to the substrate normal. The spectrometer calibration was routinely checked using the gold $4f_{7/2}$ and silver $3d_{5/2}$ peaks at 83.8 and 368.3 eV respectively.[28] Elemental sensitivity factors were determined experimentally relative to the carbon 1s (C(1s)) peak (285.0 eV) using standard compounds. These were taken as C(1s) : F(1s) : S(2p) : Na(1s) : Cl(2p) : O(1s) : N(1s) : Si(2p) = 1.00 : 0.24 : 0.49 : 0.17 : 0.5 : 0.39 : 0.65 : 1.00 respectively. The absence of any Si(2p) XPS feature following plasma polymerisation was indicative of complete coverage of the glass substrate.

6.2.4.2 VCA Characterisation

The wettability of the samples was investigated using the sessile drop technique (Section 1.8.4) employing video contact angle (VCA) apparatus (Instruments S.A. Video Contact Angle System, VCA 2500XE). A known volume of the test liquid, high purity water (B.S. 3978 grade 1) or hexadecane (Aldrich, 99% purity), was dispensed through a motorised micro-syringe and brought into contact with the surface of the sample. The contact angle of the liquid was calculated by analysis of the shape of the droplet on the sample surface.

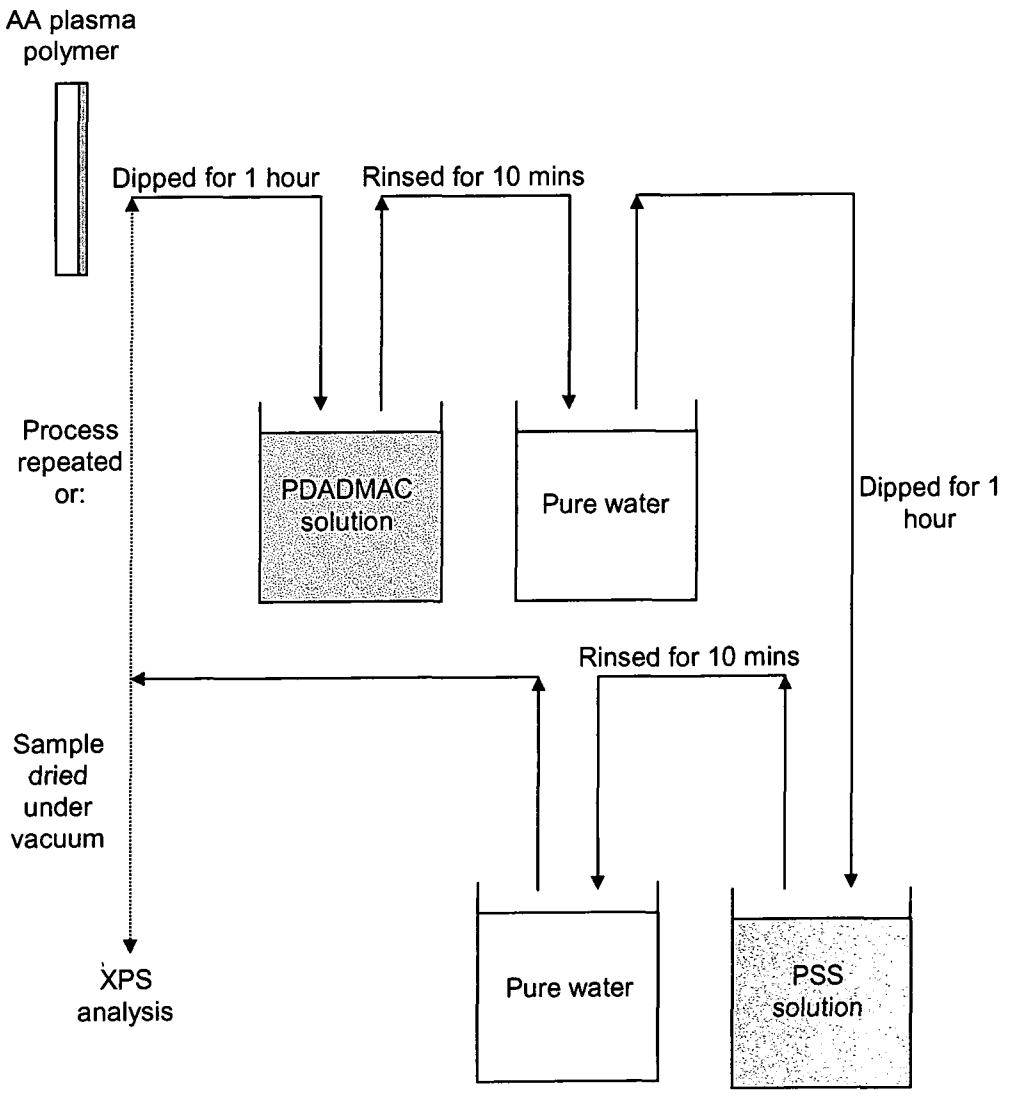

Scheme 6.1: Schematic of the PE dipping procedure.

6.3 RESULTS

High resolution XPS envelopes were fitted using a Marquardt minimisation routine. The peak shape was assumed to be Gaussian with a fixed relative full width at half maximum.[29] C(1s) regions were fitted with several different carbon functionalities depending on the elemental composition of the surface region[30] (using the hydrocarbon peak at 285.0 eV as a reference offset): aromatic -C(H)- (284.7 eV); C_xH_y (285.0 eV); C-SO_3^- (285.3 eV); C-C(=O)-O (285.7 eV); C-CF_n

(285.7 eV); C-N^+ (286.1 eV); C-O (286.6 eV); CF (287.8 eV); O-C-O / C=O (288 eV); CF-CF_n (289.0 eV); C(=O)-O (289.3 eV); CF_2 (291.2 eV); and CF_3 (293.3 eV). The first step in multilayer assembly was the plasma polymerisation of AA to form a suitable surface for attachment of the PE. AA pulsed plasma polymer (t_{on} = 20 μs, t_{off} = 4 ms, P_p = 5 W and deposition time = 30 minutes) was deposited onto a glass substrate as described in Chapter 2. The next stage was the formation of an AA plasma polymer-PDADMAC complex. Complex formation was investigated at a number of PDADMAC bulk aqueous solution concentrations. AA pulsed plasma polymer was placed into several different bulk PDADMAC concentrations for 1 hour, rinsed in pure water for 10 minutes, dried under vacuum and analysed using XPS. The N/C ratio (found from the N(1s) and C(1s) peak areas after correction for sensitivity) attached to the plasma polymer surface, and therefore the amount of PDADMAC, increased with increasing concentration and reached a maximum value of 0.09 ± 0.01 at a 20% bulk PDADMAC concentration, Figure 6.2.

The attachment of PDADMAC at a bulk concentration of 20% was then investigated as a function of treatment time. AA pulsed plasma polymer was placed into 20% bulk PDADMAC aqueous solution for varying lengths of time, rinsed in pure water for 10 minutes, dried under vacuum and analysed using XPS. The N/C ratio did not show a large dependency on treatment time, quickly reaching a plateau value of approximately 0.08 ± 0.01 after 30 minutes treatment, Figure 6.3 and 6.4.

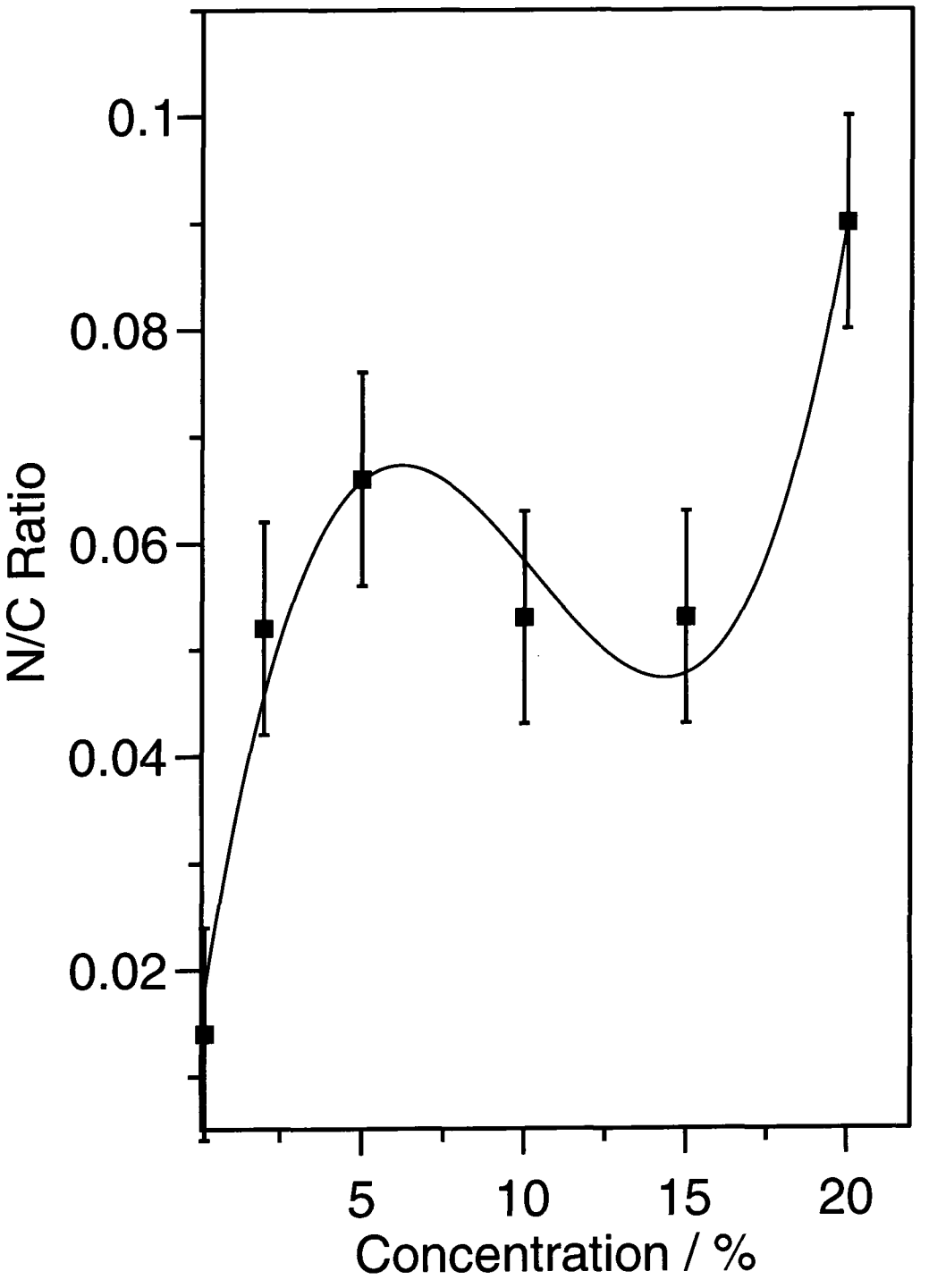

Figure 6.2: N/C ratio verses bulk PDADMAC aqueous solution concentration.

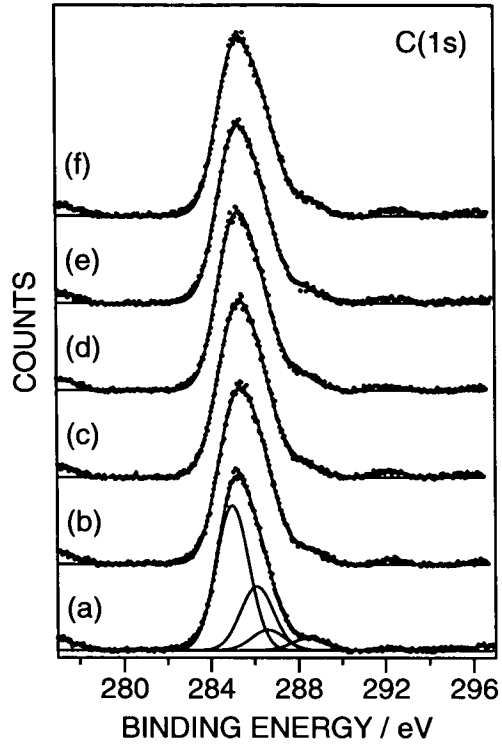

Figure 6.3: C(1s) XPS spectra of AA pulsed plasma polymer treated with 20% PDADMAC solution for various treatment times: (a) 10 minutes; (b) 30 minutes; (c) 60 minutes; (d) 100 minutes; (e) 300 minutes; and (f) overnight.

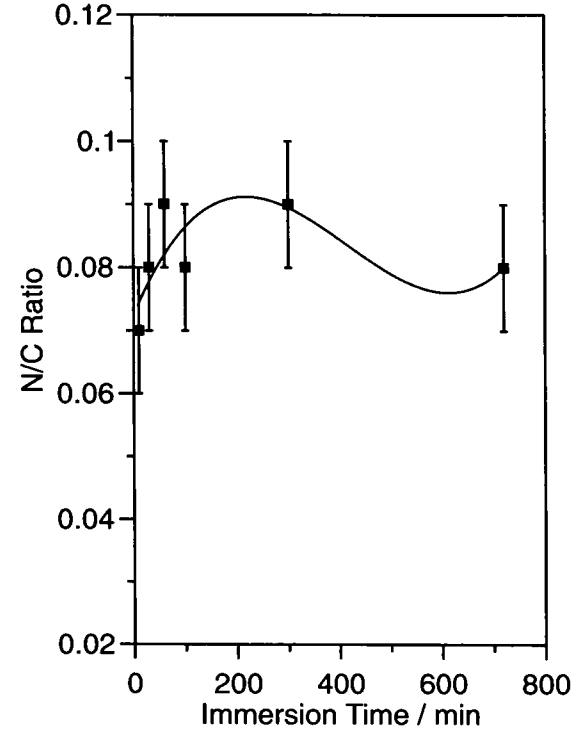

Figure 6.4: N/C ratio verses PDADMAC treatment time.

6.3.1 ATTACHMENT OF PDADMAC: LAYER 1 *AA-PDADMAC*

AA pulsed plasma polymer was placed in 20% PDADMAC aqueous solution for 1 hour, rinsed in pure water, dried under vacuum and analysed using XPS, Figures 6.5 to 6.8. The elemental composition of the surface region was compared with spin coated PDADMAC polymer (from 2% methanol solution onto glass), Table 6.1.

	%Cl	%C	%N	%O	%Si
AA plasma polymer	0	60 ± 2	0	40 ± 2	0
Spin coated PDADMAC	6 ± 1	77 ± 1	9 ± 1	10 ± 1	0
AA-PDADMAC	5 ± 1	78 ± 2	6 ± 2	13 ± 1	0

Table 6.1: Elemental composition of AA pulsed plasma polymer, spin coated PDADMAC and AA-PDADMAC complex.

Deconvolution of the C(1s) region enabled the identification of the chemical functionalities present in the surface region of the AA-PDADMAC complex, Table 6.2.

	%$\underline{C}_xH_y$	%$\underline{C}$-C(=O)-O	%$\underline{C}$-N^+	%$\underline{C}$-O	%$\underline{C}$=O /O-$\underline{C}$-O	%$\underline{C}$(=O)-O
AA plasma polymer	40 ± 1	30 ± 1	0	1 ± 1	3 ± 1	29 ± 1
Spin coated PDADMAC	44 ± 1	0	41 ± 1	8 ± 1	7 ± 1	0
AA-PDADMAC	57 ± 2	0	29 ± 2	9 ± 2	5 ± 2	0

Table 6.2: Percentage carbon groups present in the surface region of AA pulsed plasma polymer, spin coated PDADMAC and AA-PDADMAC complex.

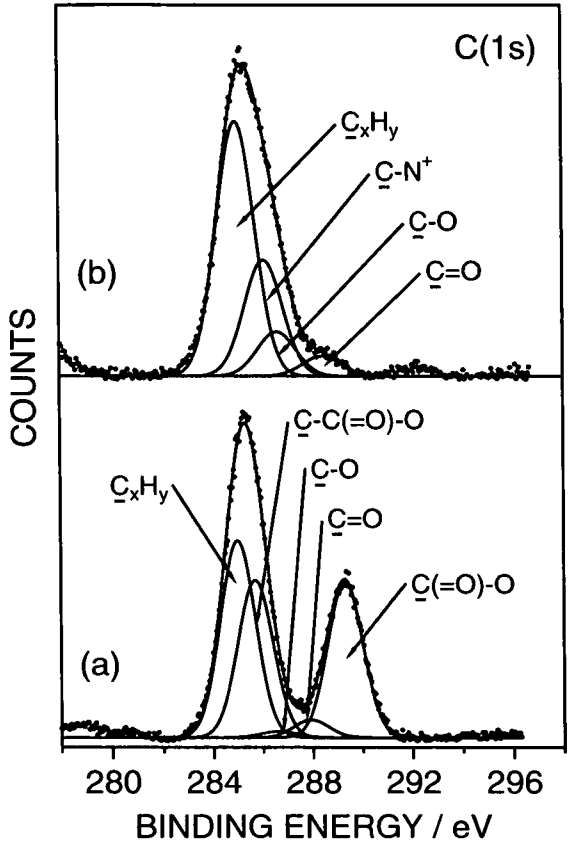

Figure 6.5: C(1s) XPS spectra of: (a) AA pulsed plasma polymer; and (b) AA pulsed plasma polymer treated with 20% PDADMAC solution for 1 hour.

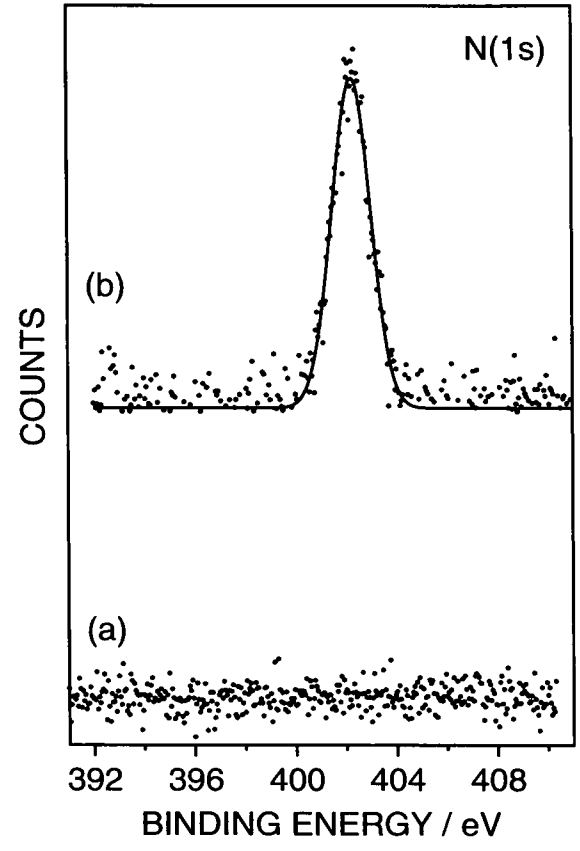

Figure 6.6: N(1s) XPS spectra of: (a) AA pulsed plasma polymer; and (b) AA pulsed plasma polymer treated with 20% PDADMAC solution for 1 hour.

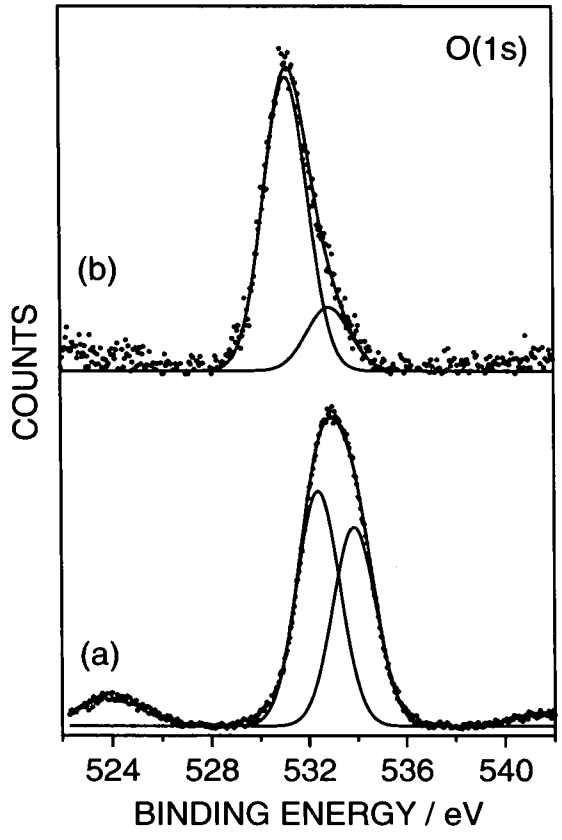

Figure 6.7: O(1s) XPS spectra of: (a) AA pulsed plasma polymer; and (b) AA pulsed plasma polymer treated with 20% PDADMAC solution for 1 hour.

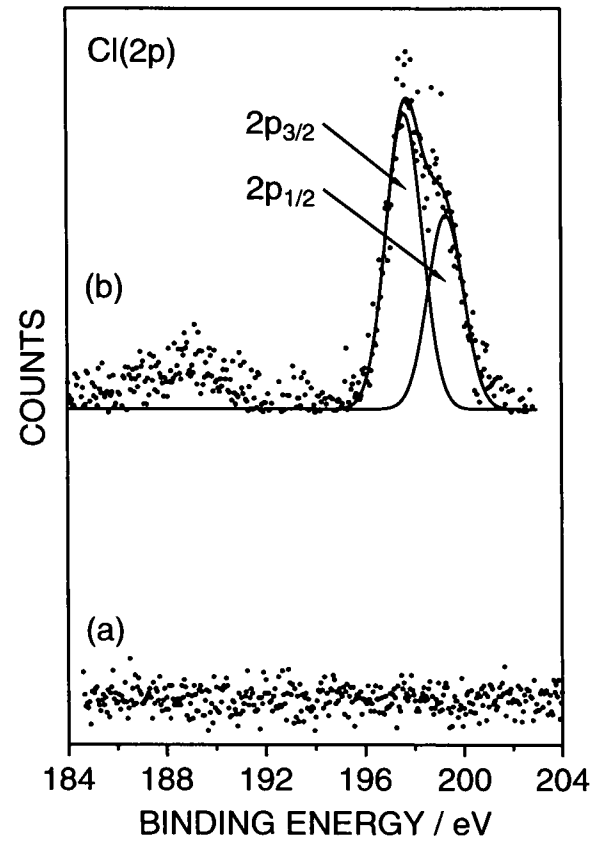

Figure 6.8: Cl(2p) XPS spectra of: (a) AA pulsed plasma polymer; and (b) AA pulsed plasma polymer treated with 20% PDADMAC solution for 1 hour.

6.3.2 ATTACHMENT OF PSS: LAYER 2 *AA-PDADMAC-PSS*

An AA-PDADMAC complex formed as described above (Section 6.3.1) was placed in a PSS aqueous solution for 1 hour, rinsed in pure water for 10 minutes, dried under vacuum and analysed using XPS, Figure 6.9 to 6.11. PSS was attached to the PDADMAC functionalised surface resulting in a S/C ratio (found from the S(2p) and C(1s) peak areas after correction for sensitivity) of 0.11 ± 0.01. The elemental composition of the surface region was calculated, Table 6.3.

	% S	%Cl	%Na	%C	%N	%O
AA-PDADMAC	0	5 ± 1	0	78 ± 2	6 ± 2	13 ± 1
AA-PDADMAC-PSS	7 ± 1	0	7 ± 1	65 ± 2	0	21 ± 2

Table 6.3: Elemental composition of AA-PDADMAC and AA-PDADMAC-PSS complexes.

Deconvolution of the C(1s) region enabled the identification of the chemical functionalities present in the surface region of the AA-PDADMAC-PSS complex, Table 6.4.

	%-<u>C</u>(H)-	%<u>C</u>$_x$H$_y$	%<u>C</u>-SO_3	%<u>C</u>-N^+	%<u>C</u>-O	%<u>C</u>=O /O-<u>C</u>-O
AA-PDADMAC	0	57 ± 2	0	29 ± 2	9 ± 2	5 ± 2
AA-PDADMAC-PSS	62 ± 2	23 ± 2	11 ± 2	0	5 ± 1	0

Table 6.4: Percentage carbon groups present in the surface region of AA-PDADMAC and AA-PDADMAC-PSS complexes.

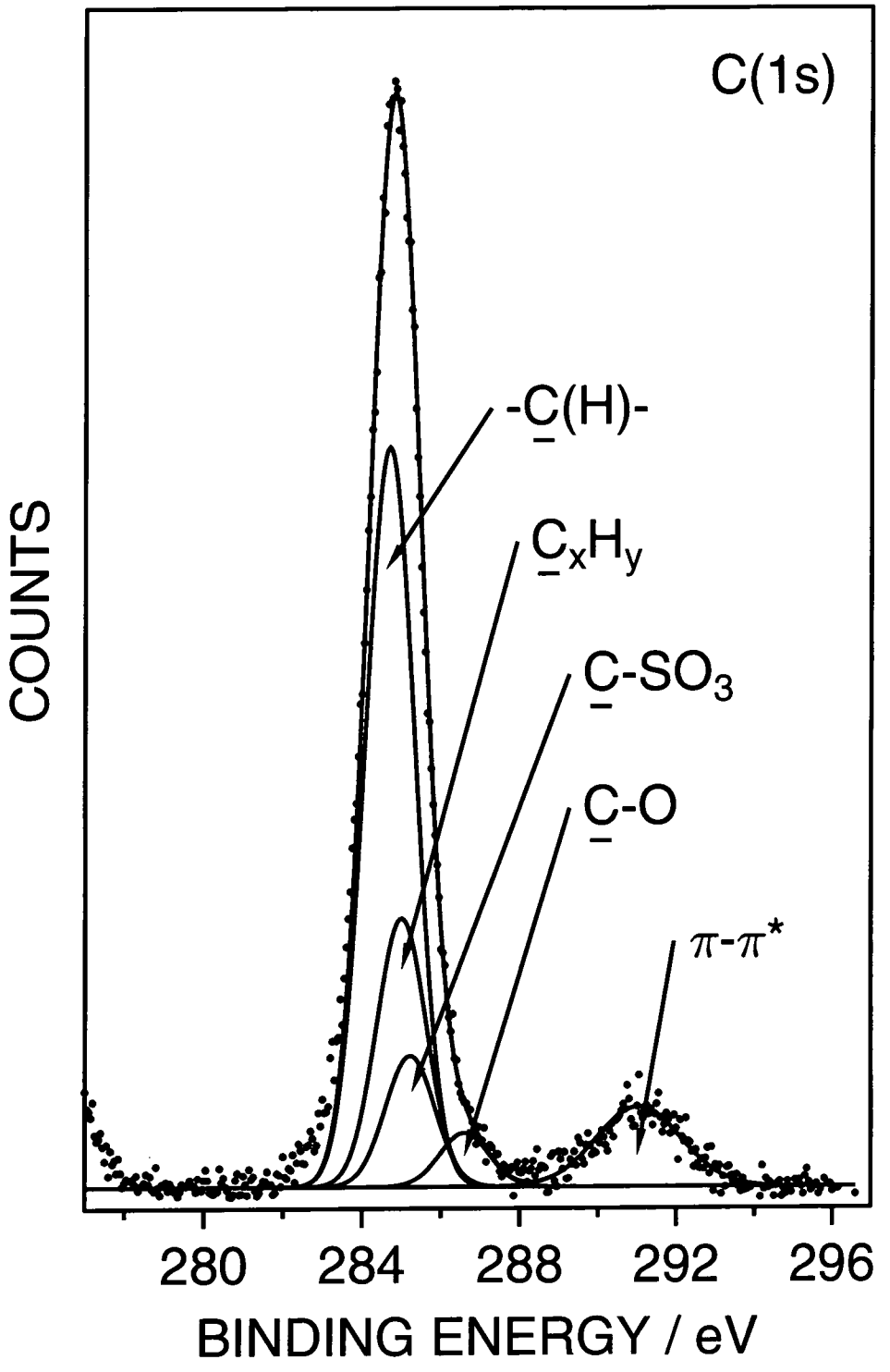

Figure 6.9: C(1s) XPS spectra of AA-PDADMAC-PSS complexes.

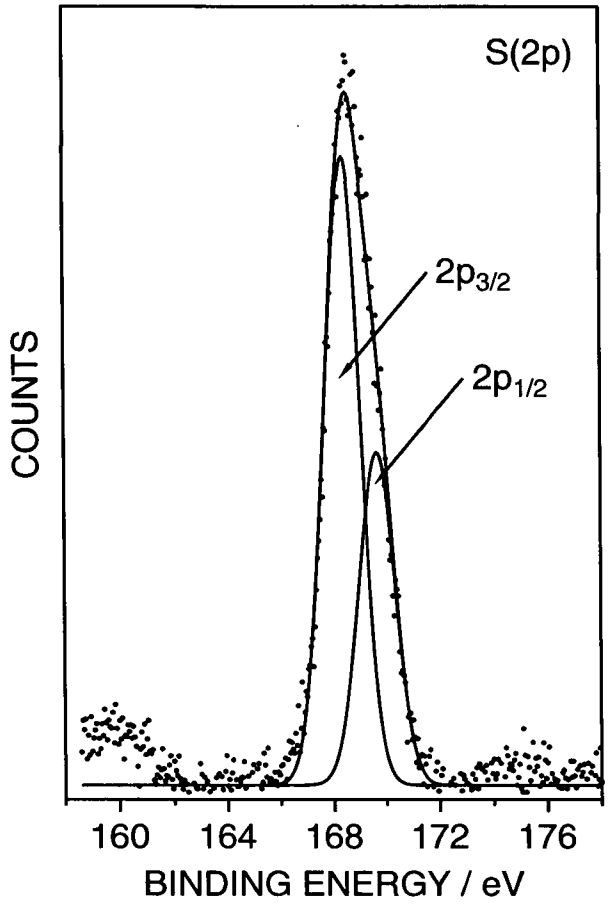

Figure 6.10: S(2p) XPS spectra of AA-PDADMAC-PSS complex.

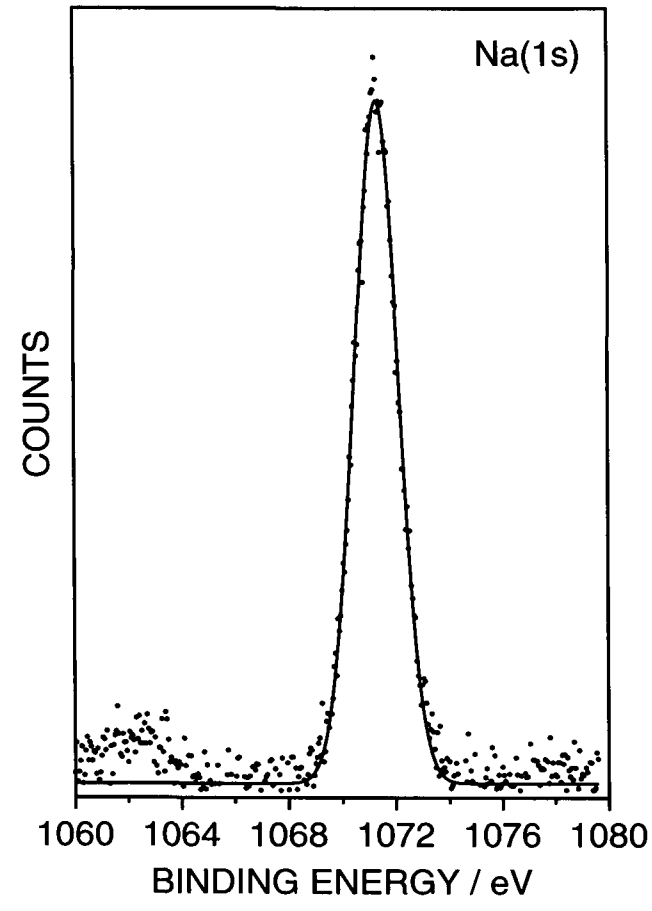

Figure 6.11: Na(1s) XPS spectra of AA-PDADMAC-PSS complex.

6.3.3 ATTACHMENT OF PDADMAC: LAYER 3 *AA-PDADMAC-PSS-PDADMAC*

The AA-PDADMAC-PSS complex was placed in 20% PDADMAC solution for 1 hour, rinsed in water for 10 minutes, dried under vacuum and analysed using XPS. A second PDADMAC polymer layer was attached to the PSS functionalised surface resulting in a N/C ratio of 0.09. The elemental composition of the surface region was calculated, Table 6.5.

	% S	%Cl	%Na	%C	%N	%O
AA-PDADMAC	0	5 ± 1	0	78 ± 1	6 ± 1	13 ± 1
AA-PDADMAC-PSS	7 ± 1	0	7 ± 1	65 ± 1	0	21 ± 1
AA-PDADMAC-PSS-PDADMAC	2 ± 1	5 ± 1	2 ± 1	74 ± 1	7 ± 1	10 ±1

Table 6.5: Elemental composition of AA-PDADMAC, AA-PDADMAC-PSS and AA-PDADMAC-PSS-PDADMAC complexes.

6.3.4 ATTACHMENT OF PSS: LAYER 4 *AA-PDADMAC-PSS-PDADMAC-PSS*

The AA-PDADMAC-PSS-PDADMAC complex was placed in PSS solution for 1 hour, rinsed in water for 10 minutes, dried under vacuum and analysed using XPS. A second PSS polymer layer was attached to the PDADMAC functionalised surface resulting in a S/C ratio of 0.11. The elemental composition of the surface region was calculated, Table 6.6.

	% S	%Cl	%Na	%C	%N	%O
AA-PDADMAC	0	5 ± 1	0	78 ± 1	6 ± 1	13 ± 1
AA-PDADMAC-PSS	7 ± 1	0	7 ± 1	65 ± 1	0	21 ± 1
AA-PDADMAC-PSS-PDADMAC	2 ± 1	5 ± 1	2 ± 1	74 ± 1	7 ± 1	10 ±1
AA-PDADMAC-PSS-PDADMAC-PSS	7 ± 1	0	5 ± 1	65 ± 1	1 ± 1	22 ± 1

Table 6.6: Elemental composition of AA-PDADMAC, AA-PDADMAC-PSS, AA-PDADMAC-PSS-PDADMAC and AA-PDADMAC-PSS-PDADMAC-PSS complexes.

6.3.5 ATTACHMENT OF PDADMAC: LAYER 5 *AA-PDADMAC-PSS-PDADMAC-PSS-PDADMAC*

The AA-PDADMAC-PSS-PDADMAC-PSS complex was placed in 20% PDADMAC solution for 1 hour, rinsed in water for 10 minutes, dried under vacuum and analysed using XPS, Figure 6.12. A third PDADMAC polymer layer was attached to the PSS functionalised surface resulting in a N/C ratio of 0.08. The elemental composition of the surface region was calculated, Table 6.7.

	% S	%Cl	%Na	%C	%N	%O
AA-PDADMAC	0	5 ± 1	0	78 ± 1	6 ± 1	13 ± 1
AA-PDADMAC-PSS	7 ± 1	0	7 ± 1	65 ± 1	0	21 ± 1
AA-PDADMAC-PSS-PDADMAC	2 ± 1	5 ± 1	2 ± 1	74 ± 1	7 ± 1	10 ±1
AA-PDADMAC-PSS-PDADMAC-PSS	7 ± 1	0	5 ± 1	65 ± 1	1 ± 1	22 ± 1
AA-PDADMAC-PSS-PDADMAC-PSS-PDADMAC	4 ± 1	1 ± 1	0	76 ± 1	6 ± 1	13 ± 1

Table 6.7: Elemental composition of AA-PDADMAC, AA-PDADMAC-PSS, AA-PDADMAC-PSS-PDADMAC, AA-PDADMAC-PSS-PDADMAC-PSS and AA-PDADMAC-PSS-PDADMAC-PSS-PDADMAC complexes.

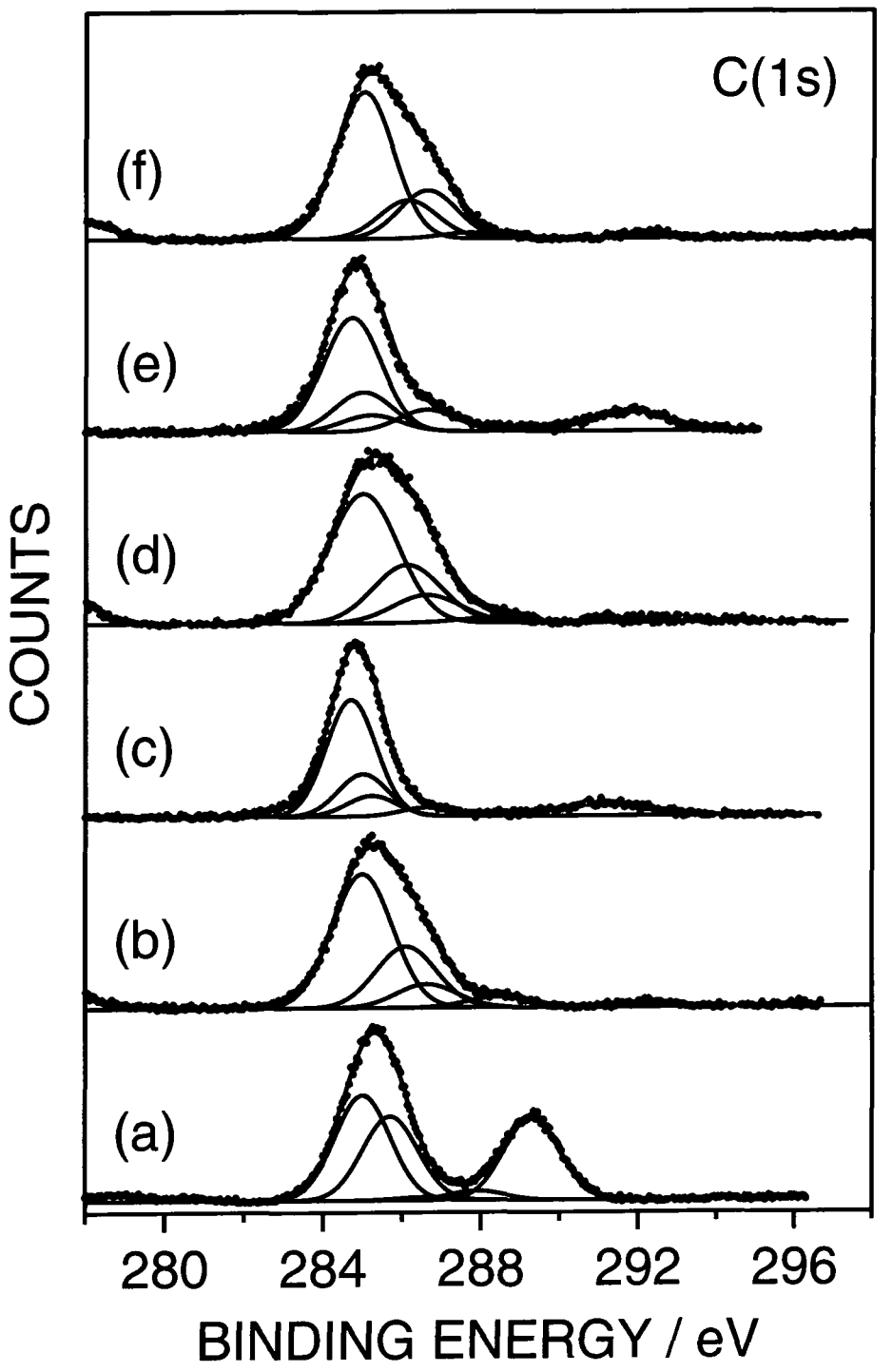

Figure 6.12: C(1s) XPS spectra of (a) AA; (b) AA-PDADMAC; (c) AA-PDADMAC-PSS; (d) AA-PDADMAC-PSS-PDADMAC; (e) AA-PDADMAC-PSS-PDADMAC-PSS; (f) AA-PDADMAC-PSS-PDADMAC-PSS-PDADMAC complexes.

6.3.6 ATTACHMENT OF CATIONIC FLUOROSURFACTANT

The ability of these PE derivatised surfaces to undergo further reaction with surface active agents was demonstrated by the fluorination of an AA-PDADMAC-PSS complex with the cationic fluorosurfactant $CF_3(CF_2)_nC_2H_5(alkyl)_3N^+$. The AA-PDADMAC-PSS complex was placed in an aqueous solution of $CF_3(CF_2)_nC_2H_5(alkyl)_3N^+$ for 1 hour, rinsed in pure water for 10 minutes, dried under vacuum and analysed using XPS, Figure 6.13. Elemental analysis of the surface region revealed a highly fluorinated structure and indicated a significant amount of surfactant attachment, Table 6.8. Deconvolution of the C(1s) XPS spectrum showed that 33% and 7% of the carbon atoms were in the $\underline{C}F_2$ and $\underline{C}F_3$ chemical environments respectively.

	%F	%S	%Cl	%Na	%C	%N	%O
AA-PDADMAC	0	0	5 ± 1	0	78 ± 1	6 ± 1	13 ± 1
AA-PDADMAC-PSS	0	7 ± 1	0	7 ± 1	65 ± 1	0	21 ± 1
AA-PDADMAC-PSS-3658	41 ± 1	3 ± 1	0	0	43 ± 1	2 ± 1	11 ±1

Table 6.8: Elemental composition of AA-PDADMAC, AA-PDADMAC-PSS and AA-PDADMAC-PSS-$CF_3(CF_2)_nC_2H_5(alkyl)_3N^+$ complexes.

The wettability of the fluorinated surface was investigated using the VCA apparatus and employing 2 test liquids, water and hexadecane. The surface interacted strongly with water and produced a contact angle of approximately 20° ± 5. However, the hexadecane contact angle measured was 81° ± 3. These unusual results were observed previously (Chapters 3 and 4).

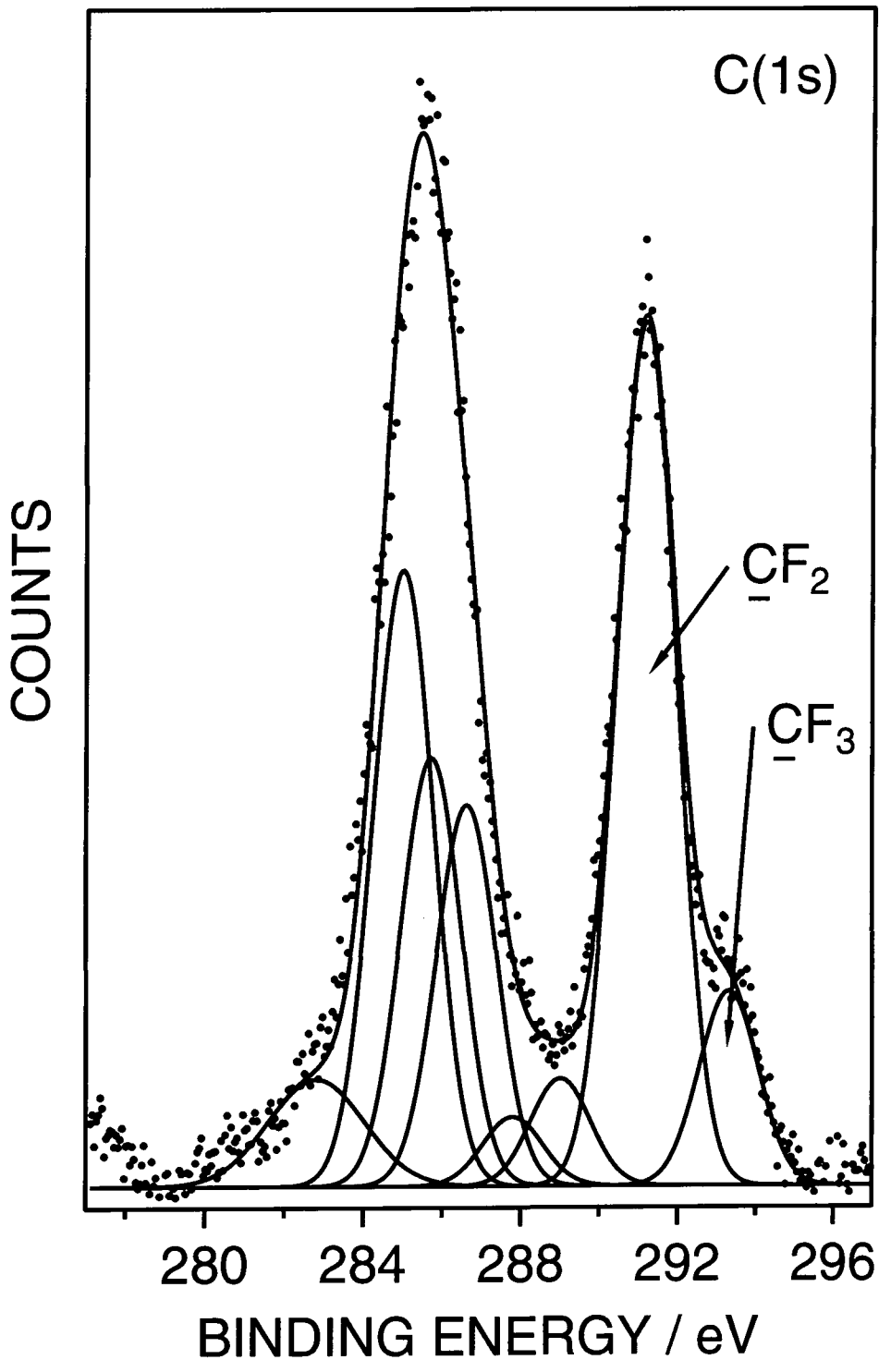

Figure 6.13: C(1s) XPS spectra of $CF_3(CF_2)_nC_2H_5(alkyl)_3N^+$ treated AA-PDADMAC-PSS complexes.

6.4 DISCUSSION

Initial experiments were performed to determine the best conditions for the adsorption of PDADMAC onto the AA plasma polymer. Nitrogen was absent from the plasma polymer and the percentage of nitrogen detected in the surface region following PDADMAC adsorption was therefore a direct measure of the amount of PDADMAC adsorbed. The results indicated that PDADMAC adsorption did not occur in appreciable amounts at low bulk solution concentrations (less than 1%). PDADMAC adsorption increased with increasing bulk solution concentration and reached a maximum value at 20%. Investigations into the rate of PDADMAC adsorption demonstrated that the adsorption process was rapid, almost reaching completion after 10 minutes. The attachment of PDADMAC onto the AA pulsed plasma polymer was irreversible, the PE could not be removed by rinsing of the sample. The mechanism of surface attachment could be via electrostatic attraction between charged acid sites on the plasma polymer surface or via weaker hydrogen bonding interactions between the acid sites and the ammonium group.[1] Unlike earlier studies,[1,2] the PDADMAC counterion was detected in relatively large concentrations (5%). This observation may indicate that the adsorption process did not proceed via electrostatic attraction. The detection of the counterion and the high percentage of nitrogen incorporation (6% in the AA-PDADMAC compared with 9% in the spin coated PDADMAC polymer) suggests that a relatively large amount of PDADMAC was adsorbed. Previous studies have reported only small percentages (approximately 1%) of nitrogen incorporation, even when the adsorbing species possessed a greater amount of nitrogen in the PE structure.[1] Furthermore, the absence of the C(=O)-O functionality in the carbon spectra adds weight to the assumption that a relatively thick layer of PDADMAC was adsorbed (thicker than the XPS sampling depth of approximately 5 nm). The PDADMAC polymer molecule attached to the plasma polymer surface may exist in a close packed arrangement with the polymer chain extending outwards from the AA pulsed plasma polymer surface. Dense PE layers have been reported by adsorption from solutions many times more dilute than the one used in this study.[27] Alternatively, the detection of the counterion suggests that the surface

may not have possessed a high positive charge after initial PDADMAC adsorption. Thus electrostatic repulsion between like charges would be reduced.

XPS analysis of the surface region following PSS adsorption revealed a S/C ratio of 0.11. The S/C ratio in the PSS polymer was 0.13, indicating that a large amount of PSS was adsorbed onto the PDADMAC. The mechanism of adsorption was likely to be electrostatic attraction between the surface bound PDADMAC PE and the oppositely charged PSS PE.[1] Nitrogen was absent from the XPS sampling region and the PSS counterion was detected in large quantities. This again suggests that a relatively large amount of PSS was adsorbed which produced a layer thicker than the XPS sampling depth. PDADMAC was adsorbed from aqueous solution onto the PSS functionalised surface to form a second PDADMAC layer with a N/C ratio of 0.9 (the N/C ratio in the PDADMAC polymer was approximately 0.13). Sulfur was detected in the XPS sampling region which indicated that less PDADMAC was adsorbed than in the first adsorption step or that the PE layers were significantly interdigitated. A second PSS layer was adsorbed onto the newly formed PDADMAC functionalised surface. The resulting S/C ratio was 0.11, less than the S/C ratio after the adsorption of the first PSS layer, indicating a decrease in PSS adsorption or an intercalated region. This assumption was further reinforced by the detection of nitrogen in large quantities (absent from the first PSS layer). Adsorption of a third PDADMAC layer resulted in a N/C ratio of 0.08 and an appreciable amount of sulfur.

A PSS functionalised surface was fluorinated by the attachment of an oppositely charged fluorosurfactant. XPS and contact angle results were similar to the results recorded for the attachment of the same fluorosurfactant onto the AA pulsed plasma polymer surface (Chapter 3). The low water and relatively high hexadecane contact angles observed indicated once again that the fluorosurfactant formed a complex surface structure with a proportion of the cationic groups oriented away from the highly oppositely charged PSS surface.

6.5 CONCLUSIONS

A multilayer assembly was formed on the AA pulsed plasma polymer. The results indicated that more than a monolayer of PE was adsorbed during the first few dipping processes. Furthermore, evidence for the adsorption of relatively thick PE layers was gained by the detection of the PE counterions. These counterions may allow the PE to adsorb in a denser layer without the need to overcome strong electrostatic repulsion between like charges. Further dipping procedures resulted in either a reduced layer thickness or a substantial amount of layer intercalation.

Fluorination of the PSS derivatised sample produced a surface with similar behaviour to fluorosurfactant treated AA surfaces. This was despite the fact that the PSS PE surface has a greater charge density.

6.6 REFERENCES

1. Phuvanartnuruks, V.; McCarthy, T. J. *Macromolecules* **1998**, *31*, 1906.
2. Hsieh, M. C.; Farris, R. J.; McCarthy, T. J. *Macromolecules* **1997**, *30*(26), 8453.
3. Decher, G.; Hong, J. D.; Schmitt, J. *Thin Solid Films* **1992**, *210/211*, 831.
4. Decher, G. In *Polymeric Materials Encyclopedia: Synthesis, Properties, and Applications*; Salamone, J. C., Ed.; CRC Press: Boca Raton, FL, 1996; Vol. 6, pp. 4540-4546; N.
5. Cheung, J. H.; Fou, A. F.; Rubner, M. F. *Thin Solid Films* **1994**, *244*, 985.
6. Bell, C. M.; Arendt, M. F.; Gomez, L.; Schmehl, R. H.; Mallouk, T. E. *J. Am. Chem. Soc.* **1994**, *116*(18), 8374.
7. Kleinfeld, E. R.; Ferguson, G. S. *Science* **1994**, *265*(15 July), 370.
8. Mao, G.; Tsao, Y.; Tirrell, M.; Davis, H. T. *Langmuir* **1993**, *9*(12), 3461.
9. Ferreira, M.; Rubner, M. F. *Macromolecules* **1995**, *28*(21), 7107.
10. Fou, A. C.; Rubner, M. F. *Macromolecules* **1995**, *28*(21), 7115.
11. Hammond, P. T.; Whitesides, G. M. *Macromolecules* **1995**, *28*(22), 7569.
12. Chen, W.; McCarthy, T. J. *Macromolecules* **1997**, *30*(1), 78.
13. Leväsalmi, J.-M.; McCarthy, T. J. *Macromolecules* **1997**, *30*(6), 1752.
14. Lvov, Y.; Decher, G.; Möhwald, H. *Langmuir* **1993**, *9*(2), 481.
15. Decher, G.; Lvov, Y.; Schmitt, J. *Thin Solid Films* **1994**, *244*, 772.
16. Sukhorukov, G. B.; Schmitt, J.; Decher, G. *Ber. Bunsenges. Phys. Chem.* **1996**, *100*(6), 948.
17. Lvov, Y.; Ariga, K.; Ichinose, I.; Kunitake, T. *J. Am. Chem. Soc.* **1995**, *117*(22), 6117.
18. Lvov, Y.; Ariga, K.; Kunitake, T. *Chem. Lett.* **1994**, 2323.
19. Watanabe, S.; Regen, S. L. *J. Am. Chem. Soc.* **1994**, *116*(19), 8855.
20. Ariga, K.; Lvov, Y.; Onda, M.; Ichinose, I.; Kunitake, T. *Chem. Lett.* **1997**, 125.
21. Onda, M.; Lvov, Y.; Ariga, K.; Kunitake, T. *J. Ferment. Bioeng.* **1996**, *82*, 502.
22. Laschewsky, A.; Mayer, B.; Wischerhoff, E.; Arys, X.; Bertrand, P.; Delcorte, A.; Jonas, A. *Thin Solid Films* **1996**, *284-285*, 334.
23. Ferreira, M.; Rubner, M. F.; Hsieh, B. R.; Fou, A. C.; Onitsuka, O. *Mat. Res. Soc. Symp. Proc.* **1995**, *369*, 575.
24. Onoda, M.; Yoshino.K. *Jpn. J. Appl. Phys., Part 2* **1995**, *34*(2B), L260.
25. Stepp, J.; Schlenoff, J. B. *J. Electrochem. Soc.* **1997**, *144*(6, June), L155.
26. Yasuda, H. *Plasma Polymerization*; Academic: London, 1985.
27. Schmitt, J.; Grünewald, T.; Decher, G.; Pershan, P. S.; Kjaer, K.; Lösche, M. *Macromolecules* **1993**, *26*(25), 7058.
28. Wagner, C. D.; Riggs, W. M.; Davis, L. E.; Moulder, J. F.; Muilenber, G. E. *Handbook of X-Ray Photoelectron Spectroscopy*; Perkin-Elmer: New York, 1978.
29. Evans, J. F.; Gibson, J. H.; Moulder, J.F.; Hammond, J. S.; Goretzki, H.; Fresenius, Z. *Anal. Chemie.* **1984**, *319*, 841.
30. Beamson, G.; Briggs, D. *High Resolution XPS of Organic Polymers, The Scienta ESCA 300 Database*; John Wiley & Sons: Chichester, 1992.

APPENDIX

CONFERENCE ATTENDED

December 1998	Materials Research Society annual fall meeting, Boston, USA.

EXAMINED LECTURE COURSES, UNIVERSITY OF DURHAM

January to May 1996	Spectroscopy (Dr. Halliday). Electron Microscopy (Dr. Durose). Experimental Design (Prof. Badyal). Mass Spectroscopy (Dr. Jones).

UNIVERSITY OF DURHAM, BOARD OF STUDIES IN CHEMISTRY, LECTURES AND SEMINARS FROM INVITED SPEAKERS

22nd October 1996	Polymers for Biomedical Applications Prof. Tighe, B.J., Aston University.
23rd October 1996	Function Based on Organisation Prof. Ringsdorf, H., Johannes Gutenberg-Universitat.
6th November 1996	Probing Dynamic Processes with Processes with Photoelectrons Dr. Reid, K.L., Nottingham University.
18th November 1996	Crossing Conventional Lines in my Chemistry of the Elements Prof. Olah, G.A., University of Southern California.

20th November 1996	Surface Light Scattering: Ripples and Relaxations Prof. Earnshaw, J.C., Belfast University.
4th December 1996	Very High Resolution ZEKE Spectroscopy Prof. Muller-Dethlefs, K., York University.
6th February 1997	Integrated Chemical Synthesis Prof. Bartlet, P., Southampton University.
3rd March 1997	Siloxanes at Surfaces Dr. Owen, M. and Dr. Gravier, D., Dow Corning.
15th October 1997	Studying Catalysis in Action Dr. Ormerod, R.M., Keele University.
22nd October 1997	Organoplatinum Chemistry and Catalysis Prof. Puddephatt, R.J., University of Western Ontario.
29th October 1997	Probing Chirality with Circular Dichroism Prof. Peacock, R.D., Glasgow University.
12th November 1997	Spectroscopy of Liquid Interfaces: From Bio-organic Chemistry to Atmospheric Chemistry Dr. Frey, J., Southampton University.
26th November 1997	A Random Walk in Polymer Science Prof. Richards, R.W., Durham University.
14th January 1998	Energy Transfer and Optical Harmonics in Molecular Systems Prof. Andrews, D.L., University of East Anglia.

18th February 1998	Surprises in the Photochemistry of Tropospheric Ozone Prof. Hancock, G., Oxford University.
11th March 1998	How to make Phthalocyanine Films and what to do with them Prof. Cook, M.J., University of East Anglia.
20th October 1998	Dynamic Electrochemistry: Small is Beautiful Prof. Unwin, P., Warwick University.
23rd October 1998	In Search of Hypervalent Free Radicals Prof. Scaiano, J.C., University of Ottawa.
26th October 1998	Reactions of the Highly Electrophilic Boranes $HB(C_6F_5)_2$ and $B(C_6F_5)_3$ with Zirconium and Tantalum Based Metallocenes Dr. Piers, W.E., University of Calgary.
28th October 1998	Tailoring Solid Surfaces Prof. Badyal, J.P.S., Durham University.
18th November 1998	Biodegradable Polymers Dr. Cameron, R.E., Cambridge University.
9th December 1998	Multinuclear Solid-State Magnetic Resonance Studies of Noncrystalline Oxides and Glasses Dr. Smith, M.E., Warwick University.
27th January 1999	Foresight of Hindsight? Some Borane Lessons and Loose Ends Prof. Wade, K., Durham University.

10th February 1999	Surfactant Adsorption and Marangoni Flow at Expanding Liquid Surfaces Dr. Bain, C.D., Oxford University
17th February 1999	Microelectrode Techniques for the Study of Enzymes and Nucleic Acids at Interfaces Dr. Horrocks, B.R., Newcastle University.